Investigating the role of membrane transporters in the adaptation of cancer cells to an acidic microenvironment

Julia Arizanova

MRC-LMS, Institute of Clinical Sciences, Imperial College London

June 2023

Submitted for the degree of

Doctor of Philosophy



Statement of Originality

The work described here was funded by the Medical Research Council (MRC) and was carried out in the Drug Transport and Tumour Metabolism group at the MRC London Institute of Medical Sciences, under the supervision of Dr Louise Fets, between October 2019 and June 2023. I declare that all work presented in this thesis is my own. Any contributions by others are clearly acknowledged or referenced throughout the text.

Copyright Statement

The copyright of this thesis rests with the author. Unless otherwise indicated, its contents are licensed under a Creative Commons Attribution-Non Commercial 4.0 International Licence (CC BY-NC). Under this licence, you may copy and redistribute the material in any medium or format. You may also create and distribute modified versions of the work. This is on the condition that: you credit the author and do not use it, or any derivative works, for a commercial purpose. When reusing or sharing this work, ensure you make the licence terms clear to others by naming the licence and linking to the licence text. Where a work has been adapted, you should indicate that the work has been changed and describe those changes. Please seek permission from the copyright holder for uses of this work that are not included in this licence or permitted under UK Copyright Law.

Acknowledgements

First and foremost I would like to thank my supervisor Louise Fets for giving me the opportunity to do my PhD project in her lab and to be the first member of the Drug Transport and Tumour Metabolism group. I am grateful for the scientific and moral support over the last 4 years, for her guidance, her patience, the meticulous feedback, the thought-provoking discussions and her truly unparalleled attention to detail. Thank you for pushing me to achieve my best.

I would also like to thank all present members of the Fets group, for their help with this project, for their encouragement, for the countless cups of coffee and all the laughter. I am grateful to the MRC for my funding, and also to Yi-Fang Wang who helped me set up the bioinformatics analysis pipeline and to Joao Mokochinski, who developed the creatine detection method and trained me on the LC-MS instrument.

A big thank you to my Cambridge family - Anna Guncheva, Steven Haworth, Giulia D'Aprile, Stefano Manca, Peter Bachev and Yasmin Surani. Also Milena Atsinov, who was there for me despite the physical distance. Thank you for keeping me sane through the tough times.

Finally, I want to thank my Mum and Grandma, for their unwavering support, always.

Abstract

As regulators of nutrient uptake, efflux, and compartmentalization, solute carrier (SLC) transporters have a significant impact on cellular metabolism, and as the metabolic interface between the cell and its environment, they are well-placed to enable cancer cells to adapt to the tumour microenvironment. While adaptations to a hypoxic microenvironment are well characterised, less is known about acidosis-specific adaptations. We hypothesised that SLC expression signatures of cancer cells change in response to acidosis, to facilitate metabolic adaptations and survival. We aimed to characterise changes in SLC expression patterns that are specifically associated with acidosis. We used a computational approach to identify samples within the TCGA database with a more or less acidic microenvironment, using transcriptional 'proxy' signatures and interrogated differential SLC expression in these samples. The creatine transporter SLC6A8 was upregulated in more 'acidic' tumours, especially in lung (LUAD) and colon adenocarcinoma (COAD). This coincided with upregulation of the glucose transporter SLC2A1 and lactate transporter SLC16A13, suggesting SLC6A8 is associated with a more glycolytic phenotype. Analysis of publicly available single-cell transcriptomics data revealed SLC6A8 is predominantly expressed on cancer cells in LUAD clinical samples, and that the transporter is upregulated in late- versus early-stage LUAD. *In vitro* however, we did not observe acidosis-specific effects of creatine on cancer cell proliferation.

In parallel, we investigated the effect of an acidic microenvironment on a panel of lung and colorectal cancer cell lines. Lung lines showed a stronger transcriptional response to acidosis, and a 'LUAD *in vitro* acidosis signature' (LIVAS) was identified. Clinically, LIVAS was associated with a favourable prognosis, and was negatively correlated with a hypoxic transcriptional signature. Interestingly, SLC6A8

was downregulated in lung cancer cell lines cultured in acidic conditions. The same was true of glycolytic enzymes and the glucose transporter SLC2A1. This data suggests acidosis in the absence of hypoxia could promote a less glycolytic and subsequently less aggressive phenotype in lung cancer.

Contents

1 Introduction **15**

1.1 SLC transporters in cancer 16

1.2 The tumour microenvironment 20

1.2.1 Metabolic interactions in the tumour microenvironment 20

1.2.2 Tumour Acidosis 21

1.3 Creatine metabolism 27

1.3.1 Creatine metabolism in healthy cells 27

1.3.2 Creatine metabolism in cancer 31

1.3.3 The Creatine transporter SLC6A8 in cancer 35

1.4 Hypothesis and project aims 36

2 Methods **37**

2.1 Computational methods 38

2.1.1 SLC family tree 38

2.1.2 TCGA data download 38

2.1.3 tSNE 38

2.1.4 TCGA differential gene expression analysis 39

2.1.5 Kaplan-Meier graphs 39

2.1.6 In-house RNAseq data processing and analysis 41

2.1.7 *In vitro* acidosis signatures 41

2.1.8 Single cell RNAseq 41

2.1.9 Blood vessel proximity data 42

2.1.10 CCLE data download 42

2.2 Cell culture methods 42

2.2.1 Cell lines . . . 42
2.2.2 pH adjustment of culture media . . . 43
2.2.3 Serum dialysis . . . 43
2.2.4 Physiological media . . . 43
2.2.5 Growth curves . . . 44
2.2.6 Hypoxia . . . 44
2.2.7 Cell mass accumulation (SRB assays) . . . 45
2.2.8 RNAseq sample preparation . . . 45
2.2.9 ATP assay . . . 47
2.2.10 Intracellular pH assay . . . 48
2.3 Molecular biology methods . . . 48
2.3.1 shRNAs . . . 48
2.3.2 Lentiviral transduction . . . 49
2.3.3 qPCR . . . 50
2.3.4 Western blots . . . 50
2.4 Metabolomics . . . 51
2.4.1 Gas chromatography - mass spectrometry (GC-MS) . . . 51
2.4.2 Liquid chromatography - mass spectrometry (LC-MS) . . . 52

3 Computationally deconvoluting SLC signatures in hypoxia and acidosis 54

3.1 Exploration of SLC signatures across cancer types . . . 55
3.1.1 TCGA clinical samples cluster by tissue of origin based on transporter expression . . . 55
3.1.2 SLC signatures vary between healthy and tumour tissue . . . 56
3.2 SLC transporter signatures in acidosis and hypoxia are cancer type-specific . . . 59
3.2.1 Different acidic signatures are associated with different clinical samples . . . 59
3.2.2 The creatine transporter SLC6A8 is upregulated in acidosis . . . 65
3.2.3 The creatine transporter SLC6A8 is upregulated in hypoxia . . . 68

3.2.4 SLC6A8 is prognostic in COAD, LUAD, LUSC and LIHC . . 69
3.2.5 SLC6A8 is upregulated away from blood vessels 69
3.3 Exploration of SLC signatures on the single cell level 75
3.3.1 Single cell RNAseq analysis reveal patient-to-patient heterogeneity in SLC expression 77
3.3.2 SLC6A8 is expressed on cancer cells, T helper cells and Macrophages 77
3.3.3 SLC6A8 is upregulated in late compared to early stage LUAD tumours 79
3.3.4 Acidosis proxies used for TCGA analysis are expressed across cell types 82
3.4 Conclusions and limitations 82

4 Investigating the role of SLC6A8 in cell adaptation to acidosis 88
4.1 Setting up an *in vitro* pH system 89
4.2 Creatine supplementation does not affect growth rates in acidic pH . 92
4.2.1 Creatine supplementation does not affect growth rates in standard and nutrient-deprived media 92
4.2.2 Creatine pre-loading does not affect growth rates in nutrient-deprived media 93
4.2.3 Knockdown of the creatine transporter SLC6A8 does not affect growth rates 93
4.2.4 Creatine supplementation does not affect growth rates in hypoxia 97
4.2.5 Quantification of creatine in foetal calf serum 97
4.2.6 Creatine supplementation does not affect growth rates in RPMI supplemented with dialysed FCS 100
4.2.7 Creatine supplementation does not affect growth rates in physiological media 103
4.3 Intracellular effects of creatine supplementation 103
4.3.1 Creatine supplementation increases intracellular creatine concentration 105

4.3.2 Creatine pre-loading affects intracellular ATP levels at pH 6.8 105
4.3.3 Creatine pre-loading does not affect intracellular pH 109
4.3.4 Creatine supplementation causes an increase in intracellular creatinine 109
4.3.5 Knockdown of SLC6A8 decreases intracellular creatinine and putrescine in RPMI 110
4.3.6 Knockdown of SLC6A8 decreases intracellular creatinine and putrescine in physiological media 113
4.4 Conclusions and limitations 117

5 Exploring SLC signatures in cancer cell lines 123
5.1 RNA sequencing of lung and colon cancer cell lines 124
5.1.1 Lung cancer cell lines show stronger transcriptional response to pH than colon cancer cell lines 124
5.1.2 SLC6A8 is downregulated in lung cancer cell models 126
5.1.3 Acidic signature has a prognostic value in lung cancer 130
5.1.4 *In vitro* acidosis signatures correlate with hypoxia in clinical samples 133
5.1.5 Adaptations to acidosis are not driven by changes in intracellular pH alone 134
5.1.6 Acidosis has a cell line-specific effect on intracellular metabolites 135
5.2 Conclusions and limitations 135

6 Discussion 142
6.1 Tumour acidosis 143
6.2 Acidosis in cell culture 145
6.3 Creatine metabolism 148
6.4 Limitations of the study 149

Appendix A Differentially expressed SLC transporters in acidosis 177

Appendix B Differentially expressed SLC transporters in hypoxia 190

List of Figures

1.1 Phylogenic tree of the SLC family 18
1.2 Cell adaptations to hypoxia result in acidosis 23
1.3 Creatine and energy storage 28
1.4 Creatine and proton buffering 30
1.5 Creatine and glycolysis 32

3.1 Clinical samples from the TCGA database 58
3.2 Expression levels of acidosis proxies across tumour types 61
3.3 Expression levels of acidosis proxies and Hallmark Hypoxia (1) 62
3.4 Expression levels of acidosis proxies and Hallmark Hypoxia (2) 63
3.5 Analysis workflow 64
3.6 Clinical samples identified as acidic or hypoxic across the analysis streams 66
3.7 Differentially expressed SLC transporters in acidosis 67
3.8 Differentially expressed SLC transporters in hypoxia 70
3.9 SLC transporters upregulated in hypoxia 71
3.10 SLC6A8 expression in cancer 72
3.11 SLC6A8 expression in tumour and healthy tissue samples 72
3.12 SLC6A8 expression in acidic and non-acidic tumour samples 73
3.13 Prognostic value of SLC6A8 74
3.14 SLC6A8 expression in glioblastoma 76
3.15 UMAP of LUAD cancer cells 78
3.16 SLC6A8 expression across cell types within the tumour in early stage LUAD 80

3.17 SLC6A8 expression across cell types within the tumour in late stage LUAD . . . 81
3.18 Upregulated SLC genes in late stage LUAD . . . 81
3.19 Expression of acidosis proxies on the single cell level in early stage LUAD . . . 83
3.20 Expression of acidosis proxies on the single cell level in late stage LUAD 84

4.1 Setting up an *in vitro* pH system . . . 91
4.2 Creatine supplementation in full media . . . 94
4.3 Cell proliferation with and without creatine supplementation in nutrient deprived media . . . 95
4.4 Creatine pre-loading . . . 96
4.5 SLC6A8 knockdown . . . 98
4.6 Creatine supplementation in hypoxia . . . 99
4.7 Creatine concentration in RPMI . . . 101
4.8 Growth rates in RPMI supplemented with dialysed FCS . . . 102
4.9 Growth rates in HPLM . . . 104
4.10 Intracellular creatine in lung cancer cell lines . . . 106
4.11 Intracellular ATP storage . . . 108
4.12 Intracellular pH . . . 110
4.13 Metabolic effect of creatine supplementation (1) . . . 111
4.14 Metabolic effect of creatine supplementation (2) . . . 112
4.15 Effects of SLC6A8 knockdown on cell metabolism (1) . . . 114
4.16 Effects of SLC6A8 knockdown on cell metabolism (2) . . . 115
4.17 Intracellular metabolite abundance in HPLM (1) . . . 116
4.18 Intracellular metabolite abundance in HPLM (2) . . . 117
4.19 Effects of SLC6A8 knockdown on cell metabolism in HPLM . . . 118
4.20 Putrescine and creatine synthesis . . . 120
4.21 Fructose metabolism in cancer . . . 121

5.1 DE genes in colon and lung cancer cell lines after 8 and 24 hours . . . 127
5.2 DE genes in lung cancer cell lines after 8 and 24 hours . . . 128

5.3 DE genes in colon cancer cell lines after 8 and 24 hours 129
5.4 DE transporters in colon and lung cancer cell lines after 8 hours . . . 131
5.5 DE transporters in colon and lung cancer cell lines after 24 hours . . 132
5.6 Prognostic value of acidosis signatures 133
5.7 Correlation of *in vitro* acidosis and hypoxia signatures 134
5.8 Changes in intracellular pH in an acidic microenvironment 136
5.9 Metabolic response of 6 cell lines to acidic pH 137
5.10 Relative expression of SLC6A8, SLC2A1 and SLC16A3 in clinical samples with acidic signatures and in lung cancer cell lines 138
5.11 Proposed model of the response to acidosis in lung adenocarcinoma . 140
5.12 Prognostic values of gene sets associated with acidosis 141

List of Tables

2.1 Rate limiting genes in glycolysis (Tanner et al., 2018) 40
2.2 Genes upregulated in lactic acidosis (J. L.-Y. Chen et al., 2008) . . . 40
2.3 Extracellular Carbonic anhydrases 40
2.4 Seeding density for Incucyte experiments in 96 well plates 44
2.5 Buffers and solutions 46
2.6 Seeding density for RNAseq in 6 well plates 47

3.1 Clinical samples from the TCGA database 56

A.1 Differentially expressed SLC transporters in Acidosis 189

B.1 Differentially expressed SLC transporters in Hypoxia 197

Chapter 1

Introduction

1.1 SLC transporters in cancer

Membrane transporters have been described as the 'gatekeepers' of biological membranes (Hediger et al., 2004). They are membrane integral proteins, distributed across all tissue types in the body. Membrane transporters are found in the cell plasma membrane, as well as organelle membranes and facilitate the passage of both endogenous and xenobiotic compounds (L. Lin et al., 2015).

Functionally, membrane transporters are generally divided into active and passive (or facilitative) transporters. Passive transporters carry their substrates across membranes, following their electrochemical gradient (Hediger et al., 2004). These include water channels and ion channels. Active transporters create ion/solute gradients across membranes, making use of an energy-coupling mechanism. They are further subdivided into primary and secondary active transporters. Primary active transporters bind or hydrolyse ATP to facilitate cross-membrane transport of a variety of substrates, such as ions, carbohydrates, lipids or xenobiotics (Borst and Elferink, 2002). These include ion pumps and members of the ATP-binding cassette (ATP) superfamily. Ion pumps generate and maintain electrochemical ion gradients across membranes, by pumping ions such as Na^+, K^+, H^+, Ca^{2+} and Cu^{2+} (Dunbar and Caplan, 2000; Hediger et al., 2004). Secondary active transporters use these electrochemical gradients to transport their substrates across the membrane, sometimes in an ion-coupled manner.

The Solute Carrier transporters (SLC) superfamily is the largest family of membrane transporters. Unlike other large gene families, they have been grouped together based on function rather than an evolutionary relationship. As of 2023, the SLC superfamily includes 458 identified members, which have been divided into 65 subfamilies, based on their structural characteristics (Pizzagalli, Bensimon, and Superti-Furga, 2021) (Figure 1.1). The SLCs include passive and secondary active members, some of which can be symporters (co-transporters) or antiporters (exchangers) (L. He, Vasiliou, and Nebert, 2009; Superti-Furga et al., 2020). They are predominantly seen as uptake transporters, while ABCs are associated with efflux. SLCs transport a broad range of substrates, including inorganic and organic ions,

sugars, essential metals, biogenic amines, neurotransmitters, vitamins, fatty acids and lipids, nucleosides and drugs (L. He, Vasiliou, and Nebert, 2009; L. Lin et al., 2015). Some SLCs, such as the organic anion transporter SLC22A6 (OAT1) have a broad substrate specificity and are able to transport xenobiotics in addition to endogenous compounds (Hediger et al., 2004). Others have a narrow specificity and high affinity to a single solute.

SLCs can be located on the plasma membrane, as well as organelle membranes. As the majority of metabolites are not membrane permeable, SLC transporters play an indispensable role in cell metabolism. They are involved in nutrient uptake, secretion of waste products and cell-to-cell signalling. SLCs are critical in the interaction between cells and their environment. As cells in different organs across the body have different metabolic needs, they express different SLC signatures (O'Hagan et al., 2018). For example, glutamate transporter SLC17A6 and glycine transporter SLC32A1 are almost exclusively expressed on neurons in the brain, and bile acid transporter SLCO1B1 is only expressed by hepatocytes in the liver (C. Hu et al., 2020; T.-T. Li et al., 2019). Some SLC subfamilies are specific for subcellular compartments. SLC25 contains 53 transporters, expressed on mitochondrial membranes specifically. The SLC25 family is cluster due to their differing evolutionary origin, rather than by substrate specificity, like the majority of other transporter families. The SLC25s have a highly diverse set of substrates. (Ruprecht and Kunji, 2020).

Many SLCs are still poorly characterised and remain 'orphans', with little known about their substrate specificity. Solute carriers have drawn a lot of attention in recent years as drug transporters or drug targets themselves, in a variety of therapeutic areas, including neurodegenerative disease, diabetes, rare disease and cancer (Aykaç and Sehirli, 2020; L. Lin et al., 2015; X. Liu, 2019; Scott et al., 2007; Superti-Furga et al., 2020). Drug targets include the serotonin transporter SLC6A4 (SERT), targeted by a class of antidepressant drugs - serotonin reuptake inhibitors (Cesar-Razquin et al., 2015). The most prominent example of SLCs with the ability to import drug molecules is the SLC22 subfamily (Koepsell, 2013; Sprowl and Sparreboom, 2014). SLC22s are divided into organic cation transporters (OCTs), zwitterion/cation transporters (OCTNs), and organic anion transporters (OATs).

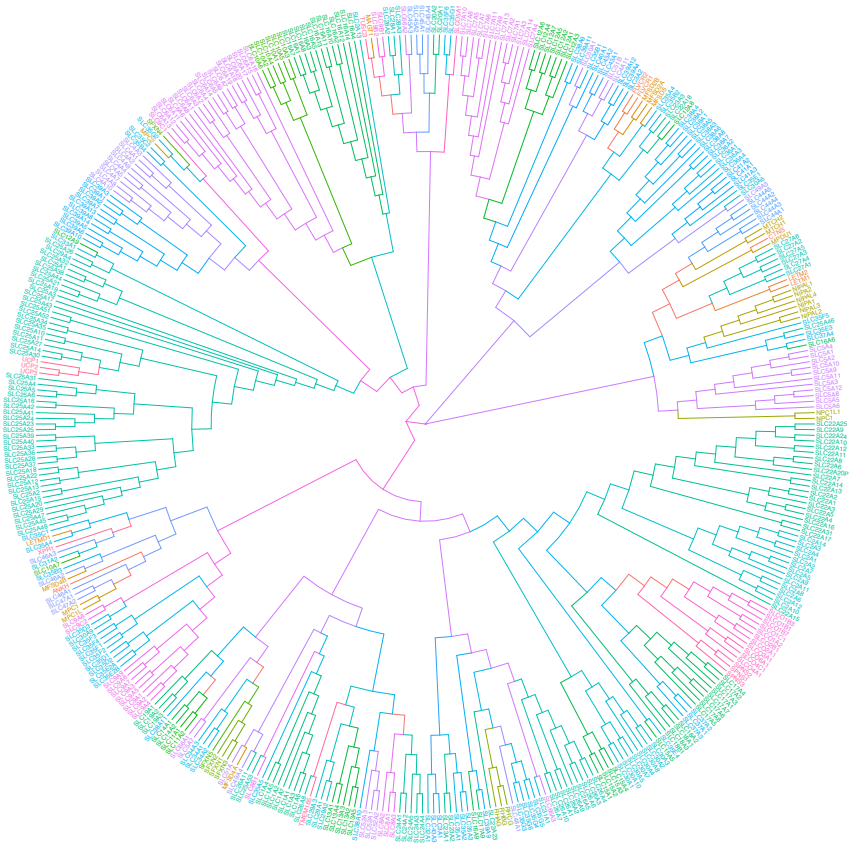


Figure 1.1: Phylogenic tree of the SLC family

They have been linked to the uptake of antibiotics, antihypertensives, antivirals, anti-inflammatory drugs, diuretics and uricosurics (Koepsell, 2013; Rizwan and Burckhardt, 2007). Other characterised drug transporters include SLC35F2 which transports the anticancer compound YM155 (Winter et al., 2014), SLC16A7 (MCT2), which mediates uptake of the pro-drug DMOG (Fets, Paul C Driscoll, et al., 2018a) and SLC19A1 which transports the antimetabolite Methotrexate (N. J. Wright et al., 2022).

SLC transporters are especially interesting in the context of cancer biology. Cancer cells divide rapidly, meaning that they have high nutritional demands. In addition, the tumour microenvironment can be a hostile growth environment, characterised by nutrient scarcity and poor vasculature. In order to survive and grow in these conditions, cancer cells need to adjust their metabolism. This is reflected in changes

in their SLC signatures. Perhaps the best characterised example is the glucose transporter SLC2A1 (GLUT1). Cancer cells are well known to increase glucose metabolism, often referred to as "The Warburg effect', and the upregulation of SLC2A1 facilitates an increased glucose uptake to maintain a rapid glycolytic rate (Murakami et al., 1992). Tumour cells are also known to have an increased demand for essential amino acids (EAA) (Hattori et al., 2017; Sheen et al., 2011). EAA are used as building blocks for macro molecules, and are sensed by the master-regulator of cell growth mammalian Target of Rapamycin (mTOR), promoting cell proliferation (Hosios et al., 2016; Jewell, R. C. Russell, and Guan, 2013). Two EAA transporters - SLC7A5 and SLC43A1 - were specifically identified as drivers of tumour progression. These were both linked to oncogenic MYC in neuroblastoma and lymphoma cell lines. MYC was demonstrated to activate SLC7A5 and SLC43A1 transcription, leading to an increased EAA uptake. EAA in turn, stimulates Myc translation, forming a feedforward loop (Yue et al., 2017). Myc oncogenes are known to regulate a number of metabolic processes, including the uptake of both glucose and glutamine (Dang, 2013; Yue et al., 2017). Another amino acid transporter - SLC43A2 - is upregulated in pancreatic and breast cancers (Bian et al., 2020). It facilitates the uptake of large neutral amino acids, such as leucine and phenylalanine, also known to promote mTOR signalling and cancer cell growth.

SLC expression is strongly altered in cancer cells compared to healthy tissue. As well as the clear implications for tumour metabolism, this presents a potential opportunity for targeted chemo-therapy, with drug molecules being internalised by cancer cells specifically while limiting off target effects on surrounding tissue. What adds complexity to this task is the fact that SLC expression patterns are also known to be highly heterogeneous between patients with the same cancer type (Nyquist, Prasad, and Mostaghel, 2017). Understanding the role of SLC transporters in cancer can also provide better understanding of mechanisms of drug resistance. One example is the nucleoside analogue Gemcitabine - a first line chemotherapy agent, which is internalised via nucleoside transporters from SLC28 and SLC29 families. Pancreatic ductal adenocarcinoma cells have been shown to develop resistance to Gemcitabine by polarising tumour associated macrophages (TAMs). The polarisa-

tion causes TAMs to release deoxycytidine, which successfully out-competes Gemcitabine for these transporters, leading to reduced uptake and resistance in cancer cells (Halbrook et al., 2019). Another transporter involved in chemoresistance is the cystine-glutamate exchanger SLC7A11. SLC7A11 imports the dipeptide cystine, which is rapidly reduced to cysteine - the rate-limiting amino acid for glutathione synthesis. Glutathione is part of a major detoxification pathway and has been linked to resistance to multiple cancer drugs (Gatti and Zunino, 2005). For one drug in particular - the anti-tumour antibiotic Geldanamycin - a direct correlation has been identified between SLC7A11 expression and drug resistance (R. Liu et al., 2007).

1.2 The tumour microenvironment

1.2.1 Metabolic interactions in the tumour microenvironment

The tumour microenvironment (TME) is often described as hostile to growth due to its poor vasculature and nutrient scarcity. It hosts a heterogeneous population of tumour cells, along with infiltrating cells of the immune system, cancer associated fibroblasts and other tissue-specific host cells. This complexity creates a unique extracellular environment, resulting from the metabolic activity of different cell types, secreted factors and extracellular matrix proteins (Finicle, Jayashankar, and A. L. Edinger, 2018; Lyssiotis and Kimmelman, 2017). Cancer cells can compete for nutrients with other cell types by upregulation of nutrient transporters. Equally, nutrient transporters can mediate commensal cell to cell interactions, which have been described across a number of cancer types.

Cancer associated Fibroblasts (CAFs) in ovarian cancer for example, are characterised by an upregulated glutamine anabolic pathway. These CAFs are able to utilise noncanonical sources of carbon and nitrogen, to synthesise and secrete glutamine even in a poor nutrient environment. Cancer cells in these tumours rely on CAF-synthesised glutamine. Targeting glutamine synthesis in stroma and glutaminase in cancer cells reduces tumour size and metastasis in mouse models of ovarian tumours (L. Yang et al., 2016). A similar metabolic interaction has been observed in pancreatic ductal adenocarcinoma. Autophagic stromal-associated pancreatic stel-

late cells (PSCs) were shown to secrete non-essential amino acids, and especially alanine in the TME. Alanine is used as an energy source by pancreatic cancer cells, preferentially to glucose and glutamine in this set up. In addition, the alanine secretion by PSCs is dependent on autophagy in stellate cells - a phenomenon only observed when they are in contact with cancer cells. Targeting PSCa inhibits cancer progression in ductal adenocarcinoma (Sousa et al., 2016).

Metabolic interactions at the whole organism level have been studied in *Drosophila* models of tumourigenesis. Tumour progression of eye tumours in *Drosophila* has been demonstrated to induce muscle wasting and systemic amino acid release, in a process mediated by Bnl - the homologue of the mammalian fibroblast growth factors (FGFs). At the same time, cancer cells upregulate expression of amino acid transporters from the SLC36 family, as a proline-scavenging strategy (Newton et al., 2020).

1.2.2 Tumour Acidosis

Cancer cells are continuously subjected to nutrient and oxygen fluctuations, as a result of poor vasculature in solid tumours. They have the ability to switch between alternative nutrient acquisition and metabolic pathways in order to survive and proliferate even under extreme stress. In solid tumours, the increased metabolic activity of cancer cells, along with the scarcity of blood vessels, often result in areas of hypoxia and acidosis. Adaptations to hypoxia are well characterised and are mainly regulated by the transcription factor Hypoxia-inducible factor 1α (HIF1α) (Corbet and Feron, 2017a; Wykoff et al., 2000). Far less is known about adaptation to low extracellular pH. Acidification of the microenvironment can occur as a consequence of hypoxia - as glucose is metabolised via anaerobic glycolysis, lactate and protons (H^+) begin to accumulate in the intracellular space. To prevent intracellular acidification, cancer cells upregulate the lactate transporters SLC16A1 (MCT1) and SLC16A3 (MCT4) (Counillon et al., 2016), and the Na^+/H^+ exchanger SLC9A1 (NHE1) (Corbet and Feron, 2017a; Reshkin et al., 2000). This prevents a drop in intracellular pH, but acidifies the extracellular space (Figure 1.1). In addition, bicarbonate importers from the SLC4 family are also upregulated. Bicarbonate

(HCO_3) is the natural pH buffering system in blood - HCO_3 and H^+ are converted to CO_2 and H_2O. This reaction can be catalysed by intracellular carbonic anhydrases (CAs), while extracellular CAs, most notably CAIX, catalyse the reverse reaction, converting CO_2 and H_2O to HCO_3 and H^+, thus further contributing to extracellular acidosis (Supuran, 2008; á. Swietach et al., 2010) (Figure 1.2). Although these events can be triggered by a hypoxic environment, cancer cells metabolise glucose by glycolysis even in the presence of oxygen - a phenomenon known as The Warburg Effect (Warburg, Wind, and Negelein, 1927). The increased metabolic rate of these cells can lead to acidosis independently of hypoxia (Corbet and Feron, 2017a). Acidification of the microenvironment has been reported to impact cell physiology in a number of ways, including changes in cell morphology, decrease in drug sensitivity and increase in cell motility, promoting metastasis. Furthermore, in some incidents acidosis alone has been shown to trigger stabilisation of HIF-1α (Mekhail et al., 2004) and HIF-2α (Corbet, Draoui, et al., 2014), and cause a dramatic change in gene expression (J. L.-Y. Chen et al., 2008).

Intracellular pH of cancer cells remains near-neutral, or slightly alkaline (G. Hao, Z. P. Xu, and L. Li, 2018; Persi et al., 2018). As the extracellular space becomes more acidic, cancer cells experience a greater difference between internal (pH_i) and external pH (pH_e) compared to healthy cells. In addition, they have an inverted pH gradient, as pH_i is higher than pH_e - the opposite of what is seen in healthy tissue (G. Hao, Z. P. Xu, and L. Li, 2018; Persi et al., 2018; Webb et al., 2011; K. A. White, Grillo-Hill, and Barber, 2017). In cancer cells pH_i has been reported between pH 7.3 - 7.6 (versus pH 7.2 in healthy cells). Fluctuations of pH_i within this narrow range can have an impact on a group of intracellular proteins, known as pH sensors (Webb et al., 2011). pH sensors are believed to enable acidosis-associated cell behaviours, although their mechanism of action remains poorly understood. There is evidence that increased pH_i blocks apoptotic signalling, as measured by downstream effects on DNA degradation (Pérez-Sala, Collado-Escobar, and Mollinedo, 1995). A more alkaline intracellular pH has also been recognised as a permissive signal for increased cell proliferation (Pouysségur et al., 1984).

The inverted pH gradient in cancer cells has been suggested to sustain nutrient up-

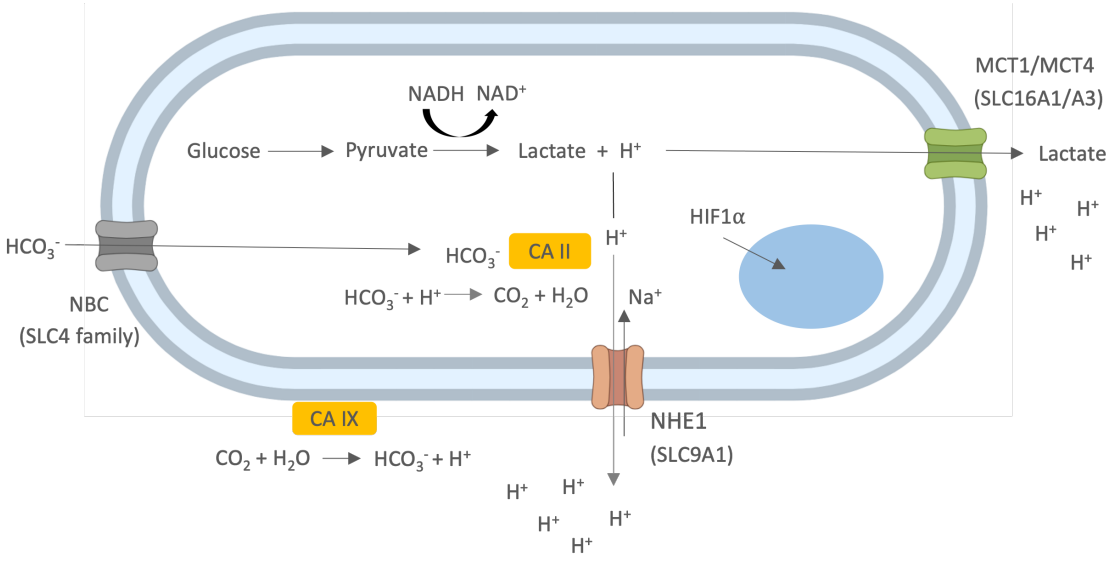


Figure 1.2: Under hypoxic conditions, glucose is metabolised to lactate and protons. Cell adaptations are mainly triggered by stabilisation of the transcriptional factor HIF-1α. To prevent acidification of the intracellular space, cancer cells upregulate monocarboxylate transporters from the SLC16 family, H^+ exchanger SLC9A1, and bicarbonate importers from the SLC4 family. Intracellular carbonic anhydrases (in this example CAII) catalyse the titration of H^+, while extracellular carbonic anhydrases (in this example CAIX catalyse the reverse reaction and contribute to the further acidification of the tumour microenvironment.

take via Proton-Nutrient Symporters (Daverio et al., 2023). Unlike healthy tissue, in cancer protons are more concentrated outside the cell than they are inside. This electrochemical gradient has a positive impact on proton-coupled nutrient uptake. H^+-driven transporter substrates include amino acids, peptides, and monocarboxylates such as pyruvate and lactate (Brown and Ganapathy, 2020; Thwaites and Anderson, 2011). Acidosis not only increases the activity of H^+-driven transporters, but is known to upregulate the expression of the glutamine transporter SLC1A5 (ASCT2) (Pérez-Escuredo et al., 2016), as well as fatty acids (Corbet, Bastien, et al., 2020) and folate uptake (Guedes et al., 2016). Because extracellular acidosis increase the cancer cells' capacity to uptake and metabolise alternative nutrients, it has been hypothesised that acidosis promotes resistance to glucose starvation (Daverio et al., 2023; Papalazarou and Maddocks, 2021). In addition, acidosis has been shown to reduce the uptake of glucose in a range of lung, colon, breast and cervix cancer cell lines (Corbet, Draoui, et al., 2014; J. Jiang et al., 2021; Prado-Garcia, Campa-Higareda, and Romero-Garcia, 2020b; J. Xie et al., 2014).

There is in fact some evidence that acidic microenvironment drives cancer metabolism away from aerobic glycolysis and towards oxidative phosphorylation (OXPHOS). Measuring ATP contribution from aerobic glycolysis and OXPHOS in a range of cancer cell lines, revealed that $23.7\% - 52.2\%$ of intracellular ATP comes from glycolysis in neutral pH, while glycolysis contribution drops to $5.7\% - 13.4\%$ in acidic conditions (H. Wu, M. Ying, and X. Hu, 2016a). Furthermore, lung cancer cell lines exposed to lactic acidosis have been shown to downregulate the glycolytic enzymes Hexokinase 1 (HK1) and pyruvate kinase (PKM) (J. Jiang et al., 2021).

Another metabolic effect which has been associated with acidosis is the onset of autophagy - a self-degradative process used as an energy source, usually as a response to nutrient stress. Melanoma, breast and colon cancer cell lines, exposed to acidic culture conditions, were shown to rapidly accumulate autophagic vesicles (Marino et al., 2012; Pellegrini et al., 2018; Wojtkowiak et al., 2012). Further, knockdown of the autophagic gene ATG5 reduces cell survival of melanoma cells in acidic conditions. Interestingly, these cells were shown to reduce glucose and leucine uptake at the same time (Marino et al., 2012). Although autophagy is normally a transient condition,

breast cancer cell lines were demonstrated to maintain autophagic vesicles for 3 months while they were exposed to acidic conditions (Wojtkowiak et al., 2012). The benefits of using autophagy as an energy source when other nutrients are available remain unclear. It could be an example of cellular adaptation to prevent further acidification of the microenvironment.

The formation of lipid droplets in cancer cells has also been commonly observed in acidic conditions (Delikatny et al., 2011; Ibrahim-Hashim and Estrella, 2019; Pillai et al., 2017). Lipid droplets are involved in fat storage, lipid metabolism and cell signalling. They could be the product of upregulation of de novo lipid synthesis, repurposing of structural lipids via enzymatic remodeling, or lipid recycling through autophagy (Petan, 2020). Recent work by Corbet, Bastien, et al. (2020) demonstrated that low pH promotes Transforming growth factor-β2 (TGF-β2) signalling, which in turn drives the formation of lipid droplets. The study shows that lipid droplets protect cancer cells from anoikis - a form of programmed cell death that occurs upon detachment from the correct extracellular matrix (Taddei et al., 2012). This makes migration and subsequent metastasis more likely. Consistent with this, the same study shows that TGF-β2 activation induces a partial epithelial-to-mesenchymal transition, and promotes fatty acid metabolism in SiHa, FaDu and HCT116 cell lines (Corbet, Bastien, et al., 2020). The presence of lipid droplets has also been positively correlated with cancer aggressiveness in breast cancer cell lines (Antalis et al., 2011; Ibrahim-Hashim and Estrella, 2019).

Acidosis has widely been linked to metastasis in cancer (Corbet and Feron, 2017b; Y.-J. Kwon et al., 2020; Riemann et al., 2016; Sculier, Nicaise, and Klastersky, 1983). Low extracellular pH promotes degradation of the extracellular matrix (Avnet et al., 2017; Rothberg et al., 2013), and high pH_i is believed to promote cell migration via pH sensors (Webb et al., 2011). In breast cancer, acidosis was shown to induce metastasis by inhibition of the circadian clock gene BMAL1, although the exact mechanism remains unclear (Y.-J. Kwon et al., 2020). In osteosarcoma, the most common primary tumour of bone, an acidic pH has been shown to remodel mesenchymal stem cells and activate the NF-*kappa*B pathway. These mesenchymal stem cells release mitogenic and chemotactic factors, driving cell division and invasion of

cancer cells (Avnet et al., 2017). In addition, acidosis has been reported to induce cell motility in a range of breast and prostate cancer cell lines (Miret et al., 2022; Riemann et al., 2016; Anne Riemann et al., 2014).

In addition to cell-to-cell interactions, acidosis has an impact on cells of the immune system. Both lactate and acidic pH have been shown to independently inhibit immune surveillance (Husain et al., 2013; Ibrahim-Hashim and Estrella, 2019; Pilon-Thomas et al., 2016). In human CD8+ T cells, both factors lead to an impairment cytolytic activity, reduced cytokine secretion and reduced expression of the T cell receptor (TCR) (Calcinotto et al., 2012). Acidic pH has been demonstrated to sequester interferon-gamma (INF-γ) mRNA and hence prevent the activation of T cells (Pilon-Thomas et al., 2016). Macrophages are also affected by acidosis - low pH is known to induce a switch from tumor-suppressive M1 phenotype to tumour-promoting M2 phenotype. In addition, acidosis induces expression of Arginase 1 in macrophages, causing arginine depletion in the microenvironment, and hence inhibition of T cell proliferation and activation (Damgaci et al., 2018; El-Kenawi et al., 2015).

Acidosis plays an important role in response to chemotherapy for several reasons. As discussed above, an acidic microenvironment can alter gene expression patterns in cancer cells. These changes can affect drug targets and lead to resistance. Acidosis can also impact SLC transporters, involved in drug uptake. This could happen as a result of changes in gene expression, but it could also be a result of transporter physiology - some transporters, like the SLC36 family of amino acid transporters, the SLC15 family of oligopeptide transporters and SLC16 family of monocarboxylate transporters, depend on a H^+-coupled transport mechanism to import their substrates, including drug molecules (Thwaites and Anderson, 2011). Lastly, acidic pH can have an impact on drug molecules themselves. Drugs have different charge states in different pH conditions, which can impact their activity and distribution (Kolosenko et al., 2017; Manallack et al., 2013). A drug screen has been conducted with the colorectal cell line HCT116, chronically adapted to pH 6.8, and the 1280 compounds from the Prestwick chemical library. The majority of compounds showed reduced efficacy in acidic pH, with only 11 compounds being more effective against

acid-adapted cells then they were against the parental cell line (Pellegrini et al., 2018).

Tumour acidosis has a profound effect on cell physiology, metabolism, tumour progression and response to therapy. Many of the driving mechanisms behind these changes are still unknown. Metabolically, acidosis has predominantly been studied in the context of hypoxia and glucose metabolism. It could however have an impact on a number of additional metabolic pathways in cancer cells. As part of the studies described within this thesis, we identified the creatine transport, SLC6A8, as being upregulated in tumours with an acidic microenvironment. As such, creatine metabolism is introduced in the next section.

1.3 Creatine metabolism

Creatine metabolism in cancer is still poorly characterised. Creatine and its analogue, cyclocreatine, have been reported to show some anti-cancer properties. A number of studies have interrogated the role of creatine, as well as the creatine transporter SLC6A8, in cancer progression, and have generated contradicting reports.

1.3.1 Creatine metabolism in healthy cells

The majority of creatine in the human body is located in the skeletal muscles, with only 10% distributed between the brain, blood and in lesser amount other tissues (Markus Wyss and Kaddurah-Daouk, 2000). Creatine synthesis is a two stage process, which takes place in the liver and kidneys. The first stage is completed in kidney cells, where guanidinoacetate is synthesised from glycine and L-arginine by the enzyme Glycine amidinotransferase (GATM). Guanidinoacetate is then exported into the circulation, by the monocarboxylate transporter SLC16A12 (MCT12) (Jomura et al., 2020). During the second stage of the process, hepatocytes in the liver internalise guanidinoacetate, suspectedly via SLC16A12 (MCT12) and SLC6A6 (Jomura et al., 2020; Tachikawa et al., 2012), and converted to creatine by the enzyme Guanidinoacetate N-methyltransferase (GAMT). Creatine is secreted into the blood

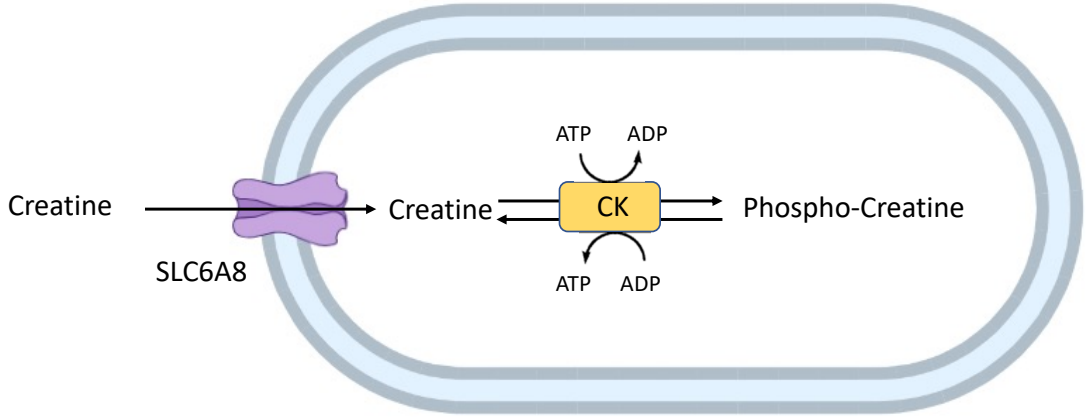


Figure 1.3: Creatine and energy storage - Creatine is internalised via the creatine transporter SLC6A8 and converter to phosphocreatine by the creatine kinase (CK)

stream and becomes available to other cell types. Suggested efflux transporters for this step are SLC16A9 (MCT9) (Futagi et al., 2020) and SLC16A12 (MCT12) (Jomura et al., 2021). Once in the blood stream, creatine can be internalised by other cell types via the creatine transporter SLC6A8 (CRT1) and can be used for intracellular energy storage, via formation of its phosphorylated form, phosphocreatine (Kazak and Cohen, 2020; Markus Wyss and Kaddurah-Daouk, 2000). Phosphocreatine can be used to regenerate ATP via transfer of the phosphate group to adenosine diphosphate (ADP) (Kazak and Cohen, 2020; Markus Wyss and Kaddurah-Daouk, 2000) (Figure 1.3).

Alternatively, creatine can be non-enzymatically converted to creatinine - a byproduct, which is considered inert and is later excreted in the urine. In humans, it has been estimated that 2% of the total creatine pool is converted to creatinine daily (Markus Wyss and Kaddurah-Daouk, 2000). There is evidence that some additional cell types are capable of creatine synthesis, including adipocytes (Maguire et al., 2021), skeletal muscle cells (A. P. Russell et al., 2014), and cancerous epithelial cells (Liwen Zhang, Zhu, et al., 2021).

Creatine and phosphocreatine are continuously converted to one another in a chemical reaction catalysed by creatine kinase (CK). Five isoforms of creatine kinase have been characterised in mammalian cells - CKM (creatine kinase muscle type), CKB (creatine kinase brain type), CKMB (creatine kinase heart type), CKMT1A and CKMT1B (creatine kinase mitochondrial type A and B).

The role of the creatine system in active muscle metabolism was studied extensively in the 1980s. Although the main function of creatine is energy storage, the system has a number of other benefits on molecular level, helping to maintain the function of muscle cells during exercise. The creatine system is considered a 'spatial energy buffer' or an 'energy transport system'. Phospho-creatine can act as an 'energy carrier', transporting ATP from subcellular sites of energy production, like glycolysis and OXPHOS, to cell compartments where ATP is utilised, for example by ATPases (Bessman and Carpenter, 1985; Jacobus, 1985; RONALD A Meyer, 1988; Ronald A Meyer, Sweeney, and Kushmerick, 1984; Ventura-Clapier et al., 1987; Theo Wallimann and Eppenberger, 1985; Theo Wallimann, Malus Wyss, et al., 1992).

The creatine system is also involved in proton buffering, and hence maintaining intracellular pH, in active muscle. As CK converts phosphocreatine to creatine, the reaction utilises ADP and H^+, preventing the buildup of H^+, and hence preventing the acidification of the intracellular space (Theo Wallimann, Malus Wyss, et al., 1992). Between 5-10% of cytosolic CK in muscle is functionally coupled to Mg^{2+}-ATPase (Schäfer and Perriard, 1988; D. C. Turner, Theo Wallimann, and Eppenberger, 1973). As both ADP and H^+ are products of ATP hydrolysis, the coupling allows muscle cells, especially during severe exercise, to break down large amounts of ATP in short periods of time, without local or global acidification of the intracellular space (Figure 1.4). The drop in intracellular pH observed in muscle cells during exercise (to pH 6.7) has been shown to activate CKM by 50%, in the direction of ATP regeneration (The Wallimann, Schlösser, and Eppenberger, 1984). By regenerating ATP, CK maintains a high ATP/ADP ratio in the vicinity of ATPases, which has been demonstrated to increase the thermodynamic efficiency of ATP hydrolysis (Kammermeier, 1987; Theo Wallimann, Malus Wyss, et al., 1992). At the same time CK controls intracellular levels of ADP, preventing ATPases inhibition by free ADP (Melkote R Iyengar, Fluellen, and C. Iyengar, 1982; Melkote Raja Iyengar, 1984).

The creatine system also has an indirect regulatory effect on metabolic pathways in muscle. Phospho-creatine is the major source of inorganic phosphate (P_i), released during muscle contraction. P_i is needed for the activation of both glycogenolysis

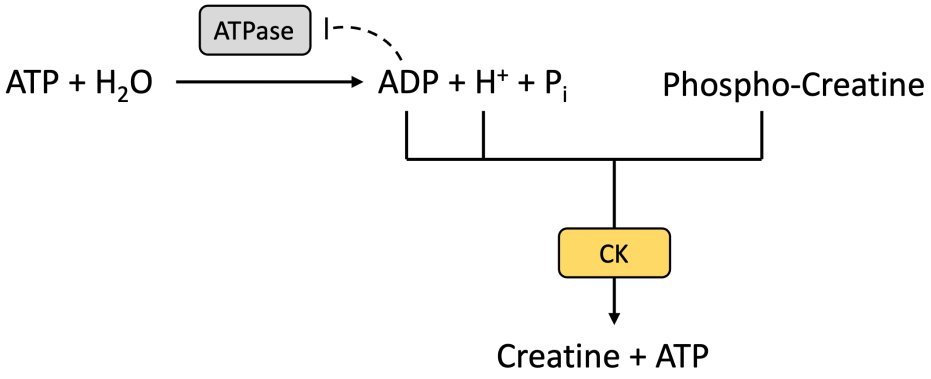


Figure 1.4: Creatine and proton buffering - As phosphocreatine is converted to creatine, an H^+ is utilised. This helps to maintain intracellular pH during exercise induces metabolic acidosis in muscle. Figure adapted from Theo Wallimann, Malus Wyss, et al. (1992).

and glycolysis. In fact, in the absence of phospho-creatine, P_i becomes limiting for glycogenolysis in muscle (Davuluri, Hird, and McLean, 1981; RONALD A Meyer et al., 1986).

There is evidence of functional coupling between CK and glycolytic enzymes. In muscle tissue, glycolytic enzymes form a glycolytic complex, localised to isotropic bands (I-bands) - bands of actin-containing thin filaments in skeletal muscles (Arnold and Pette, 1970; Bronstein and H. Knull, 1981). Interestingly, CKM is also predominantly localised to the I-bands (Wallimann et al., 1989; Wegmann et al., 1992). In addition, the amount of muscle CK correlates with the glycolytic potential of a muscle (The Wallimann, Schlösser, and Eppenberger, 1984; Theo Wallimann, Malus Wyss, et al., 1992). It has been shown that ATP, produced by glycolysis in fast twitching muscle is not accumulated, but is instead immediately incorporated in phospho-creatine. This was shown by both studies with a reconstituted glycolytic system of muscle *in vitro* (Scopes, 1973), and animal models with defective muscle glycolysis (Brumback, Gerst, and Harvey R Knull, 1983). The immediate utilisation of ATP is needed in active muscle, as free ATP would inhibit glycolysis. Interestingly, this mechanism is only observed in anaerobic glycolysis, and is suppressed in normoxic conditions (Kupriyanov et al., 1980). Further evidence for the spacial coupling of CK and glycolytic enzymes was given by Dillon and Clark (1990), who demonstrated *in vitro* coupling of CK with pyruvate kinase - the enzyme that

catalyses the conversion of phosphoenolpyruvate (PEP) to pyruvate and ATP in glycolysis. In addition, Kraft et al. (2000) demonstrated a coupling of CK with another glycolytic enzyme - phosphofructokinase (PFK) *in situ*. PFK phosphorylates Fructose-6-phosphate, and is negatively regulated by ATP (Figure 1.5). The coupling of these enzymes with CK allows immediate utilisation of ATP and prevents the negative regulation of glycolysis Kraft et al. (2000) and Theo Wallimann, Tokarska-Schlattner, and Schlattner (2011) .

High energy consumption, high glycolytic rates and buildup of H^+ intracellularly are not only typical for healthy muscle cells, but also for cancer cells (see Section 1.2.2). This makes creatine metabolism interesting in the context of cancer biology.

1.3.2 Creatine metabolism in cancer

A number of studies, conducted in rodents, suggested both creatine and its analogue, cyclocreatine, had anti-tumour activity. It has been hypothesised that cyclocreatine leads to energy deprivation in cancer cells. Cyclocreatine can be phosphorylated by CK, to form phospho-cyclocreatine. This phosphorylated form can not undergo the reverse reaction to release ATP, and hence ATP becomes 'trapped' and unavailable (Liwen Zhang and Bu, 2022). This is consistent with the fact that anti-tumour activity of cyclocreatine is higher in tumours with high expression of creatine kinase, as reported by several studies in the 1990s (Hoosein et al., 1995; Martin et al., 1996; Teicher et al., 1995).

Another hypothesis is that build up of the phosphorylated form of cyclocreatine is toxic for cancer cells (Schiffenbauer et al., 1996). Although the mechanism of action remains unclear, cyclocreatine was demonstrated to have anti-cancer properties in a number of cell lines. Schiffenbauer et al. (ibid.) demonstrated that cyclocreatine inhibits proliferation of cancer cells *in vitro* and tumour growth *in vitro* in the C6 rat glioma cells and OC238 human ovarian carcinoma cells. In pre-clinical studies, cyclocreatine in combination with cis-platin, melphalan, 4-hydroperoxycyclophosphamide, or carmustine has shown greater than additive affect against the small cell lung carcinoma cell line SW2 (Teicher et al., 1995). Cyclocreatine in combination with the anti-tumour antibiotic Adriamycin also has a synergetic effect against the prostate

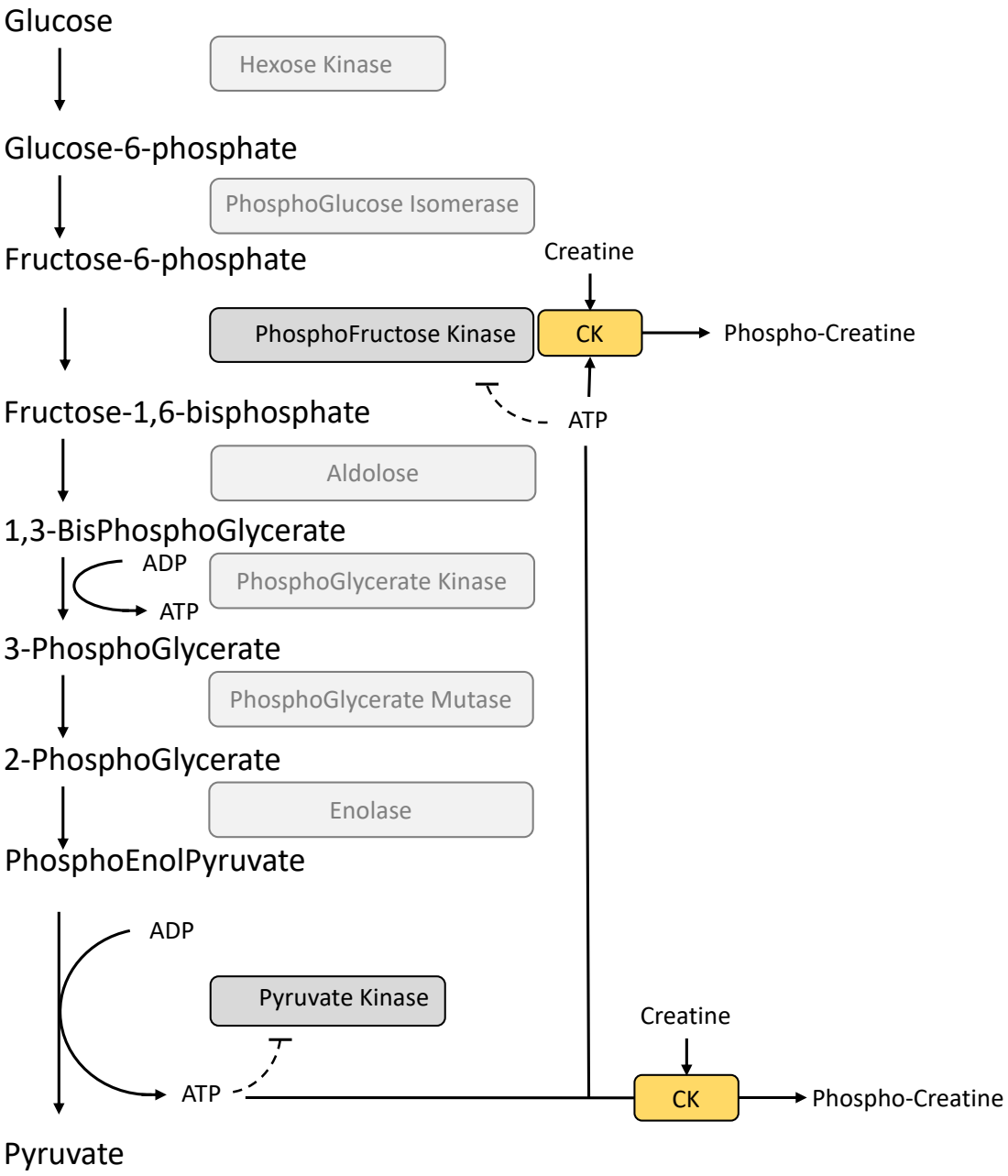


Figure 1.5: Creatine and glycolysis - As creatine is converted to phospho-creatine, ATP is utilised. The coupling of creatine kinase (CK) with glycolytic enzymes prevents the negative regulation of glycolysis by ATP.

cell line LNCaP, both in cell culture and mouse xenografts (Hoosein et al., 1995). At the same time, cyclocreatine does not inhibit the growth of healthy brain, cardiac or skeletal muscle cells in cell culture, despite high expression of CKB in these tissues (Martin et al., 1996). This would suggest differences in creatine metabolism between tumour cells and healthy tissue.

In addition, some studies have suggested that creatine itself has anti-cancer effects. One proposed mechanism is by affecting cells of the immune system, in particular T cells. Tumour infiltrating CD8+ T cells were demonstrated to upregulate the creatine transporter SLC6A8 in mice. In addition, knockdown of SLC6A8 significantly impaired anti-tumour T cell activity. The same study demonstrated that creatine supplementation suppresses tumour growth in melanoma in mouse models (Di Biase et al., 2019).

A study in rats by Campos-Ferraz and colleagues examined the effect of creatine on subcutaneous tumours. They reported a 30% reduction in tumour growth after administration of 300 mg/kg of creatine for 40 days, compared to a placebo cohort, although there was no significant difference in survival rates. The study also reported increased creatine content in the tumour and increased cytoplasmic activity of CK following creatine treatment. Interestingly, higher intracellular bicarbonate was observed in the control group compared to creatine-treated cohort (Campos-Ferraz et al., 2016). This suggests a potential dysregulation of intracellular pH caused by creatine supplementation. In consistence with this, another study reported acidic intracellular pH (pH 6.9 - pH 7.0) in tumour cells following dietary supplementation with either creatine or cyclocreatine for 2 weeks. The work was conducted in mice carrying human colon adenocarcinoma (LS174T) (Kristensen et al., 1999). The authors hypothesise the decrease in pH could be due to inhibition of oxidative phosphorylation and subsequent build up of lactate. However, high intracellular lactate concentration was not detected, so the mechanism remains unclear.

Zhang and colleagues recently demonstrated both dietary and de-novo synthesised creatine to promote colorectal and breast cancer metastasis in mice. Although creatine either suppressed or didn't affect primary tumours, it promoted metastasis of colorectal cancer to the liver. Similar results were observed with 4T1 cell-derived

breast cancer. Creatine treatment inhibited primary tumour growth, but enabled metastasis to the lung. Further, metastatic cells in the liver showed upregulation of GATM, suggesting de novo creatine synthesis (Liwen Zhang, Zhu, et al., 2021). In metastatic colon cancer, inhibition of CKB by either miRNA or small molecule inhibitors significantly suppressed liver colonisation in mouse models. The study also reports upregulation of the creatine transporter SLC6A8 in metastatic cells compared to primary colon tumours, and suggests the hypothesis that creatine, naturally synthesised in the liver, can be utilised by metastatic cells to renew intracellular ATP (Loo et al., 2015). In obesity-accelerated breast cancer, creatine was identified as a facilitating factor for tumour growth. Creatine synthesis by tumour-associated adipocytes was shown to drive tumour progression. Deletion of GATM in adipocytes or the creatine transporter SLC6A8 in tumour cells both significantly impaired tumour progression in a mouse model (Maguire et al., 2021).

Some components of the creatine system have been used as biomarkers in cancer. In hepatocellular carcinoma (HCC), an increased level of creatine has been reported in urine, and in fact has been correlated with the clinical stage of the cancer Ladep et al., 2014. Expression of CKB and CKMB is associated with poor prognosis in lung cancer (L. Liu et al., 2017), and expression of CKMT is associated with poor prognosis in lung, breast and gastric cancers (Cimino et al., 2008; Kurmi et al., 2018; Liwen Zhang and Bu, 2022).

Interestingly, recent work has also linked the expression of CKB in cancer cells to ferroptosis - a form of non-apoptotic cell death. Ferroptosis (also known as oxytosis) is dependent on iron, and is caused by uncontrolled lipid peroxidation. There is hope that ferroptosis could be explored therapeutically in drug-resistant cancer cells. Normally, ferroptosis is prevented by lipophilic antioxidants and iron chelators (Tan, Schubert, and Maher, 2001), and mostly by Glutathione Peroxidase 4 (GPX4) (Mishima and Conrad, 2023). Recent work demonstrated that CKB can phosphorylate GPX4, making it resistant to degradation by chaperone-mediated autophagy. Increased protein levels of GPX4 make cancer cells more resistant to ferroptosis (ibid.). This function of CKB is believed to be independent of its role in creatine metabolism, and reveals another axis of CKB involvement in cancer

progression.

Together, these findings suggest creatine metabolism plays a role in the metabolic rewiring of cancer cells, however, the exact mechanisms, as well as any links between acidic microenvironment and creatine metabolism, are still unclear.

1.3.3 The Creatine transporter SLC6A8 in cancer

SLC6A8 (CRT1) is known to be the main importer of creatine in mammalian cells. Substrate binding of SLC6A8 was extensively characterised by a couple of recent studies (Colas et al., 2020; Farr et al., 2022). It has been established that each SLC6A8 protein transports 15 creatine molecules per second across the plasma membrane, and has an EC_{50} of approximately 35 μM. The transporter activity is affected by both Na^+ and Cl^-, with each cycle of the transporter moving one creatine molecule, 2 Na^+ and one Cl^- (Farr et al., 2022). SLC6A8 is strictly an uptake transporter, while the monocarboxylate transporter SLC16A12 (MCT12) (Abplanalp et al., 2013; Farr et al., 2022), and potentially SLC6A6 (Jomura et al., 2020; Tachikawa et al., 2012) act as efflux transporters for creatine.

A model for the function of SLC6A8 in metastatic cancer cells was suggested by Loo and colleagues in 2015. Their work focused on colorectal adenocarcinoma metastasis to the liver. The proposed mode of action for the creatine system in this context was that extracellular ATP and extracellular creatine, synthesised by hepatocytes in the liver, are utilised to generate phospho-creatine extracellularly. This is achieved by synthesis of an extracellular soluble form of CKB by metastatic cancer cells, and subsequent internalisation of phospho-creatine via SLC6A8 (Loo et al., 2015). This work was the foundation for development of a anti-neoplastic agent, targeting SLC6A8 - the small molecule compound RGX-202. RGX-202 inhibits SLC6A8 and was demonstrated to suppress tumour growth in KRAS wild type and KRAS mutant xenografts, as well as patient-derived xenografts in mice. RGX-202 was used in phase 1 clinical trials for metastatic colorectal cancer and was demonstrated to perturbed creatine metabolism in patients. The liver is the most common metastatic site for colorectal cancer, and treatment for liver metastasis often includes 5-fluorouracil-containing chemotherapy. Combining RGX-202 with 5-fluorouracil also resulted in

inhibition of tumour growth, in xenografts from different mutational backgrounds (Kurth et al., 2021).

SLC6A8 knockdown has been demonstrated to induced apoptosis and suppressed migration in the hepatocellular carcinoma cell lines Hep3B and Huh7 (Yuan et al., 2020), and non-small cell lung cancer cell lines H1299 and H520 (Feng, Guo, and H. Tang, 2021).

As with the rest of the creatine system components, SLC6A8 is likely to be involved in cancer progression in a cancer type-specific manner, potentially by more than one mechanism of action, with further research required to achieve a mechanistic understanding of its role.

1.4 Hypothesis and project aims

We hypothesised that tumour transporter signatures change in response to tumour acidosis; not only transporters required to maintain base-acid balance, but also transporter genes that enable adaptive metabolic shifts in cancer cells. Acidosis is usually studied as a result of or in the context of hypoxia, however here we aim to characterise the effect acidosis alone can have on SLC signatures in solid tumours. The aims of this project are: 1. To identify acidosis-associated changes in SLC signatures across cancer types 2. To model these changes *in vitro* 3. To characterise the role of individual SLC transporters involved in cellular adaptation to a more acidic tumour microenvironment

Chapter 2

Methods

2.1 Computational methods

2.1.1 SLC family tree

A list of the SLC superfamily members was obtained from the HGNC website (https://www.genenames.org/data/genegroup/#!/group/752). As of December 2022, the superfamily contains 433 SLC transporters. HGNC IDs were converted to Uniprot IDs on the uniprot website (https://www.uniprot.org/uploadlists/). Four HGNC IDs were filtered out during the process, as they did not correspond to a Uniprot ID (HGNC:11043 - SLC6A10P, HGNC:31400 - SLC6A21P, HGNC:32724 - SLC7A15P and HGNC:20602 - SLC23A4P). Reviewed sequences only were downloaded as a FASTA file and aligned using ClustalW in the msa package (Bodenhofer et al., 2015) with default settings using R v4.1.2 (R Core Team, 2013) in RStudio 2022.07.2 (RStudio Team, 2020). The alignment was converted to a tree and visualised using the packages ape (Paradis and Schliep, 2019) and ggtree (G. Yu, D. Smith, et al., 2017).

2.1.2 TCGA data download

Bulk RNAseq data and metadata for 12 cancer types were downloaded from the The Cancer Genome Atlas (TCGA) database (https://www.cancer.gov/tcga) using R package TCGAbiolinks (Colaprico et al., 2015). For this work, the GRCh38 (hg38) version was used, also known as 'Harmonised' TCGA data. UUIDs and barcodes were cross-referenced using the TCGAutils package (Ramos, Schiffer, and Waldron, 2022). Downstream processing and normalisation were done with packages edgeR (Robinson, McCarthy, and Smyth, 2010) and Limma (Charity W. Law et al., 2016; Ritchie et al., 2015) and the Voom method (Charity W Law et al., 2014). The Voom-normalised reads matrix was used for all subsequent analysis.

2.1.3 tSNE

Non-supervised clustering based on SLC expression was performed using the t-distributed stochastic neighbour embedding method (tSNE) in package Rtsne (Krijthe, 2015). Expression of SLC genes was extracted from the Voom-normalised

matrix generated above. tSNE was run with the following parameters: PCA = FALSE, perplexity = 30, max_iterations = 5000, dimensions = 2 and theta = 0.2. The tSNE plot was visualised with package ggplot2 (Wickham, 2016).

2.1.4 TCGA differential gene expression analysis

As there is no direct readout for tumour acidity in the TCGA dataset, the expression of 3 gene sets were identified as proxies for acidity to enable stratification of clinical samples. 'Rate limiting genes in glycolysis' had been identified by Tanner et al. (2018) and are listed in Table 2.1. A list of 10 genes, identified as enriched in lactic acidosis, but not hypoxia, by J. L.-Y. Chen et al. (2008) are listed in Table 2.2. The original study identified a total of 1585 genes, upregulated in acidosis, but only the top 10 of them were used in this analysis. Lastly, extracellular carbonic anhydrases, which are known to acidify the extracellular space, are listed in Table 2.3. To identify hypoxic samples, the genes from GSEA Hallmark Hypoxia were used (`https://www.gsea-msigdb.org/gsea/msigdb/cards/HALLMARK_HYPOXIA.html`). Voom-normalised count matrixes were generated per cancer type (see Section 2.1.2). For each of the 4 gene sets, the analysis was done independently. Median expression was calculated for each clinical sample for each gene set. Samples with highest median expression (top 10%) within a cancer type were considered to be from an acidic microenvironment (or hypoxic, in the case of Hallmark Hypoxia). These were compared to samples with lowest median expression (bottom 10%) in the same cancer type. Differentially expressed genes were identified using the TREAT method (T-tests RElavite to A Threshold) in Limma (Charity W. Law et al., 2016; Ritchie et al., 2015). Differentially expressed SLC genes were then extracted from the full list of differentially expressed genes.

2.1.5 Kaplan-Meier graphs

Clinical data for Kaplan-Meier plots was obtained with the R package RTCGA (Kosinski and Biecek, 2021). Survival probability was calculated using the Kaplan-Meier method (Jager et al., 2008). Optimal cut point for High and Low categories was determined using the maximally selected rank statistic in the R package

Table 2.1: Rate limiting genes in glycolysis (Tanner et al., 2018)

Ensembl ID	Gene Symbol	Gene name
ENSG00000106633	GCK	Glucokinase (hexokinase 4)
ENSG00000156515	HK1	Hexokinase 1
ENSG00000159399	HK2	Hexokinase 2
ENSG00000160883	HK3	Hexokinase 3 (white cell)
ENSG00000141959	PFKL	Phosphofructokinase, liver
ENSG00000152556	PFKM	Phosphofructokinase, muscle
ENSG00000067057	PFKP	Phosphofructokinase, platelet
ENSG00000141526	SLC16A3	Monocarboxylate transporter 4
ENSG00000117394	SLC2A1	GLUT1/ glucose transporter 1
ENSG00000059804	SLC2A3	GLUT3/ glucose transporter 3

Table 2.2: Genes upregulated in lactic acidosis (J. L.-Y. Chen et al., 2008)

Ensembl ID	Gene Symbol	Gene name
ENSG00000136240	KDELR2	Endoplasmic Reticulum Protein Retention Receptor 2
ENSG00000130175	PRKCSH	Protein Kinase C Substrate 80K-H
ENSG00000087460	GNAS	Guanine Nucleotide Binding Protein
ENSG00000103769	RAB11A	Ras-Related Protein Rab-11A
ENSG00000204592	HLA-E	Major histocompatibility complex 1
ENSG00000105438	KDELR1	Endoplasmic Reticulum Protein Retention Receptor 1
ENSG00000120742	SERP1	Stress Associated Endoplasmic Reticulum Protein 1
ENSG00000010278	CD9	Cell Growth-Inhibiting Gene 2 Protein
ENSG00000138796	HADHSC	Hydroxyacyl-CoA Dehydrogenase
ENSG00000167468	GPX4	Glutathione Peroxidase 4

Table 2.3: Extracellular Carbonic anhydrases

Ensembl ID	Gene Symbol	Gene name
ENSG00000167434	CAIV	Carbonic anhydrase 4
ENSG00000107159	CAIX	Carbonic anhydrase 9
ENSG00000074410	CAXII	Carbonic anhydrase 12
ENSG00000118298	CAXIV	Carbonic anhydrase 14

Survminer (Kassambara et al., 2021).

2.1.6 In-house RNAseq data processing and analysis

Paired-end RNAseq with 60 base pair read length was done at the MRC-LMS sequencing facility. Quality control was done with the python package FastQC (Andrews, 2010). The 2013 assembly of the human genome (GRCh38) and a GTF annotation file were downloaded from UCSC (https://hgdownload.soe.ucsc.edu/goldenPath/hg38/bigZips/). Paired-end reads were aligned to UCSC GRCh38 and gene counting was performed using STAR (Dobin et al., 2013). MultiQC (Ewels et al., 2016) was applied for generating a summary report for FastQC and STAR alignment results. Data normalisation and differential expression analysis were done in the R package DESeq2 (Love, W. Huber, and Anders, 2014). Differentially expressed genes were considered any genes with adjusted p value (false discovery rate) of 0.05 or lower. No Log_2(Fold Change) cutoffs were applied.

2.1.7 *In vitro* acidosis signatures

To assign sample scores for LUAD *In vitro* Acidosis Signature (LIVAS), COAD *In vitro* Acidosis Signature (CIVAS) and Hallmark hypoxia (https://www.gsea-msigdb.org/gsea/msigdb/cards/HALLMARK_HYPOXIA.html), the R package singscore (Foroutan et al., 2018) was used. Scores were generated for individual samples in the TCGA LUAD and TCGA COAD cohorts. For CIVAS and Hypoxia, the genes provided in the gene lists are upregulated in acidosis and hypoxia respectively. In these cases, high singscore corresponds to highly acidic or highly hypoxic samples. In LIVAS however, genes in the gene list are downregulated in acidosis. For this reason, scores were arbitrarely used with a negative sign, so that high LIVAS score also corresponds to highly acidic samples.

2.1.8 Single cell RNAseq

Single cell data was accessed via the NCBI Gene Expression Omnibus database with accession code GSE131907 for N. Kim et al. (2020). Data was processed in R package Seurat (A. Butler et al., 2018; Y. Hao et al., 2021; Satija et al., 2015; T. Stuart et

al., 2019). Acidosis and hypoxia scores were assigned using the AddModuleScore function in Seurat. UMAP was run with the following parameters: FindNeighbours reduction = pca, dims = 1:10, FindClusters resolution = 0.5. Gene expression patterns in individual clusters were characterised using the packages ReactomePA (G. Yu and Q.-Y. He, 2016), clusterProfiler (T. Wu et al., 2021; G. Yu, L.-G. Wang, Y. Han, et al., 2012), enrichplot (G. Yu, 2022) and DOSE (G. Yu, L.-G. Wang, G.-R. Yan, et al., 2015).

2.1.9 Blood vessel proximity data

RNAseq data from Kumar et al. (2019) was accessed via the ArrayExpress database at EMBL-EBI under accession numbers E-MTAB-6881 and E-MTAB-6882. Ensembl IDs were converted to gene names with package biomaRt (Durinck et al., 2005). Differentially expressed (DE) genes were identified using DESeq2 (Love, W. Huber, and Anders, 2014) and SLC genes were extracted from the full list of DE genes.

2.1.10 CCLE data download

Gene expression data and metadata for cancer cell lines was downloaded from the Cancer Cell Line Encyclopedia (CCLE) database (`https://sites.broadinstitute.org/ccle/`) in June 2020. Expression data was readily available as normalised Log_2(Transcripts Per Million) and was not processed any further.

2.2 Cell culture methods

2.2.1 Cell lines

All cell lines were acquired from the American Type Culture Collection (ATCC). Unless stated otherwise, cell lines were maintained in RPMI (Gibco 12633-012) supplemented with 10% Fetal calf serum (FCS) (Sigma F7524-500ML), 2 mM L-Glutamine (Gibco 25030-081), 100 units/mL Penicillin and 50 µg/mL Streptomycin (Gibco Penicillin/Streptomycin 15140-122), at 37 °C, 5% CO_2. To split, cells were washed with Gibco dPBS (Fished Scientific 12037539) and detached with TripLE

Express (Thermo Fisher 12604013), before resuspending in fresh media at the appropriate density and seeding in new plates.

2.2.2 pH adjustment of culture media

RPMI media was buffered with either sodium bicarbonate ($NaCO_3$) or a combination of HEPES and PIPES. $NaCO_3$-buffered media was prepared from powder (Gibco 51800035) by adding 24 mM $NaCO_3$ (Sigma S8761-100ML) for pH 7.4 and 6.15 mM $NaCO_3$ for pH 6.8. HEPES/PIPES buffered media was prepared from liquid RPMI (Gibco 12633-012) by adding both HEPES (Gibco 15630-057) and PIPES (Bioworld 41620042-1) to a final concentration of 25 mM, with the addition of either 1 mL 5N NaOH (for pH 7.4) or 760 µL 37% HCl (for pH 6.8) per 500 mL of media. pH adjusted media was filter-sterilised using the Stericup system (Merck S2GPU05RE). All media was supplemented with 10% FCS (Sigma F7524-500ML), 2 mM L-Glutamine (Gibco 25030-081), 100 units/mL Penicillin and 50 µg/mL Streptomycin (Gibco Penicillin/Streptomycin 15140-122).

2.2.3 Serum dialysis

When indicated, serum was dialysed to remove small molecule metabolites and ensure a defined medium. FCS (Sigma F7524-500ML) was dialysed by placing 100 mL FCS in a 3500 Dalton molecular weight cut off (MWCO) dialysis tubing (Fisher Scientific 132724). The tubing was incubated in a beaker with 5 L PBS at 4 °C for approximately 8 hours. The tubing was then transferred to fresh 5 L of PBS and incubated at 4 °C overnight, to achieve a cumulative dilution of any <3500 Da molecules of 2500 fold. The serum was filter-sterilised with the Steriflip system (Merck SCGP00525) and stored at -20 °C until it was supplemented into culture media.

2.2.4 Physiological media

To create more physiologically-relevant conditions, fixed composition Human Plasma-Like Media (HPLM) (Fisher Scientific 17100059) was used instead of RPMI. HPLM

Table 2.4: Seeding density for Incucyte experiments in 96 well plates

Cell line	Cells per well
A549	5000
NCI-H1299	4000
NCI-H661	5000
HCT116	6000
RKO	5000
SW48	7000

was donated to us by Jason Cantor (Cantor et al., 2017). Before use, HPLM was supplemented with 10% dialysed serum (see Section 2.2.3).

2.2.5 Growth curves

All growth curves were obtained using an Incucyte Zoom in a 96 well format. Cells were seeded in 200 µL RPMI-1460 (Gibco 12633-012) supplemented with 10% FCS (Sigma F7524-500ML), 2 mM L-Glutamine (Gibco 25030-081), 100 units/mL Penicillin and 50 µg/mL Streptomycin (Gibco Penicillin/Streptomycin 15140-122). Cells were seeded at the appropriate cell density (cell line-dependent), in triplicate Table 2.4. After 24 hours, media was removed using an aspirator and replaced with 100 µL experimental media, as indicated in figure legends. Cells were imaged at 2 hour intervals. Growth curves were plotted in GraphPad Prism version 9 (GraphPad Software, San Diego, California USA, `www.graphpad.com`). For glutamine-free media experiments, RPMI-1460 (Gibco 12633-012) without added L-Glutamine was used. For glucose-free media experiments, RPMI-1640 (Gibco 11560-406) was used. For creatine-supplemented media, creatine powder (SLS C0780) was freshly prepared as a 100 mM stock solution in water, and diluted in media to a final concentration of 100 µM.

2.2.6 Hypoxia

Hypoxia experiments were done at 37 °C, 1% oxygen, 5% CO_2. Plasticware and media were equilibrated in the hypoxia chamber overnight prior to experiments, to avoid introducing additional oxygen. Cells were seeded in triplicate in 200 µL RPMI-1460 (Gibco 12633-012) at suitable density (see Table 2.4) and allowed to

attach for 12 hours in normoxic conditions. Experimental media was prepared, then split in two bottles, one of which was equilibrated in the hypoxia chamber and the other maintained in a normoxic 37 °C 5% CO_2 incubator overnight. Media was then aspirated from the 96 well plates and replaced with 100 µL experimental media. Plates incubated inside the hypoxia chamber were covered in foil to avoid exposure to light. Control plates were incubated in a 37 °C 5% CO_2 incubator. After 48 hours, an SRB assay was done.

2.2.7 Cell mass accumulation (SRB assays)

Cells were seeded in a 96 well format and exposed to experimental conditions in 100 µl of media. After 48 hours, plates were fixed with 50 µL 50% Trichloroacetic acid (TCA) per well and incubated at 4 °C for 1 hour. Plates were washed in running tab water and allowed to dry, before being stained with 100 µL of 0.4% SRB solution per well at room temperature for 30 minutes. The stain was washed four times with 1% acetic acid. When the wells had dried out, 200 µL of 10 mM Tris base was added to each well and the plates were incubated on an orbital shaker at room temperature for 30 minutes. Optical density was measured at 565 nm in a microplate reader. All solutions are detailed in Table 2.5.

2.2.8 RNAseq sample preparation

Cells were seeded in 6 well plates at the appropriate density, in triplicate, in RPMI-1460 (Gibco 12633-012) (Table 2.6). Cells were allowed to attach overnight and the following morning, the media was replaced with HEPES/PIPES supplemented RPMI, adjusted to either pH 7.4 or pH 6.8. At the appropriate time-point, RNA extraction was done using RNeasy purification kit (Qiagen 74106) according to manufacturer's instructions. Cells were scraped directly in lysis buffer (RLT) provided in the kit, using a cell lifter (Corning 3008). RNA quantity was measured on Nanodrop and the quality was assessed on Bioanalyser. RNA samples with RNA integrity number (RIN) >7 were submitted to the MRC-LMS sequencing facility for library building. RNA-Seq libraries were prepared using the NEBNext Ultra II Directional RNA Library Prep Kit with NEBNext Poly(A) mRNA Magnetic Isolation Mod-

Table 2.5: Buffers and solutions

Name	Constituents
1% Acetic acid	1% (vol/vol) acetic acid in water
0.4% SRB	0.4% sulforhodamine B (SRB) in 1% acetic acid
Laemmli buffer	1M Tris, 10% SDS, 10%Glycerol, 5% β-mercaptoethanol, 0.0002% bromophenol blue
TBS	50 mM Tris, 150 mM NaCl
Protein running buffer	2.5 mM Trizma Base, 0.2 M glycine, 0.01% SDS
Protein transfer buffer	20% methanol, 2.5 mM Trizma base, 0.2 M glycine
Blocking Solution	0.05% NaN_3, 5% Bovine Serum albumin, 200 mM PBS-0.05% Tween-20
TAE buffer	40 mM Trizma base pH 8.3, 0.1% acetic acid, 1.3 mM EDTA 0.005% SDS
PBS	137 mM NaCl, 2.7 mM KCl, 8 mM Na_2HPO_4, 1.5 mM KH_2PO_4
LB broth	1% bactotryptone, 0.5% yeast extract, 170 mM NaCl, 36 mM K_2HPO_4, 13 mM KH_2PO_4, 1.7 mM sodium citrate, 0.4 mM $MgSO_4$, 6.8 mM $(NH_4)_2SO_4$
Nigericin buffer	140 mM KCl, 1 mM $MgCl_2$, 10 mM HEPES, 10 mM PIPES, 10 µM nigericin
Tyrode's buffer	140 mM NaCl, 4.5 mM KCl, 1 mM $MgCl_2$, 11 mM Glucose, 20 mM HEPES, 2.5 mM chCaCl2

Table 2.6: Seeding density for RNAseq in 6 well plates

Cell line	Cells per well
A549 8 hours	200000
NCI-H1299 8 hours	150000
NCI-H661 8 hours	150000
HCT116 8 hours	350000
RKO 8 hours	350000
SW48 8 hours	600000
A549 24 hours	100000
NCI-H1299 24 hours	100000
NCI-H661 24 hours	100000
HCT116 24 hours	200000
RKO 24 hours	250000
SW48 24 hours	600000

ule following manufacturer's instructions. Library quality was evaluated using the Agilent 2100 High-Sensitivity DNA assay, and their concentrations measured using the Qubit dsDNA HS Assay Kit. Libraries were pooled in equimolar quantities and sequenced on a NextSeq 2000.

2.2.9 ATP assay

CellTiter-Glo assay (Promega G7570) was used to measure intracellular ATP levels. RPMI-1460 (Gibco 12633-012) was supplemented with 10% dialysed FCS, to control the amount of creatine available to the cells (see Section 2.2.3). Cells were seeded in white wall 96 well plates (Fisher Scientific 10517742), at 30000 cells per well, and allowed to attach overnight. Experimental media was prepared as HEPES/PIPES supplemented RPMI at pH 7.4 and pH 6.8, with or without 100 µM creatine. The following day, media in each 96 well plate was changed to experimental media at the indicated times. At the end of the time course, the two kit reagents (CellTiter-Glo biffer and substrate) were mixed and 50 µL of the mixture were added to each well. Luminescence was measured using a FluostarOmega plate reader. Data was analysed in Microsoft Excel (Microsoft Corporation, 2018) and plotted in GraphPad Prism.

2.2.10 Intracellular pH assay

Intracellular pH was measured using a 5-(and-6)-Carboxy SNARF (cSNARF)-based method adapted from Buckler and Vaughan-Jones (1990). Cells were seeded in black wall 96 well plates (Perkin Elmer LAS 6055300), at 30000 cells per well, and allowed to attach overnight. 10 mM cSNARF (Thermo fisher C1272) stocks were made in DMSO (Thermo Fisher 85190). cSNARF was then supplemented in Tyrode's buffer to a final concentration of 10 µM. Media was aspirated from the 96 well plates and replaced by cSNARF-containing Tyrode's buffer. Plates were incubated at room temperature for 30 minutes while wrapped in foil to protect them from light. Plates were washed once with Tyrode's buffer (without cSNARF) before adding 100 µL Tyrode's buffer (without cSNARF) at either pH 7.4 or pH 6.8. cSNARF was read at two fluorescent wavelengths on FluostarOmega plate reader - (1) excitation = 544 nm, emissions = 590 nm, and (2) excitation = 655 nm, emissions = 50 nm. Intracellular pH was determined relative to a calibration curve for each cell line.

To generate calibration curves, Nigericin buffer was adjusted to each of the following pHs: 6.25, 6.5, 7, 7.25, 7.5, 7.75. Each cell line was seeded in black wall 96 well plates (Perkin Elmer LAS 6055300), at 30000 cells per well, and allowed to attach overnight. On the following day, media was aspirated and replaced by cSNARF-containing Tyrode's buffer. Plates were incubated at room temperature for 30 minutes while wrapped in foil. Plates were washed once with Tyrode's buffer (without cSNARF) before adding 100 µL Nigericin buffer. Nigericin is a K^+/H^+ ionophore and therefore enables equilibration of intracellular pH with the external buffer solution. cSNARF fluorescence was read as before. Data was analysed in Microsoft Excel and plotted in GraphPad Prism. Buffers are detailed in Table 2.5.

2.3 Molecular biology methods

2.3.1 shRNAs

shRNAs for the silencing of SLC6A8 were received as agar stabs of *E. coli* transformed with the shRNAs in pGIPZ vector (Zeocin resistance 25 µg/mL, Ampicillin resistance 100 µg/mL). For each shRNA, bacteria were streaked out on LB agar

supplemented with 25 µg/mL Zeocin (Fisher Scientific R25001) and 50 µg/mL Carbenicillin (Fisher Bioreagents 10396833). Plates were incubated overnight at 37 °C and a single colony was inoculated in LB broth (25 µg/mL Zeocin, 50 µg/mL Carbenicillin) for midi preps. Midi preps were done with NucleoBond midi kit (Macherey-Nagel 740420.50). Purified plasmids were sent for Sanger sequencing (Genewiz) to confirm correct inserts.

Short RNAs used for SLC6A8 (sense sequence):
shRNA1 (V3LHS-411053): ACCATGAGTGCTCACTAAA
shRNA2 (V3LHS-377410): CGCTTCAACAACAACTGCT
shRNA3 (V3LHS-377412): TCCATGGTGATCGTCTTCT
shRNA4 (V3LHS-377413): AGCGTGTCCGGCGACGAGA
shRNA5 (V2LHS-56681): GTGAGTACGGAGAGTATAT

2.3.2 Lentiviral transduction

DNA mix was made for each construct by mixing 2.4 µg pMD2.g, 5.4 µg psPAX2 and 4.2 µg pGipz DNA. Transfection mix was made by combining 544 µL serum-free DMEM (Gibco 11960044) with 36 µL FuGene (Promega E2691) and incubating at room temperature for 5 minutes, before adding the DNA mix and incubating at room temperature for additional 25 minutes.
HEK293T cells were cultured in DMEM (Gibco 11960044) supplemented with 10% FCS (Sigma F7524-500ML), 2 mM L-Glutamine (Gibco 25030-081), 100 units/mL Penicillin and 50 µg/mL Streptomycin (Gibco Penicillin/Streptomycin 15140-122). Some of the media was removed, to retain exactly 6 mL of media. Transfection mix was added dropwise and cells were incubated at 37 °C, 5% CO_2. After 5 hours, media was replaced with 10 mL fresh DMEM with 10% FCS, and again with 12.5 mL DMEM with 10% FCS after 24 hours. The following day viral media was filtered through a 0.45 µm filter and polybrene (Sigma Aldrich H9268-10G) was added to a final concentration of 4 µg/mL. Media was stored at -80 °C until needed for infection. The day before infection, cells were seeded in 6 cm plates. On the day of infection, media was replaced with 3 mL viral media for 6 hours, then with fresh RPMI for

24 hours. Infected cells were selected by incubation in RPMI with puromycin (1 µg/mL, Sigma Aldrich P7255) until all cells on a control, uninfected plate, had died. Gene silencing was confirmed by qPCR.

2.3.3 qPCR

Transfected cell lines were seeded in 6 well plates, allowing them to reach 90% confluence. Cells were scraped in lysis buffer (RLT) using a cell lifter (Corning 3008). RNA extraction was performed using RNeasy purification kit (Qiagen 74106). rtPCR was done using AppliedBiosystems rtPCR kit (4387406) and a two-step programme: 37 °C for 1 hour, 95 °C for 5 minutes. qPCR was set up using SYBR Green qPCR kit (BioRad 1725271) in a 384-well format. qPCR cycles were as follows: 95 °C for 10 seconds, followed by 40 cycles of 95 °C for 10 seconds, 60 °C for 30 seconds. Melt curve: 65-95 °C at 0.5 degree increments, 3 seconds per step. qPCR primers were designed using the NCBI primer-BLAST (Ye et al., 2012).

UBC primers
123-UBC-F-1: CAGCCGGGATTTGGGTCG
124-UBC-R-1: CACGAAGATCTGCATTGTCAAGT

HPRT primers
125-HPRT1-F-1: TGAGGATTTGGAAAGGGTGT
126-HPRT1-R-1: GAGCACACAGAGGGCTACAA

GAPDH primers
121-GAPDH-F-1: GTCTCCTCTGACTTCAACAGCG
122-GAPDH-R-1: ACCACCCTGTTGCTGTAGCCAA

SLC6A8 primers
SLC6A8-F1: TTCCGCCATGAAGACTGTGC
SLC6A8-R1: AGCCTCAAGACTTTGTTCTCCC

2.3.4 Western blots

Cells were seeded in 6 well plates and allowed to reach 90% confluence. Cells were then scraped in Laemmli buffer using a cell lifter (Corning 3008). Protein concentration was measured using Pierce BCA assay (Thermo Fisher 23227). 30 µg of protein

were loaded in each well of a 4-15% mini-Protean precast gel (Biorad 456-1084). The gel was run at 100 V in a Mini-Protean Tetra vertical Electroporesis tank in Protein Running buffer. Protein was transferred to a nitrocellulose membrane in a T22 tank at 100 mA for 50 minutes, in Protein Transfer buffer. The membrane was blocked for 1 hour at room temperature in 5% milk in TBS-0.05% Tween-20 (VWR 437082Q). The primary antibodies (HIF-1a clone 54, BD Biosciences 610958 and HIF-2a D9E3, Cell signalling 7096S, used 1:1000) were diluted in Blocking solution and incubated with the membrane at 4 °C overnight. The membrane was washed three times in TBS-0.05% Tween-20. Secondary antibody (MilliporeSigma Goat-anti-rabbit IgG, Merck 12-348 and MilliporeSigma Goat-anti-mouse IgG, Merck 12-349, used 1:5000) were diluted in 5% milk in TBS-0.05% Tween-20 and incubated with the membrane for 1 hour and room temperature. The membrane was washed three times in TBS-0.05% Tween-20 and developed using Amersham ECL reagent (Fisher Scientific 10155854). Buffers are detailed in Table 2.5.

2.4 Metabolomics

2.4.1 Gas chromatography - mass spectrometry (GC-MS)

Cells were seeded in 6 cm dishes, with 4 replicates per condition, in RPMI-1640 (Gibco 12633012). The following day, media was replaced with experimental RPMI-1640 supplemented with dialysed FCS at time = 0 hours. Dialysed serum was prepared as described in Section 2.2.3. At the indicated time points cells were washed twice with ice-cold PBS (Fisher Scientific 12037539) and quenched with ice-cold methanol (Fisher Scientific 10767665), then scraped and transferred to an Eppendorf tube containing chloroform (Thermo Fisher 390760025) and water (Fisher Scientific W6-212) in final ratios 90% 9:1 MeOH/$CHCl_3$. Scyllo-inositol (Sigma Aldrich I8132) was used as an internal standard. Samples were dried down and re-suspended in 1:3:3 $ClCH_3$/MeOH/H_2O, 350 µL total volume, to separate polar and apolar metabolites. 150 µL of aqueous phase was then dried down in a vial insert using speed-vac concentrator. Samples were washed twice with 40 µL methanol, then derivatised overnight with 20 µL methoxyamine (Sigma Aldrich 593566) (20

mg/mL in pyridine (Sigma Aldrich 110-86-1)) at room temperature. 20 µL N,O-bis(trimetylsilyl)trifluoroacetamide (BSTFA) + 1% trimethylchlorosilane (TMCS) (Sigma Aldrich 25561302) was added to each sample. GC-MS analysis was performed with an Agilent 8890-5977A System. Samples were injected onto a 30 m + 10 m x 0.25 mm DB-5MS + DG column (Agilent J and W) via splitless injection at 270 °C, with a helium carrier gas in electron-impact ionization mode. Oven temperature was initially 270 °C for 2 minutes. It was increased by 12.5 °C/min to 295 °C, and further increased by 25 °C/min to 320 °C, then held at 320 °C for 3 minutes (Fets, Paul C. Driscoll, et al., 2018b). Metabolite identification and quantification was done with Agilent Masshunter Quantitative Analysis software (RRID:SCR_015040). Fractional labelling of metabolites was calculated using in-house R scripts.

2.4.2 Liquid chromatography - mass spectrometry (LC-MS)

Cells were seeded in 6 cm dishes, with 4 replicates per condition, in RPMI-1640 (Gibco 12633012). The following day, media was replaced with experimental RPMI-1640 with HEPES/PIPES, supplemented with dialysed FCS and creatine-(methyl-d_3) monohydrate (Merck 616249) to a final concentration of 100 µM , and pH adjusted to either pH 7.4 or pH 6.8. Dialysed serum was prepared as described in Section 2.2.3. Cells were incubated in experimental media for 24 hours at 37 °C, 5% CO_2. At the appropriate time point, cells were washed twice with ice-cold PBS (Fisher Scientific 12037539) and quenched in ice-cold methanol (Fisher Scientific 10767665), then scraped and transferred to an Eppendorf tube containing chloroform (Thermo Fisher 390760025) and water (Fisher Scientific W6-212) in final ratios 90% 9:1 MeOH/$CHCl_3$. ^{13}C-^{15}N-Valine-L (Sigma Aldrich 600148) was used as an internal standard. Samples were dried down in a speed-vac concentrator and biphasic extraction was done in 1:3:3 $ClCH_3$/MeOH/H_2O, 350 µL total volume. The aqueous phase was transferred to an Eppendorf tube and centrifuged 15 minutes in a bench-top centrifuge to ensure all precipitate was removed. 100 µL was then transferred to a V-bottom 96 well plate and analysed using a Q-Exactive LC-MS. Mobile phase A was 100% Acetonitrile (Merck 34967) while mobile phase B was 10 mM Ammonium acetate (Merck 73594) + 0.1% (v/v) Ammonium hydroxide (Sigma

Aldrich 338818) in water. 90% acetonitrile was used as needle washing solution and 10% isopropanol (Fisher Scientific A461212) was used as rear seal washing solution. Samples were run at a flow rate of 0.1 mL/min in 75% mobile phase A and 25% mobile phase B, on a BEH Z-HILIC 1.7 µm column (Waters Atlantis Premier PN 186009983), in both positive and negative ion mode. Data analysis was done using Xcalibur software (Thermo Fisher Scientific OPTON-30965).

For detection of creatine in media, four media formulations were tested - RPMI-1640, RPMI-1640 supplemented with 10% dialysed FCS, RPMI-1640 supplemented with 10% FCS, and finally RPMI-1640 supplemented with 10% FCS and 100 µL creatine-(methyl-d_3). All media formulations contained 25 mM HEPES and 25 mM PIPES, to represent media used in other experiments. 10 µL of media were mixed with 90 µL Acetonitrile (Merck 34967) and centrifuged 15 minutes in a bench-top centrifuge. Five replicates were run on the LC-MS for each formulation. Creatine concentration was calculated based on an external calibration curve run using the following creatine-(methyl-d_3) concentrations, spiked into extracted media: 0, 1, 3, 7, 15 and 20 µM.

Chapter 3

Computationally deconvoluting SLC signatures in hypoxia and acidosis

Cancer cells rewire their metabolism to adapt to the tumour microenvironment, including conditions of acidosis and hypoxia (Chano et al., 2016; Corbet and Feron, 2017a; Eales, Hollinshead, and Tennant, 2016; Samanta and Semenza, 2018). Since SLC transporters control fluxes of nutrients and metabolites across cell membranes, these metabolic changes can be reflected in changes in transporter expression. In this chapter, we used a computational approach to characterise SLC signatures across cancer types. We explored how SLC expression changes in tumours relative to normal tissue, and whether it varies depending on the tumour microenvironment. To capture the diversity of SLC signatures *in vivo*, clinical samples from The Cancer Genome Atlas (TCGA) database were used. The aim was to identify overall trends in SLC expression under acidic conditions, as well as cancer-type specific responses to acidosis.

3.1 Exploration of SLC signatures across cancer types

3.1.1 TCGA clinical samples cluster by tissue of origin based on transporter expression

To explore the expression patterns of SLC transporters in solid tumours, we downloaded bulk RNAseq data for 5500 clinical samples across 12 cancer types from the TCGA database (Table 3.1). As a first step in the exploratory analysis, SLC expression data was used to perform unsupervised clustering with the t-distributed stochastic neighbour embedding (tSNE) algorithm. The majority of clinical samples clustered according to cancer type (Figure 3.1A, left). Samples originating from related tissue showed a tendency to cluster together - the two types of brain tumours (LGG and GBM) formed a single cluster, as did colon adenocarcinoma (COAD) and rectum adenocarcinoma (READ) samples. Interestingly, the two types of Non-Small Cell Lung Cancer (NSCLC), LUSC and LUAD, formed two distinct clusters. Esophageal cancer (ESCA) was the only tumour type where samples populated two distinct clusters, one of which overlapped with LUAD samples. Breast cancer (BRCA) samples also formed two 'subclusters', however much closer to one another

Table 3.1: Clinical samples from the TCGA database

Abbreviation	Cancer type	Tumour samples	Healthy tissue samples
BRCA	Breast invasive carcinoma	1109	113
COAD	Colon adenocarcinoma	480	41
ESCA	Esophageal carcinoma	162	11
GBM	Glioblastoma multiforme	169	5
LGG	Brain lower grade glioma	529	0
LIHC	Liver hepatocellular carcinoma	374	50
LUAD	Lung adenocarcinoma	535	59
LUSC	Lung squamous cell carcinoma	502	49
PAAD	Pancreatic adenocarcinoma	178	4
PRAD	Prostate adenocarcinoma	499	52
READ	Rectum adenocarcinoma	167	10
SKCM	Skin cutaneous melanoma	471	1

than to any other cancer type.

Although clustering was strongly impacted by tissue of origin, cancer samples showed broader distribution, while healthy tissue samples formed tighter clusters (Figure 3.1A, right). This suggest a greater diversity in SLC expression between tumour samples, meaning there could be other factors beyond tissue of origin which impact SLC expression patterns.

3.1.2 SLC signatures vary between healthy and tumour tissue

The distinct clusters, formed by healthy and tumour samples from the same tissue type, based on SLC expression alone, revealed that cancer cells have different transporter expression signatures from healthy cells. To explore these changes in detail, SLC expression signatures in healthy tissue were compared to signatures in corresponding tumour types. Note that insufficient number of healthy control samples were available for GBM, LGG, PAAD, ESCA and SKCM. A wide variety of transporters showed changes in expression in tumour tissue. The top 30 SLCs per cancer type are shown in Figure 3.1B. Among the upregulated transporters, the SLC2 family of facilitative hexose sugar transporters were strongly represented, including the glucose transporter SLC2A1 which was increased in all 7 tumour types, and the fructose transporter SLC2A5, increased in LIHC and LUAD. Upregulation of SLC2A1 in tumour tissue is consistent with the upregulation of glycolysis, charac-

teristic of many cancer types (R. J. Gillies, Robey, and Gatenby, 2008; Hay, 2016). Fructose can also enter glycolysis, either when fructose is converted to glucose via the polyol pathway, or when fructose is metabolised to the glycolytic intermediate fructose-6-phosphate (Krause and Wegner, 2020). In healthy tissue, the conversion of fructose to glucose is mainly restricted to the liver. However, in cancer cells, polyol pathway activity has also been reported in lung cancer patients, and colon cancer mouse models (Schwab et al., 2018).

Interestingly, the orphan mitochondrial transporter SLC25A48 was increased in both types of lung cancer, LUSC and LUAD, suggesting this uncharacterised mitochondrial carrier might play a role in lung cancer progression. Another commonly upregulated transporter family was the SLCO family of organic anion transporting polypeptides. SLCO1B3 in particular was increased in COAD, LUAD, LUSC, PRAD and READ. SLCO1B3 is normally expressed in the liver, and is able to transport both endogenous and exogenous compounds, including hormones (Hagenbuch and Meier, 2004). Increasing evidence suggests extrahepatic expression of SLCO1B3 could be linked to drug resistance in cancer cells, including colorectal, lung and prostate cancer (R. Sun et al., 2020; J. L. Wright et al., 2011). Increased expression was also seen in transporters from the SLC6 family. SLC6 is one of the largest SLC families, containing 20 members. It can be subdivided into neurotransmitters, amino acid transporters, monoamine transporters and orphan members with unknown substrates (Bröer, 2006). Transporters from the SLC6 family are proton-coupled, suggesting they could be more active in an acidic microenvironment, due to the inverted pH gradient in cancer cells (Daverio et al., 2023).

Downregulated transporters included 3 members of the SLC27 family of fatty acid transporters - SLC27A6 (BRCA, COAD, LUAD, READ), SLC27A5 (LIHC) and SLC27A4 (READ). This could be a reflection of cancer cells relying more heavily on glucose metabolism rather than fatty acid oxidation for energy production.

At large the changes in transporter expression were tumour type-specific. This diversity could partially be a product of the tumour microenvironment.

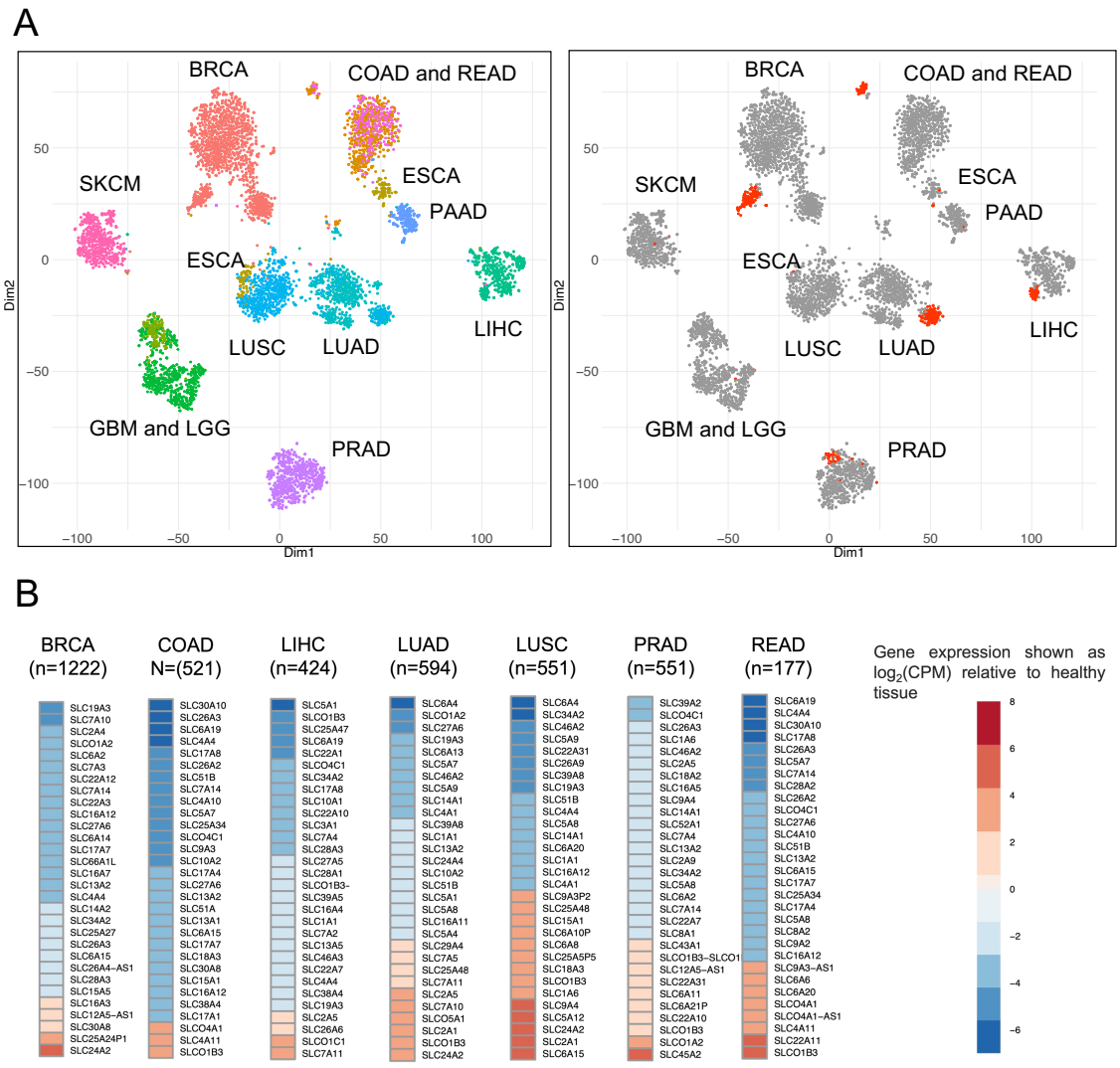


Figure 3.1: Clinical samples from the TCGA database - (A) tSNE analysis based on SLC expression. On the left, colours correspond to cancer types. On the right, cancer samples shown in grey, healthy tissue samples shown in red (B) SLC expression in tumours compared to corresponding healthy tissue. Heatmap represents mean Log_2(CPM) in tumours, relative to mean expression in healthy tissue

3.2 SLC transporter signatures in acidosis and hypoxia are cancer type-specific

3.2.1 Different acidic signatures are associated with different clinical samples

Acidosis and hypoxia are two of the main determinants in the tumour microenvironment. Both of these conditions have an impact on gene expression and metabolic rewiring of cancer cells (J. S. Fang, R. D. Gillies, and Gatenby, 2008; Gatenby et al., 2007). Although they often occur simultaneously, acidosis and hypoxia can have distinct impacts on gene expression (J. L.-Y. Chen et al., 2008; Corbet and Feron, 2017a; Zieker et al., 2008). The combined effect of the two conditions has been studied extensively, but less is known about cell adaptations to acidosis, when it occurs independently. Such adaptations are likely to be reflected in (and facilitated by) changes in membrane transporter expression patterns. The first aim of this project was to identify SLC signatures, specifically associated with acidosis in the tumour microenvironment.

Acidosis can be the result of different prerequisites in the tumour microenvironment. As there is no direct measure of acidosis in the TCGA dataset, 3 gene sets from literature were selected as 'proxies' for acidic environment. It is well documented that a high glycolytic rate in cancer cells can cause acidification of the extracellular space, due to a build up of lactate and protons. For this reason, the first proxy was a gene set of 'Rate-limiting genes in glycolysis' (Tanner et al., 2018) (later referred to as the Glycolysis proxy). The second data set contained genes, upregulated in acidosis, but not hypoxia, identified by J. L.-Y. Chen et al. (2008) (later referred to as the Acidosis proxy). The study compared transcriptional response of primary human mammary epithelial cells to hypoxia, lactic acidosis and low pH, and identified a set of genes, upregulated in lactic acidosis and low pH, but not in hypoxia. The third proxy contained extracellular carbonic anhydrases (CAs). Extracellular carbonic anhydrases, expressed by cancer cells, catalyse the conversion of CO_2 and H_2O to HCO_3 and H^+, and contribute to the acidification of the microenvironment (Supuran, 2008; á. Swietach et al., 2010).

Expression of proxy gene sets was assessed in the 5500 clinical samples, downloaded from the TCGA database. All three proxies were universally expressed across tumour types (Figure 3.2). Although the Acidosis proxy was originally identified in mammary epithelial cells, it showed comparable expression levels in BRCA and cancers originating from other tissue types. Lowest expression was seen in esophageal (ESCA) and brain tumours (GBM and LGG). The Glycolysis proxy showed lowest expression in liver (LIHC) and prostate (PRAD) tumours. The Carbonic anhydrases gene set had the lowest expression levels of the three proxies, and the broadest expression distribution between samples within the same cancer type.

As we were aiming to deconvolute acidosis from hypoxia, we next assessed the relationship between each acidosis proxy and expression of GSEA Hallmark Hypoxia. In the majority of cancer types, high expression of Hallmark Hypoxia was not associated with a dramatic increase in expression for either of the proxies (Figure 3.3, Figure 3.4). Some overlap between high expression of the Glycolysis proxy and Hallmark Hypoxia was seen in LIHC, LUAD, SKCM and brain tumours. This overlap can be explained with the fact that some of the genes in the Glycolysis proxy are HIF-1α target genes. These include HK2, PFKL, PFKP, SLC2A1 and SLC2A3. All three proxies were taken forward to be used in the downstream analysis.

To identify differentially expressed SLC transporters, each of the 12 cancer types was analysed individually. Samples with high median expression of the acidosis proxies (top 10%) were considered acidic, while samples with low median expression (bottom 10%) were considered non-acidic (Figure 3.5). The same analysis was applied using the Hallmark Hypoxia gene set, to assess the overlap between acidic and hypoxic tumour samples.

Clinical samples, selected by the different analysis streams, are summarised on Figure 3.6. The Hypoxia stream of the analysis showed strongest overlay with the Glycolysis stream across all cancer types. This was most pronounced in GBM with 20% of samples matching (7 samples). This result is consistent with the correlation seen on Figure 3.3 and Figure 3.4. The highest proportion of overlap between the Acidosis and Carbonic anhydrases streams was also observed in brain tumours, with 9% in GBM (3 samples) and 8% in LGG (11 samples). Highest similarity between

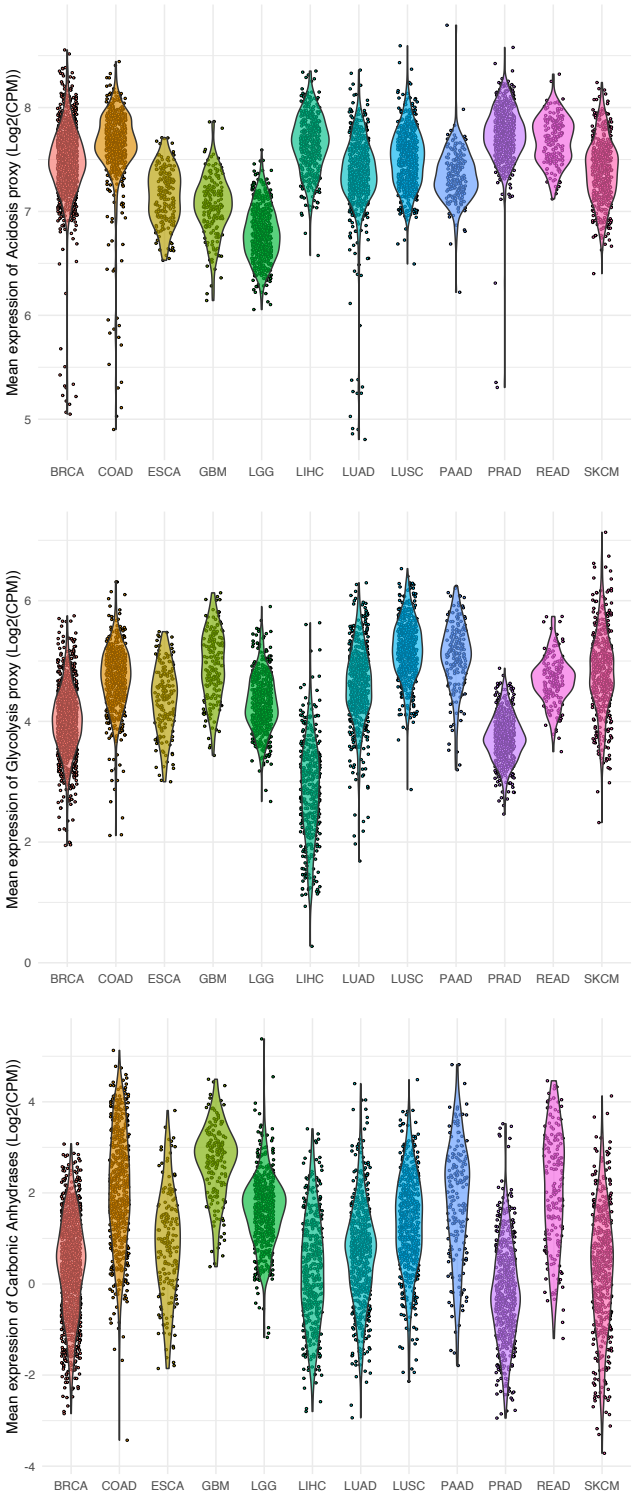


Figure 3.2: Expression levels of acidosis proxies across tumour types - Acidosis J. L.-Y. Chen et al. (2008), Glycolysis (Tanner et al., 2018) and Carbonic anhydrases gene sets were universally expressed across clinical samples from 12 cancer types. Data points represent individual clinical samples. Expression levels shown as mean expression of the gene set in each sample

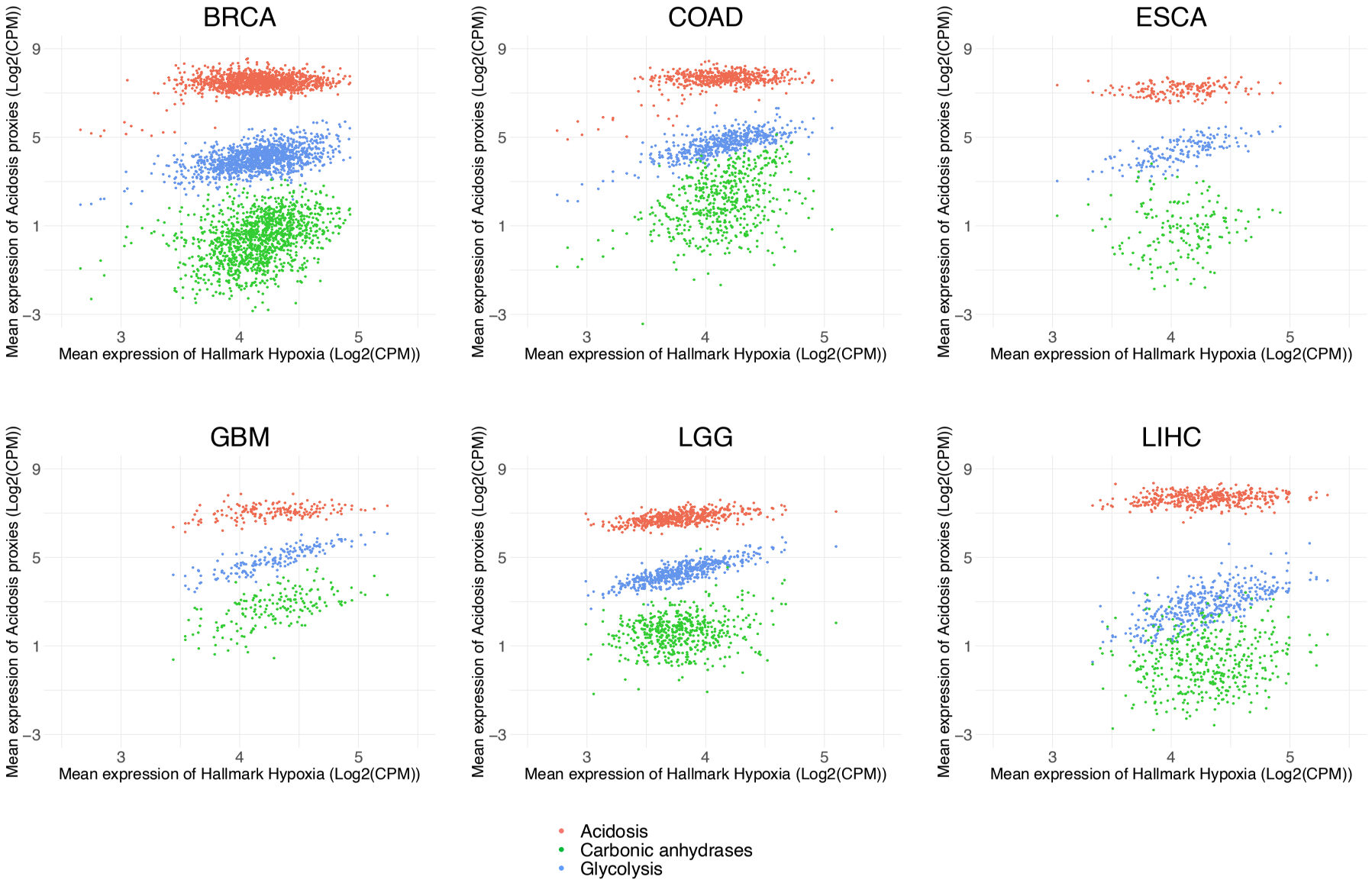


Figure 3.3: Expression levels of acidosis proxies and Hallmark Hypoxia (1) - Expression levels of Acidosis J. L.-Y. Chen et al. (2008), Glycolysis (Tanner et al., 2018) and Carbonic anhydrases shown along Y axis, expression levels of Hallmark Hypoxia shown along the X axis. Data points represent individual clinical samples. Expression levels shown as mean expression of the gene set in each sample

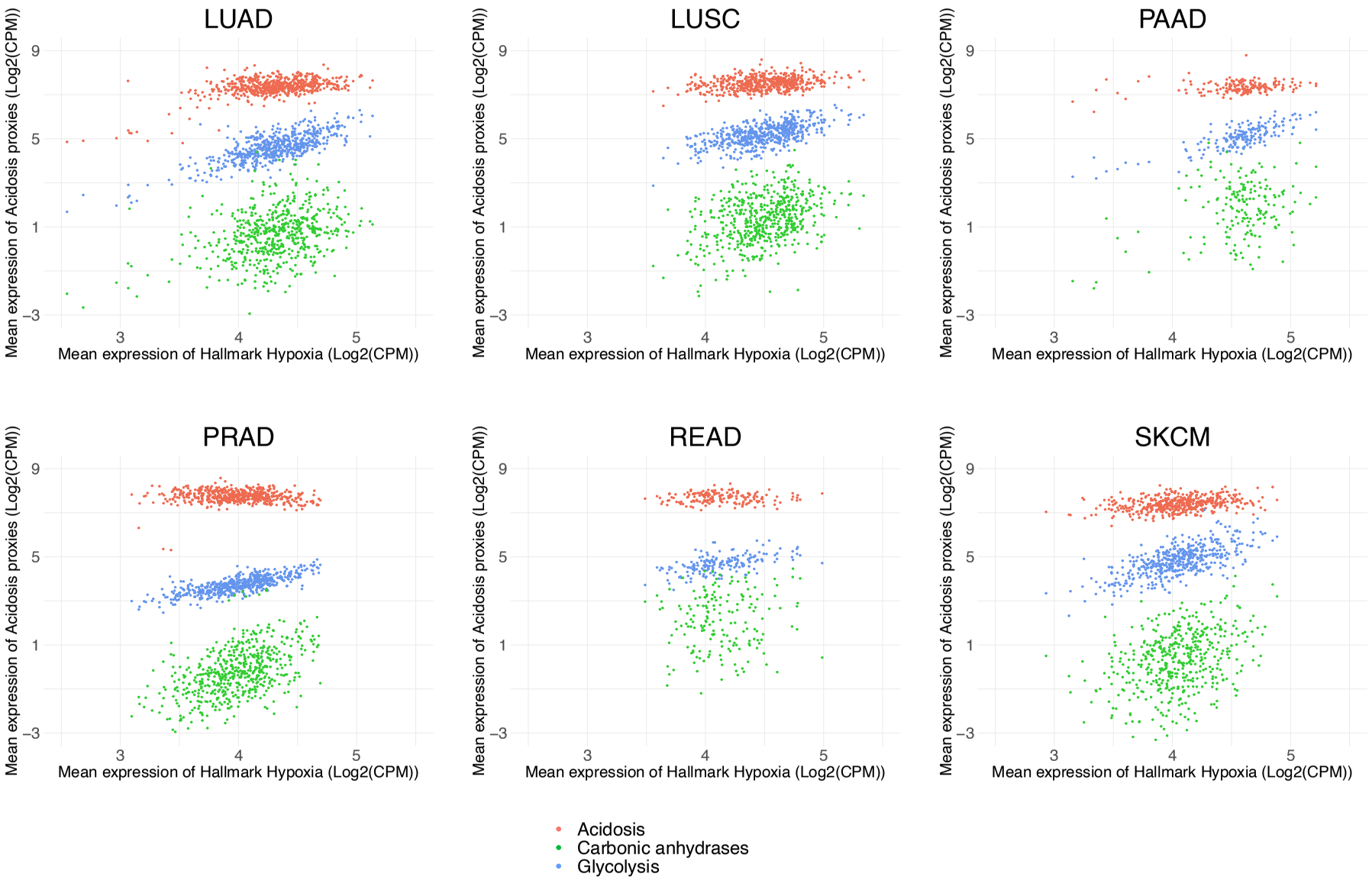


Figure 3.4: Expression levels of acidosis proxies and Hallmark Hypoxia (2) - Expression levels of Acidosis J. L.-Y. Chen et al. (2008), Glycolysis (Tanner et al., 2018) and Carbonic anhydrases shown along Y axis, expression levels of Hallmark Hypoxia shown along the X axis. Data points represent individual clinical samples. Expression levels shown as mean expression of the gene set in each sample

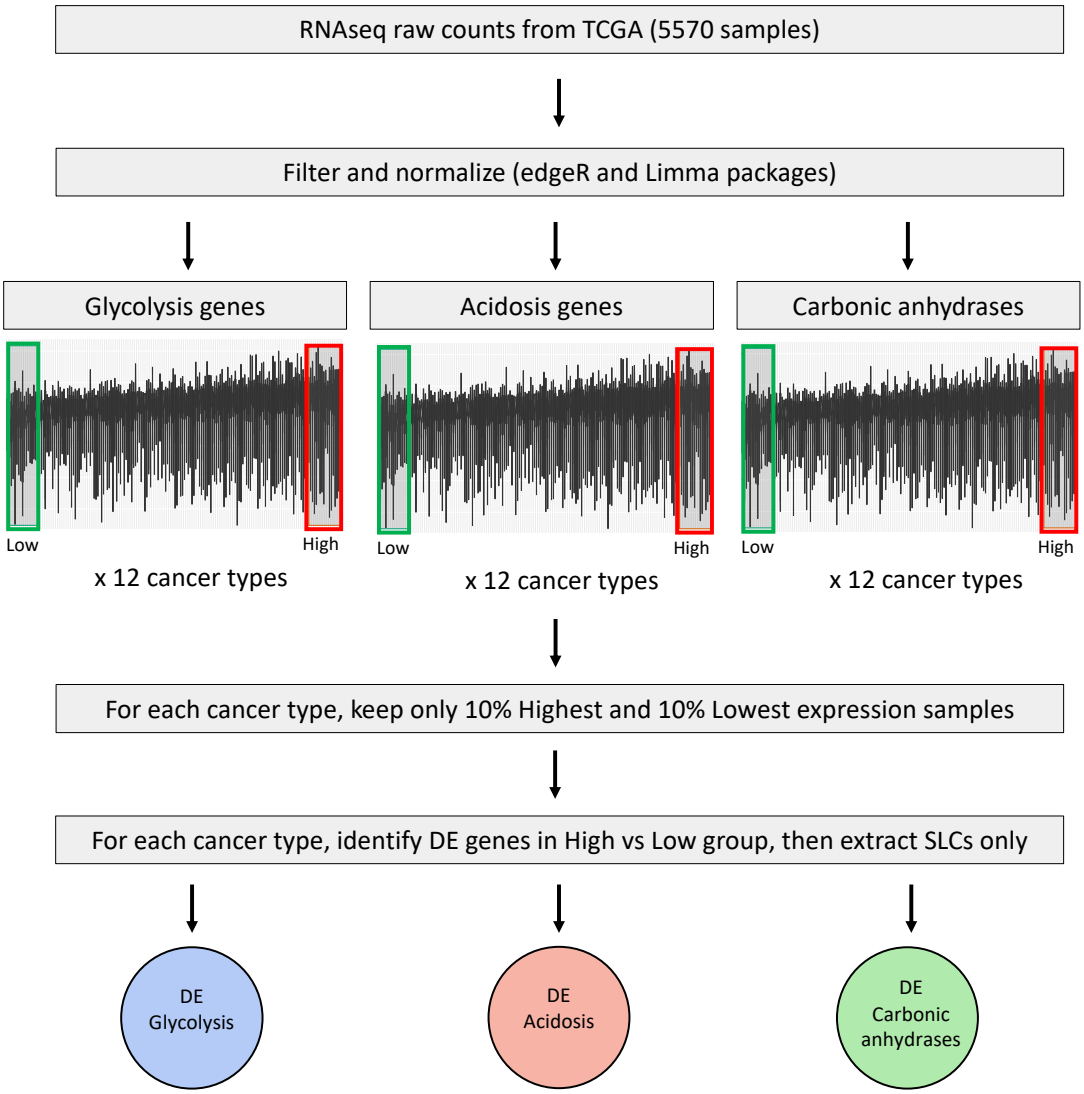


Figure 3.5: Analysis workflow - DE - differentially expressed genes

the Acidosis and Glycolysis stream (11%) showed READ (6 samples) and SKCM (15 samples). Between the Glycolysis and Carbonic anhydrases stream, highest overlap was seen in BRCA (39 samples, 12%) and LGG (12 samples, 8%). The highest number of samples, which were unanimously selected as acidic by all analysis streams, was seen in BRCA (7 samples, 2%) and LGG (5 samples, 4%).

3.2.2 The creatine transporter SLC6A8 is upregulated in acidosis

To identify transporters of interest, we performed differential expression analysis between acidic (top 10%) and non-acidic (bottom 10%) samples within each tumour type for each analysis stream (see Figure 3.5). In total, 191 transporters showed differential expression in acidic samples (Figure 3.7). Of these, 136 were upregulated in at least one cancer type. A number of transporters previously associated with acidosis were highly represented in the upregulated genes, suggesting we had successfully stratified the more acidic tumours. Sodium-hydrogen exchangers from family SLC9 were upregulated across cancer types. Bicarbonate transporters from family SLC4 were also common hits across the Glycolysis and Carbonic anhydrases stream.

Note that on a few instances, the same transporter was upregulated in one cancer type, while being downregulated in another. Such examples are SLC47A1 (also known as Multidrug and toxin extrusion protein 1) and SLC9A3 (Sodium-Hydrogen Exchanger 3). SLC9A3 has a direct impact on intracellular pH, by exchanging Na^+ for H^+ across the cell membrane. We observed an upregulation of SLC9A3 in COAD, and downregulation in PRAD, which could suggest distinct acid-base regulation mechanisms between these two cancer types. There were also rare occasions when the same transporter was picked up as upregulated in one analysis stream and downregulated in another, within the same cancer type. Such is the case with SLC10A1 (Sodium-Bile Acid Cotransporter 1) in LIHC and SLC10A6 (Sodium-Dependent Organic Anion Transporter) in PRAD. A full list of differentially expressed (DE) transporters is shown in Appendix A.

Not all streams of the analysis yielded hits in all cancer types. The Acidosis stream found no DE SLCs in ESCA, GBM, LUSC and PAAD. The Carbonic anhydrases

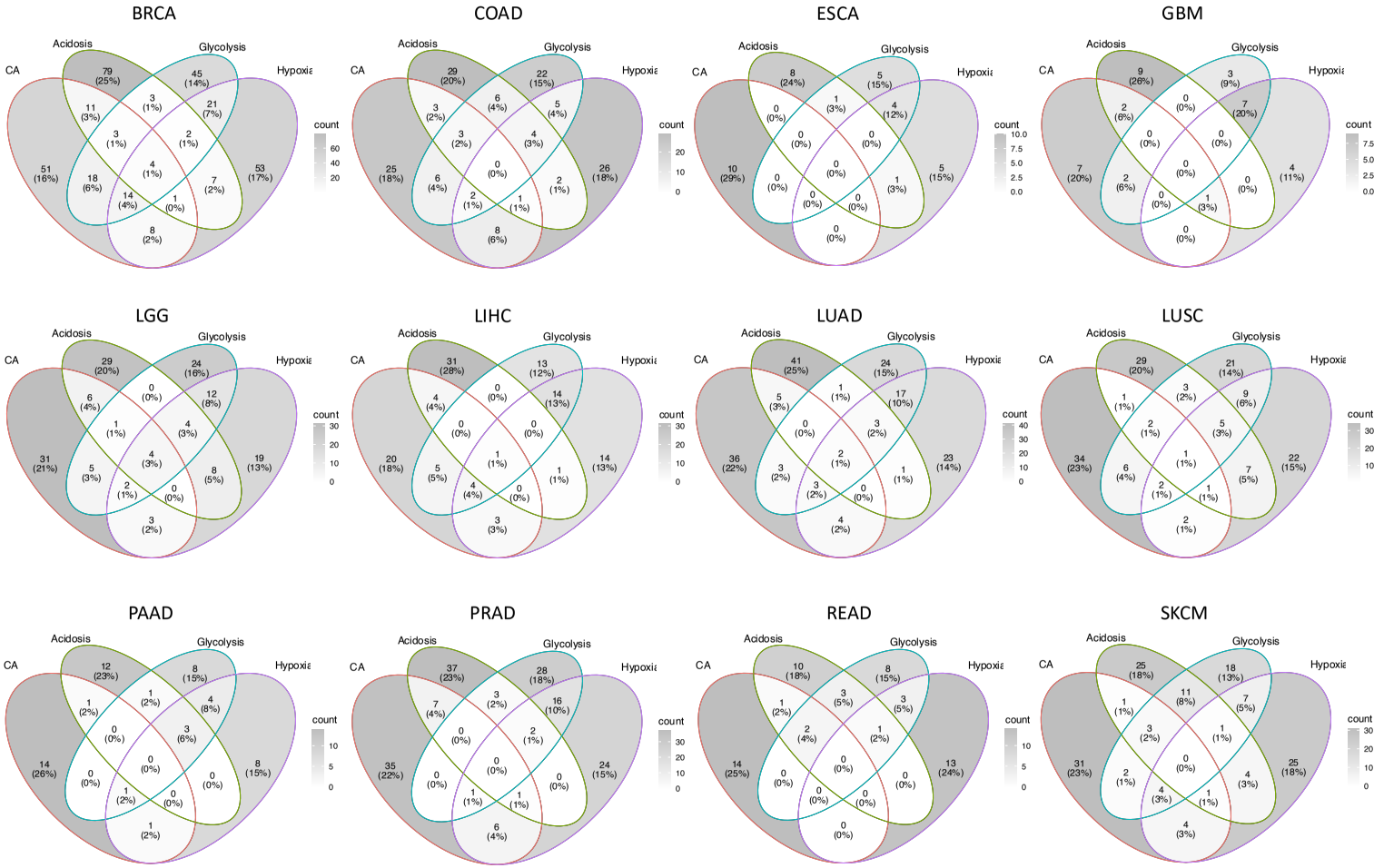


Figure 3.6: Clinical samples identified as acidic or hypoxic across the analysis streams - colour intensity corresponds to number of samples

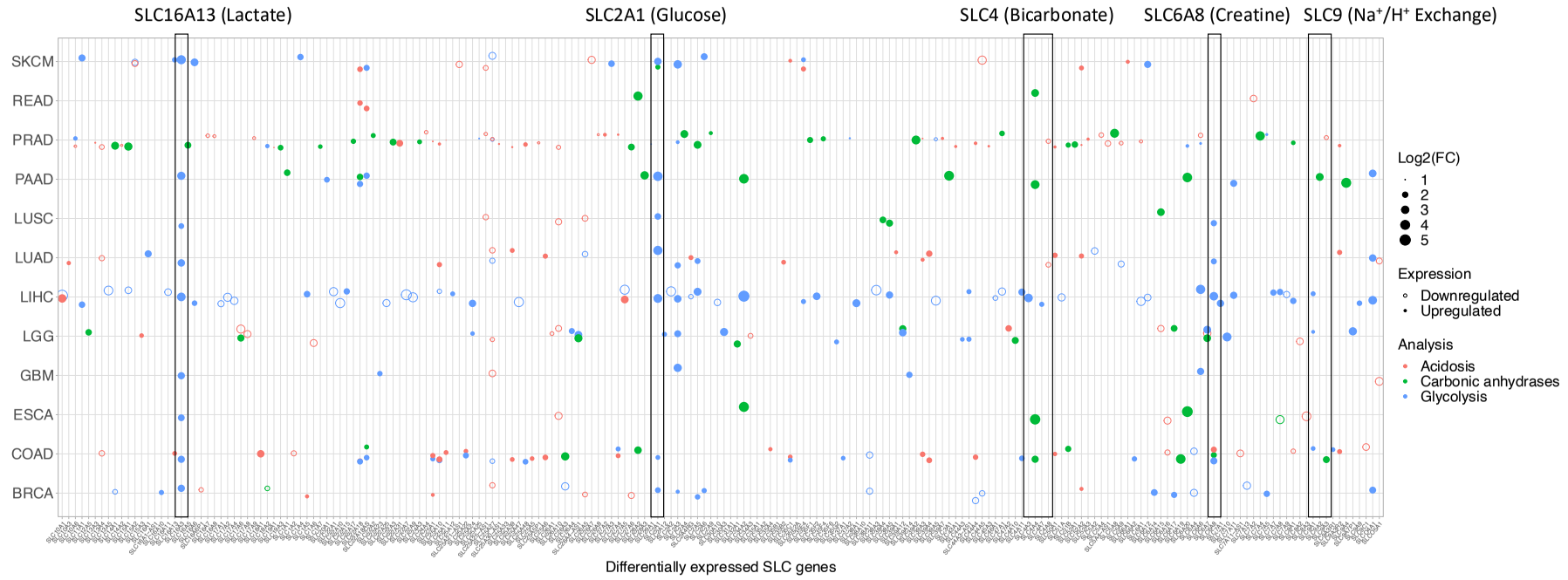


Figure 3.7: Differentially expressed SLC transporters in acidosis - DE genes identified with the R package Limma. Differential expression cut off = ($\log_2$(FC) ≥ 1, adjusted P value ≤ 0.05)

stream did not yield any hits in LIHC, LUAD and GBM. In the Glycolysis stream, no hits were identified in READ. Interestingly, some cancer types, like COAD (52 DE SLCs) and PRAD (84 DE SLCs), showed a much greater change in SLC expression, compared to others. In GBM for example, only 6 DE SLCs were identified. This could be because other factors in the microenvironment affect SLC expression. GBM tumours are characterised by extensive hypoxia (Colwell et al., 2017). It is possible that in this cancer type, hypoxia is the main determinant affecting SLC signatures, and fluctuations in pH have a lesser impact.

Differentially expressed SLCs were generally cancer type-specific. Few overlaps were observed in SLCs identified by different streams within the same cancer type. Most notably, the Glycolysis and Carbonic anhydrases streams identified 6 common hits in COAD. These included the mitochondrial transporters SLC25A1, SLC25A10 and SLC25A22, the fatty acid transporter SLC27A4, the GDP-fucose transporter SLC35C1 and the orphan transporter SLC22A18. There was only one transporter, identified by all streams of the analysis in the same cancer type - the creatine transporter SLC6A8 in COAD. SLC6A8 had a $\log_2$(FC) of 2.7 in the Glycolysis stream (adjusted P value = 0.00001), and $\log_2$(FC) = 2.2 in both the Carbonic anhydrases (adjusted P value = 0.0018) and Acidosis stream (adjusted P value = 0.0015). SLC6A8 was also identified by the Glycolysis stream in LUSC ($\log_2$(FC) = 2.3, adjusted P value = 0.01), LUAD ($\log_2$(FC) = 2.2, adjusted P value = 0.0002) and LIHC ($\log_2$(FC) = 3.7, adjusted P value = 0.0000007).

3.2.3 The creatine transporter SLC6A8 is upregulated in hypoxia

A total of 115 transporters showed differential expression in hypoxia, of which 94 were upregulated in at least one cancer type (Figure 3.8). Of the upregulated SLCs, 60 overlapped with hits from other analysis streams, and 34 were unique for hypoxia (Figure 3.9). Most pronounced was the overlap between hits from hypoxia and the Glycolysis stream. This is unsurprising, as a number of the hypoxic samples were also identified as glycolytic (see Section 3.2.1). An exception was PRAD, where many of the hypoxia hits matched with hits from the Carbonic anhydrases stream. In ESCA and READ, there were no overlaps between hypoxia and any other streams.

SLC6A8, the creatine uptake transporter, was upregulated in hypoxic samples from both COAD ($\log_2$(FC) = 2.2, adjusted P value = 0.005) and LUAD ($\log_2$(FC) = 2.1, adjusted P value = 0.0002), but not in LIHC and LUSC. A full list of DE transporters in hypoxia is shown in Appendix B.

3.2.4 SLC6A8 is prognostic in COAD, LUAD, LUSC and LIHC

SLC6A8 expression has been linked to cancer a number of times (Di Biase et al., 2019; Loo et al., 2015; Yuan et al., 2020), however the role it is playing at the mechanistic level is so far poorly understood. Results from the TCGA data analysis suggest SLC6A8 could play a role in adaptation of cancer cells to the tumour microenvironment. SLC6A8 was found to be upregulated in all streams of the analysis within COAD, as well as being identified by the Glycolysis stream in LUAD, LUSC and LIHC. For this reason it was selected for further investigation. SLC6A8 showed wide expression distribution across clinical samples, especially in COAD, LUAD and LIHC (Figure 3.10). Comparison with healthy tissue revealed SLC6A8 is upregulated in tumour samples from LUAD, LIHC and LUSC. In COAD, SLC6A8 was downregulated in tumours compared to healthy tissue (Figure 3.11). However, when tumour samples are stratified into acidic and non-acidic by the three proxy gene sets, SLC6A8 expression in acidic samples is clearly upregulated. This is particularly striking in COAD (Figure 3.12).

To examine the prognostic value of the creatine transporter, Kaplan-Maier survival analysis was done using TCGA survival data. SLC6A8 was significantly associated with unfavourable prognosis in COAD, LUAD and LIHC. Interestingly, it was associated with favourable prognosis in LUSC (Figure 3.13). This suggests creatine metabolism could play different roles in tumour progression in the two types of lung cancer.

3.2.5 SLC6A8 is upregulated away from blood vessels

The fact the SLC6A8 was associated with all 3 proxies of acidosis, as well as Hallmark Hypoxia, suggests it is likely to be upregulated in cancer cells located at a greater distance form a blood vessel, where hypoxia and acidosis commonly occur. Further

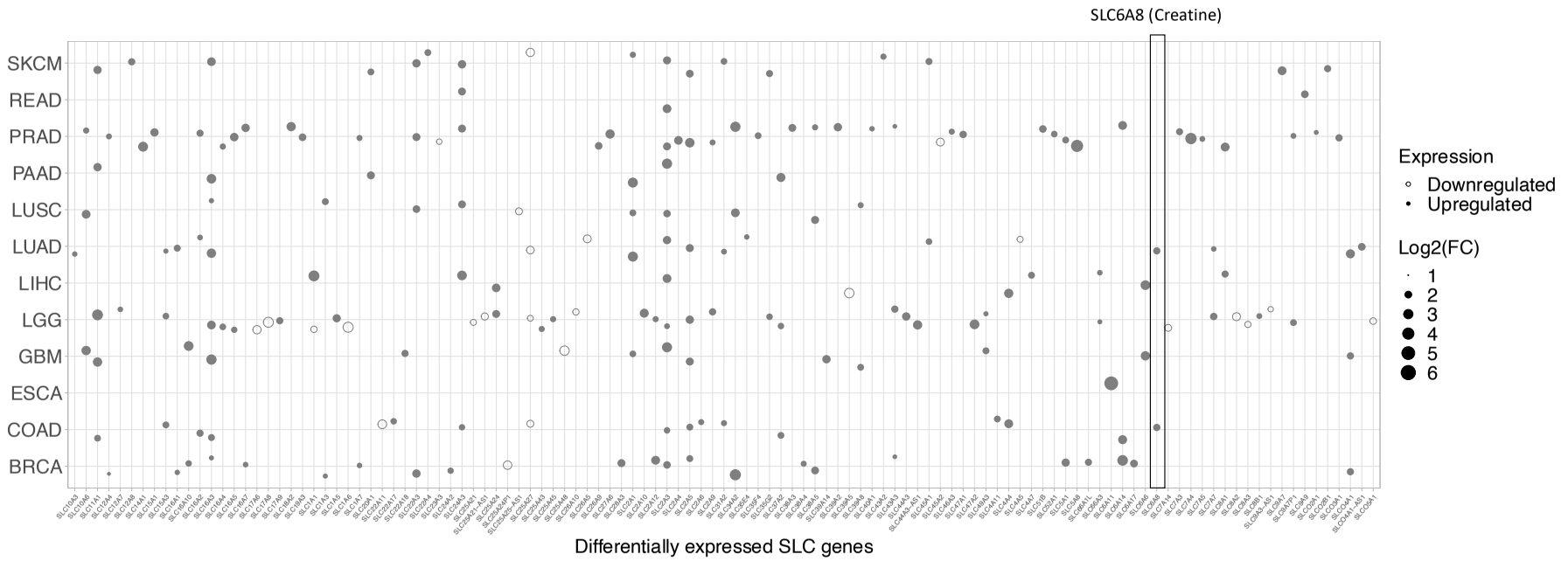


Figure 3.8: Differentially expressed SLC transporters in hypoxia - DE genes identified with the R package Limma. Differential expression cut off = ($\log_2$(FC) $\geq$ 1, adjusted P value $\leq$ 0.05)

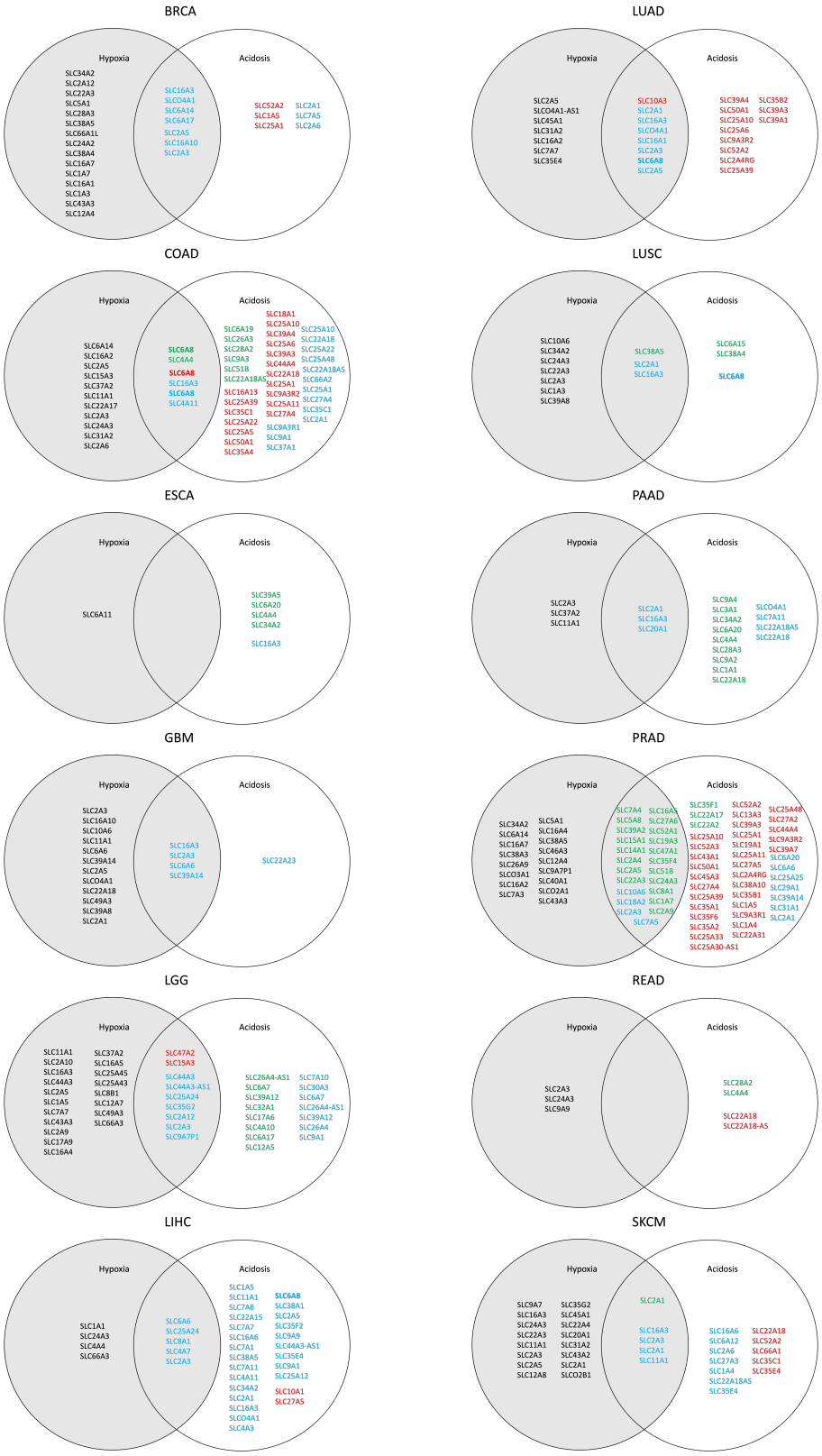


Figure 3.9: SLC transporters upregulated in hypoxia - SLC transporters with $\log_2(\text{FC}) \geq 1$, adjusted P value ≤ 0.05. Hits from the Hypoxia stream are shown in black. Hits from the Glycolysis stream are shown in blue. Hits from the Carbonic anhydrases stream are shown in green. Hits from the Acidosis stream are shown in red.

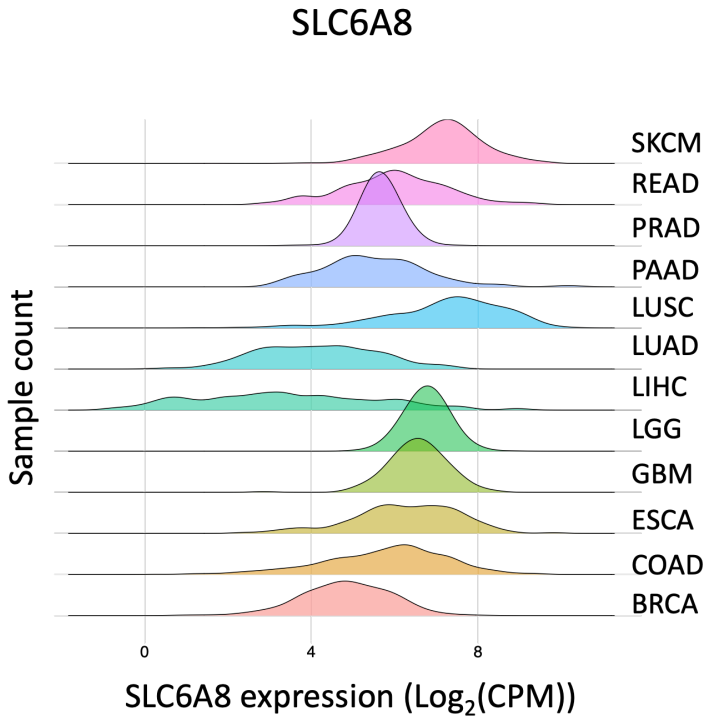


Figure 3.10: SLC6A8 expression in cancer - A ridge-plot demonstrating that SLC6A8 is heterogeneously expressed across cancer types. X axis shows transcript expression in $\log_2$(CPM), Y axis shows number of clinical samples. Expression data from the TCGA database.

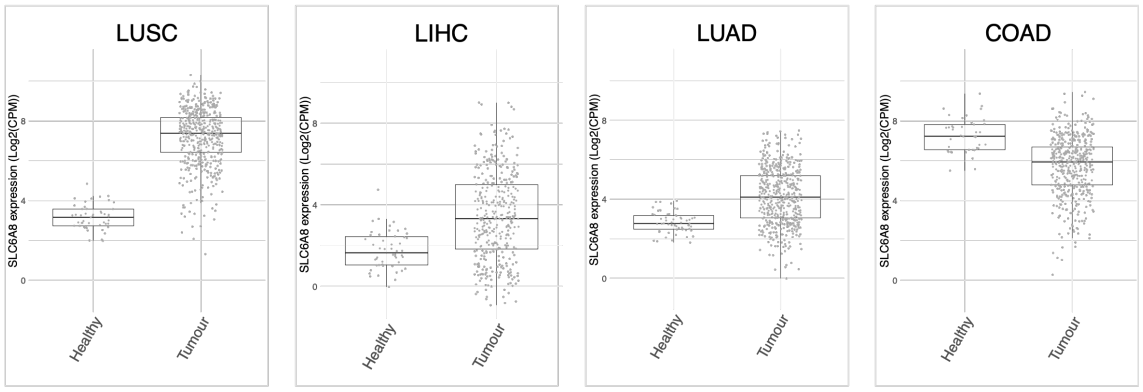


Figure 3.11: SLC6A8 expression in tumour and healthy tissue samples - Box-plots, showing SLC6A8 expression in tumour samples and corresponding healthy tissue samples from the TCGA database. Data points represent individual clinical samples.

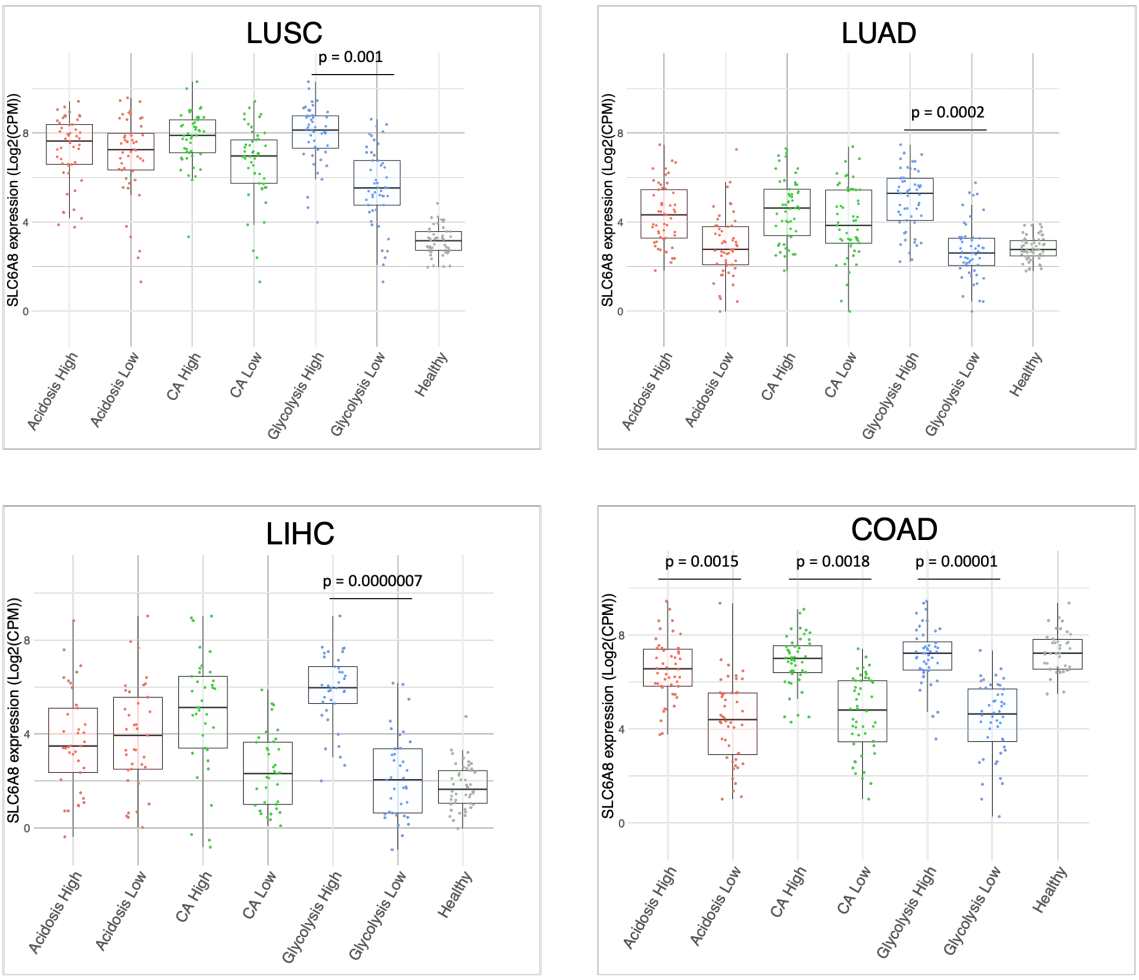


Figure 3.12: SLC6A8 expression in acidic and non-acidic tumour samples - Boxplots, showing SLC6A8 expression in tumour samples, stratified by the 3 acidosis proxies: Acidosis (J. L.-Y. Chen et al., 2008), Carbonic anhydrases (CA) and Glycolysis (Tanner et al., 2018). P values show false discovery rate for differential expression, as calculated by the R package Limma.

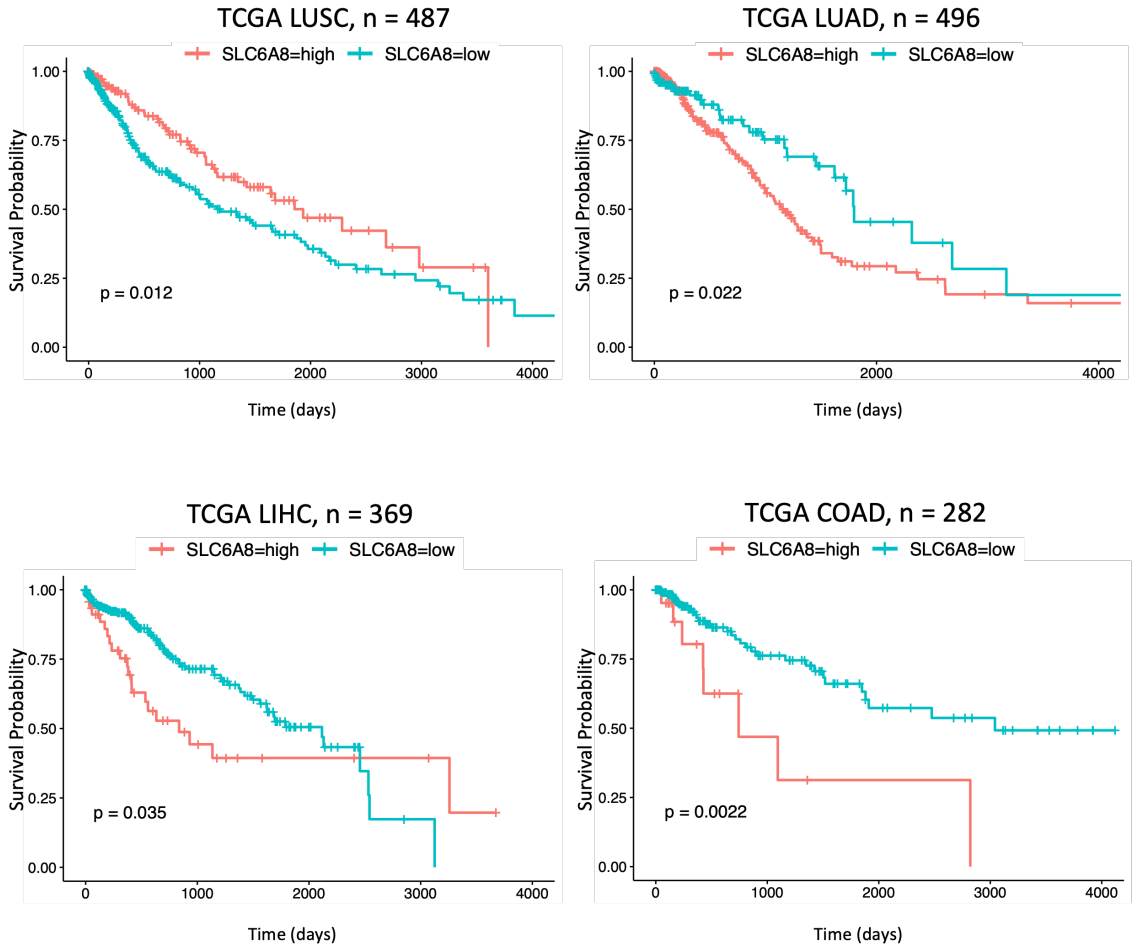


Figure 3.13: Prognostic value of SLC6A8 - Kaplan-Maier survival plots based on RNAseq and survival data obtained from the TCGA database. Optimal cut point for High and Low categories determined in the R package Survminer.

evidence for this was found in a study by Kumar et al. (2019), who investigated intra-tumoral metabolic heterogeneity in mouse models of glioblastoma. The study used injection of Hoechst dye shortly before sacrificing the mice, to allow staining of tumour cells in immediate proximity to blood vessels. Cells located at a greater distance took up decreasing amounts of dye, allowing cell sorting by FACS. Cancer cells were separated in 3 categories - High Staining (close to a blood vessel), Medium Staining (medium distance) and Low Staining (far from a blood vessel). Gene expression in these categories was examined by RNAseq.

As part of our current analysis, we examined SLC transporter expression within this RNAseq dataset to look at spatial differences in expression. It became clear that a number of transporters were differentially expressed dependent on proximity to a blood vessel in glioblastoma (Figure 3.14). The third most upregulated transporter in regions distal to blood vessels was SLC6A8. Others included the glucose transporters SLC2A1 and SLC2A3 and the monocarboxylate transporters SLC16A1 and SLC16A3, both associated with lactate transport, demonstrating that these areas are likely to be highly glycolytic.

3.3 Exploration of SLC signatures on the single cell level

TCGA data is based on bulk RNA sequencing, which could present a limitation for the analysis pipeline. Clinical tissue samples contain stromal cells in addition to cancer cells, and gene expression across different cell types affects the overall expression levels detected by bulk RNA sequencing. We aimed to determine how much of the SLC signatures we obtained could be a product of inter-patient differences within the tumour microenvironment. We explored publicly available single cell RNA sequencing (scRNAseq) data from lung tumour samples, to determine whether additional cell types could contribute to the results we saw with bulk sequencing data from TCGA.

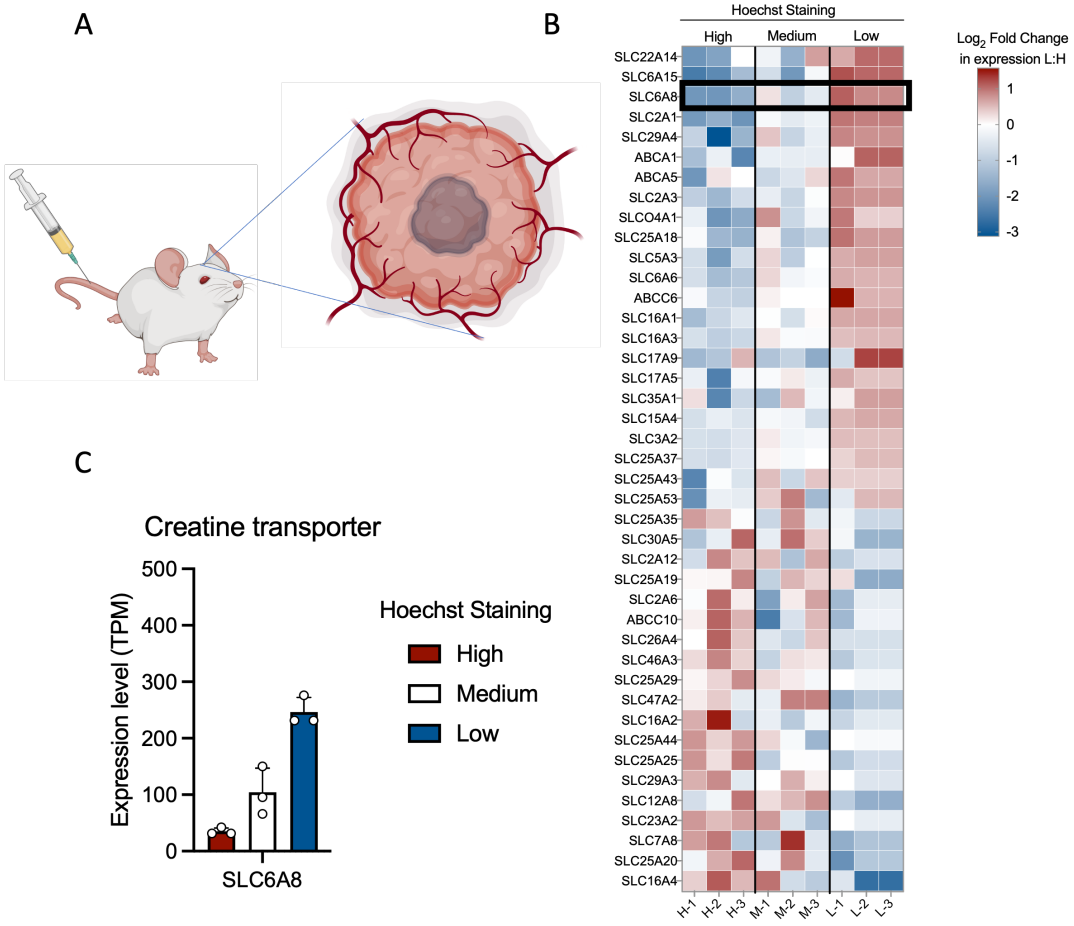


Figure 3.14: SLC6A8 expression in glioblastoma - Data from Kumar et al. (2019). (A) Orthotopic mouse models of glioblastoma were injected with Hoechst dye 5 minutes before sacrifice (B) A number of SLC transporters show changes in gene expression between the 3 groups of cancer cells: High Staining (close proximity to a blood vessel), Medium Staining (medium distance) and Low Staining (large distance from blood vessel) (C) Expression of the Creatine transporter SLC6A8 across the 3 groups

3.3.1 Single cell RNAseq analysis reveal patient-to-patient heterogeneity in SLC expression

Data from N. Kim et al. (2020) was available with cell type annotations already in place. This allowed cancer cells to be easily stratified from additional cell types in the tumour samples. A total of 31 136 cancer cells were analysed. These included cancer cells from early and late stage primary LUAD tumours, as well as brain and lymph node metastasis. We performed unsupervised clustering, using the UMAP method. The inbuilt cluster annotation function in the Seurat package revealed 20 distinct cell clusters (Figure 3.15A). Unsurprisingly, metastatic samples clustered separately from primary tumour samples. In addition, early and late stage tumour samples formed distinct clusters as well (Figure 3.15B). A closer examination of cluster composition revealed the majority of clusters in fact only contained cancer cells coming from one clinical sample (Figure 3.15C). Exceptions were Cluster 5, 6, 13, 18 and 19, where cancer cells from multiple patients were identified. On a few occasions, cells originating from the same clinical sample formed multiple clusters, in particular in the brain metastasis samples. Example are cluster 4 and 15, both originating from sample NS_12 and cluster 1 and 16, both originating from sample NS_07 (Figure 3.15E). These clustering patterns testify to the great tumour heterogeneity between LUAD clinical samples.

Next we aimed to explore SLC signatures across cell clusters. To do this, cluster markers were identified with the Seurat function ClusterMarkets, and SLC transporters were extracted from the full marker list. The creatine transporter SLC6A8 was expressed in a number of clusters across the dataset. These included the late stage LUAD cluster 0, and brain metastasis clusters 1, 4 and 7. SLC6A8 expression also overlaps with late stage LUAD cells within cluster 13 (Figure 3.15D).

3.3.2 SLC6A8 is expressed on cancer cells, T helper cells and Macrophages

To gain a more detailed understanding of SLC6A8 expression across the tumour microenvironment in LUAD, we examined all cell types across early and late stage LUAD tumours. In early stage samples, a total of 45 149 cells from 11 clinical sam-

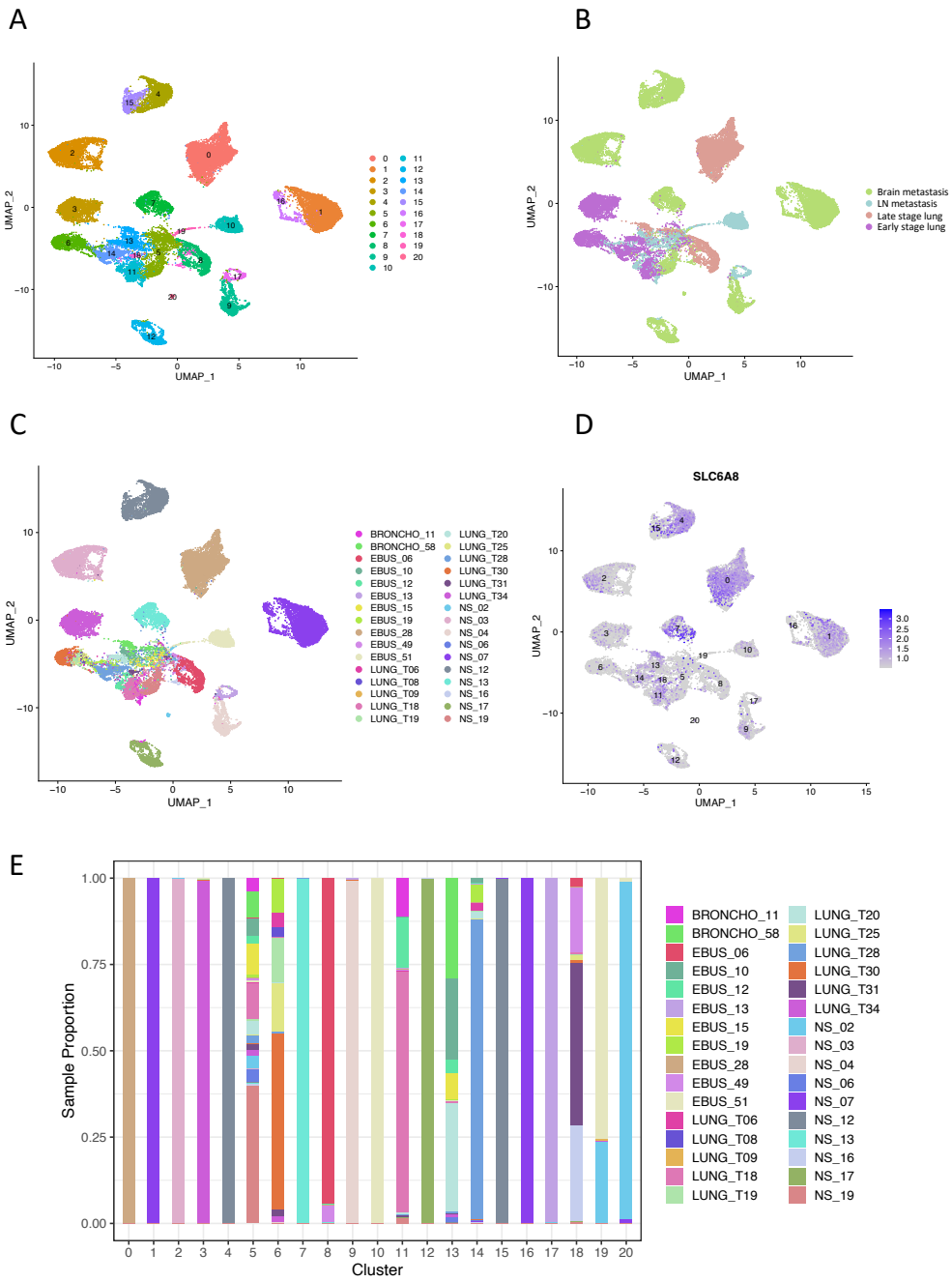


Figure 3.15: UMAP of LUAD cancer cells - UMAP analysis was performed to cluster 31 136 cancer cells across 32 clinical samples. Data from N. Kim et al. (2020). (A) cancer cells formed 20 distinct clusters. Cluster annotation was done with the Seurat package in R (B) Different cancer subtypes are associated with different clusters (C) Individual clusters are often associated with a single clinical sample (D) Expression of SLC6A8 overlaps with clusters of late stage LUAD samples and brain metastasis (E) Cluster composition. UMAP clusters shown along the X axis. Individual clinical samples shown in different colours (corresponding to panel C)

ples were clustered using UMAP. In early stage LUAD samples, SLC6A8 expression overlapped with clusters of cancer cells (Figure 3.16A). Note cancer cells are labelled as tS1, tS2 and tS3 (shown in light pink), keeping the original classification of the dataset. SLC6A8 expression was also seen in two additional clusters, populated by non-cancerous cells. Closer examination of these clusters revealed SLC6A8 was mostly expressed in T helper cells (CD+ Th and CD8+/CD4+ Mixed Th) and macrophages (annotated as mo-Mac) (Figure 3.16B).

For late stage LUAD, 12 073 cells from 4 clinical samples were clustered using UMAP (Figure 3.17). Once more, SLC6A8 expression largely overlapped with clusters of cancer cells (annotated here as Malignant cells to keep the original classification of the dataset, and shown in light pink). As before, some SLC6A8 expression was also seen amongst macrophages (mo-Mac).

3.3.3 SLC6A8 is upregulated in late compared to early stage LUAD tumours

Next we conducted a differential expression analysis of cancer cells from early and late stage LUAD samples. 19 SLC genes were identified as upregulated in late stage LUAD compared to early stage (Figure 3.18). Amongst these genes were the creatine transporter SLC6A8 ($\log2(FC) = 0.48$) and the glucose transporter SLC2A1 ($\log2(FC) = 0.27$). Interestingly, 11 of the 19 SLCs were previously identified as associated with acidosis during the TCGA analysis (Figure 3.7). These include SLC39A4 (LUAD and COAD), SLC2A4RG (PRAD), SLC22A18 and SLC22A18AS (COAD, PAAD, READ and SKCM), SLC4A11 (COAD and LIHC), SLC16A5 (PRAD), SLC22A31 (PRAD), SLC34A2 (ESCA, LIHC, PAAD), SLC25A39 (COAD, LUAD, PRAD), SLC52A2 (SKCM, PRAD, LUAD, BRCA) and SLC44A4 (PRAD and COAD). These results suggest acidosis might be a feature of late stage LUAD tumours.

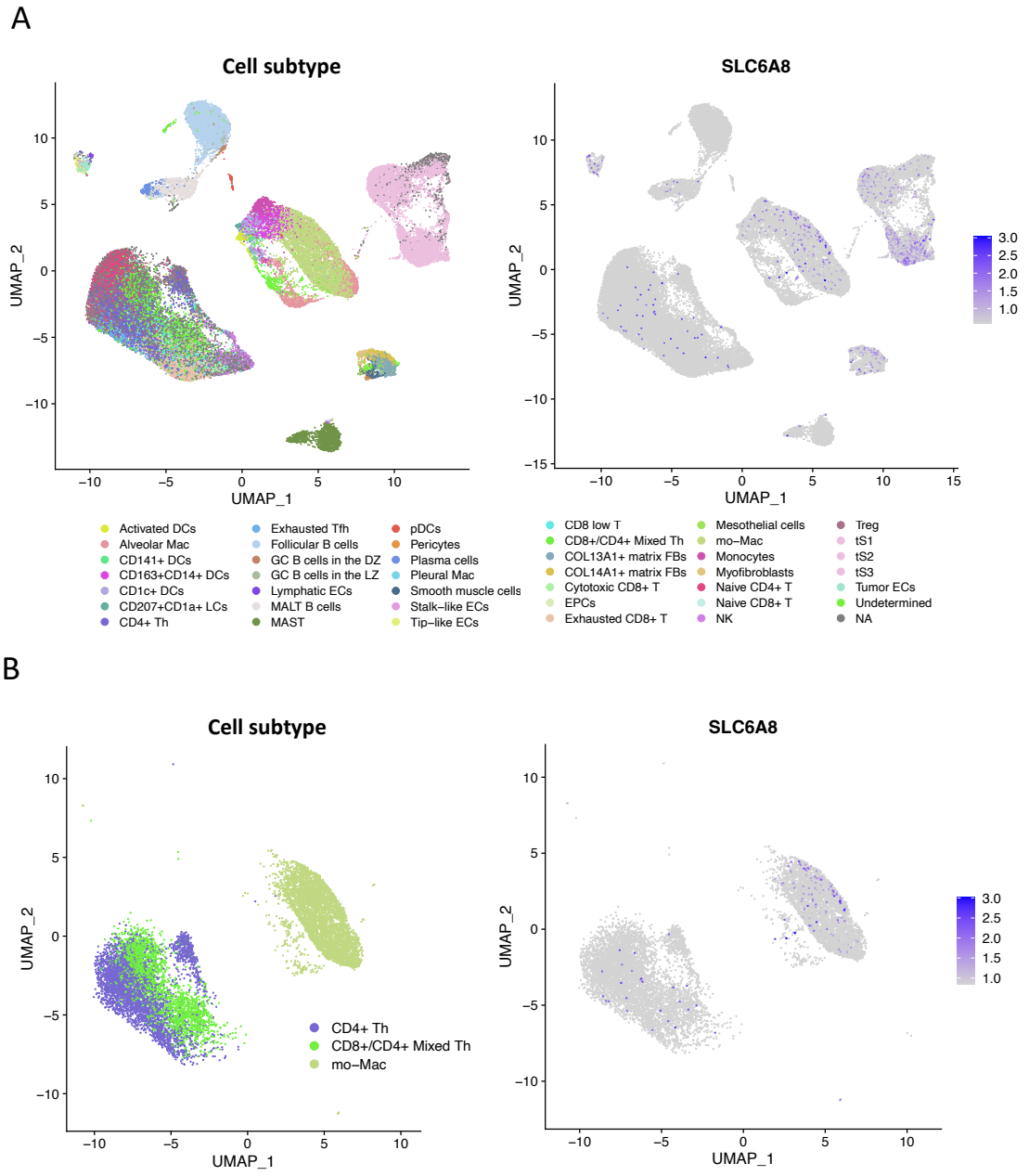


Figure 3.16: SLC6A8 expression across cell types within the tumour in early stage LUAD - UMAP analysis was performed to cluster 45 149 cells across 11 clinical samples. Cancer cells are annotated as tS1, tS2 and tS3, keeping the original classification of the dataset (N. Kim et al., 2020), and displayed in pink. A) All cell types within the tumour B) Cell types, associated with SLC6A8 expression

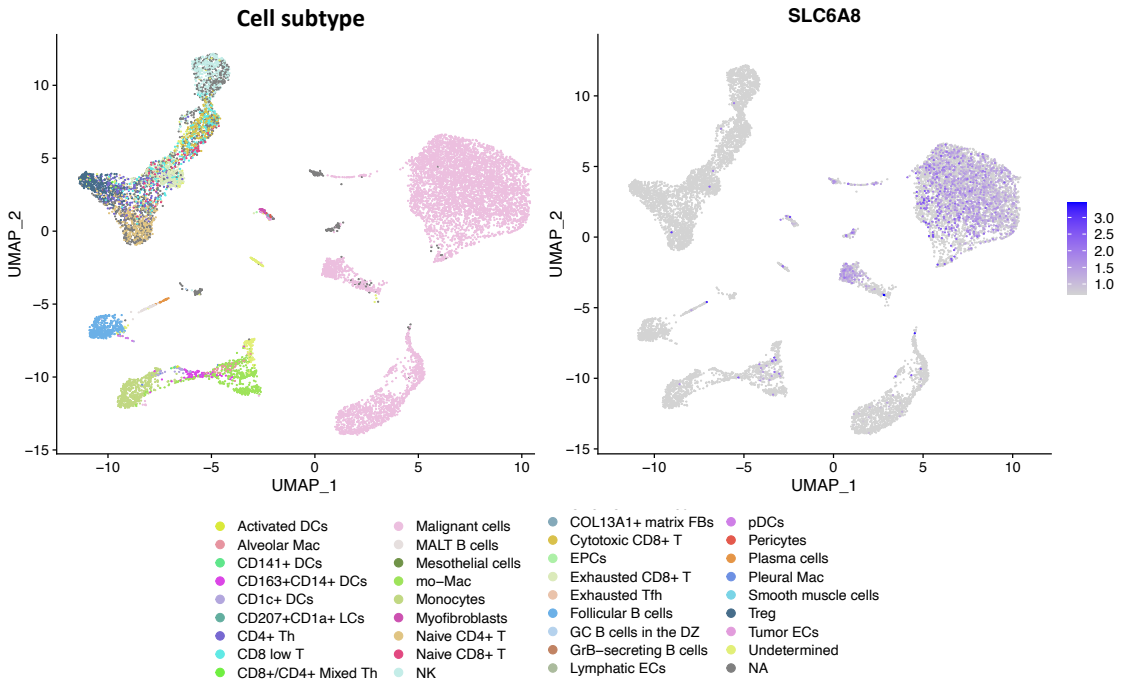


Figure 3.17: SLC6A8 expression across cell types within the tumour in late stage LUAD - UMAP analysis was performed to cluster 12 073 cells from 4 clinical samples. Cancer cells are annotated as Malignant cells, keeping the original classification of the dataset (N. Kim et al., 2020), and displayed in pink.

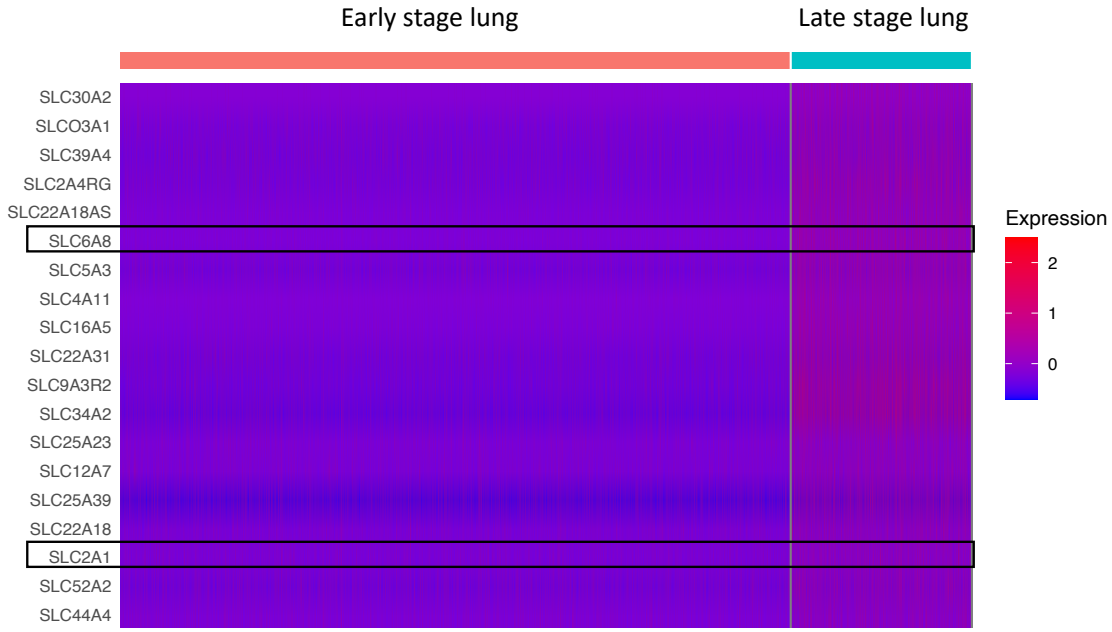


Figure 3.18: Upregulated SLC genes in late stage LUAD - Differential expression analysis performed on the single cell level with the R package Seurat. The creatine transporter SLC6A8 and glucose transporter SLC2A1 are both upregulated in cancer cells from late stage LUAD samples relative to early stage LUAD.

3.3.4 Acidosis proxies used for TCGA analysis are expressed across cell types

To evaluate the computational method, used for TCGA analysis at the beginning of this project, we examined the expression of the 4 proxies for acidosis and hypoxia across cell types. The Seurat function AddModuleScore was used to assess gene set expression across single cells. In early stage LUAD, the Acidosis proxy was expressed heterogeneously across the cancer cell clusters 4, 5, 13 and 16 (Figure 3.19). In addition, it was expressed by macrophages (mo-Mac) in clusters 3 and 6, and B cells in cluster 11. Expression of the Glycolysis proxy mostly overlapped with macrophages. The Carbonic anhydrases proxy was highly expressed by a small group of cancer cells in cluster 13. The hypoxia signature was broadly spread across both cancer cell clusters and other cell types. There was not a complete overlap between the 4 signatures, suggesting areas of hypoxia and acidosis could be separate in these tumours. Most notable overlap was seen between the Hypoxia and Glycolysis signatures in early stage lung cancer, across cluster 3 and cluster 7.

In late stage LUAD, the Acidosis proxy was expressed by a number of cell types across all clusters (Figure 3.20). The Glycolysis proxy was most highly expressed by myeloid cells in cluster 6 and 7. The Carbonic anhydrases proxy remained expressed by a small group of cells in the cancer clusters 0 and 1. The Hypoxia proxy was expressed across cell types, most upregulated in myeloid cells (cluster 6 and 7), fibroblasts (cluster 11) and cancer cells (especially cluster 9).

Overall, all 4 signatures were associated with cancer cells. However, the presence of additional cell types in clinical samples could have had some impact. For example, samples with high contents of fibroblasts could have been scored 'more acidic' using the Acidosis proxy.

3.4 Conclusions and limitations

During the clustering analysis, based on SLC transporter expression patterns, the majority of clinical samples clustered based on their tissue of origin. However, their distribution was far broader than that of corresponding normal tissues, suggesting

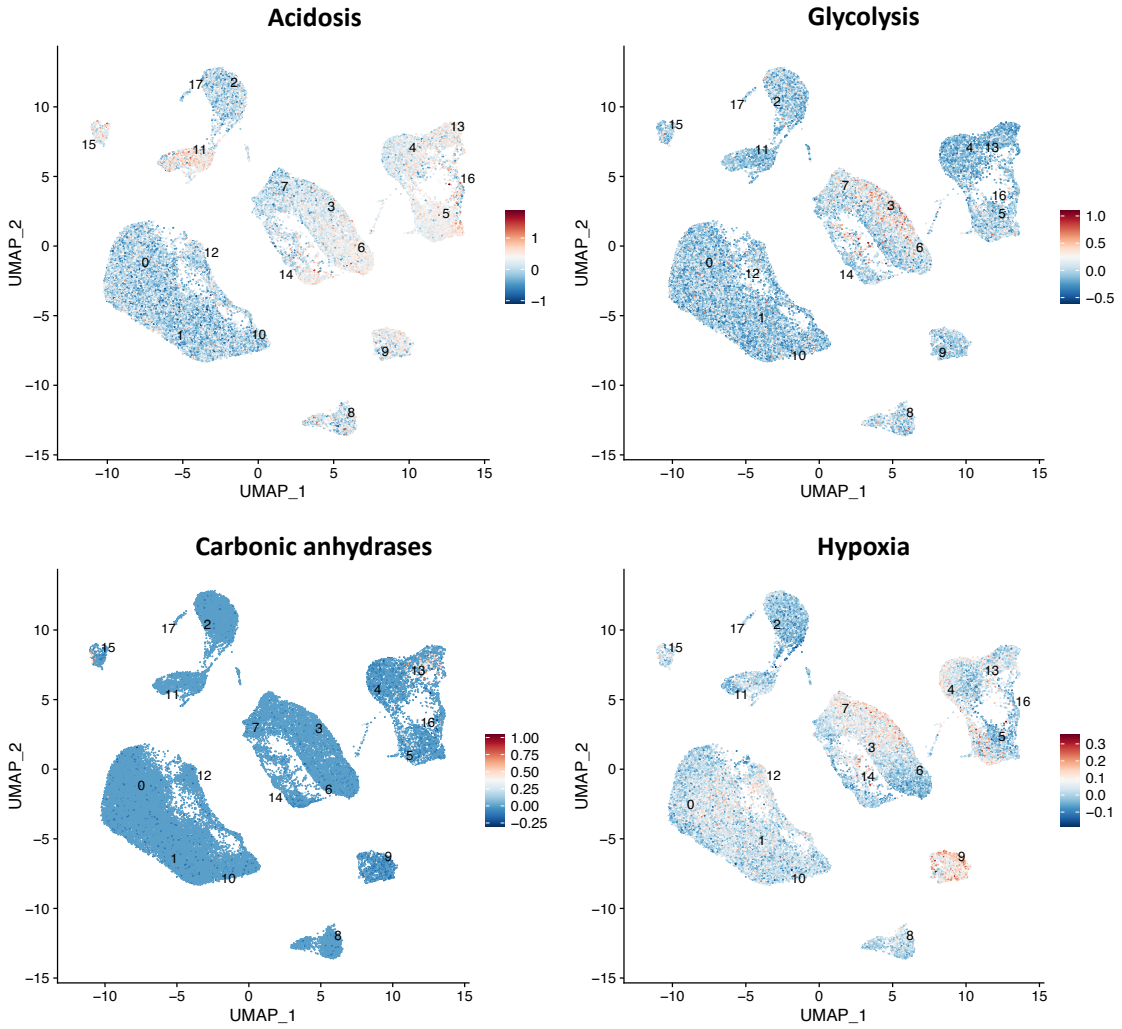


Figure 3.19: Expression of acidosis proxies on the single cell level in early stage LUAD - Expression levels calculated using the AddModileScore function in the R package Seurat. A positive score (shown in red) suggests the gene set is expressed in a particular cell more highly than would be expected, given the average expression of this gene set across the population.

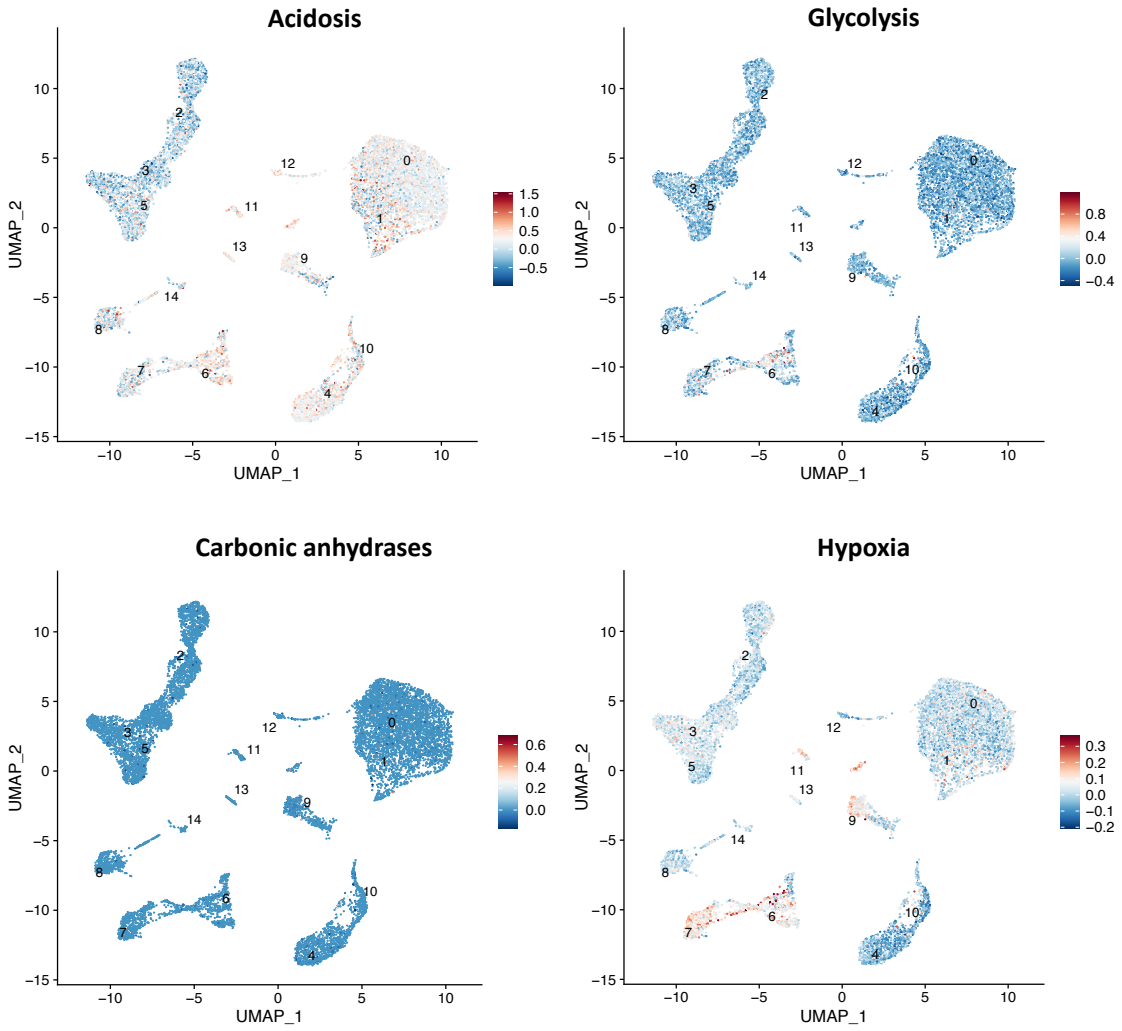


Figure 3.20: Expression of acidosis proxies on the single cell level in late stage LUAD - Expression levels calculated using the AddModuleScore function in the R package Seurat. A positive score (shown in red) suggests the gene set is expressed in a particular cell more highly than would be expected, given the average expression of this gene set across the population.

that other factors also influence SLC signatures (Figure 3.1A). It is interesting to note that healthy tissue controls for LUSC and LUAD form a single cluster, while tumour samples are clearly distinct. This could be due to the cell type of origin of LUSC and LUAD. LUSC is believed to originate from basal cells in the proximal airway, while LUAD can be developed from AT2 cells in the distal airway or club cells in bronchiolar epithelium (Sarode et al., 2020; F. Wu et al., 2021). The two cancer types are known to display differences in gene expression and signalling pathways (Anusewicz, Orzechowska, and Bednarek, 2020; Y. Yang, M. Wang, and B. Liu, 2019) and this diversity seems to also apply when it comes to SLC signatures.

ESCA was the only cancer type forming two separate clusters of tumour samples. Esophageal cancer is known to be particularly heterogeneous, with two main subtypes - Squamous cell carcinoma (SCC) and Esophageal adenocarcinoma (ECA). SCC has been shown to express more similarities to squamous carcinomas of other organs, than it does to ECA. ECA on the other hand shows genomic alterations strongly resembling the chromosomally unstable variant of gastric adenocarcinoma (J. Kim et al., 2017). This is consistent with the distributions we observed in our tSNE analysis of SLC expression. ESCA samples overlapping with the LUSC cluster are likely to be of the SCC subtype, suggesting squamous carcinomas have similar SLC signatures, resulting from similar cell types of origin.

BRCA clinical samples also formed two 'sub clusters', although they were separated from other cancer types. BRCA can be divided into two histologic subtypes - Invasive ductal carcinoma (IDC) and Invasive lobular carcinoma (ILC), with IDC accounting for 70% of all cases (Sivadas, Kok, and Ng, 2022). It is possible that the two subtypes display distinct SLC signatures and populate the different 'sub clusters' seen in the tSNE analysis.

Another important factor that is likely to impact transporter signatures is driver mutations. Unfortunately mutational burden is part of the restricted clinical data in TCGA and in-depth analysis of driver mutations was not conducted within this study.

Three different approaches were used to identify samples coming from an acidic microenvironment, and we found that there was little overlap between the hits they

identified (Figure 3.6). One possible explanation for this is that acidosis could be caused by a variety of factors. Perhaps clinical samples where acidosis occurred as a result of a highly glycolytic phenotype are in fact different from sample where it was caused by high expression of carbonic anhydrases alone.

The Acidosis proxy which is employed here, was identified by J. L.-Y. Chen et al. (2008) in primary human mammary epithelial cells subjected to lactic acidosis, low pH or hypoxia. The original study identifies 1585 genes upregulated in acidosis. Only the top 10 were used for the current analysis. It was also attempted to use a variety of larger numbers of genes but changes in the final outcome (lists of upregulated SLCs) were minimal (data not shown).

The gene set of 'Rate limiting genes in glycolysis' (Tanner et al., 2018) was selected because highly glycolytic cells have been well documented to acidify the microenvironment. However, some studies suggest in cells already growing in conditions of acidosis, glycolytic activity is reduced (Prado-Garcia, Campa-Higareda, and Romero-Garcia, 2020a; H. Wu, M. Ying, and X. Hu, 2016b). The glucose transporters SLC2A1 and SLC2A3 and lactate transporter SLC16A3 are part of the Glycolysis proxy. To validate the analysis method, these three transporters were excluded from the gene set, before running the differential expression analysis. All three were still significant hits across cancer types (data not shown), confirming glycolytic samples are being identified and the method is technically sound.

Overall there was little overlap between samples identified as acidic and samples identified as hypoxic. This suggests acidosis could occur independently of hypoxia across cancer types. The largest overlap was seen between the Hypoxia and Glycolysis streams. This is unsurprising as the relationship between highly glycolytic phenotypes and HIF-1a expression is well characterised (Corbet and Feron, 2017a; Wykoff et al., 2000).

Because the 3 analysis streams identified different clinical samples as acidic, it is unsurprising that they also yielded different SLC transporters as upregulated in acidic conditions. Despite this diversity in individual SLCs, a number of SLC families came up as upregulated in acidosis across the streams - SLC25 family of mitochondrial transporters, SLC27 (fatty acid transporters), SLC35 (nucleotide sugar

transporters), SLC39 (Zinc transporters) and SLC7 (amino acid transporters). Encouragingly, amongst the hits were also SLC transporters with known links with acidosis.

The only transporter universally identified as a hit across all analysis streams was SLC6A8 in COAD (Figure 3.7). SLC6A8 was also upregulated in hypoxia. Consistent with this, SLC6A8 was one of the most upregulated transporters further away from blood vessels in data from the Kumar et al. (2019) study. SLC6A8 was additionally associated with unfavourable prognosis in Kaplan-Maier analysis in COAD, LUAD and LIHC.

Single cell RNAseq analysis of clinical samples confirmed SLC6A8 is mostly expressed in cancer cells, especially in late stage LUAD (Figure 3.17). This suggests the increase of SLC6A8 in the bulk TCGA analysis is likely to derive from tumour rather than stromal cells. SLC6A8 and SLC2A1 were both upregulated in late stage versus early stage LUAD. These findings are consistent with the fact that SLC6A8 was associated with unfavourable prognosis in LUAD in Kaplan-Meier analysis of TCGA data (Figure 3.13). They also suggest creatine metabolism plays a role in cancer progression, especially in late stage LUAD.

These findings, as well as the unclear role of creatine in cancer, made SLC6A8 a transporter of interest and it was selected for experimental characterisation.

Chapter 4

Investigating the role of SLC6A8 in cell adaptation to acidosis

Our computational analysis of SLC signatures in clinical samples indicated that the creatine transporter SLC6A8 is upregulated in tumours with gene expression signatures associated with an acidic microenvironment. The transporter was identified in both Lung adenocarcinoma (LUAD) and Colorectal adenocarcinoma (COAD), and stratification of patients based on SLC6A8 expression level demonstrated negative prognostic value in both cancer types. This chapter focuses on our experimental characterisation of SLC6A8, using lung and colon cancer cell lines, to examine the effect of creatine and the creatine transporter on cancer cells proliferation and metabolism under acidic conditions.

4.1 Setting up an *in vitro* pH system

To study cancer cells in an acidic microenvironment *in vitro*, a stable pH system had to be established. The average pH in tumour-induced acidosis has been reported to be pH 6.8 (Griffiths, 1991; Pellegrini et al., 2018; Raghunand et al., 1999) which was therefore selected as representative of an acidic microenvironment. Two main buffering systems are used to adjust pH in cell culture - the Bicarbonate system and Non-Volatile Buffers (NVBs), most commonly the Good's buffers (Michl, K. C. Park, and P. Swietach, 2019). Both of these systems were evaluated for the current study. The Bicarbonate system controls pH based on the interaction of bicarbonate with CO_2, a relationship described by the Henderson-Hasselbalch equation (Hasselbalch, 1917; Michl, K. C. Park, and P. Swietach, 2019). The amount of bicarbonate needed to achieve the desired pH in a 5% CO_2 incubator was calculated to be 24 mM for pH 7.4 and 6.15 mM for pH 6.8. It is important to note that bicarbonate is a substrate for a number of enzymatic reactions, with a consistent concentration in blood of 20-30 mM (Morris, Murphy, and Kitabchi, 1986), therefore reducing it to unnaturally low level could have physiological effects, independent of pH. Good's buffers are zwitterionic compounds, containing both an acidic and a basic group. They buffer media pH by forming complexes with Na^+, K^+, Mg^{2+} and Ca^{2+} ions (Good et al., 1966). The advantage of the Good's system is that the same amount of bicarbonate is available to cells in both conditions. HEPES and PIPES were selected amongst other Good's buffers based in their pK_a of 7.31 (HEPES) and 6.66

(PIPES) at 37°C. This makes them suitable for maintaining a pH range of 6.8 - 8.2 (HEPES) and 6.1 - 7.5 (PIPES). In order to maintain the media formulation consistent, both buffers were used at a concentration of 25 mM and pH was adjusted using 37% HCL or 5N NaOH, and tested empirically to ensure that the correct pH was maintained after incubation at 5% CO_2. In total, 6 media formulations were tested across both systems (Figure 4.1A):

Formulation A: 24 mM Bicarbonate (pH 7.4)
Formulation B: 24 mM Bicarbonate, 25mM HEPES, 25 mM PIPES (pH 7.4)
Formulation C: 24 mM Bicarbonate, 25mM HEPES, 25 mM PIPES (pH 6.8)
Formulation D: 6.15 mM Bicarbonate (pH 7.4)
Formulation E: 6.15 mM Bicarbonate, 25mM HEPES, 25 mM PIPES (pH 6.8)
Formulation F: 6.15 mM Bicarbonate, 25mM HEPES, 25 mM PIPES (pH 7.4)

The 6 formulations were tested on two colorectal cell lines - HCT116 and RKO. Cell lines were grown in each formulation in a 5% CO_2 incubator for 4 hours. To assess any changes in metabolism that might be caused by either the use of non-physiological compounds (HEPES and PIPES) or sub-physiological levels of bicarbonate, intracellular metabolite abundances were measured by Gas chromatography-mass spectrometry (GC-MS) (Figure 4.1B).

The abundance of several metabolites was decreased in low bicarbonate media at pH 6.8 (Formulation D) for both cell lines. This effect was not observed in pH 6.8 media with standard bicarbonate levels that has been supplemented with HEPES/PIPES (Formulation C). We found no consistent trends in metabolite abundance between cell lines with HEPES/PIPES supplementation, apart from a decrease in intracellular putrescine. Based on these results, the HEPES/PIPES buffering system was selected to use going forward with the project.

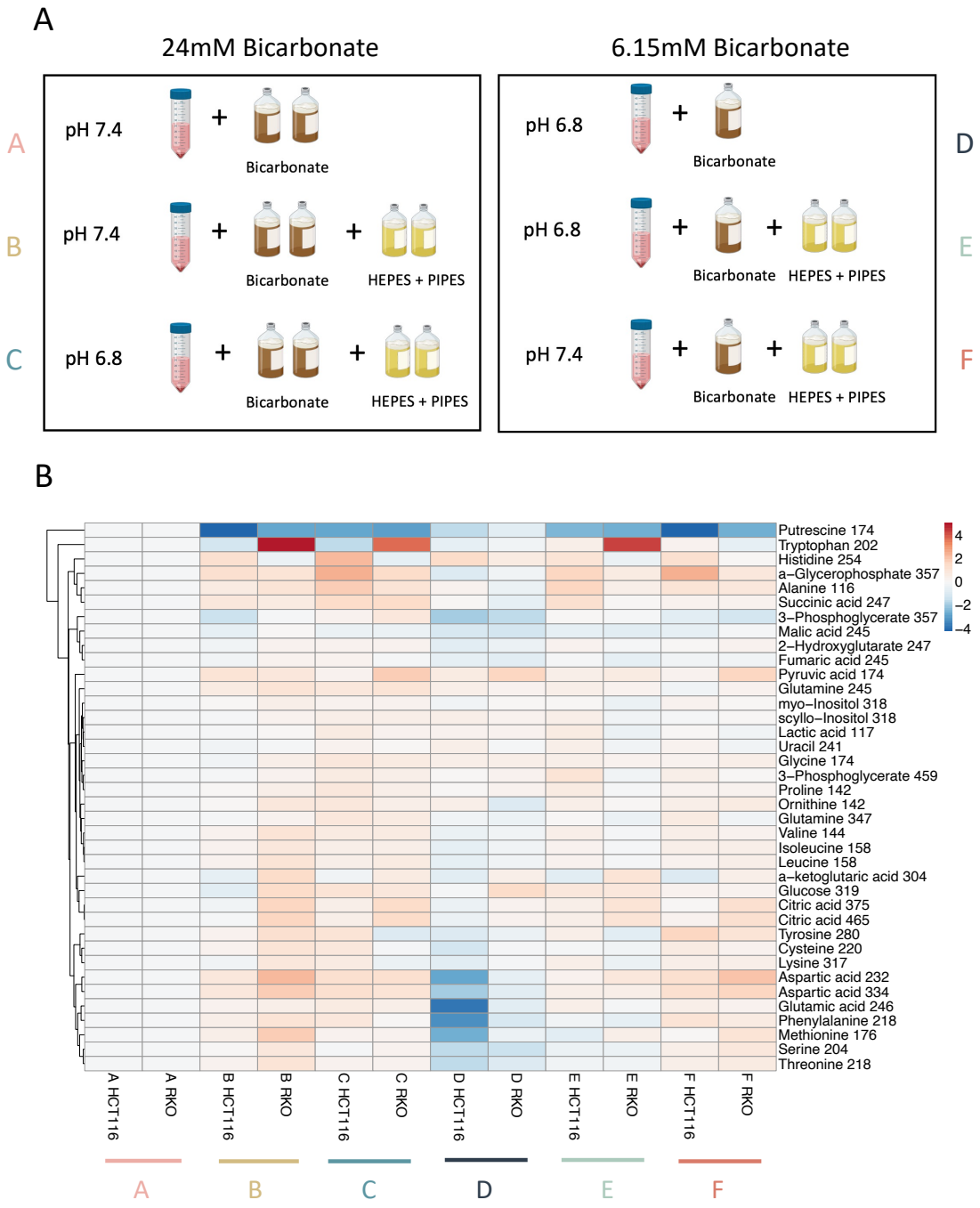


Figure 4.1: Setting up an *in vitro* pH system - (A) Six media formulations were tested, with pH adjusted with either bicarbonate or HEPES/PIPES (B) Intracellular metabolite abundance after 4 hours of incubation in indicated media formulations. Scale represents Log_2(Fold change) in metabolite abundance relative to RPMI control (pH 7.4, 24 mM Bicarbonate).

4.2 Creatine supplementation does not affect growth rates in acidic pH

4.2.1 Creatine supplementation does not affect growth rates in standard and nutrient-deprived media

As the creatine transporter SLC6A8 was found to be upregulated in tumours with more acidic signatures, we hypothesised that creatine supplementation may have a beneficial effect on cell growth under low pH conditions. The physiological concentration of creatine in human blood is reported to be between 20 and 100 µM (Poortmans et al., 1997; Markus Wyss and Kaddurah-Daouk, 2000). A concentration of 100 µM was therefore selected for culture media supplementation. The lung cancer cell line A549 and colon cancer cell line HCT116 were selected to use as models of tumour growth. Creatine was supplemented in HEPES/PIPES-buffered RPMI media and pH was adjusted to either pH 7.4 or pH 6.8. Both cell models were able to grow in the HEPES/PIPES buffered formulation, showing minimal changes in growth rates compared to standard RPMI (Figure 4.2A). In addition, both cell models showed comparable growth rates in both neutral and acidic pH. However, creatine supplementation did not affect growth rates in either pH condition, for either of the cell lines (Figure 4.2B).

RPMI is a highly nutritious medium, designed to sustain optimal cell growth. This is not necessarily representative of the conditions experienced by cancer cells within the tumour microenvironment. Areas of acidosis could coincide with regions of poor nutrient availability in solid tumours, since both can result from reduced blood supply. To mimic these microenvironment conditions, cells were grown in glutamine-free or glucose-free RPMI formulations. As before, all formulations were prepared with and without creatine supplementation and pH was adjusted to either pH 7.4 or pH 6.8. As expected, glucose and glutamine deprivation led to a decreased growth rate in both cell lines compared to full RPMI control (Figure 4.3A-B). Interestingly, under glucose-starved conditions, both A549 and HCT116 sustained growth better at pH 6.8 compared to pH 7.4 (Figure 4.3A). A549 plateaued between 40-50% confluence at pH 7.4, but were able to reach around 90% confluence at pH 6.8. HCT116

maintained growth rates comparable to control RPMI for 40 hours at pH 7.4, and up to 90 hours at pH 6.8. In glutamine-free RPMI, A549 cells plateaued around 50% confluence in both pH conditions (Figure 4.3B). HCT116 plateaued between 50-60% confluence at pH 7.4, but were able to reach 90% confluence at pH 6.8.

4.2.2 Creatine pre-loading does not affect growth rates in nutrient-deprived media

We hypothesised that creatine supplementation prior to nutrient deprivation could increase pools of phospho-creatine and as such have a stronger impact on cell growth. In the absence of major carbon sources used for ATP production (such as glucose and glutamine), phospho-creatine could be used to replenish ATP levels. To test this hypothesis, cells were grown in full RPMI, supplemented with or without 100 µM creatine for 24 hours, before exposing them to a nutrient-deprived media formulation. As before, glucose-free and glutamine-free RPMI was pH-adjusted using the HEPES/PIPES system. Consistent with previous observations, both A549 and HCT116 reached higher confluence at pH 6.8 compared to pH 7.4 in glucose-deprived media (Figure 4.4A). Creatine pre-loading however did not improve growth rates in either of the cell lines. In the glutamine-free formulation, HCT116 reached higher confluence in pH 6.8 compared to pH 7.4, while A549 plateaued around 50% confluence in both pH conditions (Figure 4.4B). However, creatine pre-loading had no significant impact on growth rates for either of the two cell lines in either pH condition.

4.2.3 Knockdown of the creatine transporter SLC6A8 does not affect growth rates

The results from creatine supplementation experiments were further confirmed by creating SLC6A8 knockdowns in A549 and HCT116, using a short-hairpin RNA interference (shRNA) based approach. Intrinsically, HCT116 has a higher expression of SLC6A8 compared to A549, according to expression data acquired from the CCLE database. (Figure 4.5A). Six shRNAs were initially tested, and transporter expression was confirmed by qPCR. shRNA 410 showed best results, reducing SLC6A8

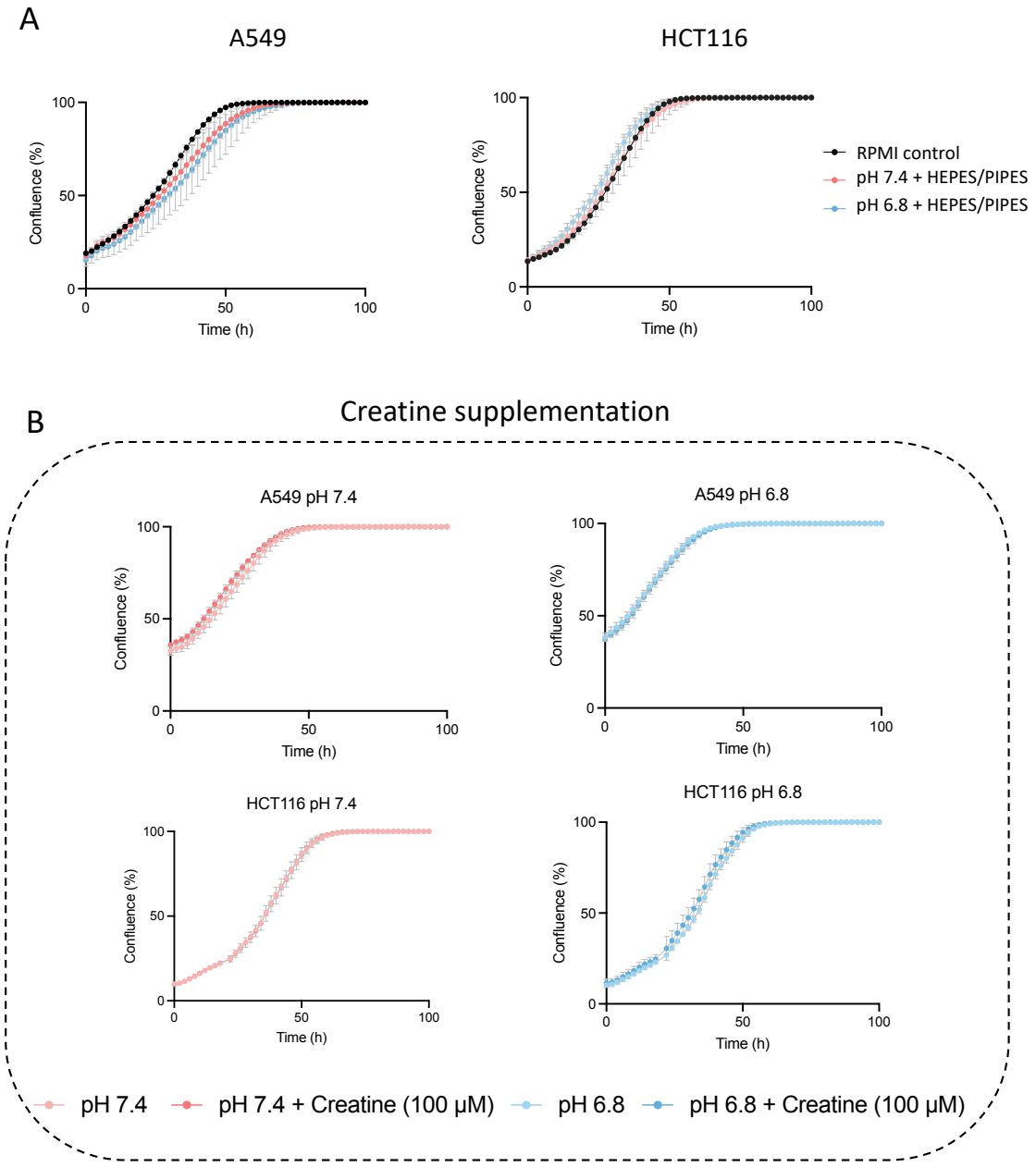


Figure 4.2: Creatine supplementation - in full media (A) Cell growth in HEPES/PIPES buffered media at pH 7.4 and pH 6.8 compared to standard RPMI control (B) Cell growth in HEPES/PIPES buffered RPMI supplemented with 100 µM creatine at pH 7.4 and pH 6.8. Experiments shown are representative of n=3 biological replicates.

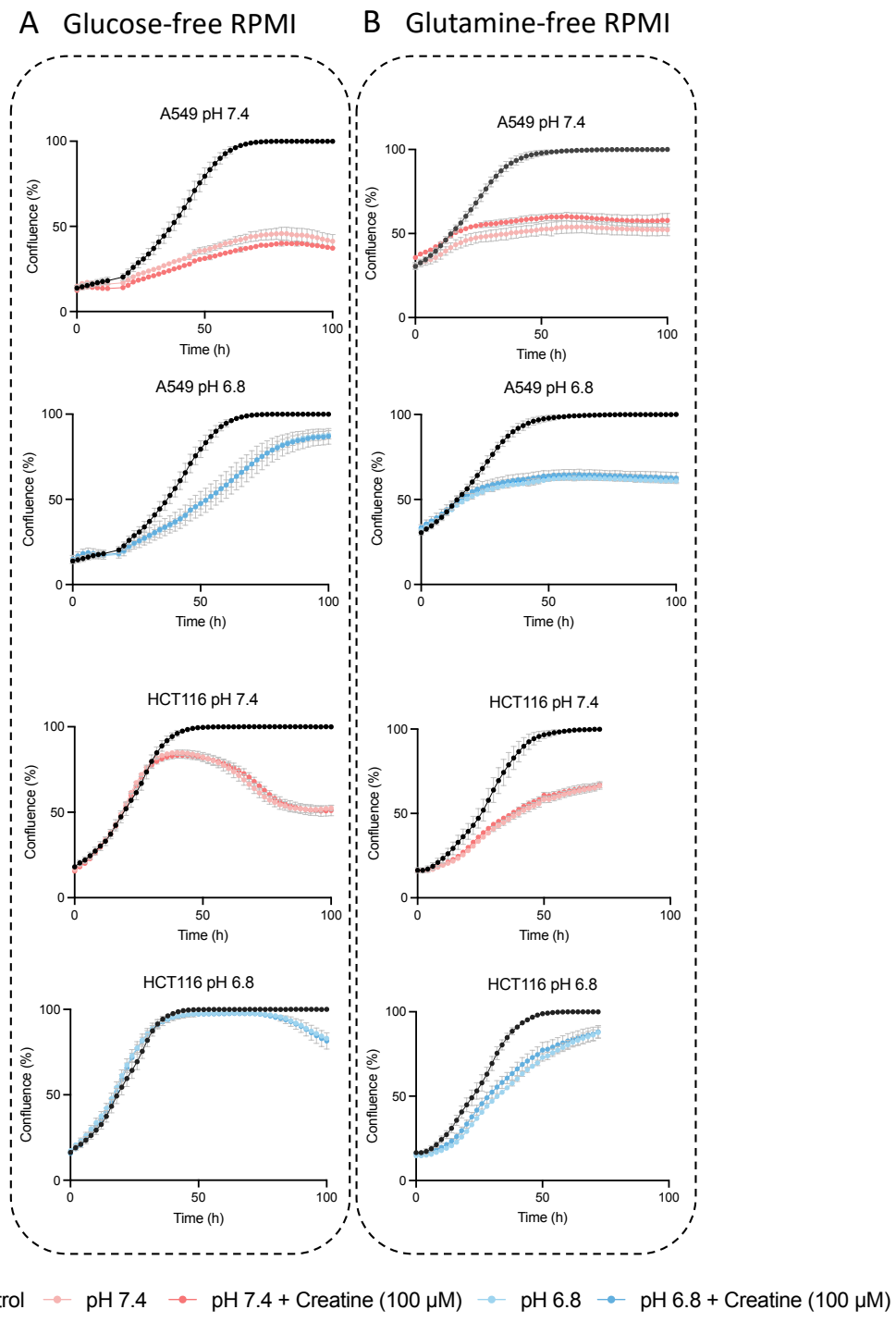


Figure 4.3: Cell proliferation with and without creatine supplementation in nutrient deprived media - (A) in glucose-free media (B) glutamine-free media. Experiments shown are representative of n=3 biological replicates.

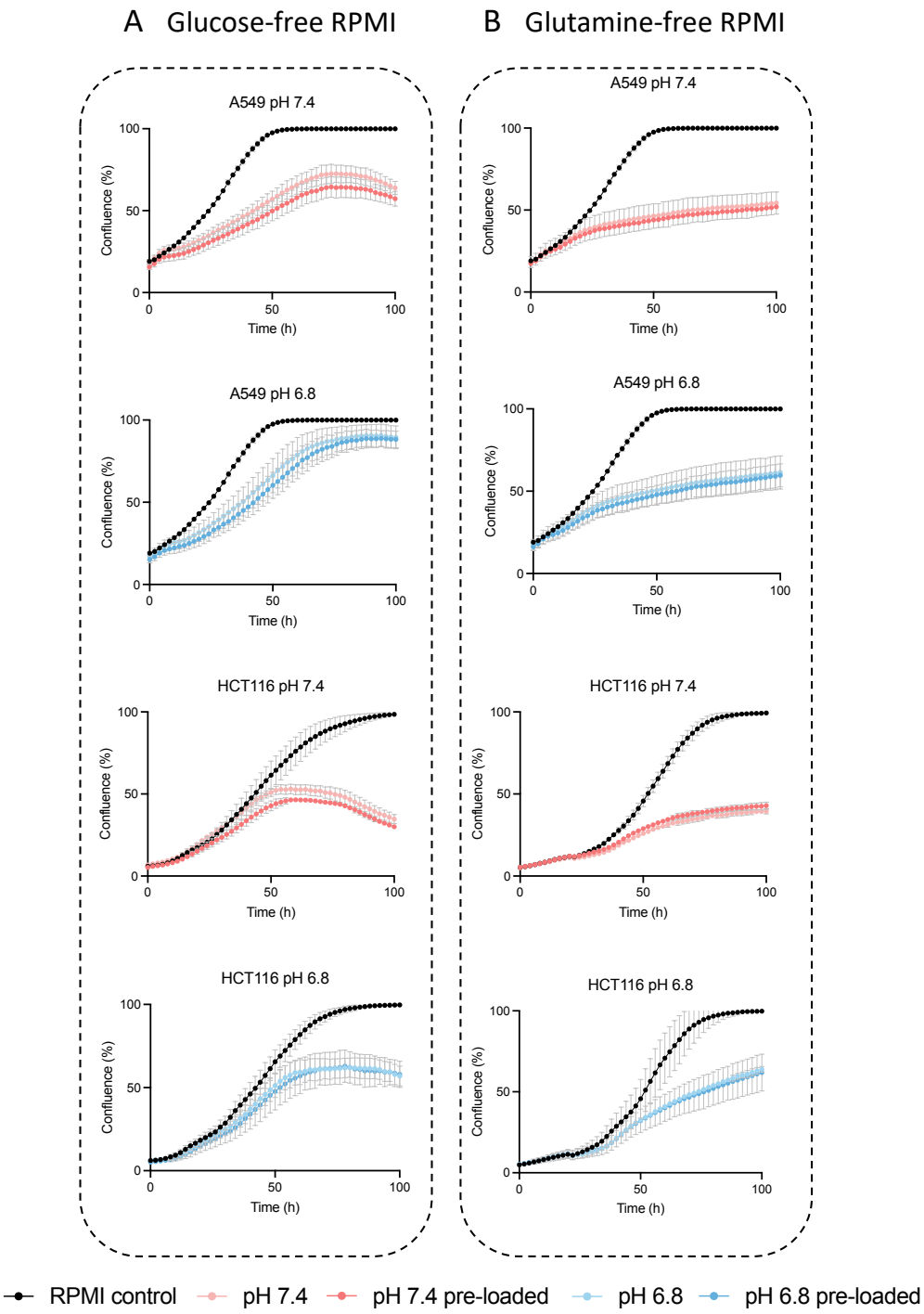


Figure 4.4: Creatine pre-loading - (A) in glucose-free media (B) glutamine-free media. Cells were incubated in RPMI, supplemented with 100 µM creatine for 24 hours, before being placed in nutrient-deprived media. No creatine was supplemented in the nutrient-deprived media. Time point 0 signifies media change to nutrient-deprived media. Experiments shown are representative of n=3 biological replicates.

expression by 83% for HCT116 and 84% for A549 (Figure 4.5B). Growth rates of the knockdown strains and an empty vector (EV) control were assessed in full RPMI at pH 7.4 and pH 6.8. Consistent with creatine supplementation experiments, we observed no difference in growth rates for either of the cell models in either of the pH conditions (Figure 4.5C).

4.2.4 Creatine supplementation does not affect growth rates in hypoxia

Although creatine supplementation had a minimal effect on cell growth in acidosis, it is important to remember that areas of acidosis often overlap with areas of hypoxia within solid tumours. Since SLC6A8 appeared as upregulated in both hypoxia and acidosis during the TCGA computational analysis (Chapter 3), it is possible that SLC6A8 only provides cancer cells with a competitive advantage when both hypoxia and acidosis are present. To explore this possibility, growth experiments were conducted in a hypoxia chamber, with 1% oxygen, by SRB assay. Western blot for HIF-1a and HIF-2a in A549 cells confirmed increase of both markers under hypoxic conditions (Figure 4.6A). A549 and HCT116 both demonstrated reduction in growth rates in hypoxic conditions compared to normoxia. Creatine supplementation however did not rescue growth rates for either of the cell models (Figure 4.6B-C). These results were further confirmed with SLC6A8 knockdown strains for HCT116. SLC6A8 knockdown did not show reduced growth rates compared to an empty vector control at either pH 7.4 or pH 6.8 (Figure 4.6D). This suggests SLC6A8 expression has no direct impact on growth rates in acidosis combined with hypoxia.

4.2.5 Quantification of creatine in foetal calf serum

FCS is a natural product, with no defined composition. For that reason, we considered the possibility that creatine is already present in its formulation, masking the effect of creatine supplementation. To measure creatine concentration, a Liquid chromatography-mass spectrometry (LC-MS) method was developed by the MRC-LMS Mass Spectrometry Facility, allowing the detection of both creatine and its byproduct creatinine (Figure 4.7A). RPMI media, lacking FCS supplementation, was used as a negative control. Creatine was in fact detected in FCS, as well as in

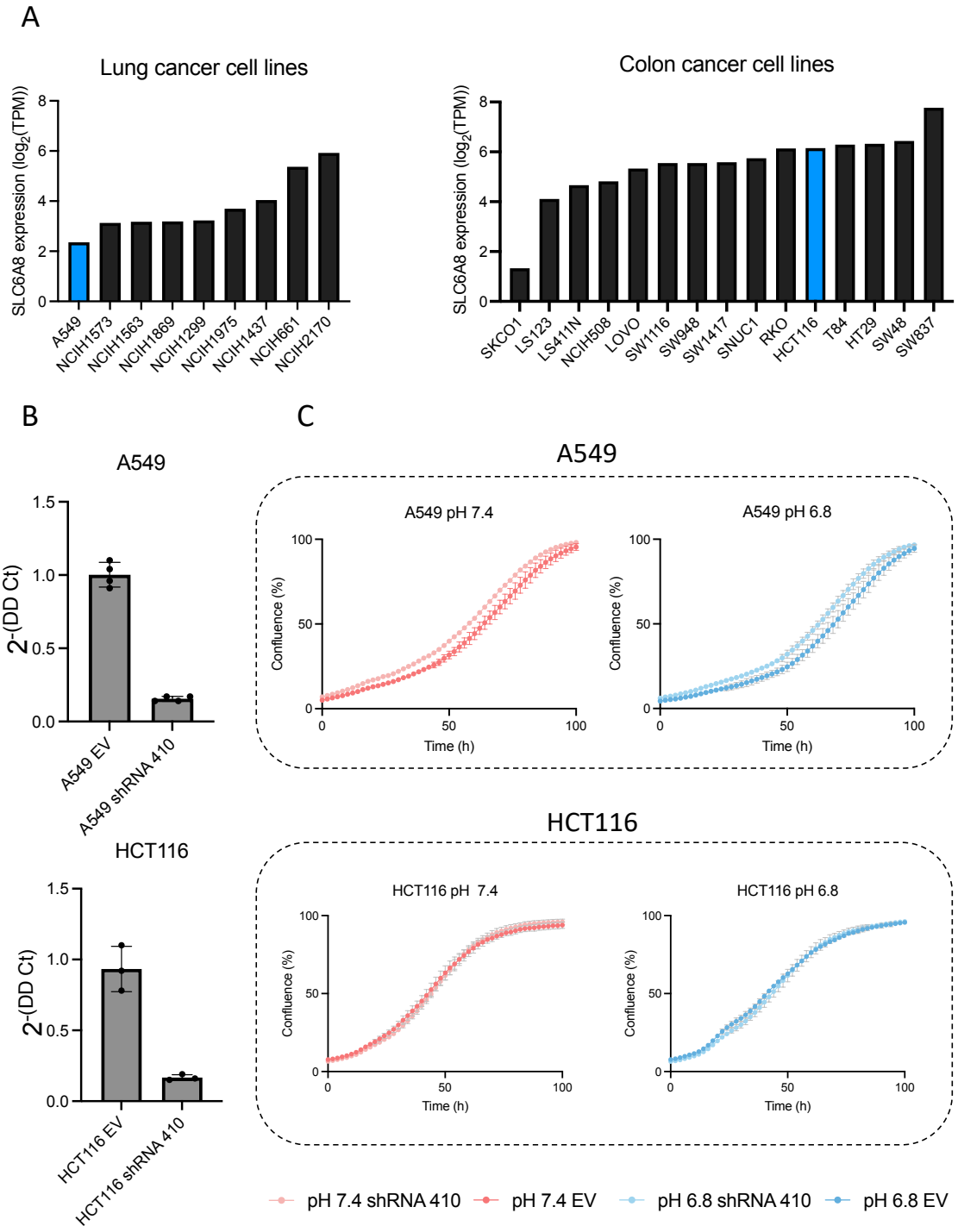


Figure 4.5: SLC6A8 knockdown - (A) SLC6A8 expression across lung and colorectal cancer cell lines available in the lab. Expression data acquired from the CCLE database. Selected cell models shown in blue (B) shRNA 410 reduced SLC6A8 expression by 70% in A549 and HCT116. Expression detected by qPCR and shown as percentage of Empty vector (EV) control (C) Knockdown of SLC6A8 had no significant effect on growth rates in full RPMI media at either pH 7.4 or pH 6.8. Data showing a representative experiment from n = 3 biological replicates.

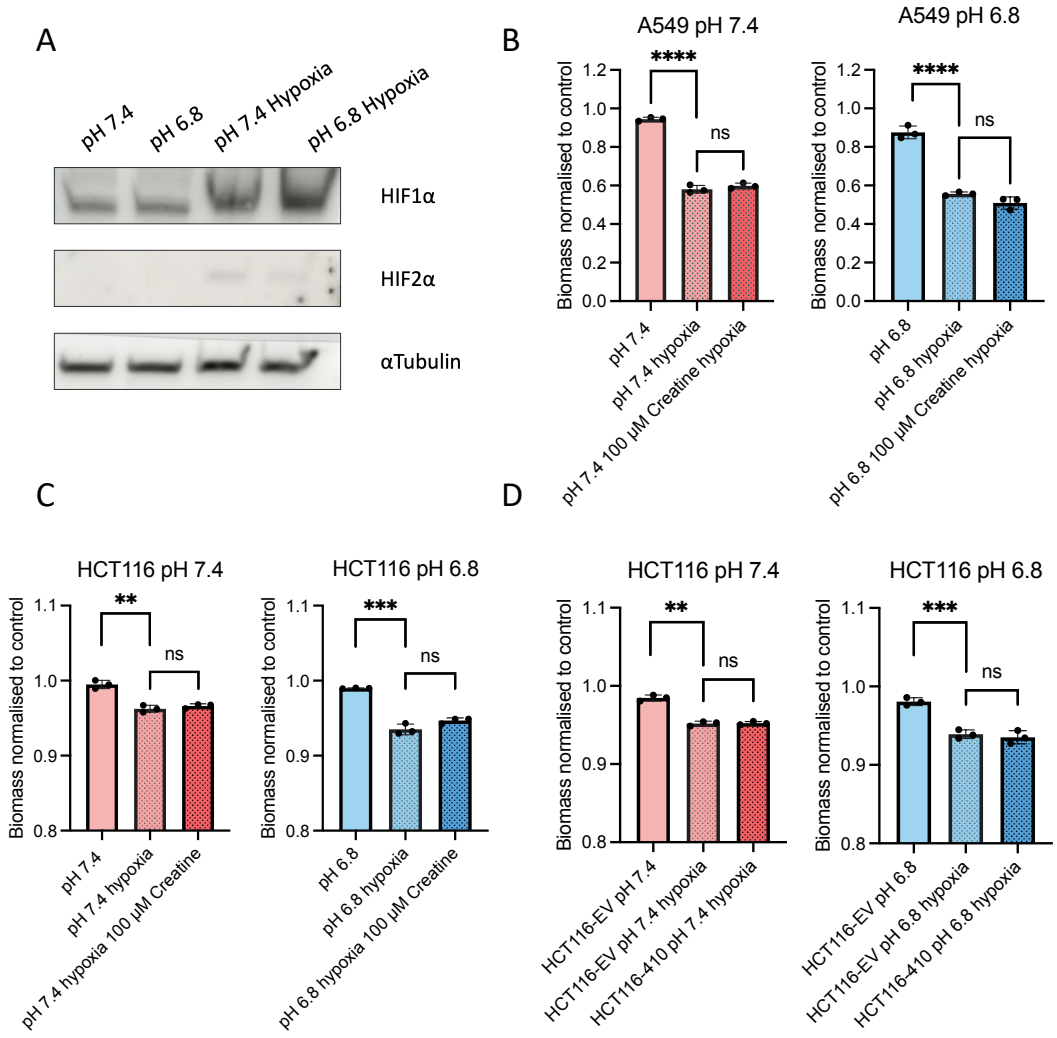


Figure 4.6: Creatine supplementation in hypoxia - (A) Western blot showing HIF-1a and HIF-2a in A549 cells (B) Growth rates of A549 in hypoxia as detected by SRB assay. Confluence shown as a percentage of A549 growing in full RPMI in normoxia (C) Growth rates of HCT116 in hypoxia as detected by SRB assay. Confluence shown as a percentage of HCT116 growing in full RPMI in normoxia (C) Knockdown of SLC6A8 in HCT116. Knockdown strain (410) showed comparable growth rate to empty vector control (EV). Confluence shown as a percentage of HCT116 growing in full RPMI in normoxia. Experiments shown are representative of n=3 biological replicates for B and C and n=2 biological replicates for D. P values obtained by a one-way ANOVA

FCS-supplemented RPMI (Figure 4.7B). Serum dialysis appeared to deplete creatine concentration almost entirely. However, creatine supplemented media had approximately 3 times higher creatine concentration compared to RPMI with FCS alone. In addition, creatine supplementation did not increase the amount of detected creatinine (Figure 4.7B). This suggests the rate of non-enzymatic conversion of creatine to creatinine is slow in RPMI and creatine remains available for cell uptake.

To quantify creatine concentration more accurately, a calibration curve was prepared using creatine-(methyl-d_3). The final creatine concentration in FCS-supplemented RPMI was calculated to be 15.8 µM. RPMI supplemented with FCS and creatine contained 82.5 µM. Although these concentrations are lower than expected (considering the 100 µM creatine supplementation), they clearly demonstrate that creatine supplementation significantly increases creatine concentration in media.

SLC6A8 has a reported affinity estimate (IC_{50}) for creatine of 35 µM (Farr et al., 2022). Creatine concentration in FCS-supplemented media is substantially lower. These results confirm FCS supplementation is insufficient to saturate SLC6A8, and is unlikely to fully mask physiological effects caused by creatine supplementation.

4.2.6 Creatine supplementation does not affect growth rates in RPMI supplemented with dialysed FCS

Although we established that pre-existing creatine in FCS-supplemented RPMI is not sufficient to saturate SLC6A8, it could potentially mask subtle effects creatine has on cell proliferation. To test this experimentally, A549 and HCT116 cells were incubated in RPMI supplemented with dialysed FCS or full FCS as a control. FCS dialysis was demonstrated to reduce creatine below the limit of detection by LC-MS (Figure 4.7B). For both cell lines, creatine supplementation in these conditions had no effect on growth rates in either of the pH conditions tested (Figure 4.8). These results confirm the creatine available in FCS is not the reason for lack of response in supplementation experiments.

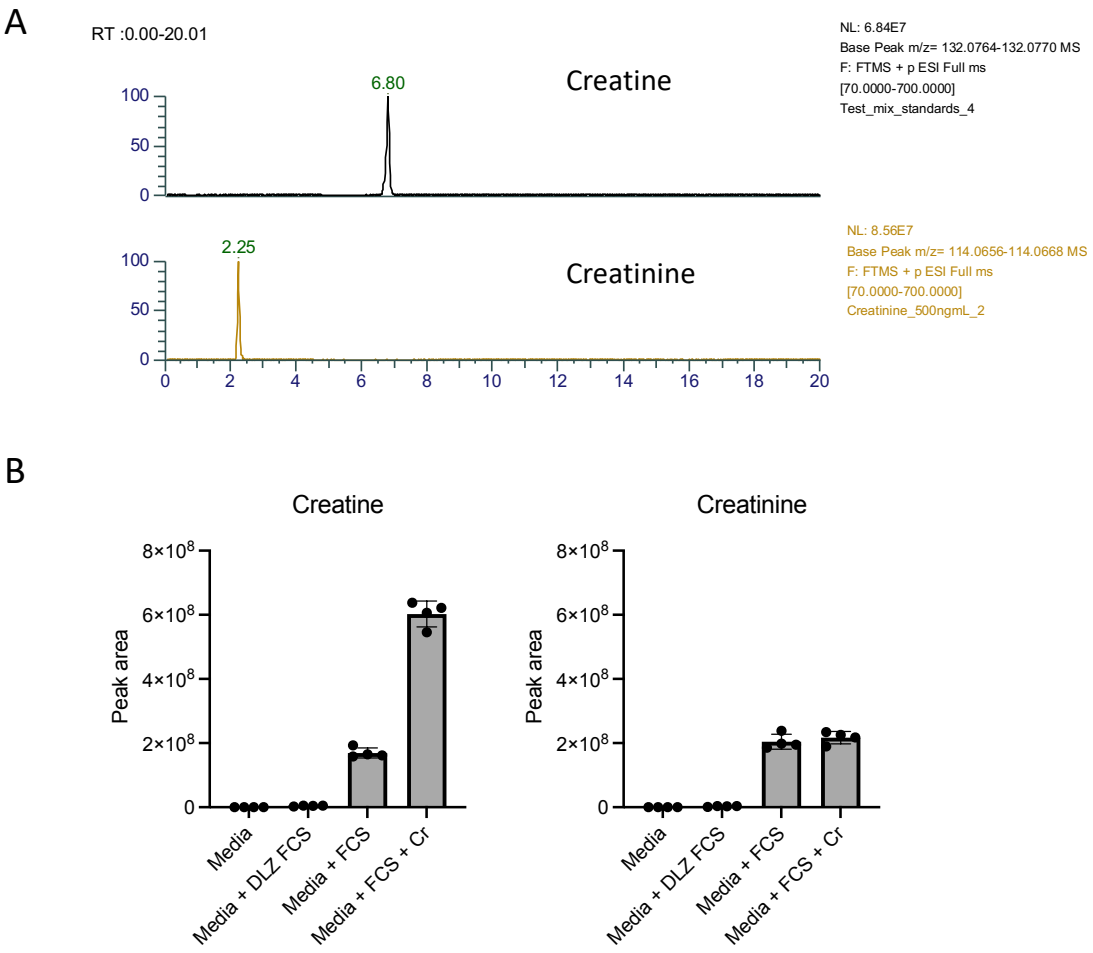


Figure 4.7: Creatine concentration in RPMI - (A) Separation of creatine and creatinine by LC-MS (B) Relative concentration of creatine in RPMI, FCS, dialysed FCS and creatine-supplemented media, as measured by LC-MS. Cr - 100 µM creatine supplementation, DLZ FCS - Dialysed FCS

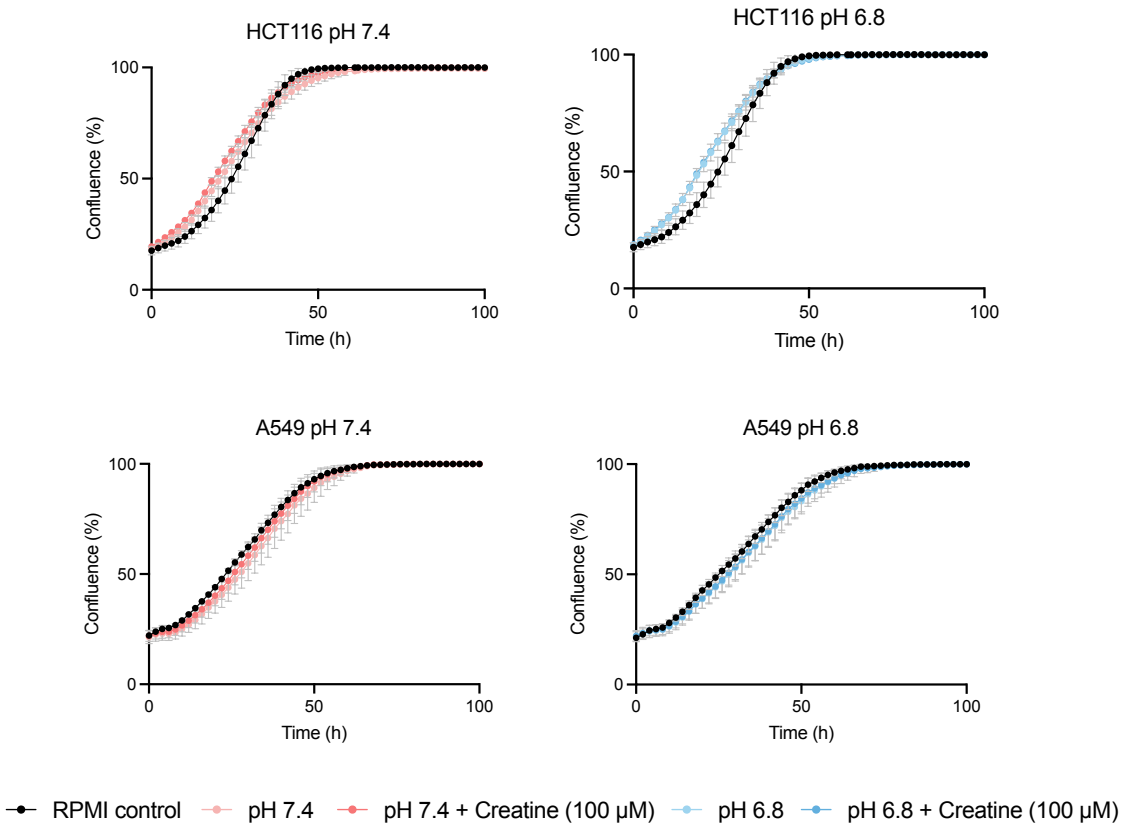


Figure 4.8: Growth rates in RPMI supplemented with dialysed FCS - Both cell lines showed growth rated comparable with RPMI control. Creatine supplementation did not affect growth rates in either of the pH conditions tested. Data shown for a representative experiment from n=3 biological replicates.

4.2.7 Creatine supplementation does not affect growth rates in physiological media

RPMI is one of the most widely used media types in cell culture experiments. It is very rich in nutrients, with a formula optimised for rapid cell proliferation (Moore, Gerner, and Franklin, 1967). To address this and mimic the tumour microenvironment further, growth experiments were also conducted in Human plasma-like media (HPLM) (Cantor et al., 2017). HPLM is a defined-composition media, aiming to represent the conditions in human plasma as closely as possible. We hypothesised creatine could have a stronger impact on cell growth and metabolism in such conditions. HPLM was supplemented with dialysed FCS and pH adjusted with HEPES/PIPES as before. It is important to note that HPLM formulation contains 35 µM creatine.

First we compared growth rates in HPLM and RPMI. Both cell lines demonstrated comparable growth rates in the two formulations (Figure 4.9A-B). As seen previously in RPMI, both A549 and HCT116 grew at comparable rates at pH 7.4 and pH 6.8 in HPLM media. pH adjustment had a minimal effect on cell growth, when compared to HPLM control (containing no HEPES/PIPES). Creatine supplementation of 100 µM made no difference to growth rates in either of the cell lines and in either of the pH conditions.

4.3 Intracellular effects of creatine supplementation

Although we did not observe differences in growth rates under the conditions tested, we wanted to know whether creatine availability has other, perhaps more subtle effects intracellularly. Small differences at the metabolic level could have an impact on cell survival and explain why SLC6A8 is increased in tumours with more acidic signatures. The creatine system is a representative of what is more generally referred to as phosphagen kinase systems - systems that synthesise a 'metabolically inert' pool of phosphorylated compounds. These compounds can then be used to replenesh ATP during periods of metabolic stress or high energetic demand (Canonaco et al.,

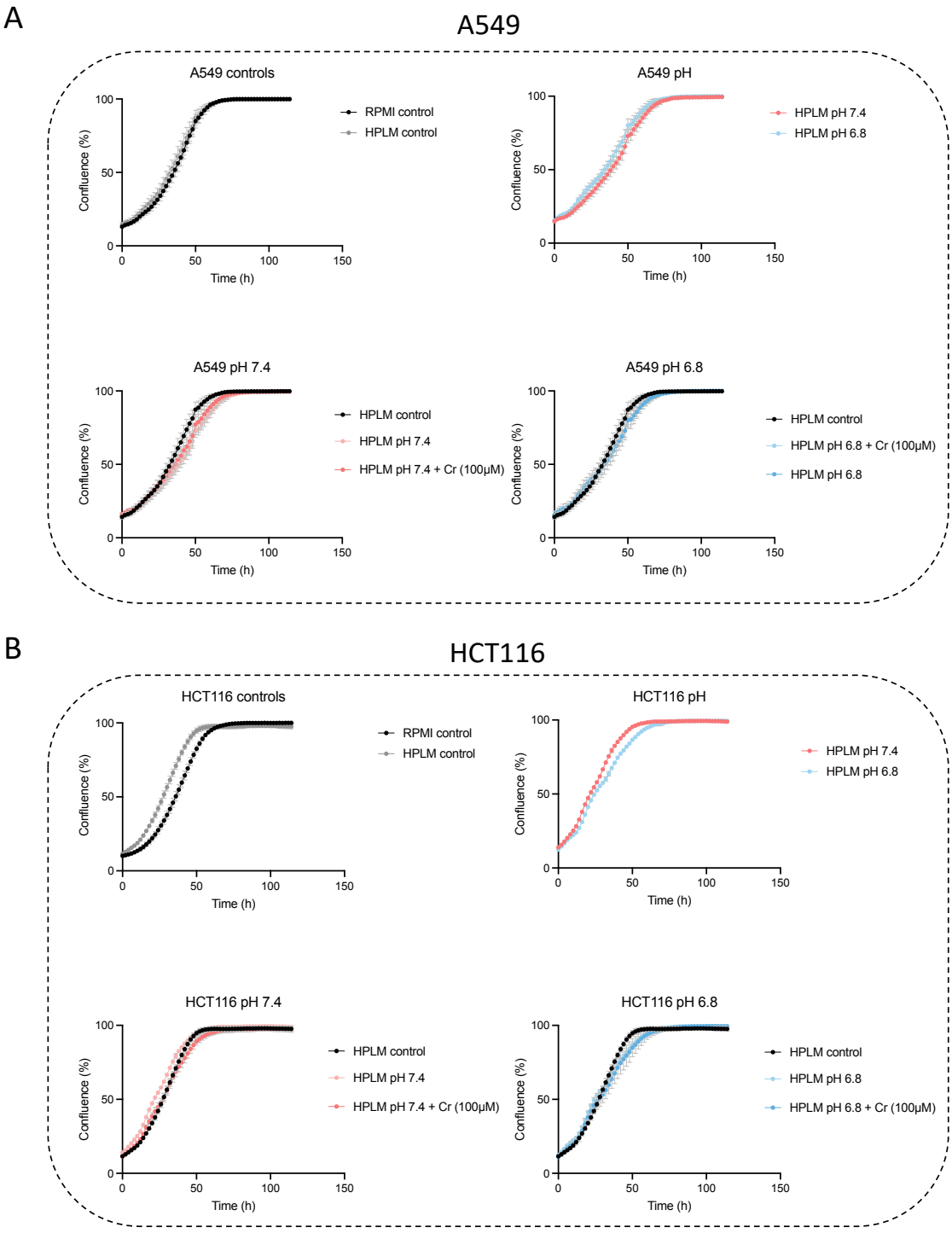


Figure 4.9: Growth rates in HPLM - Growth curves in HPLM in (A) A549 (B) HCT116. Cr - Creatine. Data shown as mean growth rates of n = 3 biological replicates

2002; Theo Wallimann, Malus Wyss, et al., 1992). In addition, the creatine system is involved in proton buffering and hence intracellular pH maintenance in muscle cells (Theo Wallimann, Malus Wyss, et al., 1992). To explore if these mechanisms are conserved in cancer cells, we tested the effect of creatine supplementation on intracellular ATP levels, intracellular pH and metabolite abundance.

4.3.1 Creatine supplementation increases intracellular creatine concentration

First we tested if increasing creatine concentration in media leads to an increase in intracellular creatine concentration. To assess the amount of creatine cancer cells take up from the media, RPMI was supplemented with 100 µM labelled creatine (creatine-(methyl-d_3), referred to here as D_3-creatine). This allowed a distinction between supplemented creatine and endogenous creatine that might be already present intracellularly. Three lung cancer cell lines were grown in RPMI supplemented with D_3-creatine or RPMI control formulation for 24 hours at pH 7.4 and pH 6.8. Both RPMI formulations were supplemented with dialysed serum. Intracellular creatine concentration was measured by LC-MS.

All cell lines showed an increase in intracellular D_3-creatine following D_3-creatine supplementation (Figure 4.10A). This was true in both pH 7.4 and pH 6.8, and intracellular abundance was not pH-dependent.

Endogenous creatine was detected in all cell lines (Figure 4.10B) and endogenous creatine levels were consistent between the two pH conditions. Interestingly, there was a trend towards a decrease in endogenous creatine when exogenous creatine was available to the cells. These results suggest the tested cell lines could be capable of synthesising creatine intrinsically. However, when creatine is available extracellularly, uptake could be the preferred method for obtaining intracellular creatine.

4.3.2 Creatine pre-loading affects intracellular ATP levels at pH 6.8

The conversion of creatine to phospho-creatine by the creatine kinase requires ATP, and the reverse reaction makes ATP available to the cell (Markus Wyss and Kaddurah-Daouk, 2000) (Figure 4.11A). As such, creatine availability can affect intracellular

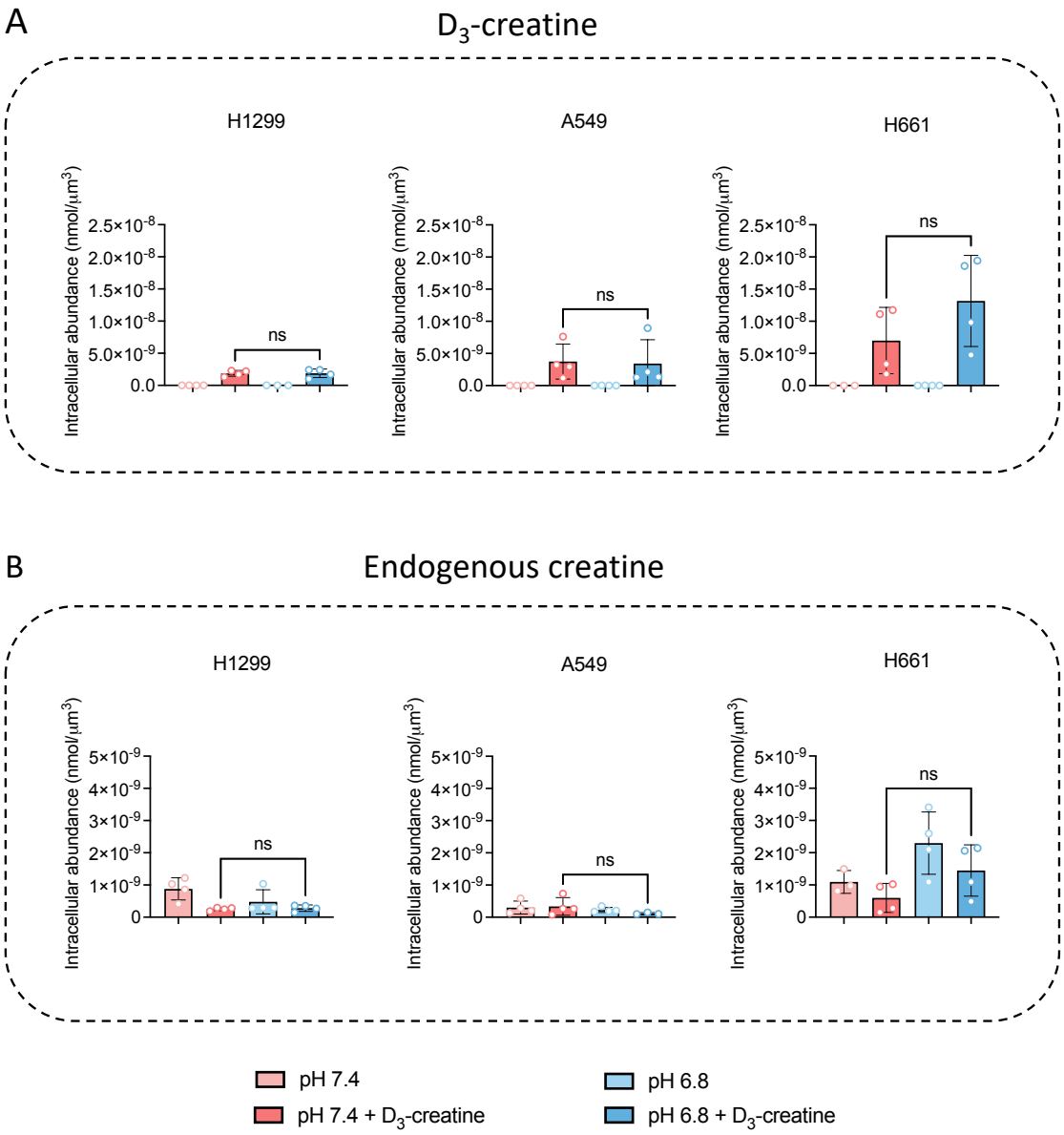


Figure 4.10: Intracellular creatine in lung cancer cell lines - (A) Intracellular abundance of Creatine-(methyl-d_3 (D_3-creatine) following D_3-creatine supplementation in media (B) Endogenous creatine abundance following D_3-creatine supplementation in media. Intracellular creatine levels detected by LC-MS. P values obtained by one-way ANOVA

ATP levels. We wanted to know if acidic pH could have an impact on this process. To test this, cells were pre-loaded with 100 µM creatine in full RPMI media for 24 hours, then exposed to media at pH 6.8 or pH 7.4 as control. Intracellular ATP levels were measured at 1 hour intervals using CellTiter Glo assay.

In control A549 cells, there was no significant difference in intracellular ATP level between the two pH conditions (Figure 4.11B). HCT116 cells had marginally higher intracellular levels of ATP at pH 6.8 compared to pH 7.4 (Figure 4.11C). In both cell lines, cells pre-loaded with creatine showed no change in intracellular ATP levels compared to control at pH 7.4. However, in HCT116, pre-loaded cells had lower levels of intracellular ATP at pH 6.8 compared to control. A similar trend was observed in A549, although it did not reach significance. These results suggest intracellular creatine leads to a decrease in intracellular ATP in acidic pH, but not in neutral pH.

In muscle, ATP depletion by the creatine system is a mechanism to support glycolysis (Theo Wallimann, Tokarska-Schlattner, and Schlattner, 2011). The cytosolic isoform of creatine kinase can be coupled with glycolytic enzymes, which are either involved in ATP production (such as pyruvate kinase (Dillon and Clark, 1990)), or are negatively regulated by ATP (such as phosphofructokinase (PFK) (Kraft et al., 2000)) (see Figure 1.5). In active muscle, this coupling allows ATP to be immediately removed from the glycolytic microcompartment by creatine kinase, incorporating ATP into phosphocreatine, to prevents the inhibition of glycolysis (Theo Wallimann, Tokarska-Schlattner, Neumann, et al., 2007; Theo Wallimann, Tokarska-Schlattner, and Schlattner, 2011). Interestingly, the interaction between creatine kinase and PFK is pH dependent, and it is stronger in acidic pH compared to neutral pH. This is physiologically relevant in muscle, as intracellular pH drops during muscle activation (Theo Wallimann, Tokarska-Schlattner, and Schlattner, 2011). Our results, showing a decrease in intracellular ATP at low pH when creatine is available, suggest a similar mechanism could also be employed by cancer cells. Importantly for this hypothesis, expression data from the CCLE database indicates that both cancer cell models, HCT116 and A549, express the cytosolic form of creatine kinase (CKB) (see Figure 4.20C).

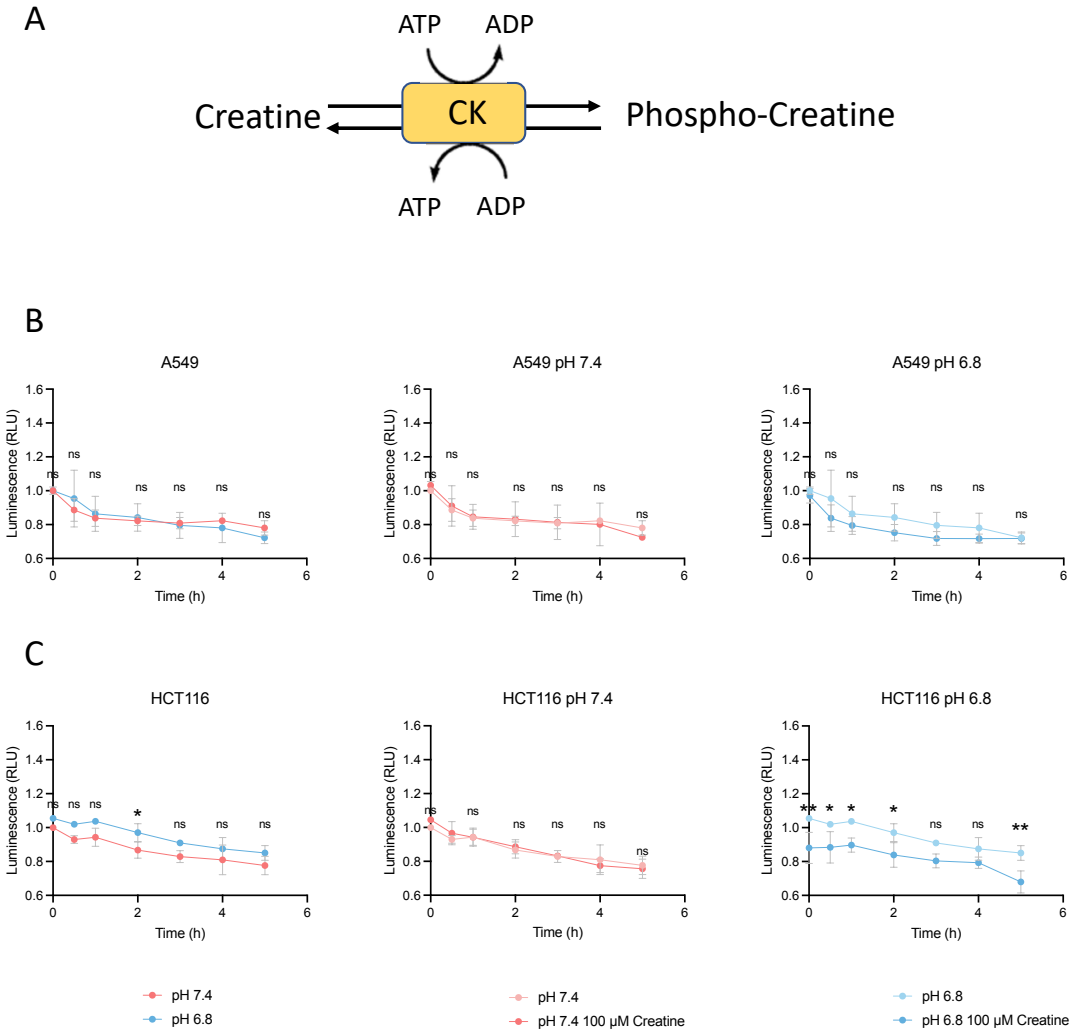


Figure 4.11: Intracellular ATP storage - (A) ATP gets depleted during the conversion of creatine to phosphocreatine by creatine kinase (CK), and ATP is generated during the reverse reaction (B) A549 cells: Intracellular ATP is not significantly different between pH 7.4 and pH 6.8. No significant changes in intracellular ATP following creatine preloading at pH 7.4 or pH 6.8. (C) HCT116 cells: Intracellular ATP is not significantly different between pH 7.4 and pH 6.8. Creatine pre-loading caused an increase in intracellular ATP at pH 6.8. Data shown from n=3 biological replicates, normalised to RPMI at pH 7.4 at time point 0 for each cell line. P values obtained by one-way ANOVA.

4.3.3 Creatine pre-loading does not affect intracellular pH

Many of the cellular adaptations observed in acidosis help cancer cells to maintain intracellular pH constant when extracellular pH drops (Corbet and Feron, 2017b). One proposed function of the creatine system in muscle is proton buffering. The CK reaction in the direction of ATP regeneration utilises not only ADP, but also a proton. As both of these are produced during ATP hydrolysis, the coupling of creatine kinase with ATPases has been proposed as a mechanism of preventing intracellular acidification in muscle cells (Theo Wallimann, Malus Wyss, et al., 1992) (see Figure 1.4). In addition, other phosphagen kinase systems have been demonstrated to aid cell survival in acidosis. For example, the expression of arginine kinase in yeast makes cells more resistant to transient reduction in extracellular pH (Canonaco et al., 2002). To test whether creatine could be involved in a mechanism for maintaining intracellular pH in cancer cells, A549 and HCT116 were pre-loaded with 100 µM creatine for 24 hours. Cells were then transferred from pH 7.4 to pH 6.8, and intracellular pH was measured 5 minutes later using a cSNARF-based method. In both cell lines, a drop of around 0.5 pH unit was observed in intracellular pH (Figure 4.12). There was no significant difference between control and pre-loaded cells.

4.3.4 Creatine supplementation causes an increase in intracellular creatinine

Next we explored the effect of creatine supplementation on cell metabolism. HCT116 and A549 were incubated in media, with and without creatine supplementation, for 24 hours, before extracting polar metabolites and analysing them via GC-MS. Media was supplemented with dialysed serum. Although creatine itself cannot be detected by GC-MS, creatine supplementation caused a significant increase in intracellular creatinine in both cell lines across pH conditions (Figure 4.13A-B). Creatine is converted to creatinine at low rates in a non-enzymatic manner, therefore this result suggests cancer cells are taking up additional creatine when it is available in the media.

Interestingly, low pH was associated with a decrease in intracellular amino acids,

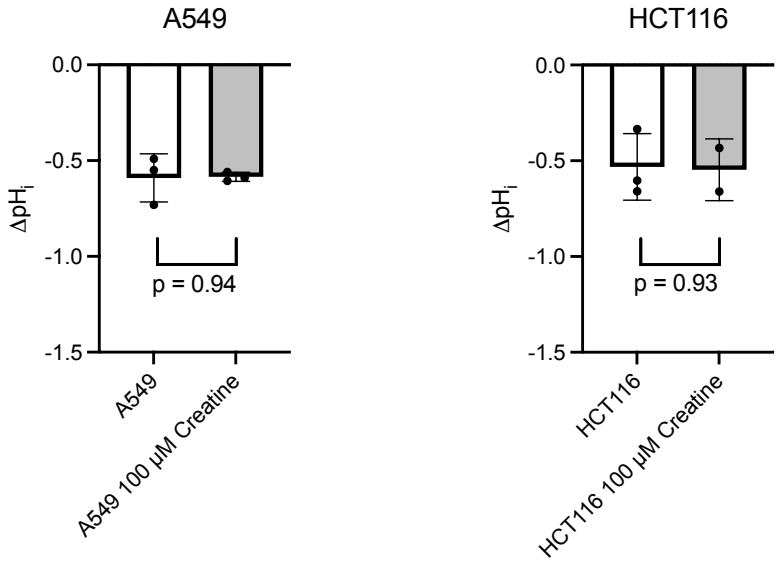


Figure 4.12: Intracellular pH - Change in intracellular pH in A549 and HCT116, 5 minutes after cells were transferred from pH 7.4 into pH 6.8. Creatine pre-loading did not affect change in intracellular pH (δpH_i). Data points show biological replicates. P values obtained by unpaired t test.

independent of creatine supplementation. In HCT116 this trend reached significance for asparagine and aspartate (Figure 4.13C). In A549, the same trend was observed but did not reach significance Figure 4.14).

4.3.5 Knockdown of SLC6A8 decreases intracellular creatinine and putrescine in RPMI

To assess the impact of SLC6A8 knockdown on metabolism, a metabolomics experiment was done with HCT116 empty vector and knockdown strain in RPMI supplemented with dialysed serum and 100 µM creatine. Consistent with the previous metabolomics experiment, low pH was associated with a decrease in intracellular amino acids. This pH-specific effect was conserved across the empty vector control (HCT116-EV) and the knockdown strain (HCT116-410), and included phenylalanine and methionine as previously observed, but also tyrosine and the branched chain amino acids valine, leucine and isoleucine (Figure 4.15).

We also observed an increase in intracellular glucose and fructose in acidic pH. However the majority of glycolytic intermediates remained unaffected (Figure 4.16A).

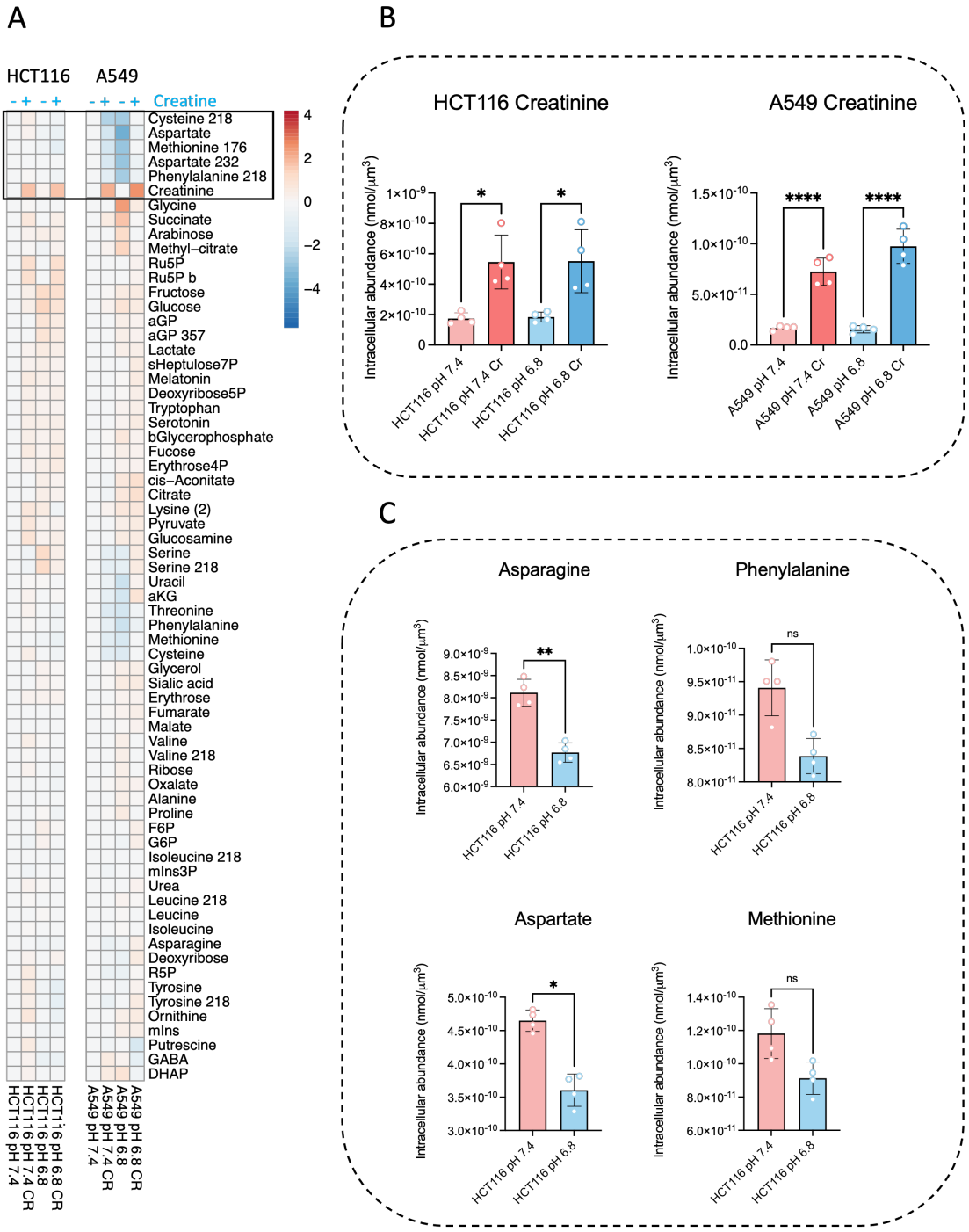


Figure 4.13: Metabolic effect of creatine supplementation (1) - (A) Overall changes in intracellular metabolites in HCT116 and A549 following 24 hours of creatine supplementation. Metabolite abundance has been normalised to cell volume and is shown as $\log_2$(Fold change) over RPMI control at pH 7.4 for each cell line (B) Changes in intracellular creatinine following creatine supplementation for 24h in HCT116 and A549. (C) pH-dependent changes in intracellular amino acids in HCT116. P values obtained by one-way ANOVA

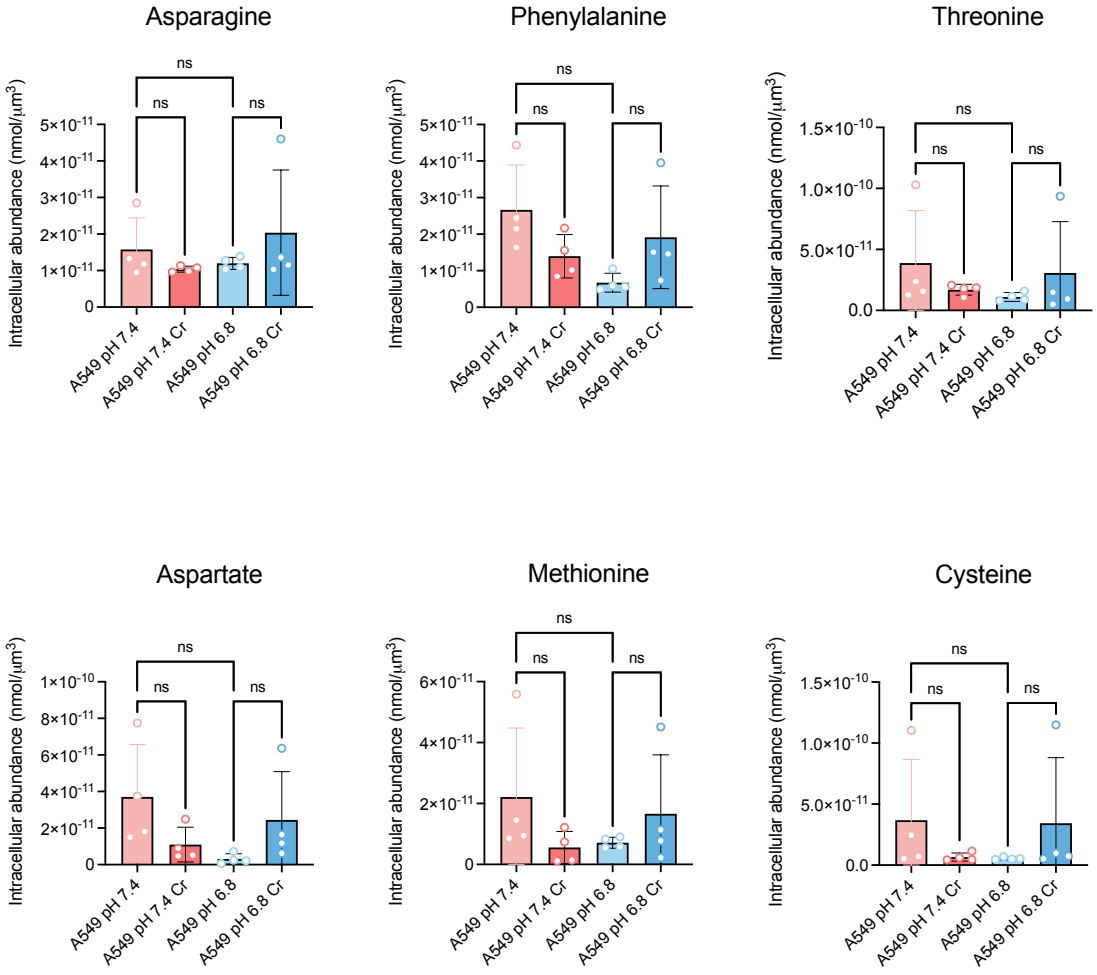


Figure 4.14: Metabolic effect of creatine supplementation (2) - pH-dependent decrease in intracellular amino acids was observed in A549, similar to HCT116. However this trend did not reach significance. Intracellular amino acid abundance was not affected by creatine supplementation. P values obtained by one-way ANOVA

Knockdown of SLC6A8 resulted in a decrease in intracellular creatinine, independently of pH (Figure 4.16B). This is consistent with results from the creatine supplementation experiment (Figure 4.13B), and suggests that knockdown of the transporter does decrease the levels of creatine within the cell. Interestingly, knockdown of SLC6A8 was also associated with a reduction of intracellular putrescine (Figure 4.16B). One explanation for this could be the fact that both putrescine and creatine are synthesised from arginine. It is possible that arginine is preferentially used for creatine synthesis as creatine uptake is impaired by knockdown of the creatine transporter. This would be consistent with the suggestion that HCT116 cells can synthesise creatine intracellularly, as discussed in Section 4.3.1.

4.3.6 Knockdown of SLC6A8 decreases intracellular creatinine and putrescine in physiological media

The metabolic effects of acidic pH were further assessed in HCT116 and A549 cultured in HPLM. As observed previously, low pH was associated with a significant decrease in intracellular amino acids (Figure 4.17A). Affected amino acids included lysine, asparagine, ornithine, tyrosine, phenylalanine, as well as the branched chain amino acids valine, leucine and isoleucine (Figure 4.17B). The increase in intracellular glucose and fructose, previously observed in RPMI, was also evident in physiological media (Figure 4.18).

Finally, we conducted a targeted metabolomics experiment with HCT116 SLC6A8 knockdowns in HPLM (Figure 4.19A). Consistent with what was seen in the parental strain, we observed an increase in intracellular glucose and fructose in acidic pH. For glucose, this effect was conserved between the empty vector control (HCT116-EV) and the SLC6A8 knockdown strain (HCT116-410). For fructose, the effect was lost in HCT116-410 (Figure 4.19B). We also observed a pH-dependent decrease in amino acids, including valine and phenylalanine. As previously seen in RPMI, knockdown of the creatine transporter resulted in a decrease in intracellular creatinine and putrescine (Figure 4.19C). However, this trend only reached significance at pH 7.4 in HPLM.

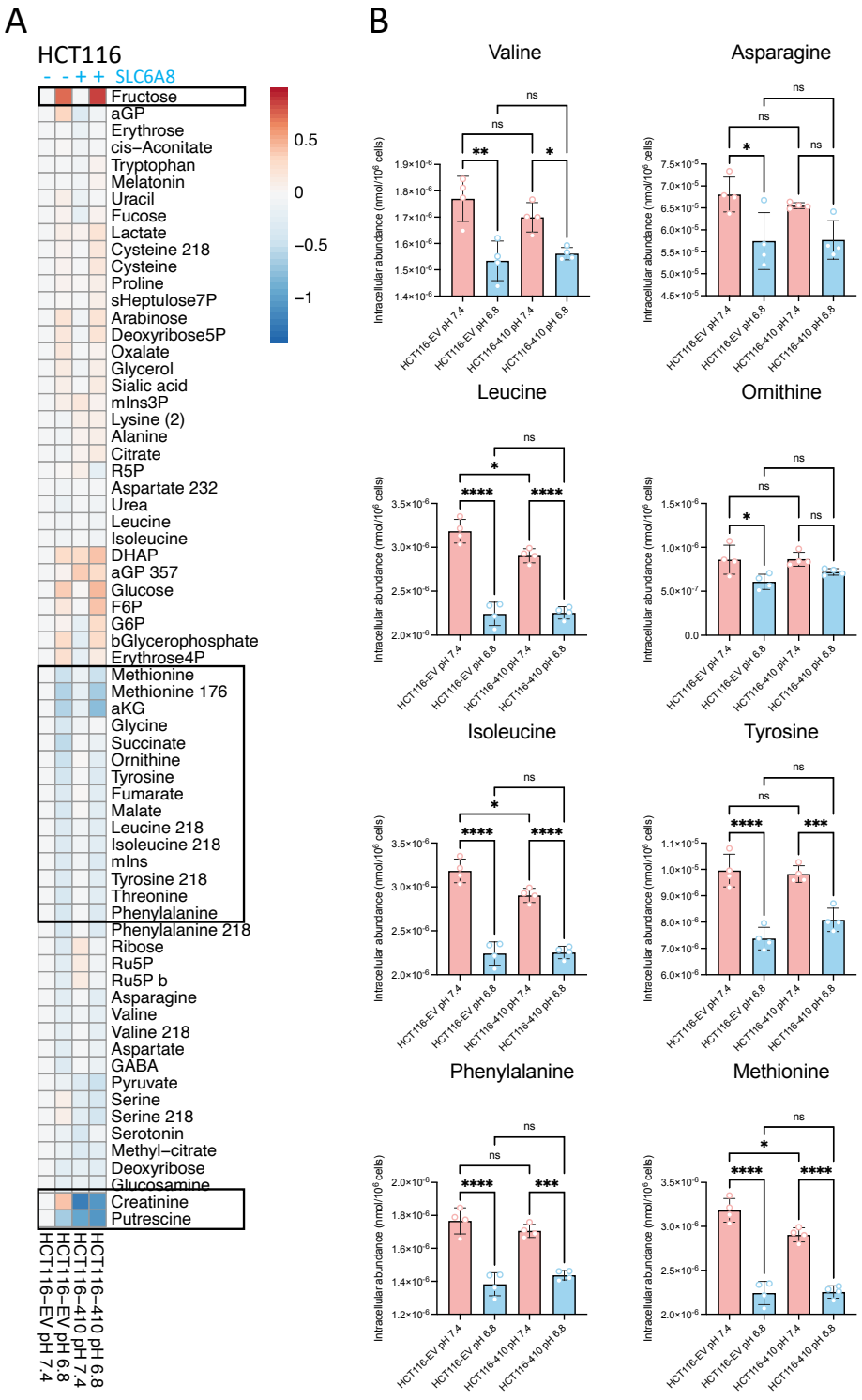


Figure 4.15: Effects of SLC6A8 knockdown on cell metabolism (1) - (A) Overall changes in intracellular metabolites in HCT116-EV and HCT116-410. Metabolite abundance has been normalised to cell count, and is shown as $\log_2$(Fold change) over HCT116-EV at pH 7.4. EV - empty vector, 410 - knockdown strain generated with shRNA 410 (B) pH-specific decrease in intracellular amino acids in HCT116. P values obtained by one-way ANOVA.

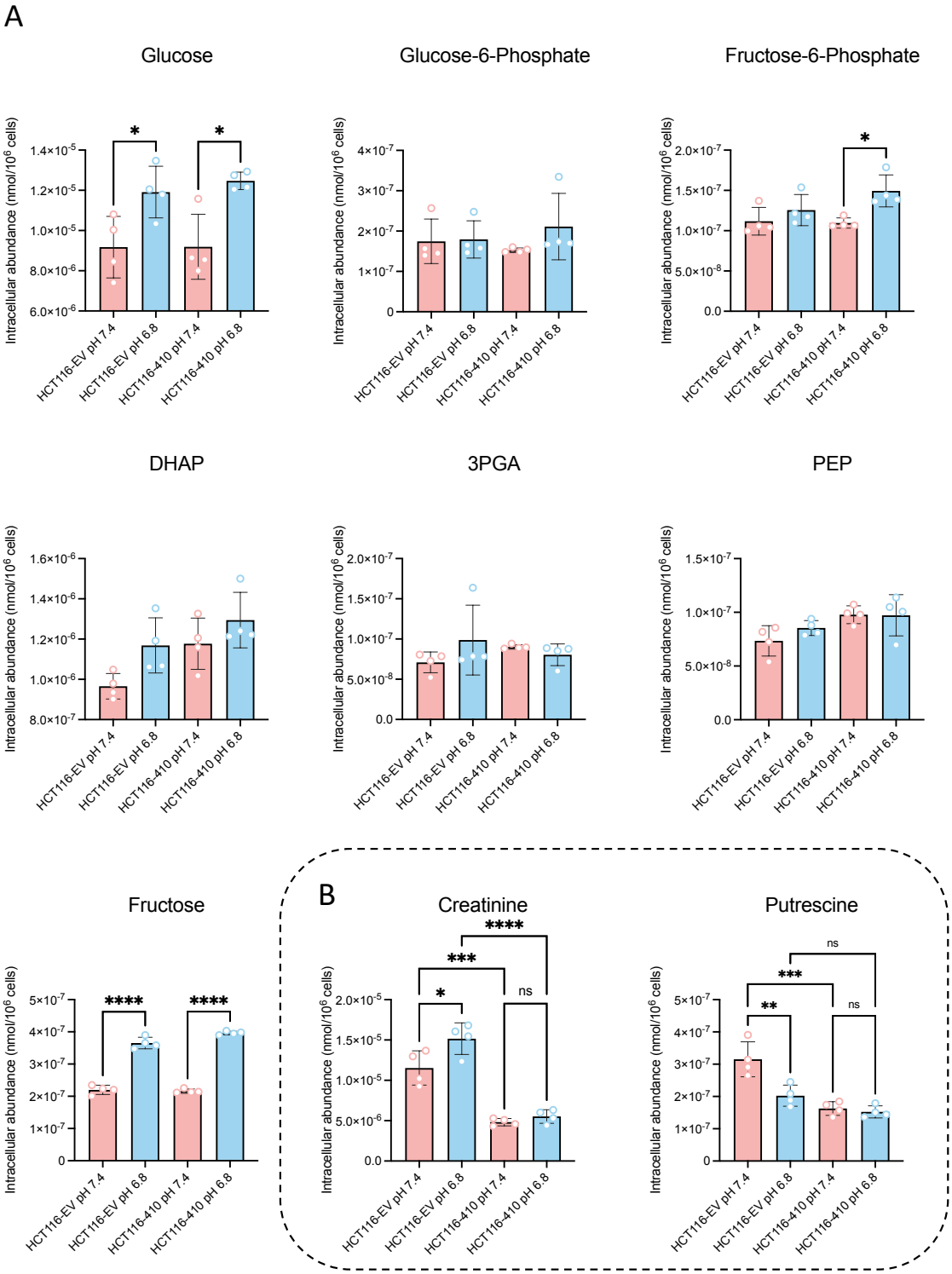


Figure 4.16: Effects of SLC6A8 knockdown on cell metabolism (2) - (A) Glycolytic intermediates (B) SLC6A8 knockdown is associated with a decrease in intracellular creatinine and putrescine. EV - empty vector, 410 - knockdown strain generated with shRNA 410. P values obtained by one-way ANOVA.

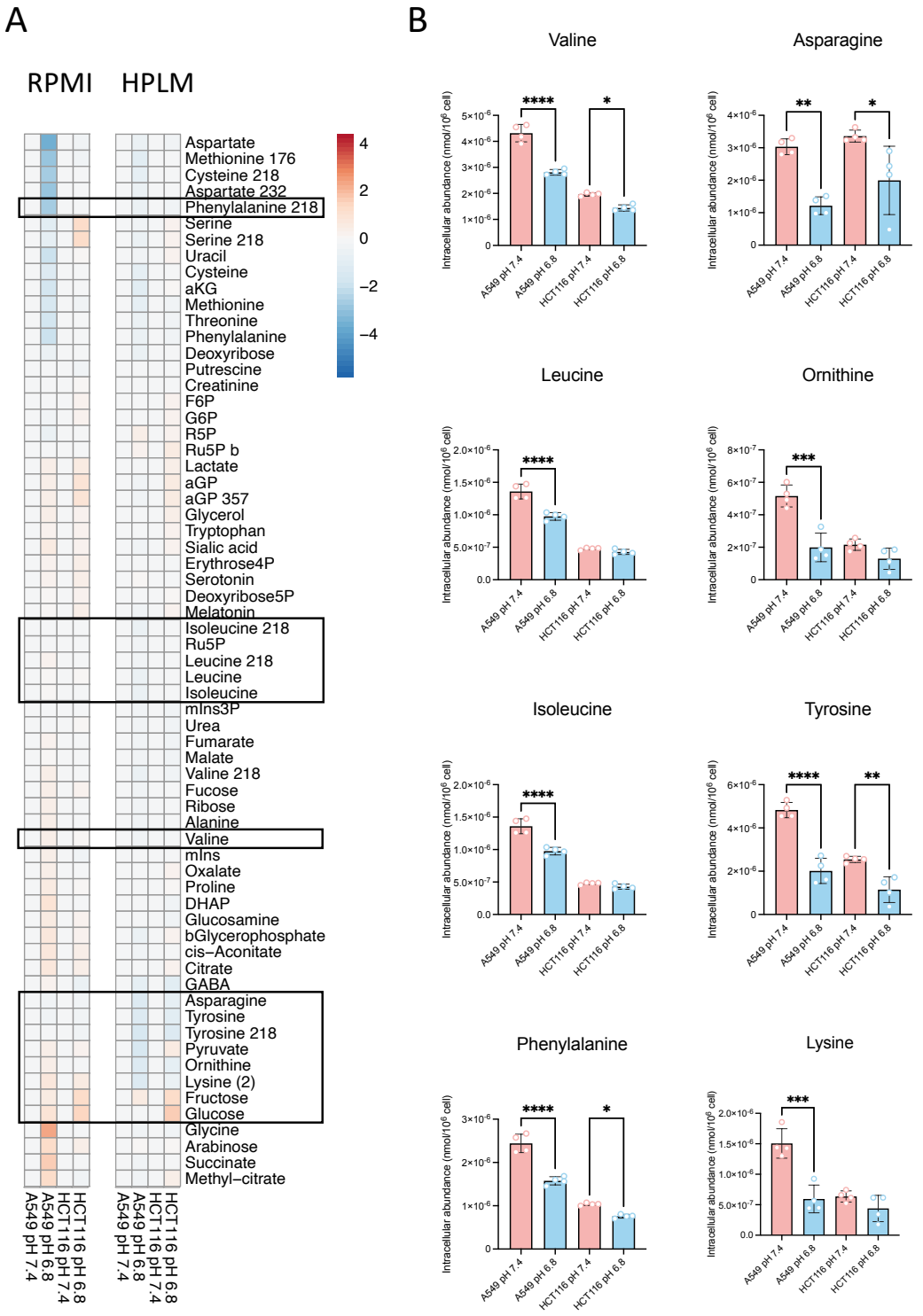


Figure 4.17: Intracellular metabolite abundance in HPLM (1) - (A) Metabolite abundance in A549 and HCT116 cells cultured in HPLM compared to RPMI. Metabolite abundance normalised to cell count, shown as $\log_2$(Fold change) over pH 7.4 for each cell line in each media type. Data for RPMI media shown previously in Figure 4.13 (B) pH-specific decrease in intracellular amino acids in A549 and HCT116 cells cultured in HPLM media for 24 hours. P values obtained by one-way ANOVA.

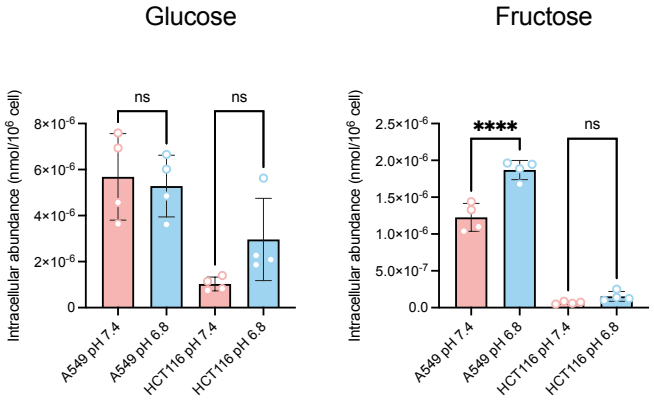


Figure 4.18: Intracellular metabolite abundance in HPLM (2) - Intracellular abundance of glucose and fructose in A549 and HCT116 cells cultured in HPLM media for 24 hours. P values obtained by one-way ANOVA.

4.4 Conclusions and limitations

The majority of experiments conducted in acidic pH suggested creatine does not have a major impact on cell growth in normoxia or hypoxia, or on intracellular pH. However, we demonstrated that creatine supplementation results in increased intracellular creatine and creatinine, confirming it is imported by cancer cells. In HCT116, creatine supplementation was also associated with a decrease in intracellular ATP in acidic conditions. Knockdown of the creatine transporter SLC6A8 caused a decrease in intracellular creatinine and putrescine in both cell models tested. In addition, we observed a reduction in intracellular amino acids and build up of glucose and fructose in acidic pH.

Creatinine is a non-enzymatic by-product of creatine and as creatine uptake is reduced in SLC6A8 knockdown strains, it is unsurprising to see a reduction in creatinine as well. The reduction in intracellular putrescine however was unexpected. Putrescine is a polyamine which can be synthesised from arginine via ornithine (Kanehisa et al., 2023; Sourkes and Missala, 1981). Arginine (along with glycine) is also a precursor of creatine. One possible explanation for the decrease in putrescine in SLC6A8 knockdown lines could be that arginine is redirected towards creatine synthesis as creatine uptake is impaired by knockdown of the creatine transporter (Figure 4.20A). Intracellular creatine detection by LC-MS revealed that lung cancer cell lines had endogenous creatine, along with the labelled creatine taken up from

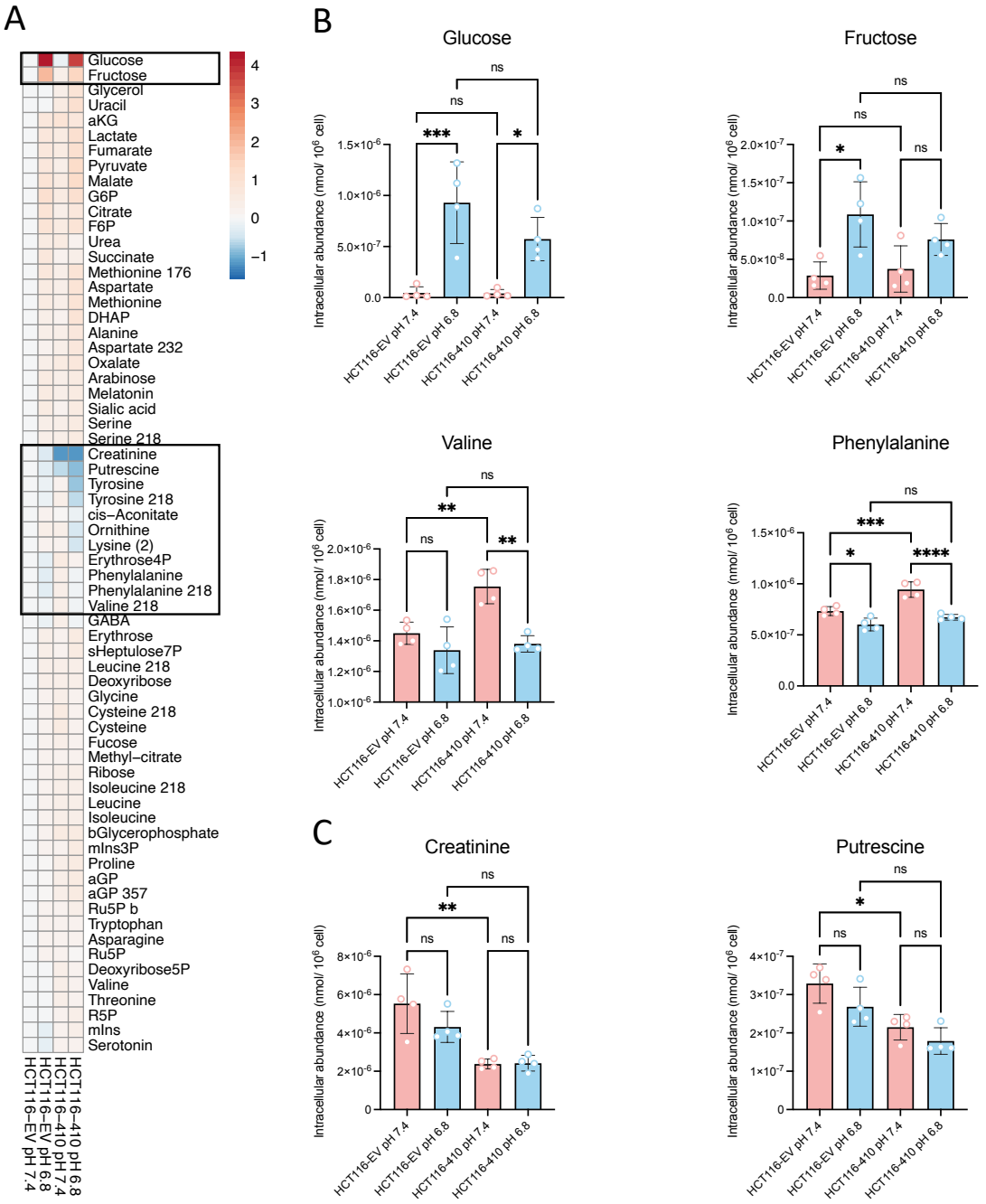


Figure 4.19: Effects of SLC6A8 knockdown on cell metabolism in HPLM - (A) Metabolite abundance in HCT116-EV and HCT116-410 cultured in HPLM for 24 hours. Metabolite abundance normalised to cell count, shown as $\log_2$(Fold change) over Empty vector (EV) control at pH 7.4 (B) pH-specific changes in intracellular glucose, fructose and amino acids (C) knockdown of SLC6A8 is associated with a decrease in intracellular creatinine and putrescine in HPLM

culture media (Figure 4.10). In addition, expression data from the CCLE database suggests a number of cancer cell lines express enzymes involved in creatine synthesis. All three of the lung cancer cell lines used in this study express guanidinoacetate methyltransferase (GAMT) (Figure 4.20B). GAMT is also expressed in the colon cancer cell line HCT116. Similarly, all lung cancer cell lines, as well as HCT116, express at least one creatine kinase, allowing them to convert creatine to phospho-creatine (Figure 4.20C). In lung cancer cell lines the cytosolic isoform, CKB, has the highest expression levels. Unfortunately, we were unable to detect and quantify phospho-creatine using the existing LC-MS method. Therefore we have no indication as to how much of the intracellular creatine, endogenously made or exogenously supplemented, is converted to phospho-creatine.

Multiple studies have reported that acidosis can inhibit glycolysis in cancer cells (Abrego et al., 2017; Corbet, Draoui, et al., 2014; Gao et al., 2020; J. Y. Lee et al., 2019). This is consistent with growth experiments, where we observed a lesser impact of glucose depletion on cell growth in pH 6.8 compared to pH 7.4 (Figure 4.3A). The increase in intracellular glucose we observed in acidic pH, could be a sign of glucose build up due to suppression of glycolysis. The increase in intracellular fructose could suggest that glucose is converted to fructose via the polyol pathway, instead of entering glycolysis (Figure 4.21).

Another metabolic change observed in acidic pH was a decrease in intracellular amino acids. Amino acids are involved in a number of metabolic processes in cancer cells, including biomass production, energetic regulation, redox balance, and resistance to metabolic stress (Lieu et al., 2020). The decrease in intracellular amino acids could suggest a downregulation of mTOR activity in acidic conditions.

A number of amino acid depletion strategies are currently under clinical evaluation as cancer therapies (M. Butler, Meer, and Leeuwen, 2021). For example, asparaginase, an enzyme which hydrolyses asparagine to aspartic acid and ammonia, leading to asparagine depletion, has been successfully used to treat pediatric acute lymphoblastic leukemia (M. Butler, Meer, and Leeuwen, 2021; Cools, 2012). Asparaginase is now under clinical investigation for the treatment of a number of additional cancer types, including glioblastoma, ovarian, breast, gastric and liver cancer (Chiu et al.,

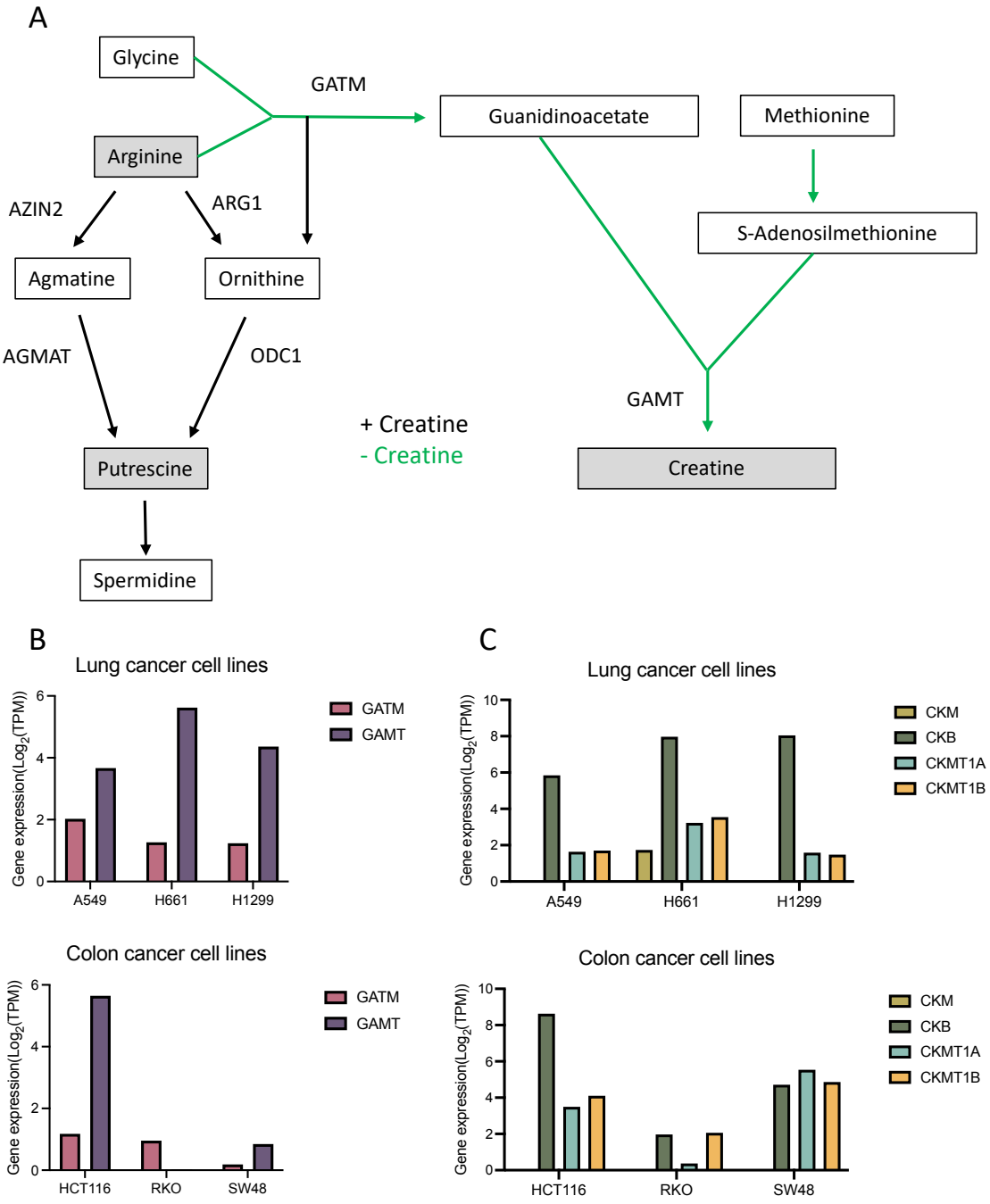


Figure 4.20: Putrescine and creatine synthesis - (A) Arginine can be a precursor for both putrescine and creatine (B) Expression of creatine synthesis components across lung and colon cancer cell lines (C) Expression of creatine kinases across lung and colon cancer cell lines. Expression data for (B) and (C) obtained from the CCLE database. CKM - creatine kinase muscle type, CKB - creatine kinase brain type, CKMT1/2 - mitochondrial creatine kinase 1/2, GATM - Glycine Amidinotransferase, GAMT - Guanidinoacetate N-methyltransferase, AZIN2 - Antizyme inhibitor 2, AGMAT - Agmatinase, ARG1 - Arginase 1, ODC1 - Ornithine decarboxylase 1.

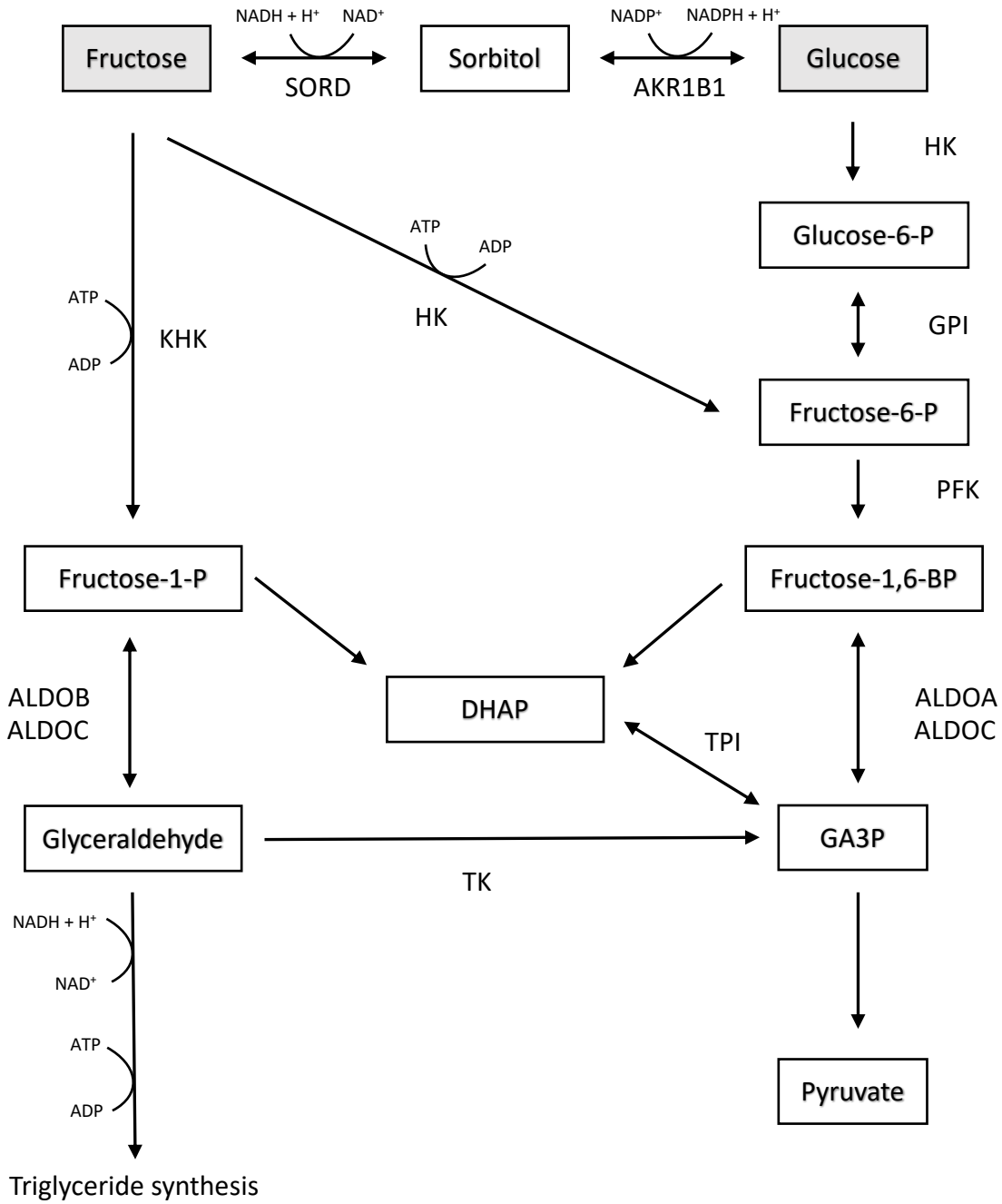


Figure 4.21: Fructose metabolism in cancer - Glucose can be metabolised to fructose via the polyol pathway instead of entering glycolysis in cancer cells. Figure adapted from Krause and Wegner (2020). SORD - Sorbitol dehydrogenase, AKR1B1 - Aldo-keto reductase 1B, KHK - Ketohexokinase, HK - Hexokinase 1, GPI - Glucose-6-Phosphate isomerase, PFK - Phosphofructokinase, ALDOA - Aldolase A, ALDOB - Aldolase B, ALDOC - Aldolase C, TK - Thymidine kinase 1, TPI - Triosephosphate isomerase 1, GA3P - Glyceraldehyde-3-phosphate.

2020; Knott et al., 2018). Promising anti-tumour effects have also been seen with enzymatic depletion of methionine. The bacterially derived enzyme L-methionine-gamma-lyase (METase) has been used to target methionine *in vitro* as well as *in vivo* in colorectal cancer, melanoma, and brain tumours and has shown limited toxicity in Phase I clinical trials (M. Butler, Meer, and Leeuwen, 2021; Fernandes et al., 2017; Hoffman, Kokkinakis, and Frenkel, 2019). The decrease we observed in intracellular amino acids in acidic pH could therefore be a natural vulnerability of cancer cells.

Chapter 5

Exploring SLC signatures in cancer cell lines

The creatine transporter SLC6A8 was identified as upregulated in tumours with acidic transcriptional signatures using a computational approach on publicly available clinical data (Chapter 3). However, this finding was not recreated in lung and colorectal cancer cell culture models (Chapter 4). To assess the transcriptional response of cell lines to acidic pH, we took a complementary, untargeted approach. A panel of three lung and three colorectal cell lines were incubated in acidic and neutral pH, and their SLC signatures were interrogated by RNA sequencing. This chapter explores the response of these cell lines to acidosis and draws a parallel between what is seen in clinical conditions and what is seen in cancer cell models.

5.1 RNA sequencing of lung and colon cancer cell lines

5.1.1 Lung cancer cell lines show stronger transcriptional response to pH than colon cancer cell lines

To explore SLC signatures in acidosis directly, we selected a panel of 6 cancer cell lines: A549, NCI-H1299 (H1299) and NCI-H661 (H661) were selected as representative of lung adenocarcinoma while HCT116, RKO and SW48 were selected as representative of colon adenocarcinoma. The six cell models were incubated at either pH 6.8 or pH 7.4 as control. RNA was collected after 8 and 24 hours and sent for RNA sequencing. Overall transcriptional response was stronger in lung cancer compared to colon cancer cell lines at both time points (Figure 5.1).

At the 8 hour time point, the majority of DE genes across all cell lines were downregulated, with the strongest transcriptional response seen in A549 and H1299. The two cell lines had 110 DE genes in common (Figure 5.2A). Of these, two genes were consistently downregulated in all lung cancer cell lines - F2RL1 and RCL1. F2RL1 (F2R like trypsin receptor 1) is a member of the G-protein coupled receptor 1 family and is known to promote angiogenesis in lung, colon and breast cancer (Yong Li et al., 2022; Nag et al., 2023; Nassar et al., 2021). RCL1 (RNA terminal phosphate cyclase like 1) is predicted to enable endoribonuclease activity. Interestingly, RCL1 is believed to be a hypoxia-regulated gene (Ren et al., 2022), however, this data

suggests acidosis alone also affects RCL1 expression. SMAD7 showed downregulation in A549 and H1299, as well as HCT116 and RKO. SMAD7 (Mothers against decapentaplegic homolog 7) is a member of the TGF-β signaling pathway and has a context-specific role in cancer. It has been reported to support the development of lung, colon, pancreatic and skin cancer. At the same time, SMAD7 is believed to inhibit metastasis in breast cancer, melanoma and hepatocellular carcinoma (Stolfi et al., 2014).

The colorectal cell lines had a heterogeneous transcriptional response with fewer overlaps in DE genes at the 8 hour time point. However, one gene, PDCD4, was upregulated across all colorectal cell lines. PDCD4 (Programmed cell death protein 4) is a tumour suppressor gene, which acts by inhibiting the transcription of p53 (Wedeken, Singh, and Klempnauer, 2011), and has been associated with inhibition of cancer invasion in both lung and colon cancer (Allgayer, 2010; Y. Chen et al., 2003). PDCD4 was also upregulated in the lung cancer cell line A549. In addition, HCT116 and RKO had 8 more DE genes in common, of which POSTN was strongly upregulated (Figure 5.3A). POSTN (Periostin) is known to bind integrins to support migration of epithelial cells during development, and has been linked to metastasis in melanoma. Like SMAD7, POSTN is also inducible by TGF-β (Soikkeli et al., 2010). POSTN expression has been linked to 5-fluorouracil resistance in colon cancer and in HCT116 cells (T. Liu et al., 2021). This result suggest acidosis could be a contributing factor for resistance, by inducing upregulation of POSTN.

At the 24 hour time point, the majority of DE genes remained downregulated. Lung cancer cell lines shared 18 DE genes in common (Figure 5.2B). Nine of these (PMEPA1, SGK1, INSIG1, JPT2, TPM1, ANGPTL4, ESAM, FHOD1, MMP9) were consistent with DE genes identified at the 8 hour time point. Interestingly, one of the downregulated genes is LDHA - the enzyme, converting glucose-derived pyruvate to lactate. This suggests lung cancer cells could be reducing the production of lactate to prevent further acidification of the microenvironment. Three other glycolytic genes were downregulated in H661 - PGK1 (Log_2(FC) = -0.24, adjusted p value = 0.04), PGAM1 (Log_2(FC) = -0.32, adjusted p value = 0.01) and PKM (Log_2(FC) = -0.20, adjusted p value = 0.03).

Another downregulated gene, shared between all lung cancer cell lines, was SGK1. SGK1 has been identified as a master regulator of ion channels and SLC transporters, including the creatine transporter SLC6A8 and the glucose transporter SLC2A1 (Palmada et al., 2006; Strutz-Seebohm et al., 2007). In addition, A549 and H1299 shared 35 more DE genes in common (Figure 5.2C). Of these, 11 were consistent with DE genes identified at the 8 hour time point (Figure 5.2A).

The three colon cancer cell lines had 3 DE genes in common at the 24 hour time point (Figure 5.3B). These were not consistent with DE genes seen at the 8 hour time point, or DE genes identified in lung cancer cell lines. LANCL2, which was downregulated across all 3 cell lines, has been identified as a driver of tumorigenesis (Y. Lou et al., 2021). In addition, HCT116 and RKO shared 11 more DE genes in common (Figure 5.3B). Of these, SMAD7 was consistent with the 8 hour time point, and CBX7 was consistent with lung cancer cell lines. CBX7 supresses genes expression via chromatin modification as part of the PRC1 complex (polycomb repressive complex 1) (Jun Li et al., 2021). Expression of CBX7 is associated with favourable prognosis in colon cancer patients (Pallante et al., 2010).

Unfortunately the limited transcriptional response observed meant that the DE genes were insufficient for a meaningful GO terms analysis.

5.1.2 SLC6A8 is downregulated in lung cancer cell models

Consistent with the overall changes in gene expression, the majority of DE transporters were downregulated in acidic conditions. At the 8 hour time point, there were 37 differentially expressed SLCs, only 10 of which were upregulated (Figure 5.4). The majority of upregulated SLCs (9 out of 10) were identified in the lung cancer cell line A549. There was some overlap in downregulated SLCs between cell models. Sodium-phosphate symporter SLC20A1 was downreglulated in HCT116, H661 and A549. In contrast with the TCGA analysis, these 3 cell lines showed downregulation of the glucose transporter SLC2A1. The creatine transporter SLC6A8 was also downregulated in A549, with $\log_2$(FC) of -0.28. Interestingly, SLC16A13, which was recently validated as a lactate uptake transporter (Schumann et al., 2021), was downregulated in A549. The downregulation of SLC16A13 and SLC2A1, along

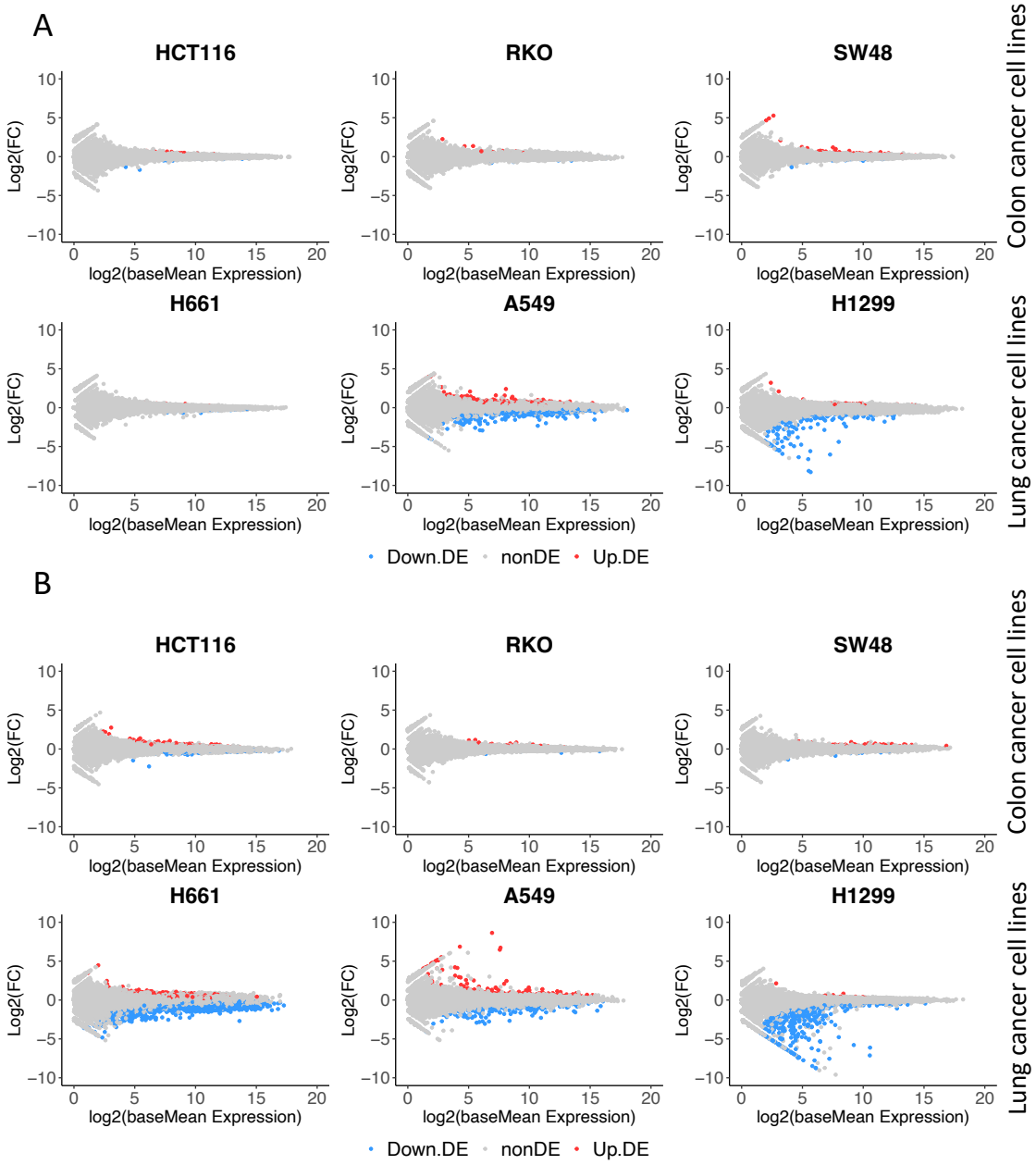


Figure 5.1: DE genes in colon and lung cancer cell lines after 8 and 24 hours of incubation at pH 6.8 - Differentially expressed (DE) genes after (A) 8 hours and (B) 24 hours in pH 6.8 relative to pH 7.4. Differential expression analysis conducted with the Deseq2 package in R. Upregulated genes shown in red, downregulated genes shown in blue. Non-DE genes shown in grey. DE cut off was adjusted P value of 0.05. No log fold change cut offs were applied.

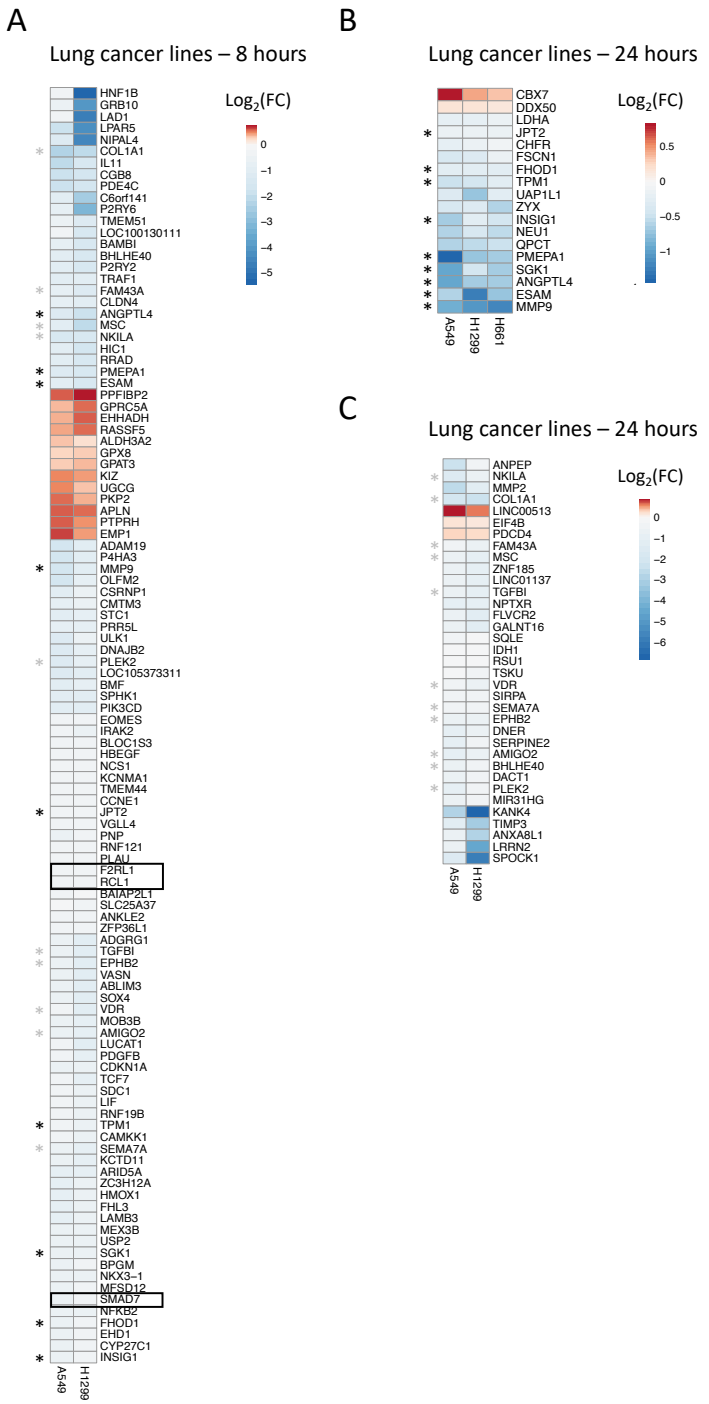


Figure 5.2: DE genes in lung cancer cell lines after 8 and 24 hours - Differentially expressed (DE) genes were considered any genes with false discovery rate (adjusted p value) of 0.05 or lower. No log fold change cut offs were applied. Heatmaps show $\log_2$(FC) in pH 6.8 relative to pH 7.4 in full RPMI. Each cell line shown as average values of n=3 technical replicates. A) DE genes in common in A549 and H1299 after 8 hours B) DE genes in common in A549, H1299 and H661 after 24 hours C) DE genes in common in A549 and H1299 after 24 hours. Asterisks mark DE genes, consistent between the 8 hour and 24 hour time point.

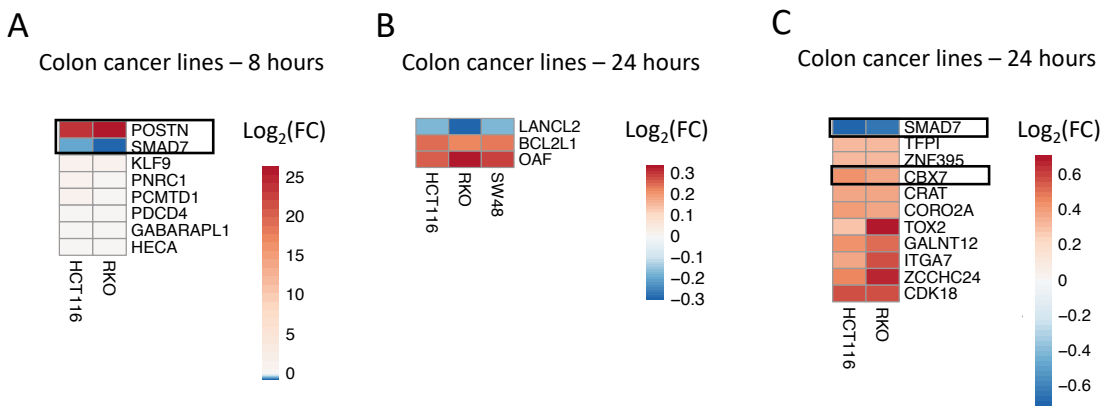


Figure 5.3: DE genes in colon cancer cell lines after 8 and 24 hours - Differentially expressed (DE) genes were considered any genes with false discovery rate (adjusted p value) of 0.05 or lower. No log fold change cut offs were applied. Heatmaps show $\log_2$(FC) in pH 6.8 relative to pH 7.4 in full RPMI. Each cell line shown as average values of n=3 technical replicates. A) DE genes in common in HCT116 and RKO after 8 hours B) DE genes in common in HCT116, RKO and SW48 after 24 hours C) DE genes in common in HCT116 and RKO after 24 hours.

with the downregulation of LDHA we observed in A549 (Section 5.1.1) are both adaptations to reduce the build up of lactate intracellularly. Interestingly, SLC16A7 (MCT2), which is also a known lactate uptake transporter, was upregulated in A549. However, SLC16A7 has been demonstrated to have a higher propensity for pyruvate (Fets, Paul C Driscoll, et al., 2018a). It is an example of a nutrient-proton symporter. This type of transporters are believed to be enhanced by the reversed pH gradient in acidosis, which facilitates nutrient uptake (Daverio et al., 2023).

At the 24 hour time point, changes in SLC expression remained mostly cell line specific (Figure 5.5). HCT116 was the only colon cancer cell line where DE SLCs were present. The glucose transporter SLC2A1 was downregulated in two lung cancer cell lines, H661 and A549. In H661, four additional glucose transporters showed differential expression - SLC2A6 and SLC2A8 were downregulated, while SLC2A10 and SLC2A12 were upregulated at the same time. SLC2A6 and SLC2A8 are both retained to intracellular compartments, predominantly lysosomes and endosomes, and are not expressed on the plasma membrane (Augustin, Riley, and Moley, 2005; Holman, 2020; Uldry et al., 2002). SLC2A10 and SLC2A12 are also predominantly associated with intracellular vesicles (Aerni-Flessner, Otu, and Moley, 2011; Pyla et

al., 2013). SLC2A12 can be recruited to the plasma membrane in response to external stimuli, like insulin stimulation (C. A. Stuart et al., 2009). Lactate transporters SLC16A1 and SLC16A13 were downregulated in A549, consistent with the 8 hour time point. The sodium-coupled amino acid transporter SLC38A5 was downregulated in HCT116 and A549, which is consistent with the decrease in intracellular amino acid abundance observed in these two cell lines during metabolomics experiments (Chapter 4). The creatine transporter SLC6A8 remained downregulated, with $\log_2$(FC) = -0.29 in H661 and $\log_2$(FC) = -0.28 in A549. Interestingly, the cytosolic isoform of creatine kinase, CKM, was downregulated in H1299 ($\log_2$(FC) = -3.57), and the mitochondrial isoform CKMT1B was downregulated in H661($\log_2$(FC) = -0.79).

5.1.3 Acidic signature has a prognostic value in lung cancer

A number of DE genes in the acidosis signature, identified in lung cancer cell lines, have been linked to angiogenesis and tumour progression. These includes PMEPA1 (Vo Nguyen et al., 2014), SGK1 (Z. Tang et al., 2018; Xiaobo et al., 2016), INSIG1 (D. Xu et al., 2020), FSCN1 (Jawhari et al., 2003; Jie Li et al., 2018; Pelosi et al., 2003), ZYX (Zhong et al., 2019), UAP1L1 (Qi et al., 2020) and FHOD1 (C. Jiang et al., 2021). All of these genes appear to be downregulated in acidic pH (Figure 5.2B). For simplicity, we refer to the 16 genes, downregulated across all lung cancer cell lines, as LIVAS - 'LUAD *In Vitro* Acidosis Signature'. To test the prognostic value of LIVAS, we used clinical data from the LUAD cohort in TCGA. LIVAS was prognostic of a favourable clinical outcome, with p = 0.0047 (Figure 5.6A). This result suggests acidosis could be associated with a less aggressive phenotype in lung cancer.

Colorectal cell lines only shared 3 DE genes after incubation in acidic pH for 24 hours. For that reason, we used upregulated genes, shared between HCT116 and RKO only, as an acidic signature in colon cancer (Figure 5.3C). We refer to this signature as CIVAS - 'COAD *In Vitro* Acidosis Signature'. To assess prognostic value of this signature, we used the COAD cohort in TCGA. CIVAS was not prognostic in COAD (p = 0.24) (Figure 5.6B).

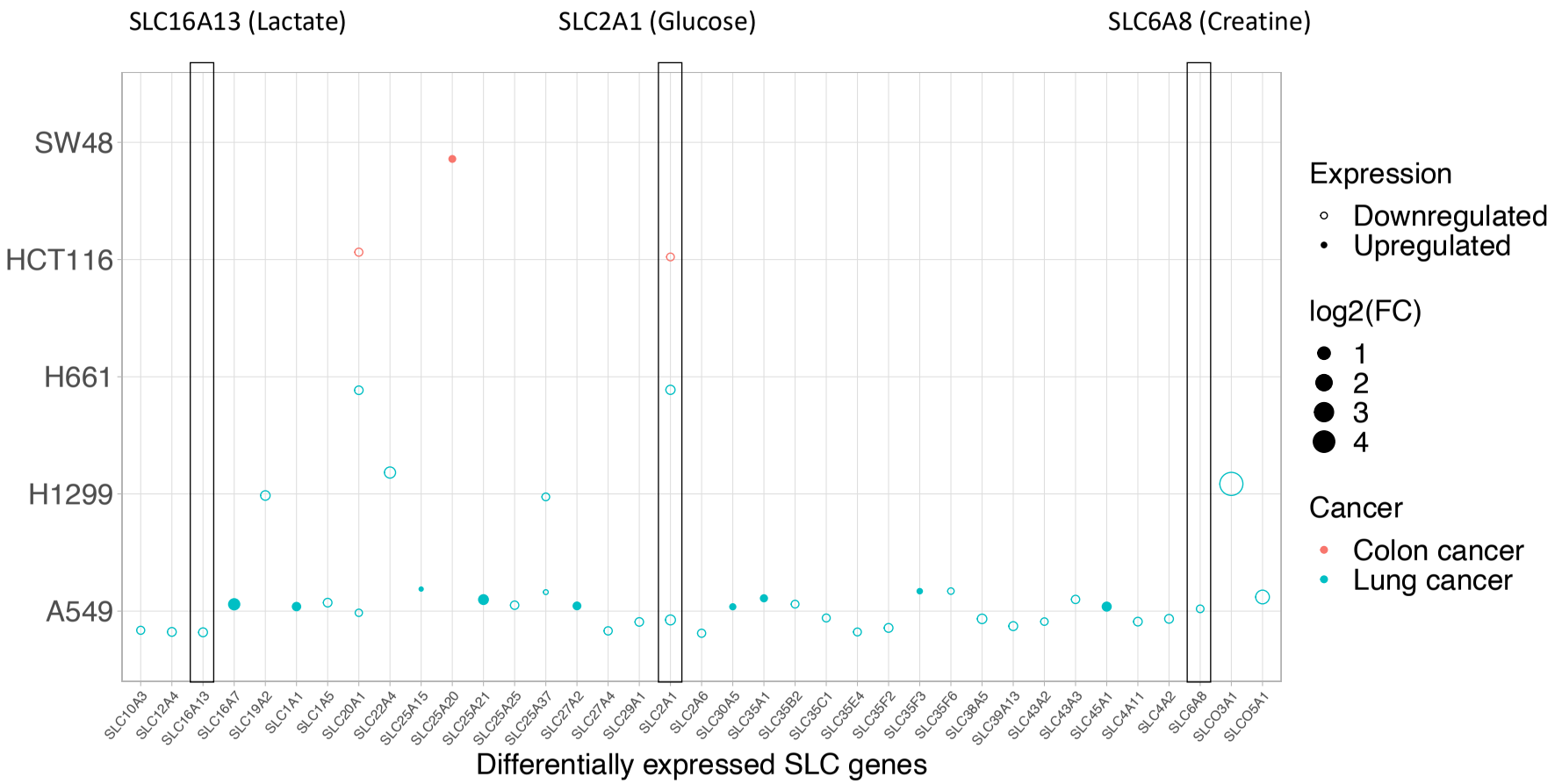


Figure 5.4: DE transporters in colon and lung cancer cell lines after 8 hours - Differentially expressed (DE) transporter genes after 8 hours at acidic pH. Colon cancer cell lines shown in red, lung cancer cell lines shown in blue. Differential expression analysis conducted with the Deseq2 package in R. DE cut off was adjusted P value of 0.05

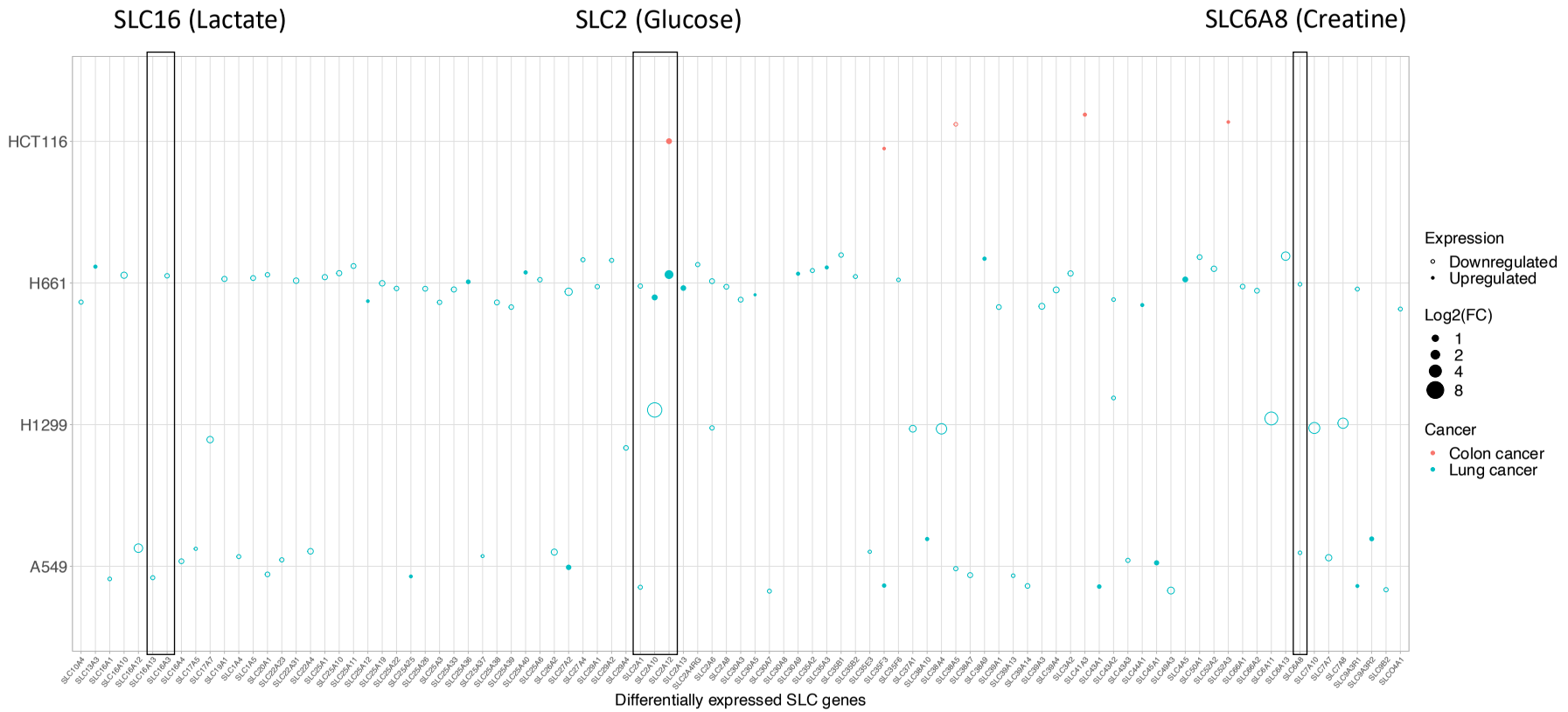


Figure 5.5: DE transporters in colon and lung cancer cell lines after 24 hours - Differentially expressed (DE) transporter genes after 24 hours at acidic pH. Colon cancer cell lines shown in red, lung cancer cell lines shown in blue. Differential expression analysis conducted with the Deseq2 package in R. DE cut off was adjusted P value of 0.05

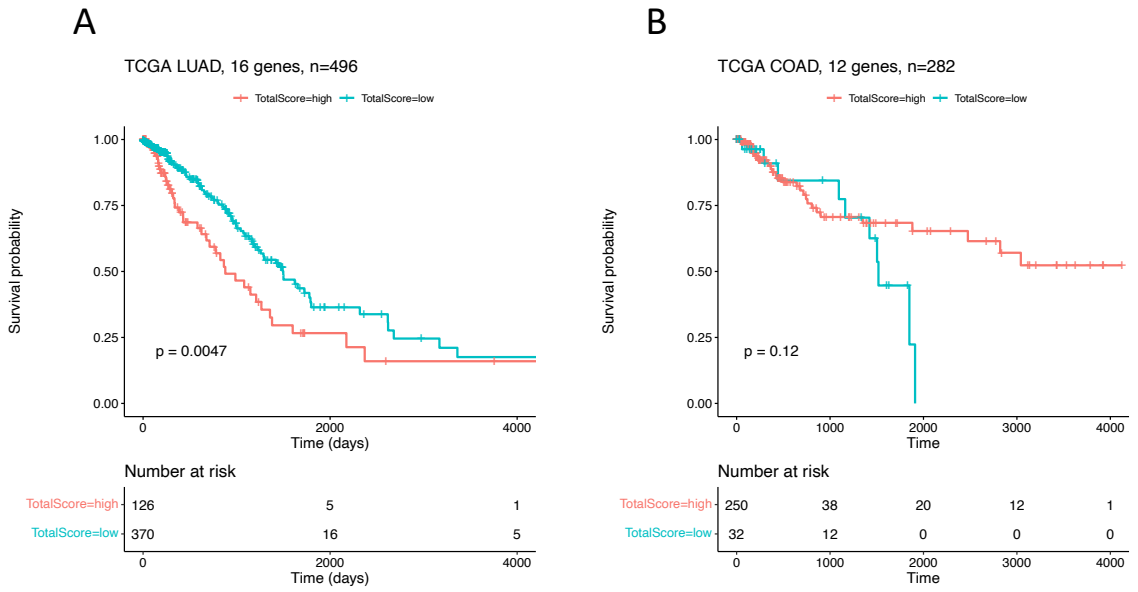


Figure 5.6: Prognostic value of acidosis signatures - (A) Prognostic value of the 16 downregulated genes, identified in lung cancer cell lines (LIVAS), based on 496 samples in the TCGA LUAD cohort (B) Prognostic value of the 12 upregulated genes, identified in HCT116 and RKO (CIVAS), based on 282 samples in the TCGA COAD cohort. P values calculated using the Cox regression method.

5.1.4 *In vitro* acidosis signatures correlate with hypoxia in clinical samples

The RNAseq experiment we conducted was done in normoxic conditions. We hypothesised that the *in vitro* signatures we uncovered would correspond to clinical samples, where cancer cells are growing in conditions of acidosis, but not hypoxia. To test this hypothesis, we used expression data from the COAD and LUAD cohort in the TCGA database. Expression scores for acidosis were calculated based on LIVAS and CIVAS expression. Expression score for hypoxia was calculated based on GSEA Hallmark Hypoxia. Scores were calculated for each signature in each sample using the R package singscore.

In LUAD, there was a strong negative correlation between the Acidosis score and Hypoxia score (R = -0.62) (Figure 5.7A). This confirms the LIVAS phenotype corresponds to areas with low expression of Hallmark hypoxia *in vivo*. In COAD samples, there was a moderate positive correlation between Acidosis and Hypoxia scores (R = 0.44) (Figure 5.7B). This data suggests in COAD, the CIVAS signature is also

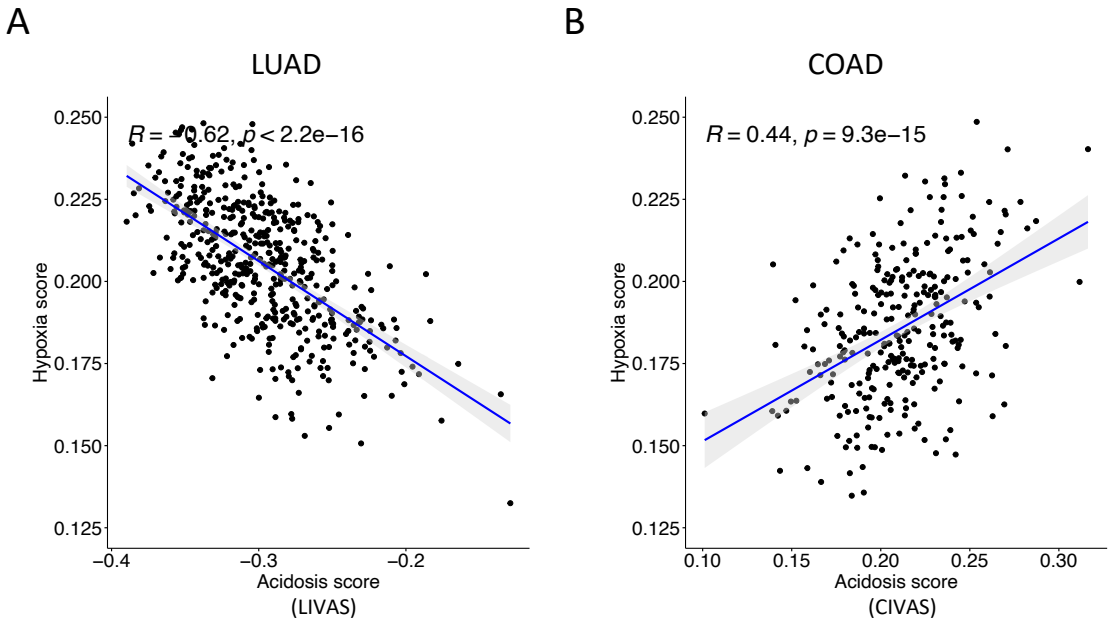


Figure 5.7: Correlation of *in vitro* acidosis and hypoxia signatures - (A) Pearson correlation of Hallmark hypoxia and Acidosis score based on LIVAS, in TCGA LUAD cohort (B) Pearson correlation of Hallmark hypoxia and Acidosis score based on CIVAS, in the TCGA COAD cohort. P and rho (R) values of Pearson correlation.

associated with hypoxia.

5.1.5 Adaptations to acidosis are not driven by changes in intracellular pH alone

The results from the RNAseq experiment clearly show that there are differences in response to acidic pH between lung and colon cancer cell lines. We hypothesised this could be due to the fact that the colon cancers originate from a more acidic environment in the first place (G. Hao, Z. P. Xu, and L. Li, 2018; Ilhan et al., 2017), and hence are naturally 'adapted' to acidosis. This is consistent with the fact lung cancer cell lines showed greater changes in gene expression compared to colon cell lines in acidic conditions. As cell adaptations to acidosis are often related to maintaining intracellular pH, one possibility is that colon cancer cell lines are intrinsically capable of regulating their intracellular pH better than lung cancer cell lines. To test this, the panel was exposed to acidic pH media, and the immediate change in intracellular pH was measured using a cSNARF-based method. Across the

cell panel, intracellular pH decreased by approximately one pH unit (Figure 5.8A). We observed no differences between lung and colorectal cell lines (Figure 5.8B). This finding suggests there are other driving factors to the adaptations observed in lung cancer cell lines.

5.1.6 Acidosis has a cell line-specific effect on intracellular metabolites

In addition to gene expression, we explored the effect of acidosis on intracellular metabolites across the cell panel. The majority of acidosis-induced changes were cell line-specific (Figure 5.9). A large number of metabolites were reduced in SW48 in acidic pH. Consistent with previous observations, there was a trend towards increased intracellular glucose and fructose in acidic pH, although for glucose this trend did not reach significance in any of the cell lines. The increase of intracellular fructose in H661 is consistent with a downregulation in ketohexokinase (KHK) after 24 hours in acidic pH (Log_2(FC) = -0.7, adjusted p value = 0.008). KHK catalyzes the phosphorylation of fructose to produce fructose-1-phosphate. Fructose-1-phosphate can be further metabolised to form the glycolytic intermediate glyceraldehyde 3-phosphate (Hannou et al., 2018). The drop in intracellular amino acids we observed previously was conserved to different extents in all lung lines, and some of the colorectal cell lines.

5.2 Conclusions and limitations

RNA sequencing of cancer cell lines in culture revealed differences in the way lung and colon cancer models respond to acidosis. Lung cancer cell lines showed a stronger transcriptional response compared to colon cancer models. The acidosis gene signature we identified in lung cancer cell lines (LIVAS) was associated with a favourable prognosis in LUAD patients (Figure 5.6A). This result suggests acidosis promotes a less aggressive phenotype in lung cancer. The acidic signature correlated with low expression of Hallmark hypoxia across LUAD clinical samples (Figure 5.7A), suggesting this phenotype could be triggered *in vivo* by acidosis alone.

The creatine transporter SLC6A8 was downregulated in lung cancer cell lines in

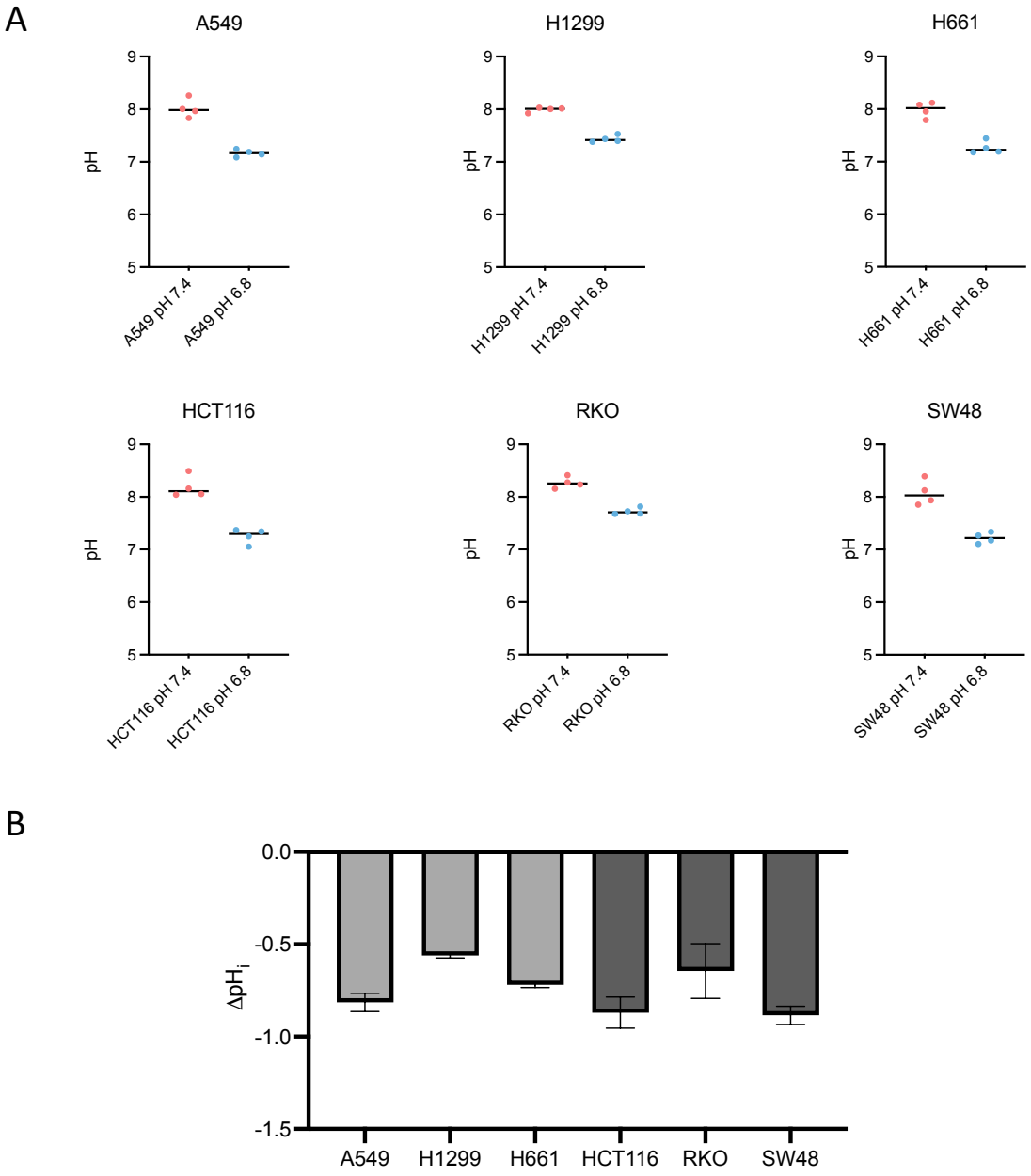


Figure 5.8: Changes in intracellular pH in an acidic microenvironment - (A) one representative biological replicate (n = 4 technical replicates) per cell line. Intracellular pH was measured 5 minutes after media was changed from full RPMI at pH 7.4 to full RPMI at pH 6.8. (B) Change in pH across the cell panel of 6 cell lines. Data shown for n=2 biological replicates. Lung cancer and colon cancer panel showed comparable change in intracellular pH

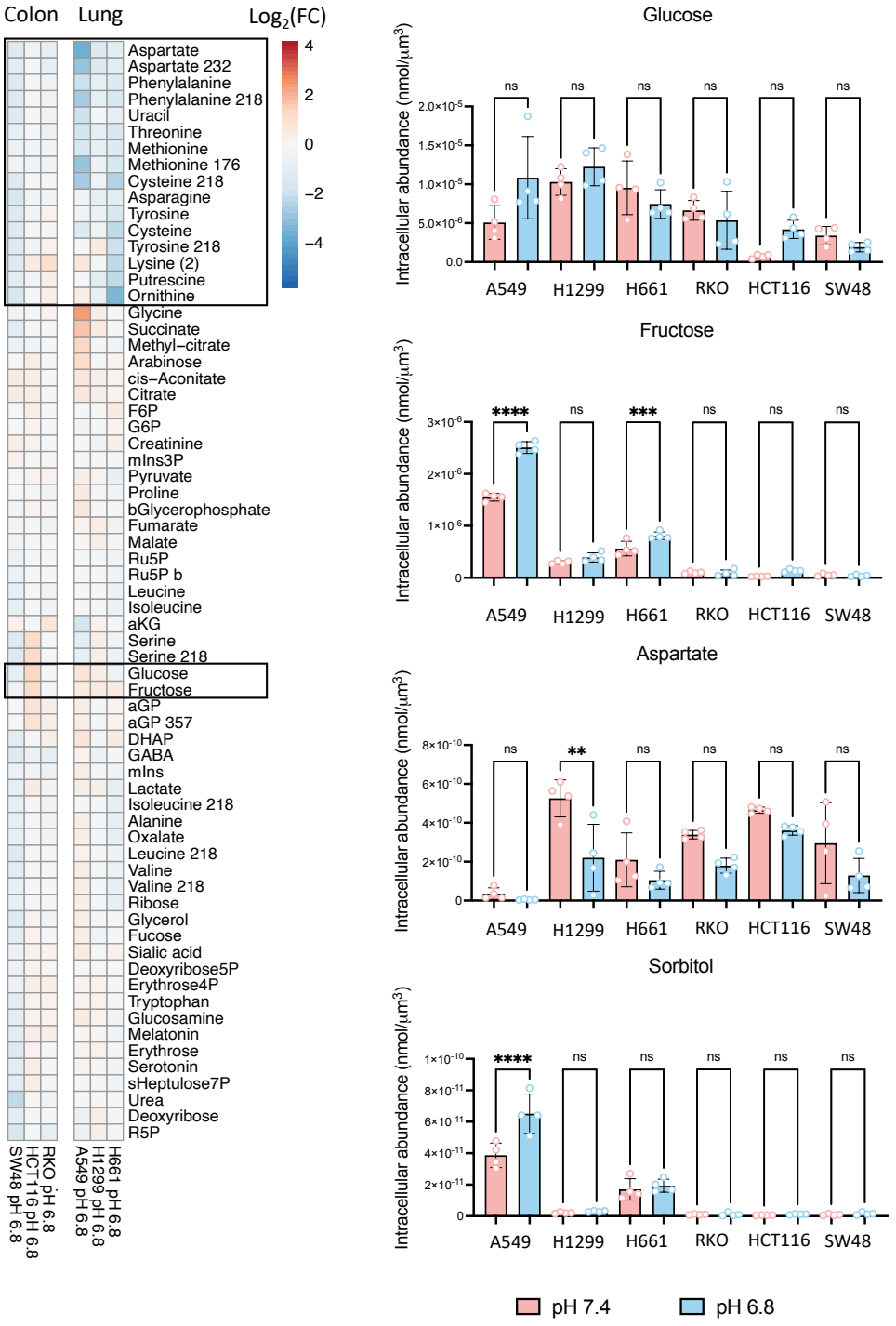


Figure 5.9: Metabolic response of 6 cell lines to acidic pH - cells grown in RPMI supplemented with dialysed FCS at either pH 7.4 of pH 6.8 for 24 hours. Heatmap shows intracellular metabolite abundance as $\log_2$(FC) at pH 6.8 relative to pH 7.4. Average values for n = 4 technical replicates, normalised to cell volume. p values obtained by one-way ANOVA. Data for HCT116 and A549 previously shown in Figure 4.13

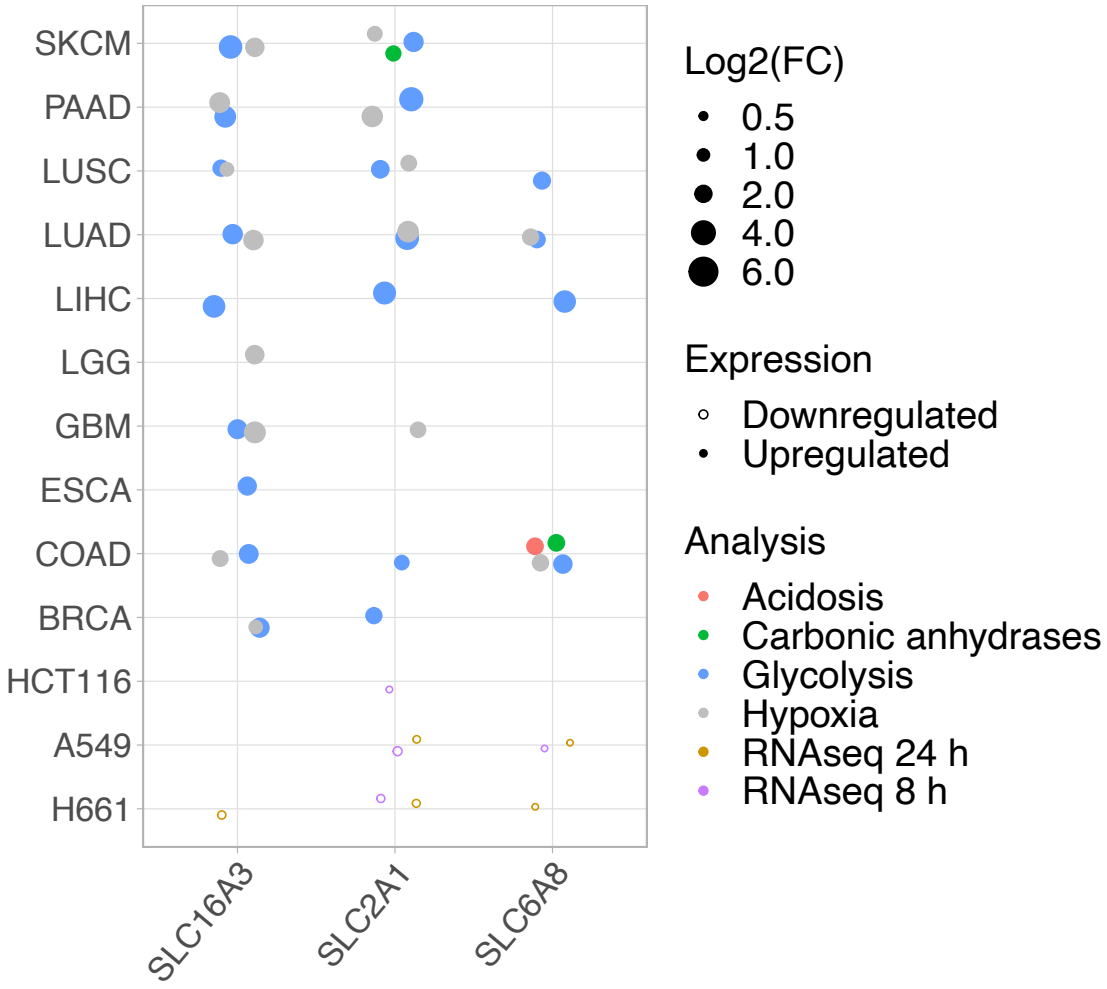


Figure 5.10: Relative expression of SLC6A8, SLC2A1 and SLC16A3 in clinical samples with acidic signatures and in lung cancer cell lines - All 3 transporters are upregulated in TCGA samples associated with acidic signatures, but downregulated in RNAseq of lung cancer cell lines in acidic pH

acidic conditions, contrary to our TCGA analysis (Chapter 3). This was also true of the glucose transporter SLC2A1 and the lactate transporter SLC16A3 (Figure 5.10). All of these transporters were identified as upregulated in a number of cancer types by the Hypoxia and Glycolysis stream of the TCGA computational analysis. The discrepancy we see in transporter expression between the analysis of *in vivo* clinical samples and the *in vitro* RNAseq experiment could be explained by the interplay of acidosis and hypoxia. The RNAseq experiment was conducted in normoxic conditions. We observed a downregulation in the glucose transporter SLC2A1, as well as LDHA and the lactate transporter SLC16A3. In addition, metabolomics data showed build-up of intracellular glucose in acidic pH. These changes point at

lower rates of glucose conversion to lactate. We hypothesise this would reduce the lactate, exported in the extracellular space, preventing further acidification of the tumour microenvironment. This is consistent with the idea that glycolysis can be inhibited by acidic pH - a phenomenon that has previously been described in literature (Abrego et al., 2017; Corbet, Draoui, et al., 2014; Gao et al., 2020; J. Y. Lee et al., 2019). It is also consistent with the resistance to glucose starvation we observed in acidic pH in Chapter 4 (Figure 4.3A, Figure 4.4A). In the context of lung cancer, this less glycolytic phenotype is associated with favourable patient outcome (Figure 5.6A). However, we propose in conditions of hypoxia, the stabilisation of HIF transcription factors overwrites this effect and leads to a more glycolytic phenotype, manifested by upregulation of the glucose transporter SLC2A1, lactate transporter SLC16A3 and creatine transporter SLC6A8 (Figure 5.11). We hypothesise this could lead to a more aggressive phenotype in lung cancer.

In fact, the 4 acidosis-related gene sets we have discussed in this study exemplify this hypothesis. The gene signature we identified in lung cancer cell lines (LIVAS), as well as the Acidosis gene set by J. L.-Y. Chen et al. (2008) are associated with acidosis exclusively. Both of these gene sets have favourable prognostic value in the LUAD cohort in TCGA (Figure 5.12). On the other hand, 'Rate-limiting genes in glycolysis' (Tanner et al., 2018) and extracellular carbonic anhydrases have been associated with both acidosis and hypoxia. In fact, some of the genes in these gene sets are HIF-1α target genes. These include CA9, HK2, PFKL, PFKP, SLC2A1 and SLC2A3, according to a HIF-1α target gene list, obtained from the NCBI (Gene ID 3091, accessed May 2023, `https://www.ncbi.nlm.nih.gov/gene/3091`). Both 'Rate-limiting genes in glycolysis' and extracellular carbonic anhydrases are associated with unfavourable prognosis, although in the case of carbonic anhydrases this tendency does not reach significance (Figure 5.12).

The creatine system has previously been linked to high glycolysis (Dillon and Clark, 1990; Kraft et al., 2000; Theo Wallimann, Tokarska-Schlattner, and Schlattner, 2011). In active muscle, functional pairing of creatine kinase with glycolytic enzymes allows glycolytic ATP to be incorporated in phospho-creatine immediately and prevents the inhibition of glycolysis by free ATP (Figure 1.5). This is con-

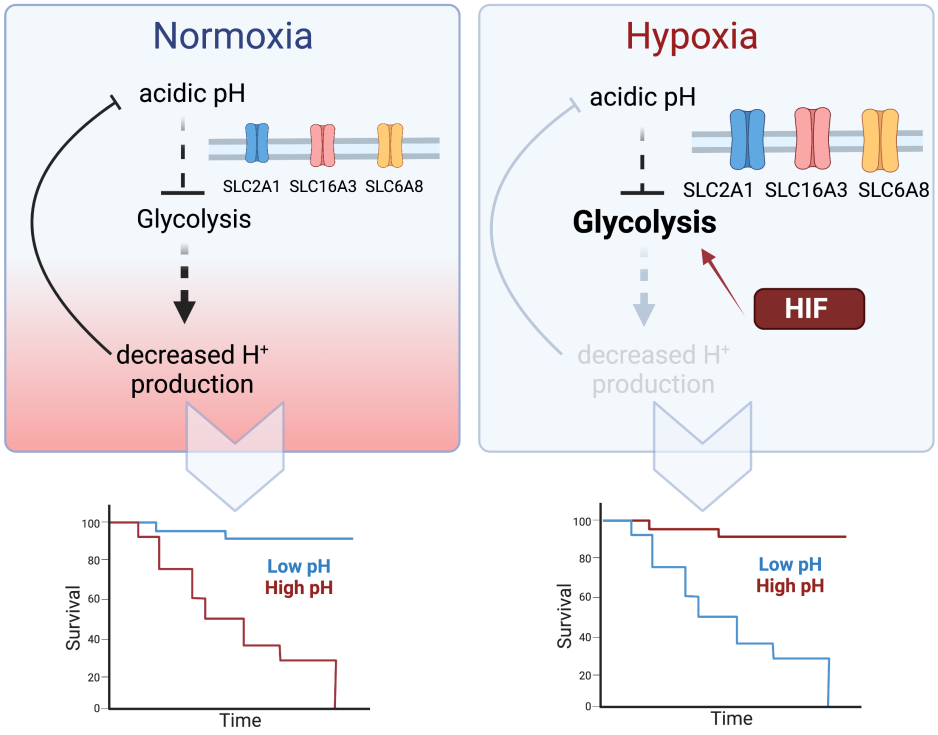


Figure 5.11: Proposed model of the response to acidosis in lung adenocarcinoma

sistent with the upregulation of SLC6A8 we have observed along with SLC2A1 and SLC16A3 in clinical samples. It is also consistent with the downregulation of SLC6A8 (in A549 and H661) and the creatine kinase (in A549 and H1299) observed in acidic conditions in the RNAseq experiment. If the creatine system acts the same way in cancer cells as it does in active muscle, it would no longer be needed in acidic conditions, if glycolysis is downregulated.

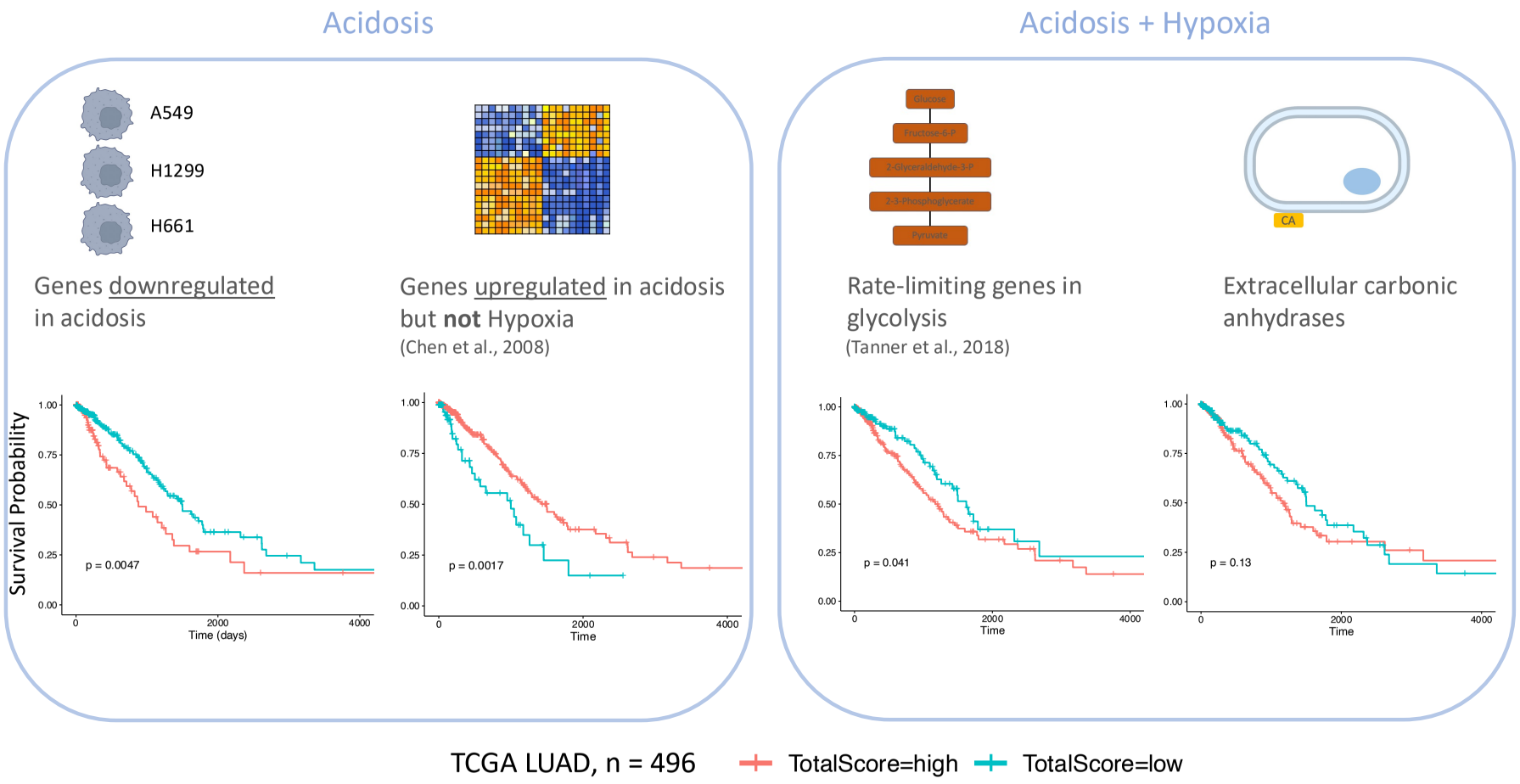


Figure 5.12: Prognostic values of gene sets associated with acidosis - in the presence and absence of hypoxia. Kaplan-Meier plots based on 496 samples in TCGA LUAD cohort. P values calculated using the Cox regression method

Chapter 6

Discussion

This chapter summarises the work completed within the project, and discusses the results in the context of what is currently known about tumour acidosis and creatine metabolism. The chapter also aims to acknowledge technical limitations and suggest key points for further investigation.

6.1 Tumour acidosis

Acidification of the tumour microenvironment can occur as a result of hypoxia, high glycolytic rates, poor vasculature, or all of these factors combined. This was reflected in our results from TCGA data analysis. We used 3 'acidic proxy' transcriptional signatures to identify tumours with an acidic microenvironment. Different samples were identified by the different proxies (Figure 3.6), supporting the hypothesis that different conditions can result in acidosis independently. While each of these scenarios resulted in upregulation of a different selection of SLC transporters, some transporters were associated with all three proxy-signatures across a range of cancer types (Figure 3.7). This result demonstrates the complex and heterogeneous nature of SLC signatures in cancer. *In vivo*, the majority of adaptations are probably influenced by both acidosis and hypoxia, and it is a challenging task to pinpoint the exact contribution of each of these factors to the overall changes, observed in tumours.

Within the scope of this project, we focused on the creatine transporter SLC6A8, as it was identified by all acidosis proxy signatures. SLC6A8 expression was associated with both hypoxic and acidic signatures in clinical samples from LUAD and COAD tumours. However, SLC6A8 was associated with acidosis, but not hypoxia, in LUSC and LIHC (Figure 3.9). LUSC and LIHC cell lines were not used in this study due to technical limitations. It is possible that creatine supplementation under acidic conditions could produce stronger phenotypes in such cell lines.

A number of additional DE transporters were identified in the TCGA analysis, many of which were associated with a single acidic proxy and not with hypoxia (Figure 3.9). These transporters could be studied in a cancer-type specific manner. COAD, LIHC and PRAD had the greatest number of SLCs associated with acidosis and not hypoxia. This could suggest that acidosis and hypoxia tend to occur independently

in these cancers. Response to hypoxia is mostly regulated by hypoxia inducible factors (HIFs) (Harris, 2002) while acidosis can activate acid-sensing G protein-coupled receptors (GPCRs), triggering downstream signalling cascades (Justus, Dong, and L. V. Yang, 2013). If the two occur independently, this could explain the different changes in gene expression we observed.

The riboflavin transporter SLC52A2 was associated with the Acidosis proxy (J. L.-Y. Chen et al., 2008), but not Hallmark Hypoxia, in LUAD, BRCA, PRAD and SKCM (Figure 3.9). Riboflavin, also known as vitamin B_2, is metabolised intracellularly to flavin mononucleotide (FMN) and flavin adenine dinucleotide (FAD). FMN and FAD play a key role as cofactors in energy metabolism, by catalysing oxidation/reduction reactions in the mitochondrial electron transport chain (Suwannasom et al., 2020). Enhanced riboflavin uptake has been reported in breast tumours (Bareford et al., 2008). However, there is no known link between riboflavin and acidosis.

Two members of the mitochondrial family SLC25 were also associated with the Acidosis (J. L.-Y. Chen et al., 2008) and Glycolysis (Tanner et al., 2018) proxies, but not with Hallmark Hypoxia – mitochondrial citrate carrier SLC25A1 (COAD, BRCA, PRAD) and mitochondrial dicarboxylate transporter SLC25A10 (COAD, LUAD, PRAD). SLC25A1 exports citrate from the mitochondria into the cytosol in exchange for malate (Mosaoa et al., 2021) and has previously been implicated in cancer adaptation to acidosis (Corbet, Pinto, et al., 2016). Corbet and colleagues demonstrated that under acidic pH, glucose metabolism is downregulated and fatty acid oxidation becomes the main source of acetyl-coenzyme A in SiHa, FaDu and HCT116 cell lines. All three cell lines upregulated SLC25A1 expression in acidic pH. This leads to an increased citrate efflux to the cytosol, which the authors propose allows for NADPH production, through the action of the malic enzyme, compensating for decreased pentose phosphate pathway flux in the absence of glucose. The same mechanism has been described in macrophages, grown in low glucose medium (Palmieri et al., 2015).

SLC25A10 transports dicarboxylates such as malate and succinate across the inner mitochondrial membrane in exchange for phosphate and sulfate (Dolce, Cappello, and Capobianco, 2014). High expression of this transporters has been associated

with unfavourable clinical outcome and metastasis in Osteosarcoma patients (G. Wang et al., 2020). To our knowledge, there are no known links between SLC25A10 and acidosis. SLC52A2 and SLC25A10 would both be an interesting subject for further investigation in the context of cancer cells adaptation to acidosis.

An interesting continuation of the current project would also be to investigate therapeutic vulnerabilities, caused by adaptations to acidosis. Our TCGA analysis suggested acidosis leads to upregulation of some members of the SLC22 family of drug transporters - SLC22A23 in GBM, SLC22A15 in LIHC, SLC22A2, SLC22A17 and SLC22A31 in PRAD. The orphan transporter SLC22A18 was upregulated in COAD, PAAD, READ and SKCM. Given the associations of the SLC22 family with transport of exogenous small molecules, these changes in SLC expression could lead to an increased drug uptake of particular chemotherapeutic compounds in acidic conditions. SLC22A2 for example has been associated with Metformin transport (Sajib et al., 2018). However, RNAseq of cancer cell lines revealed SLC22A17 and SLC22A31, along with SLC22A4 are all downregulated in lung cancer cell lines (Figure 5.4, Figure 5.5). These results reinforce the idea the effect of acidosis on SLC expression is cancer type specific. Pellegrini and colleagues performed a drug screen in HCT116 cell, chronically adapted to acidic pH (Pellegrini et al., 2018). The great majority of tested compounds showed a significant reduction in efficacy under acidic conditions. The study identified only 11 compounds, which showed consistent cytotoxicity towards control and acid-adapted cells. Verteporfin and Auranofin were the only clinical compounds, showing increased activity against acid-adapted cells. This study highlights the importance of the tumour microenvironment, not only in cancer progression but also in drug resistance. As acidosis is one of the most common characteristics of solid tumours, expanding this research to additional cell lines and cancer types would provide valuable insights on cancer sensitivity to chemotherapy in the clinic.

6.2 Acidosis in cell culture

Cell culture experiments provided the ability to separate acidosis from hypoxia in a way which is not plausible *in vivo*. It is important to mention that acidosis

could be mimicked by lowering media pH, achieved via additional buffering, or by media supplementation with lactic acid. The two conditions have been reported to produce similar transcriptional responses in breast cancer cell lines (J. L.-Y. Chen et al., 2008). However, they might have distinct effects on other cancer types, including non-small lung cancer cell lines (Daverio et al., 2023). Lactate is involved in a number of metabolic processes in cancer cells, independent of pH. The majority of solid tumours contain a population of glycolytic cells (often growing in hypoxic conditions) and a population of oxidative cells (Dhup et al., 2012). While glycolytic cells preferentially take up glucose and metabolise it to lactate, it is believed that oxidative cells are able to take up lactate via SLC16A1 and use it as a carbon source. Lactate can be oxidised to pyruvate, and enter the TCA cycle. This has been described as a 'metabolic symbiosis' in solid tumours (Dhup et al., 2012; Feron, 2009; Whitaker-Menezes et al., 2011). Evidence for this process has been observed in mouse models with MDA-MB-231 breast cancer xenografts (Bonuccelli et al., 2010) and mice bearing the human squamous carcinoma cell lines SiHa and WiDr (Sonveaux et al., 2008). In addition, lactate can act as a signalling molecule in cancer cells. Lactate was also shown to act as a hypoxia-mimetic, and activate the transcription factor HIF-1a in normoxic conditions, in glioma cell lines (Lu, Forbes, and Verma, 2002) as well as SiHa and WiDr cells (De Saedeleer et al., 2012). In this work, we have focused on the effects of acidic pH. To avoid any off-target metabolic effects of lactate in cancer cells, acidosis in culture media was achieved by a HEPES/PIPES based buffering system, rather than lactic acid supplementation.

Tumour acidosis has been proposed to facilitate survival during glucose starvation. This is linked to increased activity of proton-nutrient symporters and upregulation of fatty acids, glutamine and folate uptake (Daverio et al., 2023; Papalazarou and Maddocks, 2021). Consistent with this, our results showed the lung cancer cell line A549 and the colorectal cancer cell line HCT116 were both able to maintain higher growth rates in glucose-free media in acidic pH, compared to a neutral pH control (Figure 4.4, Figure 4.5).

In fact, there is evidence in literature that acidosis inhibits glycolysis, and cancer cells growing in acidic conditions show a preference for alternative nutrient sources

(Corbet, Draoui, et al., 2014; Corbet, Pinto, et al., 2016; J. Jiang et al., 2021; H. Wu, M. Ying, and X. Hu, 2016a). Consistent with this, our RNAseq data revealed downregulation of glycolytic genes in acidic pH, across a panel of 3 lung cancer cell lines. The lactate-producing enzyme LDHA was downregulated in all 3 cell lines (A549, H1299 and H661) (Figure 5.2B). Three additional glycolytic genes - PGK1, PGAM1 and PKM - were downregulated in H661. The glucose importer SLC2A1 was downregulated in A549 and H661 (Figure 5.4, Figure 5.5). SGK1, which is known to activate SLC2A1 (Palmada et al., 2006), was downregulates in all 3 cell lines. Finally, the lactate transporter SLC16A13 was downregulated in A549. All of these expression changes suggest a downregulation of glycolysis.

Our metabolomics data revealed an increase in intracellular fructose in HCT116 (Figure 4.16), A549 and H661 (Figure 5.9) in acidic pH. In addition, we observed an increase in intracellular sorbitol in A549. Cancer cells are able to metabolise glucose to fructose via sorbitol, using the polyol pathway. Fructose can then be further metabolised to dihydroxyacetone phosphate (DHAP) and glyceraldehyde (Krause and Wegner, 2020) (Figure 4.21). It is possible that these cell lines redirect glucose towards the polyol pathway instead of glycolysis in acidic pH. There are however no previous reports of this phenomenon in literature.

Colorectal cell lines showed a lesser response to acidic pH. However, HCT116 was also characterised by an increase in intracellular glucose (Figure 5.9) and downregulation of the glucose transporter SLC2A1 (Figure 5.4). These results suggest glycolysis could be inhibited by acidic pH in colorectal as well as lung cancer cell lines. Acidic pH was associated with a small but significant drop in intracellular amino acids in both HCT116 (Figure 4.15) and A549 (Figure 4.17). This could potentially be linked to a downregulation of mTOR activity and subsequently a slowing of cell proliferation. However mTOR signalling was not tested within this project due to time restraints.

A downregulation of mTOR activity would result in a reduction in cell growth and tumour progression. This would be consistent with the fact that the acidosis gene expression signatures we identified in lung cancer cell lines (LIVAS) was associated with better clinical outcomes (Figure 5.6). Similar results was reported by J. L.-Y.

Chen et al. (2008). The study identified an *in vitro* gene expression signature in mammary epithelial cells in response to low pH. The signature was associated with good survival outcomes in breast cancer, and was associated with tumours displaying a metabolic preference for aerobic respiration rather than glycolysis. The top 10 genes from this study were used here for identification of acidic samples in the TCGA analysis (Table 2.2). Interestingly, none of these genes were upregulated in our RNAseq data.

We hypothesise that acidosis promotes a less glycolytic and subsequently less aggressive phenotype in lung cancer, associated with a downregulation of the the glucose transporter SLC2A1, the lactate transporter SLC16A3 and the creatine transporter SLC6A8. However, this effect is not conserved if acidosis is combined with hypoxia. The two conditions promote a more glycolytic phenotype, associated with poorer clinical outcomes (Figure 5.11).

6.3 Creatine metabolism

Creatine metabolism was extensively studied in the 1980s and 1990s, mostly in the context of muscle cells. Little is known about the role of creatine in cancer progression, but in recent years there is an increased interest in the components of the creatine system. Although no direct mechanism linking acidosis to creatine metabolism was uncovered here, we demonstrated that lung cancer cell lines take up additional creatine, when it is available to them (Figure 4.10A). We also observed the presence of endogenous creatine in all three lung cancer cell lines tested (Figure 4.10B). Expression data from the CCLE database confirmed expression of creatine synthesis enzymes in lung cancer cells (Figure 4.20B), indicating these cell lines could indeed be capable of creatine synthesis. We showed the creatine transporter SLC6A8 is predominantly expressed in cancer cells in LUAD clinical samples (Figure 3.16, Figure 3.17), and is further upregulated in late stage LUAD tumours (Figure 3.18). Together, these results suggest creatine metabolism may play an important role in lung cancer progression.

In muscle cells, the creatine system is involved in maintaining intracellular pH by proton buffering. It is also implicated in allowing rapid ATP utilisation by ATPases

and continuous glycolysis in active muscle (The Wallimann, Schlösser, and Eppenberger, 1984; Theo Wallimann, Tokarska-Schlattner, and Schlattner, 2011; Theo Wallimann, Malus Wyss, et al., 1992). Some or all of these mechanisms could be conserved in cancer cells. We observed a decrease in intracellular ATP, following creatine supplementation in HCT116 cells in acidic pH (Figure 4.11). This could be a result of creatine and ATP being consumed to form phosphocreatine and ADP. This could be a mechanism to remove free ATP that could otherwise be inhibitory to glycolytic enzymes. No difference in intracellular ATP was observed in neutral pH control, suggesting this mechanism may be specific for acidosis.

Although targeting creatine metabolism alone is unlikely to be a successful cancer therapy, it is possible that combined with existing approaches, it could improve treatment outcomes. Both creatine and cyclocreatine have shown some therapeutic potential in animal models. In addition, RGX-202, which inhibits SLC6A8 specifically, is currently in clinical trials for colorectal cancer.

6.4 Limitations of the study

The results of our computational analysis (Chapter 3) were not reproducible *in vitro* in cell lines (Chapter 4). This could be due to a number of contributing factors, which are missing in 2D culture. The tumour microenvironment combines multiple cell types, and cells are subjected to oxygen, pH and nutrient fluctuations. In addition, many metabolites, including lactate, are involved in cell to cell interactions, and their impact on host cells can indirectly affect cancer progression. Lactate has been implicated in the inhibition of effector T cells, reduced motility of monocytes and macrophages and inhibition of the differentiation of monocytes to dendritic cells (Fischer et al., 2007; Gottfried et al., 2006; Hirschhaeuser, Sattler, and Mueller-Klieser, 2011). This aspect of acidosis could be modelled more accurately by co-culturing cancer cells with cells of the immune system, or culturing cancer cells in immune cells-conditioned media. In addition, cells in the core of solid tumours are likely to grow in a more acidic and highly hypoxic microenvironment, while cancer cells located in the tumour periphery are more likely to have access to nutrients and oxygen. This could be modelled *in vitro* using spheroids. It is possible that

although creatine supplementation had no impact on growth rates in 2D culture, it may impact other parameters of tumour growth in acidic pH, such as spheroid formation, shape, proliferation or invasiveness.

Some aspects of adaptation to acidosis are likely to be cancer type or even cell-line specific. Some of these adaptations are likely to be affected by driver mutations. This project took an exploratory approach to investigate SLC signatures across different tumours. Although we did not find any pan-cancer trends, we were able to identify a less aggressive phenotype in lung adenocarcinoma cell lines, associated with acidosis. Perhaps an RNAseq experiment performed with a panel of cell lines sharing the same driver mutations could reveal clearer trends and more specific adaptations, associated with particular oncogenic mutations in LUAD.

Machine learning based predictive models are gaining popularity in modelling biological systems. Perhaps modelling transcriptional changes in this manner can help in deconvoluting the effects of acidosis and hypoxia. Such computational approaches are already being applied to the tumour microenvironment. A study by Zeng et al. (2020) used machine learning to examine immune cells under hypoxic conditions in oral squamous cell carcinoma (OSCC). The study used DNA methylation data to identify a set of genes, likely to be activated in a hypoxic microenvironment. Peng and colleagues have developed a machine learning based pipeline using single cell transcriptomics data, to investigate ligand-receptor mediated intercellular communication in the tumour microenvironment (Peng et al., 2022). Perhaps similar approaches could be used to characterise SLC expression patterns in cancer cells.

The role of SLC transporters in cancer metabolism is an area of ongoing investigation. While numerous members of the SLC superfamily have been demonstrated to be involved in cancer progression, the molecular mechanism for many of them remain uncharacterised. Finally, further research is needed to unravel the expression patterns, functional significance and regulatory mechanisms of SLCs in cancer; given their emerging roles in both cancer metabolism and drug uptake, investigating the potential of targeting SLC transporters for cancer treatment holds promise for developing new therapeutic approaches.

Bibliography

Abplanalp, Jeannette et al. (2013). "The cataract and glucosuria associated monocarboxylate transporter MCT12 is a new creatine transporter". In: *Human molecular genetics* 22.16, pp. 3218–3226.

Abrego, Jaime et al. (2017). "GOT1-mediated anaplerotic glutamine metabolism regulates chronic acidosis stress in pancreatic cancer cells". In: *Cancer letters* 400, pp. 37–46.

Aerni-Flessner, Lauren B, Mitch C Otu, and Kelle H Moley (2011). "The amino acids upstream of NH (2)-terminal dileucine motif play a role in regulating the intracellular sorting of the Class III transporters GLUT8 and GLUT12". In: *Molecular membrane biology* 28.1, pp. 30–41.

Allgayer, Heike (2010). "Pdcd4, a colon cancer prognostic that is regulated by a microRNA". In: *Critical reviews in oncology/hematology* 73.3, pp. 185–191.

Andrews, S (June 2010). *FastQC: A Quality Control Tool for High Throughput Sequence Data*.

Antalis, Caryl J et al. (2011). "Migration of MDA-MB-231 breast cancer cells depends on the availability of exogenous lipids and cholesterol esterification". In: *Clinical & experimental metastasis* 28, pp. 733–741.

Anusewicz, Dorota, Magdalena Orzechowska, and Andrzej K Bednarek (2020). "Lung squamous cell carcinoma and lung adenocarcinoma differential gene expression regulation through pathways of Notch, Hedgehog, Wnt, and ErbB signalling". In: *Scientific reports* 10.1, pp. 1–15.

Arnold, Heidwolf and Dirk Pette (1970). "Binding of aldolase and triosephosphate dehydrogenase to F-actin and modification of catalytic properties of aldolase". In: *European Journal of Biochemistry* 15.2, pp. 360–366.

Augustin, Robert, Joan Riley, and Kelle H Moley (2005). "GLUT8 contains a [DE] XXXL [LI] sorting motif and localizes to a late endosomal/lysosomal compartment". In: *Traffic* 6.12, pp. 1196–1212.

Avnet, Sofia et al. (2017). "Cancer-associated mesenchymal stroma fosters the stemness of osteosarcoma cells in response to intratumoral acidosis via NF-κB activation". In: *International journal of cancer* 140.6, pp. 1331–1345.

Aykaç, Asli and Ahmet Ozer Sehirli (2020). "The role of the SLC transporters protein in the neurodegenerative disorders". In: *Clinical Psychopharmacology and Neuroscience* 18.2, p. 174.

Bareford, Lisa M et al. (2008). "Intracellular processing of riboflavin in human breast cancer cells". In: *Molecular pharmaceutics* 5.5, pp. 839–848.

Bessman, Samuel P and Christopher L Carpenter (1985). "The creatine-creatine phosphate energy shuttle". In: *Annual review of biochemistry* 54.1, pp. 831–862.

Bian, Yingjie et al. (2020). "Cancer SLC43A2 alters T cell methionine metabolism and histone methylation". In: *Nature* 585.7824, pp. 277–282.

Bodenhofer, Ulrich et al. (2015). "msa: an R package for multiple sequence alignment". In: *Bioinformatics* 31.24, pp. 3997–3999. DOI: 10.1093/bioinformatics/btv494.

Bonuccelli, Gloria et al. (2010). "Ketones and lactate "fuel" tumor growth and metastasis: Evidence that epithelial cancer cells use oxidative mitochondrial metabolism". In: *Cell cycle* 9.17, pp. 3506–3514.

Borst, P and R Oude Elferink (2002). "Mammalian ABC transporters in health and disease". In: *Annual review of biochemistry* 71.1, pp. 537–592.

Bröer, Stefan (2006). "The SLC6 orphans are forming a family of amino acid transporters". In: *Neurochemistry international* 48.6-7, pp. 559–567.

Bronstein, WW and HR Knull (1981). "Interaction of muscle glycolytic enzymes with thin filament proteins". In: *Canadian journal of biochemistry* 59.7, pp. 494–499.

Brown, Timothy P and Vadivel Ganapathy (2020). "Lactate/GPR81 signaling and proton motive force in cancer: Role in angiogenesis, immune escape, nutrition, and Warburg phenomenon". In: *Pharmacology & therapeutics* 206, p. 107451.

Brumback, Roger A, Jeffery W Gerst, and Harvey R Knull (1983). "High energy phosphate depletion in a model of defective muscle glycolysis". In: *Muscle & Nerve: Official Journal of the American Association of Electrodiagnostic Medicine* 6.1, pp. 52–55.

Buckler, K. J. and R. D. Vaughan-Jones (1990). "Application of a new pH-sensitive fluoroprobe (carboxy-SNARF-1) for intracellular pH measurement in small, isolated cells". In: *Pflügers Archiv* 417.2, pp. 234–239. ISSN: 0031-6768. DOI: 10.1007/bf00370705.

Butler, Andrew et al. (2018). "Integrating single-cell transcriptomic data across different conditions, technologies, and species". In: *Nature Biotechnology* 36, pp. 411–420. DOI: 10.1038/nbt.4096.

Butler, Miriam, Laurens T van der Meer, and Frank N van Leeuwen (2021). "Amino acid depletion therapies: starving cancer cells to death". In: *Trends in Endocrinology & Metabolism* 32.6, pp. 367–381.

Calcinotto, Arianna et al. (2012). "Modulation of Microenvironment Acidity Reverses Anergy in Human and Murine Tumor-Infiltrating T LymphocytespH and T-Cell Anergy". In: *Cancer research* 72.11, pp. 2746–2756.

Campos-Ferraz, PL et al. (2016). "Exploratory studies of the potential anti-cancer effects of creatine". In: *Amino acids* 48, pp. 1993–2001.

Canonaco, Fabrizio et al. (2002). "Functional expression of phosphagen kinase systems confers resistance to transient stresses in Saccharomyces cerevisiae by buffering the ATP pool". In: *Journal of Biological Chemistry* 277.35, pp. 31303–31309.

Cantor, Jason R. et al. (2017). "Physiologic Medium Rewires Cellular Metabolism and Reveals Uric Acid as an Endogenous Inhibitor of UMP Synthase". In: *Cell* 169.2, 258–272.e17. ISSN: 0092-8674. DOI: 10.1016/j.cell.2017.03.023.

Cesar-Razquin, Adrian et al. (2015). "A call for systematic research on solute carriers". In: *Cell* 162.3, pp. 478–487.

Chano, Tokuhiro et al. (2016). "Tumour-specific metabolic adaptation to acidosis is coupled to epigenetic stability in osteosarcoma cells". In: *American journal of cancer research* 6.4, p. 859.

Chen, Julia Ling-Yu et al. (2008). "The Genomic Analysis of Lactic Acidosis and Acidosis Response in Human Cancers". In: *PLoS Genetics* 4.12. lactic ac, e1000293. ISSN: 1553-7390. DOI: 10.1371/journal.pgen.1000293.

Chen, Yuan et al. (2003). "Loss of PDCD4 expression in human lung cancer correlates with tumour progression and prognosis". In: *The Journal of Pathology: A Journal of the Pathological Society of Great Britain and Ireland* 200.5, pp. 640–646.

Chiu, Martina et al. (2020). "Asparagine synthetase in cancer: beyond acute lymphoblastic leukemia". In: *Frontiers in Oncology* 9, p. 1480.

Cimino, Daniela et al. (2008). "Identification of new genes associated with breast cancer progression by gene expression analysis of predefined sets of neoplastic tissues". In: *International journal of cancer* 123.6, pp. 1327–1338.

Colaprico, Antonio et al. (2015). "TCGAbiolinks: An R/Bioconductor package for integrative analysis of TCGA data". In: *Nucleic Acids Research*. DOI: 10.1093/nar/gkv1507.

Colas, Claire et al. (2020). "Studies of structural determinants of substrate binding in the Creatine Transporter (CreaT, SLC6A8) using molecular models". In: *Scientific Reports* 10.1, p. 6241.

Colwell, Nicole et al. (2017). "Hypoxia in the glioblastoma microenvironment: shaping the phenotype of cancer stem-like cells". In: *Neuro-oncology* 19.7, pp. 887–896.

Cools, Jan (2012). "Improvements in the survival of children and adolescents with acute lymphoblastic leukemia". In: *Haematologica* 97.5, pp. 635–635.

Corbet, Cyril, Estelle Bastien, et al. (2020). "TGFβ2-induced formation of lipid droplets supports acidosis-driven EMT and the metastatic spreading of cancer cells". In: *Nature communications* 11.1, p. 454.

Corbet, Cyril, Nihed Draoui, et al. (2014). "The SIRT1/HIF2α Axis Drives Reductive Glutamine Metabolism under Chronic Acidosis and Alters Tumor Response to TherapyAcidosis-Triggered Reprogramming of Tumor Metabolism". In: *Cancer research* 74.19, pp. 5507–5519.

Corbet, Cyril and Olivier Feron (2017a). "Tumour acidosis: from the passenger to the driver's seat". In: *Nature Reviews Cancer* 17.10, nrc.2017.77. ISSN: 1474-1768. DOI: 10.1038/nrc.2017.77.

— (2017b). "Tumour acidosis: from the passenger to the driver's seat". In: *Nature Reviews Cancer* 17.10, pp. 577–593.

Corbet, Cyril, Adán Pinto, et al. (2016). "Acidosis drives the reprogramming of fatty acid metabolism in cancer cells through changes in mitochondrial and histone acetylation". In: *Cell metabolism* 24.2, pp. 311–323.

Counillon, Laurent et al. (2016). "Na+/H+ antiporter (NHE1) and lactate/H+ symporters (MCTs) in pH homeostasis and cancer metabolism". In: *Biochimica et Biophysica Acta (BBA)-Molecular Cell Research* 1863.10, pp. 2465–2480.

Damgaci, Sultan et al. (2018). "Hypoxia and acidosis: immune suppressors and therapeutic targets". In: *Immunology* 154.3, pp. 354–362.

Dang, Chi V (2013). "MYC, metabolism, cell growth, and tumorigenesis". In: *Cold Spring Harbor perspectives in medicine* 3.8, a014217.

Daverio, Zoé et al. (2023). "How Warburg-Associated Lactic Acidosis Rewires Cancer Cell Energy Metabolism to Resist Glucose Deprivation". In: *Cancers* 15.5, p. 1417.

Davuluri, Siva Prasad, FJR Hird, and RM McLean (1981). "A re-appraisal of the function and synthesis of phosphoarginine and phosphocreatine in muscle". In: *Comparative Biochemistry and Physiology Part B: Comparative Biochemistry* 69.3, pp. 329–336.

De Saedeleer, Christophe J et al. (2012). "Lactate activates HIF-1 in oxidative but not in Warburg-phenotype human tumor cells". In.

Delikatny, E James et al. (2011). "MR-visible lipids and the tumor microenvironment". In: *NMR in biomedicine* 24.6, pp. 592–611.

Dhup, Suveera et al. (2012). "Multiple biological activities of lactic acid in cancer: influences on tumor growth, angiogenesis and metastasis". In: *Current pharmaceutical design* 18.10, pp. 1319–1330.

Di Biase, Stefano et al. (2019). "Creatine uptake regulates CD8 T cell antitumor immunity". In: *Journal of Experimental Medicine* 216.12, pp. 2869–2882.

Dillon, Patrick F and Joseph F Clark (1990). "The theory of diazymes and functional coupling of pyruvate kinase and creatine kinase". In: *Journal of theoretical Biology* 143.2, pp. 275–284.

Dobin, Alexander et al. (2013). "STAR: ultrafast universal RNA-seq aligner". In: *Bioinformatics*. DOI: 10.1093/bioinformatics/bts635.

Dolce, Vincenza, Anna Rita Cappello, and Loredana Capobianco (2014). "Mitochondrial tricarboxylate and dicarboxylate–tricarboxylate carriers: from animals to plants". In: *IUBMB life* 66.7, pp. 462–471.

Dunbar, Lisa A and Michael J Caplan (2000). "The cell biology of ion pumps: sorting and regulation". In: *European journal of cell biology* 79.8, pp. 557–563.

Durinck, Steffen et al. (2005). "BioMart and Bioconductor: a powerful link between biological databases and microarray data analysis". In: *Bioinformatics* 21, pp. 3439–3440.

Eales, Katherine L, Kate ER Hollinshead, and Daniel A Tennant (2016). "Hypoxia and metabolic adaptation of cancer cells". In: *Oncogenesis* 5.1, e190–e190.

Ewels, Philip et al. (2016). "MultiQC: Summarize analysis results for multiple tools and samples in a single report". In: *Bioinformatics*. DOI: 10.1093/bioinformatics/btw354.

Fang, Jennifer S, Robert D Gillies, and Robert A Gatenby (2008). "Adaptation to hypoxia and acidosis in carcinogenesis and tumor progression". In: *Seminars in cancer biology*. Vol. 18. 5. Elsevier, pp. 330–337.

Farr, Clemens V et al. (2022). "Cooperative Binding of Substrate and Ions Drives Forward Cycling of the Human Creatine Transporter-1". In: *Frontiers in Physiology*, p. 1311.

Feng, Yan, Xiangyu Guo, and Huaping Tang (2021). "SLC6A8 is involved in the progression of non-small cell lung cancer through the Notch signaling pathway". In: *Annals of Translational Medicine* 9.3.

Fernandes, HS et al. (2017). "Amino acid deprivation using enzymes as a targeted therapy for cancer and viral infections". In: *Expert opinion on therapeutic patents* 27.3, pp. 283–297.

Feron, Olivier (2009). "Pyruvate into lactate and back: from the Warburg effect to symbiotic energy fuel exchange in cancer cells". In: *Radiotherapy and oncology* 92.3, pp. 329–333.

Fets, Louise, Paul C Driscoll, et al. (2018a). "MCT2 mediates concentration-dependent inhibition of glutamine metabolism by MOG". In: *Nature chemical biology* 14.11, pp. 1032–1042.

Fets, Louise, Paul C. Driscoll, et al. (2018b). "MCT2 mediates concentration-dependent inhibition of glutamine metabolism by MOG". In: *Nature Chemical Biology* 14.11, pp. 1032–1042. ISSN: 1552-4450. DOI: 10.1038/s41589-018-0136-y.

Finicle, Brendan T, Vaishali Jayashankar, and Aimee L Edinger (2018). "Nutrient scavenging in cancer". In: *Nature Reviews Cancer* 18.10, pp. 619–633.

Fischer, Karin et al. (2007). "Inhibitory effect of tumor cell–derived lactic acid on human T cells". In: *Blood* 109.9, pp. 3812–3819.

Foroutan, Momeneh et al. (2018). "Single sample scoring of molecular phenotypes". In: *BMC bioinformatics* 19.1, pp. 1–10.

Futagi, Yuya et al. (2020). "Molecular characterization of the orphan transporter SLC16A9, an extracellular pH-and Na+-sensitive creatine transporter". In: *Biochemical and Biophysical Research Communications* 522.2, pp. 539–544.

Gao, Jiayue et al. (2020). "Differential metabolic responses in breast cancer cell lines to acidosis and lactic acidosis revealed by stable isotope assisted metabolomics". In: *Scientific reports* 10.1, p. 21967.

Gatenby, Robert A et al. (2007). "Cellular adaptations to hypoxia and acidosis during somatic evolution of breast cancer". In: *British journal of cancer* 97.5, pp. 646–653.

Gatti, Laura and Franco Zunino (2005). "Overview of tumor cell chemoresistance mechanisms". In: *Chemosensitivity: Volume II: In VIVO Models, Imaging, and Molecular Regulators*, pp. 127–148.

Gillies, Robert J, Ian Robey, and Robert A Gatenby (2008). "Causes and consequences of increased glucose metabolism of cancers". In: *Journal of Nuclear Medicine* 49.Suppl 2, 24S–42S.

Good, Norman E et al. (1966). "Hydrogen ion buffers for biological research". In: *biochemistry* 5.2, pp. 467–477.

Gottfried, Eva et al. (2006). "Tumor-derived lactic acid modulates dendritic cell activation and antigen expression". In: *Blood* 107.5, pp. 2013–2021.

Griffiths, J (1991). "Are cancer cells acidic?" In: *British Journal of Cancer* 64, pp. 425–427. DOI: 10.1038/bjc.1991.326.

Guedes, Marta et al. (2016). "Modulation of the uptake of critical nutrients by breast cancer cells by lactate: Impact on cell survival, proliferation and migration". In: *Experimental cell research* 341.2, pp. 111–122.

Hagenbuch, Bruno and Peter J Meier (2004). "Organic anion transporting polypeptides of the OATP/SLC21 family: phylogenetic classification as OATP/SLCO superfamily, new nomenclature and molecular/functional properties". In: *Pflügers Archiv* 447, pp. 653–665.

Halbrook, Christopher J et al. (2019). "Macrophage-released pyrimidines inhibit gemcitabine therapy in pancreatic cancer". In: *Cell metabolism* 29.6, pp. 1390–1399.

Hannou, Sarah A et al. (2018). "Fructose metabolism and metabolic disease". In: *The Journal of clinical investigation* 128.2, pp. 545–555.

Hao, Guanyu, Zhi Ping Xu, and Li Li (2018). "Manipulating extracellular tumour pH: an effective target for cancer therapy". In: *RSC advances* 8.39, pp. 22182–22192.

Hao, Yuhan et al. (2021). "Integrated analysis of multimodal single-cell data". In: *Cell*. DOI: 10.1016/j.cell.2021.04.048.

Harris, Adrian L (2002). "Hypoxia—a key regulatory factor in tumour growth". In: *Nature reviews cancer* 2.1, pp. 38–47.

Hasselbalch, K (1917). "Die Berechnung der Wasserstoffzahl des Blutes aus der freien und gebundenen Kohlensäure und die Sauerstoffbindung des Blutes als Funktion der Wasserstoffzahl". In: *Biochem Z* 78, p. 113.

Hattori, Ayuna et al. (2017). "Cancer progression by reprogrammed BCAA metabolism in myeloid leukaemia". In: *Nature* 545.7655, pp. 500–504.

Hay, Nissim (2016). "Reprogramming glucose metabolism in cancer: can it be exploited for cancer therapy?" In: *Nature Reviews Cancer* 16.10, pp. 635–649.

He, Lei, Konstandinos Vasiliou, and Daniel W Nebert (2009). "Analysis and update of the human solute carrier (SLC) gene superfamily". In: *Human genomics* 3.2, pp. 1–12.

Hediger, Matthias A et al. (2004). "The ABCs of solute carriers: physiological, pathological and therapeutic implications of human membrane transport proteins: Introduction". In: *Pflügers Archiv* 447, pp. 465–468.

Hirschhaeuser, Franziska, Ulrike GA Sattler, and Wolfgang Mueller-Klieser (2011). "Lactate: a metabolic key player in cancer". In: *Cancer research* 71.22, pp. 6921–6925.

Hoffman, Robert M, Demetrius M Kokkinakis, and Eugene P Frenkel (2019). "Total methionine restriction treatment of cancer". In: *Methionine Dependence of Cancer and Aging: Methods and Protocols*, pp. 163–171.

Holman, Geoffrey D (2020). "Structure, function and regulation of mammalian glucose transporters of the SLC2 family". In: *Pflügers Archiv-European Journal of Physiology* 472.9, pp. 1155–1175.

Hoosein, NM et al. (1995). "Antiproliferative effects of cyclocreatine on human prostatic carcinoma cells." In: *Anticancer research* 15.4, pp. 1339–1342.

Hosios, Aaron M et al. (2016). "Amino acids rather than glucose account for the majority of cell mass in proliferating mammalian cells". In: *Developmental cell* 36.5, pp. 540–549.

Hu, Chengliang et al. (2020). "The solute carrier transporters and the brain: Physiological and pharmacological implications". In: *Asian journal of pharmaceutical sciences* 15.2, pp. 131–144.

Husain, Zaheed et al. (2013). "Tumor-derived lactate modifies antitumor immune response: effect on myeloid-derived suppressor cells and NK cells". In: *The Journal of Immunology* 191.3, pp. 1486–1495.

Ibrahim-Hashim, Arig and Veronica Estrella (2019). "Acidosis and cancer: from mechanism to neutralization". In: *Cancer and Metastasis Reviews* 38, pp. 149–155.

Ilhan, Zehra Esra et al. (2017). "pH-mediated microbial and metabolic interactions in fecal enrichment cultures". In: *Msphere* 2.3, e00047–17.

Iyengar, Melkote R, Cathryn E Fluellen, and Chungwha Iyengar (1982). "Creatine kinase from the bovine myometrium: purification and characterization". In: *Journal of Muscle Research & Cell Motility* 3, pp. 231–246.

Iyengar, Melkote Raja (1984). "Creatine kinase as an intracellular regulator". In: *Journal of Muscle Research & Cell Motility* 5.5, pp. 527–534.

Jacobus, William E (1985). "Respiratory control and the integration of heart high-energy phosphate metabolism by mitochondrial creatine kinase". In: *Annual review of physiology* 47.1, pp. 707–725.

Jager, Kitty J. et al. (2008). "The analysis of survival data: the Kaplan–Meier method". In: *Kidney International* 74.5, pp. 560–565. ISSN: 0085-2538. DOI: 10.1038/ki.2008.217.

Jawhari, Aida U et al. (2003). "Fascin, an actin-bundling protein, modulates colonic epithelial cell invasiveness and differentiation in vitro". In: *The American journal of pathology* 162.1, pp. 69–80.

Jewell, Jenna L, Ryan C Russell, and Kun-Liang Guan (2013). "Amino acid signalling upstream of mTOR". In: *Nature reviews Molecular cell biology* 14.3, pp. 133–139.

Jiang, Chengfei et al. (2021). "FHOD1 is upregulated in gastric cancer and promotes the proliferation and invasion of gastric cancer cells". In: *Oncology letters* 22.4, pp. 1–11.

Jiang, Jun et al. (2021). "Lactate modulates cellular metabolism through histone lactylation-mediated gene expression in non-small cell lung cancer". In: *Frontiers in oncology* 11, p. 647559.

Jomura, Ryuta et al. (2020). "Monocarboxylate transporter 12 as a guanidinoacetate efflux transporter in renal proximal tubular epithelial cells". In: *Biochimica et Biophysica Acta (BBA)-Biomembranes* 1862.11, p. 183434.

— (2021). "Contribution of monocarboxylate transporter 12 to blood supply of creatine on the sinusoidal membrane of the hepatocytes". In: *American Journal of Physiology-Gastrointestinal and Liver Physiology* 321.2, G113–G122.

Justus, Calvin R, Lixue Dong, and Li V Yang (2013). "Acidic tumor microenvironment and pH-sensing G protein-coupled receptors". In: *Frontiers in physiology* 4, p. 354.

Kammermeier, H (1987). "Interrelationship between the free energy change of ATP-hydrolysis, cytosolic inorganic phosphate and cardiac performance during hypoxia and reoxygenation." In: *Biomedica Biochimica Acta* 46.8-9, S499–504.

Kanehisa, Minoru et al. (2023). "KEGG for taxonomy-based analysis of pathways and genomes". In: *Nucleic Acids Research* 51.D1, pp. D587–D592.

Kassambara, Alboukadel et al. (2021). *Drawing Survival Curves using 'ggplot2'*. R package version 0.4.9.

Kazak, Lawrence and Paul Cohen (2020). "Creatine metabolism: energy homeostasis, immunity and cancer biology". In: *Nature Reviews Endocrinology* 16.8, pp. 421–436.

El-Kenawi, Asmaa E et al. (2015). "Extracellular acidosis alters polarization of macrophages". In: *Cancer Research* 75.15_Supplement, pp. 3213–3213.

Kim, Jihun et al. (2017). "Integrated genomic characterization of oesophageal carcinoma". In: *Nature* 541.7636, pp. 169–175. ISSN: 0028-0836. DOI: 10.1038/nature20805.

Kim, Nayoung et al. (2020). "Single-cell RNA sequencing demonstrates the molecular and cellular reprogramming of metastatic lung adenocarcinoma". In: *Nature communications* 11.1, p. 2285.

Knott, Simon RV et al. (2018). "Asparagine bioavailability governs metastasis in a model of breast cancer". In: *Nature* 554.7692, pp. 378–381.

Koepsell, Hermann (2013). "The SLC22 family with transporters of organic cations, anions and zwitterions". In: *Molecular aspects of medicine* 34.2-3, pp. 413–435.

Kolosenko, Iryna et al. (2017). "Therapeutic implications of tumor interstitial acidification". In: *Seminars in Cancer Biology*. Vol. 43. Elsevier, pp. 119–133.

Kosinski, Marcin and Przemyslaw Biecek (2021). *RTCGA: The Cancer Genome Atlas Data Integration*. R package version 1.24.0.

Kraft, Theresia et al. (2000). "Coupling of creatine kinase to glycolytic enzymes at the sarcomeric I-band of skeletal muscle: a biochemical study in situ". In: *Journal of muscle research and cell motility* 21.7, p. 691.

Krause, Nils and Andre Wegner (2020). "Fructose metabolism in cancer". In: *Cells* 9.12, p. 2635.

Krijthe, Jesse H. (2015). *Rtsne: T-Distributed Stochastic Neighbor Embedding using Barnes-Hut Implementation*. R package version 0.16.

Kristensen, CA et al. (1999). "Creatine and cyclocreatine treatment of human colon adenocarcinoma xenografts: 31P and 1H magnetic resonance spectroscopic studies". In: *British journal of cancer* 79.2, pp. 278–285.

Kumar, Saran et al. (2019). "Intra-Tumoral Metabolic Zonation and Resultant Phenotypic Diversification Are Dictated by Blood Vessel Proximity". In: *Cell Metabolism* 30.1, 201–211.e6. ISSN: 1550-4131. DOI: 10.1016/j.cmet.2019.04.003.

Kupriyanov, VV et al. (1980). "Phosphocreatine production coupled to the glycolytic reactions in the cytosol of cardiac cells". In: *Biochimica et Biophysica Acta (BBA)-Bioenergetics* 592.2, pp. 197–210.

Kurmi, Kiran et al. (2018). "Tyrosine phosphorylation of mitochondrial creatine kinase 1 enhances a druggable tumor energy shuttle pathway". In: *Cell metabolism* 28.6, pp. 833–847.

Kurth, Isabel et al. (2021). "Therapeutic targeting of SLC6A8 creatine transporter suppresses colon cancer progression and modulates human creatine levels". In: *Science advances* 7.41, eabi7511.

Kwon, Yong-Jin et al. (2020). "Extracellular acidosis promotes metastatic potency via decrease of the BMAL1 circadian clock gene in breast cancer". In: *Cells* 9.4, p. 989.

Ladep, Nimzing G et al. (2014). "Discovery and validation of urinary metabotypes for the diagnosis of hepatocellular carcinoma in West Africans". In: *Hepatology* 60.4, pp. 1291–1301.

Law, Charity W et al. (2014). "voom: precision weights unlock linear model analysis tools for RNA-seq read counts". In: *Genome Biology* 15.R29. DOI: 10.1186/gb-2014-15-2-r29.

Law, Charity W. et al. (2016). "RNA-seq analysis is easy as 1-2-3 with limma, Glimma and edgeR". In: *F1000 Research*. DOI: 10.12688/f1000research.9005.3.

Lee, Ji Young et al. (2019). "Extrinsic acidosis suppresses glycolysis and migration while increasing network formation in pulmonary microvascular endothelial cells". In: *American Journal of Physiology-Lung Cellular and Molecular Physiology* 317.2, pp. L188–L201.

Li, Jie et al. (2018). "FSCN1 promotes epithelial-mesenchymal transition through increasing snail1 in ovarian cancer cells". In: *Cellular Physiology and Biochemistry* 49.5, pp. 1766–1777.

Li, Jun et al. (2021). "CBX7 is dualistic in cancer progression based on its function and molecular interactions". In: *Frontiers in Genetics* 12, p. 740794.

Li, Ting-Ting et al. (2019). "Overview of organic anion transporters and organic anion transporter polypeptides and their roles in the liver". In: *World Journal of Clinical Cases* 7.23, p. 3915.

Li, Yong et al. (2022). "PAR2 promotes tumor-associated angiogenesis in lung adenocarcinoma through activating EGFR pathway". In: *Tissue and Cell* 79, p. 101918.

Lieu, Elizabeth L et al. (2020). "Amino acids in cancer". In: *Experimental & molecular medicine* 52.1, pp. 15–30.

Lin, Lawrence et al. (2015). "SLC transporters as therapeutic targets: emerging opportunities". In: *Nature reviews Drug discovery* 14.8, pp. 543–560.

Liu, Lei et al. (2017). "Lactate dehydrogenase and creatine kinase as poor prognostic factors in lung cancer: A retrospective observational study". In: *PLoS One* 12.8, e0182168.

Liu, Ruqing et al. (2007). "Cystine-glutamate transporter SLC7A11 mediates resistance to geldanamycin but not to 17-(allylamino)-17-demethoxygeldanamycin". In: *Molecular pharmacology* 72.6, pp. 1637–1646.

Liu, Tao et al. (2021). "mRNA expression level of CDH2, LEP, POSTN, TIMP1 and VEGFC modulates 5-fluorouracil resistance in colon cancer cells". In: *Experimental and Therapeutic Medicine* 22.3, pp. 1–12.

Liu, Xiaodong (2019). "SLC family transporters". In: *Drug Transporters in Drug Disposition, Effects and Toxicity*, pp. 101–202.

Loo, Jia Min et al. (2015). "Extracellular metabolic energetics can promote cancer progression". In: *Cell* 160.3, pp. 393–406.

Lou, Yuqing et al. (2021). "Akt kinase LANCL2 functions as a key driver in EGFR-mutant lung adenocarcinoma tumorigenesis". In: *Cell Death & Disease* 12.2, p. 170.

Love, Michael I., Wolfgang Huber, and Simon Anders (2014). "Moderated estimation of fold change and dispersion for RNA-seq data with DESeq2". In: *Genome Biology* 15 (12), p. 550. DOI: 10.1186/s13059-014-0550-8.

Lu, Huasheng, Robert A Forbes, and Ajay Verma (2002). "Hypoxia-inducible factor 1 activation by aerobic glycolysis implicates the Warburg effect in carcinogenesis". In: *Journal of Biological Chemistry* 277.26, pp. 23111–23115.

Lyssiotis, Costas A and Alec C Kimmelman (2017). "Metabolic interactions in the tumor microenvironment". In: *Trends in cell biology* 27.11, pp. 863–875.

Maguire, Olivia A et al. (2021). "Creatine-mediated crosstalk between adipocytes and cancer cells regulates obesity-driven breast cancer". In: *Cell metabolism* 33.3, pp. 499–512.

Manallack, David T et al. (2013). "The significance of acid/base properties in drug discovery". In: *Chemical Society Reviews* 42.2, pp. 485–496.

Marino, Maria Lucia et al. (2012). "Autophagy is a protective mechanism for human melanoma cells under acidic stress". In: *Journal of Biological Chemistry* 287.36, pp. 30664–30676.

Martin, K et al. (1996). "Specific targeting of tumor cells by the creatine analog cyclocreatine". In: *International Journal of Oncology* 9.5, pp. 993–999.

Mekhail, Karim et al. (2004). "HIF activation by pH-dependent nucleolar sequestration of VHL". In: *Nature cell biology* 6.7, pp. 642–647.

Meyer, RONALD A (1988). "A linear model of muscle respiration explains monoexponential phosphocreatine changes". In: *American Journal of Physiology-Cell Physiology* 254.4, pp. C548–C553.

Meyer, Ronald A, H Lee Sweeney, and Martin J Kushmerick (1984). "A simple analysis of the" phosphocreatine shuttle"". In: *American Journal of Physiology-Cell Physiology* 246.5, pp. C365–C377.

Meyer, RONALD A et al. (1986). "Phosphagen and intracellular pH changes during contraction of creatine-depleted rat muscle". In: *American Journal of Physiology-Cell Physiology* 250.2, pp. C264–C274.

Michl, Johanna, Kyung Chan Park, and Pawel Swietach (2019). "Evidence-based guidelines for controlling pH in mammalian live-cell culture systems". In: *Communications biology* 2.1, p. 144.

Microsoft Corporation (Sept. 24, 2018). *Microsoft Excel*. Version 2019 (16.0).

Miret, Noelia V et al. (2022). "Extracellular acidosis stimulates breast cancer cell motility through aryl hydrocarbon receptor and c-src kinase activation". In: *Journal of Cellular Biochemistry* 123.7, pp. 1197–1206.

Mishima, Eikan and Marcus Conrad (2023). "Nonmetabolic role for CKB in ferroptosis". In: *Nature Cell Biology*, pp. 1–2.

Moore, George E, Robert E Gerner, and H Addison Franklin (1967). "Culture of normal human leukocytes". In: *Jama* 199.8, pp. 519–524.

Morris, Lawrence R, Mary Beth Murphy, and Abbas E Kitabchi (1986). "Bicarbonate therapy in severe diabetic ketoacidosis". In: *Annals of internal medicine* 105.6, pp. 836–840.

Mosaoa, Rami et al. (2021). "The mitochondrial citrate carrier SLC25A1/CIC and the fundamental role of citrate in cancer, inflammation and beyond". In: *Biomolecules* 11.2, p. 141.

Murakami, Takashi et al. (1992). "Identification of two enhancer elements in the gene encoding the type 1 glucose transporter from the mouse which are responsive to serum, growth factor, and oncogenes." In: *Journal of Biological Chemistry* 267.13, pp. 9300–9306.

Nag, Jeetendra Kumar et al. (2023). "RNF43 induces the turnover of protease-activated receptor 2 in colon cancer". In: *The FASEB Journal* 37.1, e22675.

Nassar, Eyyad et al. (2021). "Syndecan-1 promotes angiogenesis in triple-negative breast cancer through the prognostically relevant tissue factor pathway and additional angiogenic routes". In: *Cancers* 13.10, p. 2318.

Newton, Holly et al. (2020). "Systemic muscle wasting and coordinated tumour response drive tumourigenesis". In: *Nature communications* 11.1, p. 4653.

Nyquist, Michael D, Bhagwat Prasad, and Elahe A Mostaghel (2017). "Harnessing solute carrier transporters for precision oncology". In: *Molecules* 22.4, p. 539.

O'Hagan, Steve et al. (2018). "GeneGini: Assessment via the Gini coefficient of reference "housekeeping" genes and diverse human transporter expression profiles". In: *Cell systems* 6.2, pp. 230–244.

Pallante, Pierlorenzo et al. (2010). "The loss of the CBX7 gene expression represents an adverse prognostic marker for survival of colon carcinoma patients". In: *European journal of cancer* 46.12, pp. 2304–2313.

Palmada, Monica et al. (2006). "SGK1 kinase upregulates GLUT1 activity and plasma membrane expression". In: *Diabetes* 55.2, pp. 421–427.

Palmieri, Erika M et al. (2015). "Acetylation of human mitochondrial citrate carrier modulates mitochondrial citrate/malate exchange activity to sustain NADPH production during macrophage activation". In: *Biochimica et Biophysica Acta (BBA)-Bioenergetics* 1847.8, pp. 729–738.

Papalazarou, Vasileios and Oliver DK Maddocks (2021). "Supply and demand: Cellular nutrient uptake and exchange in cancer". In: *Molecular Cell* 81.18, pp. 3731–3748.

Paradis, E. and K. Schliep (2019). "ape 5.0: an environment for modern phylogenetics and evolutionary analyses in R". In: *Bioinformatics* 35, pp. 526–528.

Pellegrini, Paola et al. (2018). "A drug screening assay on cancer cells chronically adapted to acidosis". In: *Cancer Cell International* 18.1, pp. 1–15.

Pelosi, G et al. (2003). "Independent prognostic value of fascin immunoreactivity in stage I nonsmall cell lung cancer". In: *British journal of cancer* 88.4, pp. 537–547.

Peng, Lihong et al. (2022). "Cell–cell communication inference and analysis in the tumour microenvironments from single-cell transcriptomics: data resources and computational strategies". In: *Briefings in Bioinformatics* 23.4, bbac234.

Pérez-Escuredo, Jhudit et al. (2016). "Lactate promotes glutamine uptake and metabolism in oxidative cancer cells". In: *Cell cycle* 15.1, pp. 72–83.

Pérez-Sala, Dolores, Dolores Collado-Escobar, and Faustino Mollinedo (1995). "Intracellular Alkalinization Suppresses Lovastatin-induced Apoptosis in HL-60 Cells through the Inactivation of a pH-dependent Endonuclease". In: *Journal of Biological Chemistry* 270.11, pp. 6235–6242.

Persi, Erez et al. (2018). "Systems analysis of intracellular pH vulnerabilities for cancer therapy". In: *Nature communications* 9.1, p. 2997.

Petan, Toni (2020). "Lipid droplets in cancer". In.

Pillai, Smitha et al. (2017). "Enhanced dependence on lipid metabolism is a cellular adaptation to acidic microenvironment". In: *Cancer Research* 77.13_Supplement, pp. 3538–3538.

Pilon-Thomas, Shari et al. (2016). "Neutralization of tumor acidity improves antitumor responses to immunotherapy". In: *Cancer research* 76.6, pp. 1381–1390.

Pizzagalli, Mattia D, Ariel Bensimon, and Giulio Superti-Furga (2021). "A guide to plasma membrane solute carrier proteins". In: *The FEBS journal* 288.9, pp. 2784–2835.

Poortmans, JR et al. (1997). "Effect of short-term creatine supplementation on renal responses in men". In: *European journal of applied physiology and occupational physiology* 76, pp. 566–567.

Pouysségur, Jacques et al. (1984). "A specific mutation abolishing Na+/H+ antiport activity in hamster fibroblasts precludes growth at neutral and acidic pH." In: *Proceedings of the National Academy of Sciences* 81.15, pp. 4833–4837.

Prado-Garcia, Heriberto, Andrea Campa-Higareda, and Susana Romero-Garcia (2020a). "Lactic Acidosis in the Presence of Glucose Diminishes Warburg Effect in Lung Adenocarcinoma Cells". In: *Frontiers in Oncology* 10, p. 807. ISSN: 2234-943X. DOI: 10.3389/fonc.2020.00807.

Prado-Garcia, Heriberto, Andrea Campa-Higareda, and Susana Romero-Garcia (2020b). "Lactic acidosis in the presence of glucose diminishes Warburg effect in lung adenocarcinoma cells". In: *Frontiers in oncology* 10, p. 807.

Pyla, Rajkumar et al. (2013). "Expression of conventional and novel glucose transporters, GLUT1,-9,-10, and-12, in vascular smooth muscle cells". In: *American Journal of Physiology-Cell Physiology*.

Qi, Jing et al. (2020). "Identification of UAP1L1 as tumor promotor in gastric cancer through regulation of CDK6". In: *Aging (Albany NY)* 12.8, p. 6904.

R Core Team (2013). *R: A Language and Environment for Statistical Computing*. R Foundation for Statistical Computing. Vienna, Austria.

Raghunand, N et al. (1999). "Enhancement of chemotherapy by manipulation of tumour pH". In: *British journal of cancer* 80.7, pp. 1005–1011.

Ramos, Marcel, Lucas Schiffer, and Levi Waldron (2022). *TCGAutils: TCGA utility functions for data management*. R package version 1.14.1.

Ren, Xueting et al. (2022). "Identification of a combined apoptosis and hypoxia gene signature for predicting prognosis and immune infiltration in breast cancer". In: *Cancer Medicine* 11.20, pp. 3886–3901.

Reshkin, Stephan J et al. (2000). "Na+/H+ exchanger-dependent intracellular alkalinization is an early event in malignant transformation and plays an essential role in the development of subsequent transformation-associated phenotypes". In: *The FASEB Journal* 14.14, pp. 2185–2197.

Riemann, A et al. (2016). "Acidosis promotes metastasis formation by enhancing tumor cell motility". In: *Oxygen Transport to Tissue XXXVII*. Springer, pp. 215–220.

Riemann, Anne et al. (2014). "Acidic priming enhances metastatic potential of cancer cells". In: *Pflügers Archiv-European Journal of Physiology* 466, pp. 2127–2138.

Ritchie, Matthew E et al. (2015). "limma powers differential expression analyses for RNA-sequencing and microarray studies". In: *Nucleic Acids Research* 43.7, e47. DOI: 10.1093/nar/gkv007.

Rizwan, Ahsan N and Gerhard Burckhardt (2007). "Organic anion transporters of the SLC22 family: biopharmaceutical, physiological, and pathological roles". In: *Pharmaceutical research* 24, pp. 450–470.

Robinson, Mark D, Davis J McCarthy, and Gordon K Smyth (2010). "edgeR: a Bioconductor package for differential expression analysis of digital gene expression data". In: *Bioinformatics* 26.1, pp. 139–140. DOI: 10.1093/bioinformatics/btp616.

Rothberg, Jennifer M et al. (2013). "Acid-mediated tumor proteolysis: contribution of cysteine cathepsins". In: *Neoplasia* 15.10, 1125–IN9.

RStudio Team (2020). *RStudio: Integrated Development Environment for R*. RStudio, PBC. Boston, MA.

Ruprecht, Jonathan J and Edmund RS Kunji (2020). "The SLC25 mitochondrial carrier family: structure and mechanism". In: *Trends in biochemical sciences* 45.3, pp. 244–258.

Russell, Aaron P et al. (2014). "Creatine transporter (SLC6A8) knockout mice display an increased capacity for in vitro creatine biosynthesis in skeletal muscle". In: *Frontiers in physiology* 5, p. 314.

Sajib, Abu Ashfaqur et al. (2018). "Interaction of rs316019 variants of SLC22A2 with metformin and other drugs-an in silico analysis". In: *Journal of Genetic Engineering and Biotechnology* 16.2, pp. 769–775.

Samanta, Debangshu and Gregg L Semenza (2018). "Metabolic adaptation of cancer and immune cells mediated by hypoxia-inducible factors". In: *Biochimica et Biophysica Acta (BBA)-Reviews on Cancer* 1870.1, pp. 15–22.

Sarode, Poonam et al. (2020). "Epithelial cell plasticity defines heterogeneity in lung cancer". In: *Cellular Signalling* 65, p. 109463.

Satija, Rahul et al. (2015). "Spatial reconstruction of single-cell gene expression data". In: *Nature Biotechnology* 33, pp. 495–502. DOI: 10.1038/nbt.3192.

Schäfer, Beat W and Jean-Claude Perriard (1988). "Intracellular targeting of isoproteins in muscle cytoarchitecture." In: *The Journal of cell biology* 106.4, pp. 1161–1170.

Schiffenbauer, YAEL S et al. (1996). "Cyclocreatine transport and cytotoxicity in rat glioma and human ovarian carcinoma cells: 31P-NMR spectroscopy". In: *American Journal of Physiology-Cell Physiology* 270.1, pp. C160–C169.

Schumann, Tina et al. (2021). "Deletion of the diabetes candidate gene Slc16a13 in mice attenuates diet-induced ectopic lipid accumulation and insulin resistance". In: *Communications Biology* 4.1, p. 826.

Schwab, Annemarie et al. (2018). "Polyol Pathway Links Glucose Metabolism to the Aggressiveness of Cancer CellsPolyol Pathway in Aggressive Cancers". In: *Cancer research* 78.7, pp. 1604–1618.

Scopes, Robert K (1973). "Studies with a reconstituted muscle glycolytic system. The rate and extent of creatine phosphorylation by anaerobic glycolysis". In: *Biochemical Journal* 134.1, pp. 197–208.

Scott, Laura J et al. (2007). "A genome-wide association study of type 2 diabetes in Finns detects multiple susceptibility variants". In: *science* 316.5829, pp. 1341–1345.

Sculier, JP, C Nicaise, and J Klastersky (1983). "Lactic acidosis: a metabolic complication of extensive metastatic cancer". In: *European Journal of Cancer and Clinical Oncology* 19.5, pp. 597–601.

Sheen, Joon-Ho et al. (2011). "Defective regulation of autophagy upon leucine deprivation reveals a targetable liability of human melanoma cells in vitro and in vivo". In: *Cancer cell* 19.5, pp. 613–628.

Sivadas, Ambily, Victor C Kok, and Ka-Lok Ng (2022). "Multi-omics analyses provide novel biological insights to distinguish lobular ductal types of invasive breast cancers". In: *Breast Cancer Research and Treatment* 193.2, pp. 361–379.

Soikkeli, Johanna et al. (2010). "Metastatic outgrowth encompasses COL-I, FN1, and POSTN up-regulation and assembly to fibrillar networks regulating cell adhesion, migration, and growth". In: *The American journal of pathology* 177.1, pp. 387–403.

Sonveaux, Pierre et al. (2008). "Targeting lactate-fueled respiration selectively kills hypoxic tumor cells in mice". In: *The Journal of clinical investigation* 118.12, pp. 3930–3942.

Sourkes, TL and K Missala (1981). "Putrescine metabolism and the study of diamine oxidase activity in vivo". In: *Agents and Actions* 11, pp. 20–27.

Sousa, Cristovão M et al. (2016). "Pancreatic stellate cells support tumour metabolism through autophagic alanine secretion". In: *Nature* 536.7617, pp. 479–483.

Sprowl, Jason A and Alex Sparreboom (2014). "Uptake carriers and oncology drug safety". In: *Drug Metabolism and Disposition* 42.4, pp. 611–622.

Stolfi, C et al. (2014). "A functional role for Smad7 in sustaining colon cancer cell growth and survival". In: *Cell death & disease* 5.2, e1073–e1073.

Strutz-Seebohm, Nathalie et al. (2007). "PIKfyve in the SGK1 mediated regulation of the creatine transporter SLC6A8". In: *Cellular physiology and biochemistry* 20.6, pp. 729–734.

Stuart, Charles A et al. (2009). "Insulin-stimulated translocation of glucose transporter (GLUT) 12 parallels that of GLUT4 in normal muscle". In: *The Journal of Clinical Endocrinology & Metabolism* 94.9, pp. 3535–3542.

Stuart, Tim et al. (2019). "Comprehensive Integration of Single-Cell Data". In: *Cell* 177, pp. 1888–1902. DOI: 10.1016/j.cell.2019.05.031.

Sun, Ruipu et al. (2020). "The emerging role of the SLCO1B3 protein in cancer resistance". In: *Protein and Peptide Letters* 27.1, pp. 17–29.

Superti-Furga, Giulio et al. (2020). "The RESOLUTE consortium: unlocking SLC transporters for drug discovery". In: *Nature reviews Drug discovery* 19.7, pp. 429–430.

Supuran, Claudiu T (2008). "Carbonic anhydrases: novel therapeutic applications for inhibitors and activators". In: *Nature reviews Drug discovery* 7.2, pp. 168–181.

Suwannasom, Nittiya et al. (2020). "Riboflavin: The Health Benefits of a Forgotten Natural Vitamin". In: *International Journal of Molecular Sciences* 21.3. ISSN: 1422-0067.

Swietach, áP et al. (2010). "New insights into the physiological role of carbonic anhydrase IX in tumour pH regulation". In: *Oncogene* 29.50, pp. 6509–6521.

Tachikawa, Masanori et al. (2012). "γ-Aminobutyric acid transporter 2 mediates the hepatic uptake of guanidinoacetate, the creatine biosynthetic precursor, in rats". In: *PloS one* 7.2, e32557.

Taddei, ML et al. (2012). "Anoikis: an emerging hallmark in health and diseases". In: *The Journal of pathology* 226.2, pp. 380–393.

Tan, Shirlee, David Schubert, and Pamela Maher (2001). "Oxytosis: a novel form of programmed cell death". In: *Current topics in medicinal chemistry* 1.6, pp. 497–506.

Tang, Zhiyuan et al. (2018). "Serum and glucocorticoid-regulated kinase 1 (SGK1) is a predictor of poor prognosis in non-small cell lung cancer, and its dynamic pattern following treatment with SGK1 inhibitor and γ-ray irradiation was elucidated". In: *Oncology Reports* 39.3, pp. 1505–1515.

Tanner, Lukas Bahati et al. (2018). "Four Key Steps Control Glycolytic Flux in Mammalian Cells". In: *Cell Systems* 7.1, 49–62.e8. ISSN: 2405-4712. DOI: 10.1016/j.cels.2018.06.003.

Teicher, Beverly A et al. (1995). "Cyclocreatine in cancer chemotherapy". In: *Cancer chemotherapy and pharmacology* 35, pp. 411–416.

Thwaites, David T and Catriona MH Anderson (2011). "The SLC36 family of proton-coupled amino acid transporters and their potential role in drug transport". In: *British journal of pharmacology* 164.7, pp. 1802–1816.

Turner, David C, Theo Wallimann, and Hans M Eppenberger (1973). "A protein that binds specifically to the M-line of skeletal muscle is identified as the muscle form of creatine kinase". In: *Proceedings of the National Academy of Sciences* 70.3, pp. 702–705.

Uldry, Marc et al. (2002). "GLUT2 is a high affinity glucosamine transporter". In: *FEBS letters* 524.1-3, pp. 199–203.

Ventura-Clapier, RENEE et al. (1987). "Reversible MM-creatine kinase binding to cardiac myofibrils". In: *American Journal of Physiology-Cell Physiology* 253.3, pp. C444–C455.

Vo Nguyen, Thanh Thao et al. (2014). "TMEPAI/PMEPA 1 enhances tumorigenic activities in lung cancer cells". In: *Cancer science* 105.3, pp. 334–341.

Wallimann, T et al. (1989). "Subcellular compartmentation of creatine kinase isoenzymes, regulation of CK and octameric structure of mitochondrial CK: important aspects of the phosphoryl-creatine circuit." In: *Progress in clinical and biological research* 315, pp. 159–176.

Wallimann, The, T Schlösser, and Hans M Eppenberger (1984). "Function of M-line-bound creatine kinase as intramyofibrillar ATP regenerator at the receiving end of the phosphorylcreatine shuttle in muscle." In: *Journal of Biological Chemistry* 259.8, pp. 5238–5246.

Wallimann, Theo and Hans M Eppenberger (1985). *Localization and function of M-line-bound creatine kinase: M-band model and creatine phosphate shuttle*. Springer.

Wallimann, Theo, Malgorzata Tokarska-Schlattner, Dietbert Neumann, et al. (2007). "The phosphocreatine circuit: molecular and cellular physiology of creatine kinases, sensitivity to free radicals, and enhancement by creatine supplementation". In: *Molecular system bioenergetics: Energy for life*, pp. 195–264.

Wallimann, Theo, Malgorzata Tokarska-Schlattner, and Uwe Schlattner (2011). "The creatine kinase system and pleiotropic effects of creatine". In: *Amino acids* 40, pp. 1271–1296.

Wallimann, Theo, Malus Wyss, et al. (1992). "Intracellular compartmentation, structure and function of creatine kinase isoenzymes in tissues with high and fluctuating energy demands: the'phosphocreatine circuit'for cellular energy homeostasis." In: *Biochemical Journal* 281.Pt 1, p. 21.

Wang, Gaoyuan et al. (2020). "SLC25A10 performs an oncogenic role in human osteosarcoma". In: *Oncology Letters* 20.4, pp. 1–1.

Warburg, Otto, Franz Wind, and Erwin Negelein (1927). "The metabolism of tumors in the body". In: *The Journal of general physiology* 8.6, p. 519.

Webb, Bradley A et al. (2011). "Dysregulated pH: a perfect storm for cancer progression". In: *Nature Reviews Cancer* 11.9, pp. 671–677.

Wedeken, Lena, Priyanka Singh, and Karl-Heinz Klempnauer (2011). "Tumor suppressor protein Pdcd4 inhibits translation of p53 mRNA". In: *Journal of Biological Chemistry* 286.50, pp. 42855–42862.

Wegmann, Gabi et al. (1992). "In situ compartmentation of creatine kinase in intact sarcomeric muscle: the acto-myosin overlap zone as a molecular sieve". In: *Journal of Muscle Research & Cell Motility* 13, pp. 420–435.

Whitaker-Menezes, Diana et al. (2011). "Evidence for a stromal-epithelial "lactate shuttle" in human tumors: MCT4 is a marker of oxidative stress in cancer-associated fibroblasts". In: *Cell cycle* 10.11, pp. 1772–1783.

White, Katharine A, Bree K Grillo-Hill, and Diane L Barber (2017). "Cancer cell behaviors mediated by dysregulated pH dynamics at a glance". In: *Journal of cell science* 130.4, pp. 663–669.

Wickham, Hadley (2016). *ggplot2: Elegant Graphics for Data Analysis*. Springer-Verlag New York. ISBN: 978-3-319-24277-4.

Winter, Georg E et al. (2014). "The solute carrier SLC35F2 enables YM155-mediated DNA damage toxicity". In: *Nature chemical biology* 10.9, pp. 768–773.

Wojtkowiak, Jonathan W et al. (2012). "Chronic Autophagy Is a Cellular Adaptation to Tumor Acidic pH MicroenvironmentsChronic Autophagic Response to Extracellular Acidosis". In: *Cancer research* 72.16, pp. 3938–3947.

Wright, Jonathan L et al. (2011). "Expression of SLCO transport genes in castration-resistant prostate cancer and impact of genetic variation in SLCO1B3 and SLCO2B1 on prostate cancer outcomes". In: *Cancer Epidemiology, Biomarkers & Prevention* 20.4, pp. 619–627.

Wright, Nicholas J et al. (2022). "Methotrexate recognition by the human reduced folate carrier SLC19A1". In: *Nature* 609.7929, pp. 1056–1062.

Wu, Fengying et al. (2021). "Single-cell profiling of tumor heterogeneity and the microenvironment in advanced non-small cell lung cancer". In: *Nature Communications* 12.1, p. 2540. DOI: 10.1038/s41467-021-22801-0.

Wu, Hao, Minfeng Ying, and Xun Hu (2016a). "Lactic acidosis switches cancer cells from aerobic glycolysis back to dominant oxidative phosphorylation". In: *Oncotarget* 7.26, p. 40621.

— (2016b). "Lactic acidosis switches cancer cells from aerobic glycolysis back to dominant oxidative phosphorylation". In: *Oncotarget* 7.26, pp. 40621–40629. ISSN: 1949-2553. DOI: 10.18632/oncotarget.9746.

Wu, Tianzhi et al. (2021). "clusterProfiler 4.0: A universal enrichment tool for interpreting omics data". In: *The Innovation* 2.3, p. 100141. DOI: 10.1016/j.xinn.2021.100141.

Wykoff, C C et al. (2000). "Hypoxia-inducible expression of tumor-associated carbonic anhydrases." In: *Cancer research* 60.24, pp. 7075–83. ISSN: 0008-5472.

Wyss, Markus and Rima Kaddurah-Daouk (2000). "Creatine and creatinine metabolism". In: *Physiological reviews* 80.3, pp. 1107–1213.

Xiaobo, Yu et al. (2016). "Serum and glucocorticoid kinase 1 promoted the growth and migration of non-small cell lung cancer cells". In: *Gene* 576.1, pp. 339–346.

Xie, Jiansheng et al. (2014). "Beyond Warburg effect–dual metabolic nature of cancer cells". In: *Scientific reports* 4.1, p. 4927.

Xu, Daqian et al. (2020). "The gluconeogenic enzyme PCK1 phosphorylates INSIG1/2 for lipogenesis". In: *Nature* 580.7804, pp. 530–535.

Yang, Lifeng et al. (2016). "Targeting stromal glutamine synthetase in tumors disrupts tumor microenvironment-regulated cancer cell growth". In: *Cell metabolism* 24.5, pp. 685–700.

Yang, Yang, Meng Wang, and Bao Liu (2019). "Exploring and comparing of the gene expression and methylation differences between lung adenocarcinoma and squamous cell carcinoma". In: *Journal of cellular physiology* 234.4, pp. 4454–4459.

Ye, Jian et al. (2012). "Primer-BLAST: A tool to design target-specific primers for polymerase chain reaction". In: *BMC Bioinformatics* 13. DOI: 10.1186/1471-2105-13-134.

Yu, Guangchuang (2022). *enrichplot: Visualization of Functional Enrichment Result*. R package version 1.14.2.

Yu, Guangchuang and Qing-Yu He (2016). "ReactomePA: an R/Bioconductor package for reactome pathway analysis and visualization". In: *Molecular BioSystems* 12.12, pp. 477–479. DOI: 10.1039/C5MB00663E.

Yu, Guangchuang, David Smith, et al. (2017). "ggtree: an R package for visualization and annotation of phylogenetic trees with their covariates and other associated

data." In: *Methods in Ecology and Evolution* 8 (1), pp. 28–36. DOI: 10.1111/2041-210X.12628.

Yu, Guangchuang, Li-Gen Wang, Yanyan Han, et al. (2012). "clusterProfiler: an R package for comparing biological themes among gene clusters". In: *OMICS: A Journal of Integrative Biology* 16.5, pp. 284–287. DOI: 10.1089/omi.2011.0118.

Yu, Guangchuang, Li-Gen Wang, Guang-Rong Yan, et al. (2015). "DOSE: an R/Bioconductor package for Disease Ontology Semantic and Enrichment analysis". In: *Bioinformatics* 31.4, pp. 608–609. DOI: 10.1093/bioinformatics/btu684.

Yuan, Lu et al. (2020). "SLC6A8 knockdown suppresses the invasion and migration of human hepatocellular carcinoma Huh-7 and Hep3B cells". In: *Technology in Cancer Research & Treatment* 19, p. 1533033820983029.

Yue, Ming et al. (2017). "Oncogenic MYC activates a feedforward regulatory loop promoting essential amino acid metabolism and tumorigenesis". In: *Cell reports* 21.13, pp. 3819–3832.

Zeng, Hao et al. (2020). "Machine learning analysis of DNA methylation in a hypoxia-immune model of oral squamous cell carcinoma". In: *International Immunopharmacology* 89, p. 107098.

Zhang, Liwen and Pengcheng Bu (2022). "The two sides of creatine in cancer". In: *Trends in Cell Biology* 32.5, pp. 380–390.

Zhang, Liwen, Zijing Zhu, et al. (2021). "Creatine promotes cancer metastasis through activation of Smad2/3". In: *Cell Metabolism* 33.6, pp. 1111–1123.

Zhong, Chenhan et al. (2019). "Zyxin as a potential cancer prognostic marker promotes the proliferation and metastasis of colorectal cancer cells". In: *Journal of cellular physiology* 234.9, pp. 15775–15789.

Zieker, Derek et al. (2008). "Lactate modulates gene expression in human mesenchymal stem cells". In: *Langenbeck's archives of surgery* 393, pp. 297–301.

Appendix A

Differentially expressed SLC transporters in acidosis

gene_name	log2FC	adj.P.Val	cancer	Analysis
SLC27A6	-2.253888168	3.065473E-3	BRCA	Acidosis
SLC25A27	-1.942221945	1.8732500000000001E-4	BRCA	Acidosis
SLC26A5	-1.769920205	9.510335E-3	BRCA	Acidosis
SLC16A6P1	-1.6191256439999999	4.7559957999999999E-2	BRCA	Acidosis
SLC25A1	1.4412753039999999	6.664629E-3	BRCA	Acidosis
SLC1A5	1.5130384859999999	7.0667780000000001E-3	BRCA	Acidosis
SLC52A2	1.5135972209999999	9.8764160000000007E-3	BRCA	Acidosis
SLC7A11-AS1	-2.631873068	1.0946697E-2	COAD	Acidosis
SLC9C1	-2.5702828769999999	2.0371159999999998E-3	COAD	Acidosis
SLC13A4	-2.0118591289999999	8.4228500000000002E-4	COAD	Acidosis
SLC6A16	-1.8999103930000001	2.8836245E-2	COAD	Acidosis
SLC1A2	-1.874421584	3.9051629999999997E-2	COAD	Acidosis
SLC8A1	-1.6076796900000001	4.0239342999999997E-2	COAD	Acidosis
SLC35A4	1.55679251	4.2354376999999999E-2	COAD	Acidosis
SLC50A1	1.591608205	2.9372728000000001E-2	COAD	Acidosis
SLC25A5	1.683534393	1.2125980999999999E-2	COAD	Acidosis

SLC25A22	1.685786966	4.4958063999999999E-2	COAD	Acidosis
SLC35C1	1.705297227	9.6313739999999998E-3	COAD	Acidosis
SLC25A39	1.729697338	2.3419651E-2	COAD	Acidosis
SLC16A13	1.732707494	6.1436299999999998E-3	COAD	Acidosis
SLC27A4	1.767869082	9.5325659999999993E-3	COAD	Acidosis
SLC25A11	1.769344185	8.5500000000000003E-3	COAD	Acidosis
SLC9A3R2	1.8217931650000001	2.4452387999999999E-2	COAD	Acidosis
SLC25A1	1.8845302230000001	3.1138440000000002E-3	COAD	Acidosis
SLC22A18	1.9347640260000001	1.0295515E-2	COAD	Acidosis
SLC44A4	1.9692951919999999	7.2718800000000003E-4	COAD	Acidosis
SLC39A3	2.000284679	1.0421219999999999E-3	COAD	Acidosis
SLC25A6	2.0958479890000001	2.9310999999999999E-3	COAD	Acidosis
SLC39A4	2.1388605049999998	1.547631E-2	COAD	Acidosis
SLC6A8	2.242172547	1.5406669999999999E-3	COAD	Acidosis
SLC25A10	2.2436732500000001	9.7028399999999997E-4	COAD	Acidosis
SLC18A1	2.9906234789999999	2.352214E-3	COAD	Acidosis
SLC8A3	-3.8096110900000002	2.5260408000000002E-2	ESCA	Acidosis
SLC26A10	-2.7936750469999998	4.9971282999999998E-2	ESCA	Acidosis
SLC6A16	-2.7606156799999999	4.6629906999999998E-2	ESCA	Acidosis
SLCO5A1	-3.2410842529999999	3.1086539999999999E-2	GBM	Acidosis
SLC25A27	-2.560857387	2.6350913E-2	GBM	Acidosis
SLC17A6	-3.3794500379999999	2.3779859999999999E-3	LGG	Acidosis
SLC6A7	-2.970567886	4.1314126E-2	LGG	Acidosis
SLC17A8	-2.7396860360000002	1.92809E-2	LGG	Acidosis
SLC1A6	-2.6918187009999999	1.0317951000000001E-2	LGG	Acidosis
SLC8A2	-2.6046648889999999	2.5262850000000001E-3	LGG	Acidosis
SLC6A15	-2.3942527509999998	3.4347709999999997E-2	LGG	Acidosis
SLC26A10	-2.2246657390000002	1.7594299999999999E-4	LGG	Acidosis
SLC34A3	-1.7758007010000001	1.4333340999999999E-2	LGG	Acidosis

SLC25A27	-1.5514225960000001	2.5262850000000001E-3	LGG	Acidosis
SLC26A1	-1.455043742	3.4824453999999998E-2	LGG	Acidosis
SLC15A3	1.6837829980000001	4.6724490000000004E-3	LGG	Acidosis
SLC47A2	2.4532984610000002	8.5988899999999997E-3	LGG	Acidosis
SLC27A5	3.1622842360000001	4.0639049999999996E-3	LIHC	Acidosis
SLC10A1	3.5939981849999998	3.0194151999999998E-2	LIHC	Acidosis
SLCO5A1	-2.2277771720000001	4.1670550000000002E-3	LUAD	Acidosis
SLC25A27	-2.0224915280000002	2.0811190000000002E-3	LUAD	Acidosis
SLC13A4	-1.9246716260000001	1.30167E-3	LUAD	Acidosis
SLC4A8	-1.728669359	2.1563129E-2	LUAD	Acidosis
SLC39A1	1.484166724	3.2757741E-2	LUAD	Acidosis
SLC39A3	1.491231762	4.8951110999999999E-2	LUAD	Acidosis
SLC10A3	1.5827353799999999	4.4510772999999997E-2	LUAD	Acidosis
SLC35B2	1.732515721	1.3632819999999999E-3	LUAD	Acidosis
SLC25A39	1.7603264329999999	1.3117637999999999E-2	LUAD	Acidosis
SLC2A4RG	1.7887213230000001	1.1102107E-2	LUAD	Acidosis
SLC52A2	1.8712348320000001	9.3361639999999992E-3	LUAD	Acidosis
SLC9A3R2	1.874449788	3.3480068000000002E-2	LUAD	Acidosis
SLC25A6	1.8788876219999999	8.0144199999999995E-3	LUAD	Acidosis
SLC25A10	1.8972902389999999	3.869782E-3	LUAD	Acidosis
SLC50A1	1.9541658719999999	2.4776000000000003E-4	LUAD	Acidosis
SLC39A4	2.4144164180000001	2.03005E-4	LUAD	Acidosis
SLC26A10	-2.3264580690000001	2.5279000000000002E-4	LUSC	Acidosis
SLC26A5	-2.1646778289999999	1.2548027E-2	LUSC	Acidosis
SLC25A25-AS1	-1.9837876329999999	4.4517599999999999E-3	LUSC	Acidosis
SLC5A4-AS1	-2.0158456340000002	7.6451269999999998E-3	PRAD	Acidosis
SLC13A4	-1.7417121440000001	2.19E-5	PRAD	Acidosis

SLC5A4	-1.659007498	1.319808E-3	PRAD	Acidosis
SLC6A6	-1.6228494499999999	3.9700000000000002E-7	PRAD	Acidosis
SLC4A8	-1.590355027	3.4300000000000002E-6	PRAD	Acidosis
SLC26A10	-1.553052095	2.0742100000000001E-4	PRAD	Acidosis
SLC9A3	-1.5029786140000001	1.3227034E-2	PRAD	Acidosis
SLC5A9	-1.421990997	2.1816349999999999E-3	PRAD	Acidosis
SLC16A7	-1.389186544	4.8912700000000001E-4	PRAD	Acidosis
SLC24A4	-1.370760626	5.1973000000000002E-3	PRAD	Acidosis
SLC25A25-AS1	-1.329403084	5.9563200000000002E-4	PRAD	Acidosis
SLC25A27	-1.321218161	1.359273E-3	PRAD	Acidosis
SLC6A1	-1.276761445	3.7677829999999998E-3	PRAD	Acidosis
SLC16A8	-1.2367016719999999	2.4275082E-2	PRAD	Acidosis
SLC17A9	-1.2330376750000001	1.7018300000000001E-3	PRAD	Acidosis
SLC10A6	-1.1550457430000001	4.8246689000000002E-2	PRAD	Acidosis
SLC25A5P1	-1.1227466269999999	3.3118789000000003E-2	PRAD	Acidosis
SLC26A8	-1.1021736070000001	3.2030034999999998E-2	PRAD	Acidosis
SLC14A2	-1.0991195149999999	3.903939E-2	PRAD	Acidosis
SLC25A11	1.0061600850000001	2.5867109999999998E-3	PRAD	Acidosis
SLC19A1	1.0258767449999999	3.9929620000000001E-3	PRAD	Acidosis
SLC25A1	1.0535016450000001	1.319808E-3	PRAD	Acidosis
SLC39A3	1.05642861	1.8386380000000001E-3	PRAD	Acidosis
SLC13A3	1.075326537	1.0964883E-2	PRAD	Acidosis
SLC52A2	1.0846114499999999	9.9297399999999994E-3	PRAD	Acidosis
SLC25A30-AS1	1.088322072	1.7385402000000001E-2	PRAD	Acidosis
SLC25A39	1.0995992539999999	1.5802979999999999E-3	PRAD	Acidosis
SLC27A4	1.1383330700000001	2.0774000000000001E-4	PRAD	Acidosis
SLC45A3	1.162563609	2.1367862000000001E-2	PRAD	Acidosis

SLC50A1	1.262547077	1.08E-6	PRAD	Acidosis
SLC43A1	1.271660389	9.2763700000000008E-3	PRAD	Acidosis
SLC52A3	1.2892272010000001	1.0575444999999999E-2	PRAD	Acidosis
SLC25A10	1.291048559	7.0810600000000001E-4	PRAD	Acidosis
SLC39A7	1.2956861799999999	1.9099999999999999E-6	PRAD	Acidosis
SLC9A3R2	1.363567033	1.91E-5	PRAD	Acidosis
SLC44A4	1.3701226989999999	8.6999999999999997E-6	PRAD	Acidosis
SLC27A2	1.4370571940000001	3.9100000000000002E-5	PRAD	Acidosis
SLC25A48	1.6447090550000001	2.807515E-3	PRAD	Acidosis
SLC22A31	2.6386003179999999	2.76E-5	PRAD	Acidosis
SLC7A2	-2.5036730349999998	2.4565535999999999E-2	READ	Acidosis
SLC22A18	1.9893878570000001	9.1524829999999995E-3	READ	Acidosis
SLC22A18AS	2.1148057979999999	1.0126075E-2	READ	Acidosis
SLC44A5	-3.4672962709999999	1.6604250000000001E-3	SKCM	Acidosis
SLC26A7	-2.835010499	1.782732E-3	SKCM	Acidosis
SLC25A21-AS1	-2.3633232689999999	3.1936145999999999E-2	SKCM	Acidosis
SLC15A2	-2.2427243020000001	8.5925770000000005E-3	SKCM	Acidosis
SLC25A25-AS1	-1.7608934009999999	2.6629462999999999E-2	SKCM	Acidosis
SLC35C1	1.4354780220000001	2.8218445000000002E-2	SKCM	Acidosis
SLC66A1	1.4968800600000001	2.3185095999999999E-2	SKCM	Acidosis
SLC52A2	1.7913854760000001	1.255866E-3	SKCM	Acidosis
SLC35E4	1.852165649	2.0557200000000001E-2	SKCM	Acidosis
SLC22A18	2.0598125650000001	3.744711E-3	SKCM	Acidosis
SLC22A18AS	1.81433193	4.5588640000000001E-3	COAD	CA
SLC6A8	2.225951475	1.803874E-3	COAD	CA
SLC51B	2.313501976	1.8330864999999998E-2	COAD	CA
SLC9A3	2.678279571	9.9807909999999993E-3	COAD	CA

SLC4A4	2.8231870840000002	3.4258560000000001E-3	COAD	CA
SLC28A2	3.011811228	6.9173200000000002E-3	COAD	CA
SLC26A3	3.4707974369999999	8.8759719999999993E-3	COAD	CA
SLC6A19	4.4197011599999998	4.0899999999999998E-6	COAD	CA
SLC7A8	-3.3443202630000002	3.7938696000000001E-2	ESCA	CA
SLC34A2	4.7440495619999998	1.5094382999999999E-2	ESCA	CA
SLC4A4	5.010213351	2.7437356999999999E-2	ESCA	CA
SLC6A20	5.3664853800000003	1.3117225E-2	ESCA	CA
SLC39A5	6.2712940000000001	3.7686379999999999E-3	ESCA	CA
SLC12A5	2.4674672000000002	1.9743523999999998E-2	LGG	CA
SLC6A17	2.5949191470000001	3.3772209999999997E-2	LGG	CA
SLC4A10	2.7204906379999998	2.7846260000000001E-3	LGG	CA
SLC17A6	2.8023899120000002	3.0442547E-2	LGG	CA
SLC32A1	2.8263703140000001	3.1272442999999997E-2	LGG	CA
SLC39A12	2.846073069	1.4433995999999999E-2	LGG	CA
SLC6A7	3.1155574349999999	3.1272442999999997E-2	LGG	CA
SLC26A4-AS1	3.3536216259999998	3.1484400000000002E-3	LGG	CA
SLC38A4	2.5794658990000001	2.9434439999999999E-2	LUSC	CA
SLC38A5	2.7713195129999999	1.7799999999999999E-5	LUSC	CA
SLC6A15	3.1119523280000001	1.7750377000000001E-2	LUSC	CA
SLC22A18	2.4771161720000001	3.1152830999999999E-2	PAAD	CA
SLC1A1	2.4912512690000002	1.8284584999999999E-2	PAAD	CA
SLC9A2	3.2250384150000002	4.9778189E-2	PAAD	CA
SLC28A3	3.5778367609999999	1.0521631E-2	PAAD	CA
SLC4A4	3.833648894	3.1250539999999999E-3	PAAD	CA
SLC6A20	4.3794062299999998	1.2460934E-2	PAAD	CA
SLC34A2	4.4026007480000002	6.8824059999999998E-3	PAAD	CA
SLC3A1	4.5789200980000002	7.4535929999999997E-3	PAAD	CA

SLC9A4	4.7067599180000004	1.5318317999999999E-2	PAAD	CA
SLC2A9	1.501322716	2.4158911000000002E-2	PRAD	CA
SLC1A7	1.6610152229999999	2.8153259999999999E-2	PRAD	CA
SLC8A1	1.677618096	1.6822325999999999E-2	PRAD	CA
SLC24A3	1.780422368	1.3685660000000001E-3	PRAD	CA
SLC22A2	1.8062390399999999	3.8230543999999998E-2	PRAD	CA
SLC51B	1.8876661299999999	4.3725680000000003E-3	PRAD	CA
SLC35F4	1.888628505	1.027083E-3	PRAD	CA
SLC22A17	1.9436947389999999	9.3200000000000001E-8	PRAD	CA
SLC47A1	2.0634722970000001	7.8000000000000005E-7	PRAD	CA
SLC19A3	2.1006353610000001	2.4243474000000001E-2	PRAD	CA
SLC35F1	2.2725988890000002	1.33E-5	PRAD	CA
SLC52A1	2.4494305289999998	2.2900000000000001E-5	PRAD	CA
SLC27A6	2.6310496950000002	2.0553699999999999E-4	PRAD	CA
SLC16A5	2.635752632	1.3399999999999999E-8	PRAD	CA
SLC22A3	2.6595246260000001	4.0500000000000002E-5	PRAD	CA
SLC2A5	3.1979550689999998	1.66E-7	PRAD	CA
SLC2A4	3.22112255	7.2699999999999996E-14	PRAD	CA
SLC14A1	3.2519997429999998	3.5899999999999997E-8	PRAD	CA
SLC15A1	3.449056707	5.5400000000000001E-7	PRAD	CA
SLC39A2	3.8920914369999999	3.7500000000000001E-7	PRAD	CA
SLC5A8	3.947275522	5.6799999999999999E-8	PRAD	CA
SLC7A4	4.1936773150000004	9.53E-8	PRAD	CA
SLC4A4	3.1649855929999999	1.7123329999999999E-3	READ	CA
SLC28A2	4.1051510230000003	1.7123329999999999E-3	READ	CA
SLC2A1	1.862881419	4.6264187999999998E-2	SKCM	CA
SLC7A13	-2.9125542709999999	3.7899999999999999E-7	BRCA	Glycolysis
SLC26A3	-2.9040947799999999	1.6096099999999999E-4	BRCA	Glycolysis
SLC6A4	-2.7747394339999998	4.1733800000000001E-4	BRCA	Glycolysis

SLC44A4	-2.3588656100000001	1.7755030000000002E-2	BRCA	Glycolysis
SLC38A11	-2.306985697	4.9300000000000002E-6	BRCA	Glycolysis
SLC44A5	-2.0194631709999999	3.5043364E-2	BRCA	Glycolysis
SLC14A1	-1.7215304309999999	2.5076889000000002E-2	BRCA	Glycolysis
SLC2A3	1.5204058819999999	8.9872370000000004E-3	BRCA	Glycolysis
SLC16A10	1.8724956939999999	1.3920320000000001E-3	BRCA	Glycolysis
SLC2A6	1.887438669	2.2099999999999998E-5	BRCA	Glycolysis
SLC2A5	1.983707908	4.6699999999999997E-5	BRCA	Glycolysis
SLC2A1	2.1235571489999998	1.6100000000000001E-11	BRCA	Glycolysis
SLC6A17	2.3211955290000001	8.48123E-4	BRCA	Glycolysis
SLC7A5	2.3875694200000002	8.09E-7	BRCA	Glycolysis
SLC6A14	2.612587671	4.9603292E-2	BRCA	Glycolysis
SLCO4A1	2.673755791	1.49E-9	BRCA	Glycolysis
SLC16A3	2.881007232	2.4099999999999999E-29	BRCA	Glycolysis
SLC6A4	-2.5289492020000002	3.1475633000000003E-2	COAD	Glycolysis
SLC38A11	-2.3903896590000002	2.3381972000000001E-2	COAD	Glycolysis
SLC25A27	-1.6860458760000001	4.3747542E-2	COAD	Glycolysis
SLC37A1	1.6836589310000001	6.6701590000000002E-3	COAD	Glycolysis
SLC9A1	1.7038670490000001	1.0423465999999999E-2	COAD	Glycolysis
SLC9A3R1	1.709136295	3.2101987999999998E-2	COAD	Glycolysis
SLC2A1	1.7345829989999999	1.9784446000000001E-2	COAD	Glycolysis
SLC35C1	1.790682031	4.495733E-3	COAD	Glycolysis
SLC27A4	1.804730173	1.6426435E-2	COAD	Glycolysis
SLC25A1	1.848565485	1.7154584E-2	COAD	Glycolysis
SLC66A2	1.940313867	8.1340500000000001E-4	COAD	Glycolysis
SLC22A18AS	2.0474903360000001	2.0366939999999999E-3	COAD	Glycolysis
SLC4A11	2.0707199639999998	9.5194200000000007E-3	COAD	Glycolysis
SLC25A48	2.1105535010000001	2.3501358E-2	COAD	Glycolysis
SLC25A22	2.2093499140000001	2.8293200000000001E-4	COAD	Glycolysis

SLC22A18	2.2110992669999998	4.53571E-4	COAD	Glycolysis
SLC25A10	2.238540091	3.8220300000000001E-3	COAD	Glycolysis
SLC6A8	2.7296789719999999	1.1199999999999999E-5	COAD	Glycolysis
SLC16A3	2.8218344530000001	5.1600000000000002E-15	COAD	Glycolysis
SLC16A3	2.6253819709999999	1.7367126E-2	ESCA	Glycolysis
SLC22A23	1.9754850989999999	1.8861169000000001E-2	GBM	Glycolysis
SLC39A14	2.3716823150000002	7.5015009999999998E-3	GBM	Glycolysis
SLC6A6	2.8258122380000001	1.4425832E-2	GBM	Glycolysis
SLC16A3	2.8592219330000002	8.0099999999999995E-5	GBM	Glycolysis
SLC2A3	3.4549425039999999	4.3500000000000002E-7	GBM	Glycolysis
SLC9A1	1.4459203430000001	2.0101376000000001E-2	LGG	Glycolysis
SLC25A24	1.6311706720000001	2.8748969999999999E-2	LGG	Glycolysis
SLC44A3	1.69673524	4.8879752999999998E-2	LGG	Glycolysis
SLC35G2	1.7950376539999999	6.7602570000000004E-3	LGG	Glycolysis
SLC2A12	1.831090106	8.2334680000000007E-3	LGG	Glycolysis
SLC44A3-AS1	1.8752016199999999	2.1110951999999999E-2	LGG	Glycolysis
SLC26A4	2.2426213420000001	7.5334410000000001E-3	LGG	Glycolysis
SLC2A3	2.6827476419999998	4.2E-10	LGG	Glycolysis
SLC39A12	3.047687571	9.9568399999999994E-4	LGG	Glycolysis
SLC26A4-AS1	3.1077113399999998	1.6357765E-2	LGG	Glycolysis
SLC6A7	3.1988703959999998	4.0124594999999999E-2	LGG	Glycolysis
SLC30A3	3.3540557880000001	7.6369940000000002E-3	LGG	Glycolysis
SLC9A7P1	3.4441370980000001	1.6099999999999999E-8	LGG	Glycolysis
SLC7A10	3.885371921	3.24743E-4	LGG	Glycolysis
SLC10A1	-5.3489523849999996	5.1800000000000004E-6	LIHC	Glycolysis
SLC22A7	-4.693609887	5.41E-5	LIHC	Glycolysis
SLC38A3	-4.3455435859999998	1.15E-6	LIHC	Glycolysis

SLC25A47	-4.1324477249999996	5.7846590000000002E-3	LIHC	Glycolysis
SLC22A10	-4.0956260379999998	7.4800000000000002E-5	LIHC	Glycolysis
SLC2A2	-4.0893344279999999	2.94E-5	LIHC	Glycolysis
SLC22A9	-4.035275145	2.3499999999999999E-6	LIHC	Glycolysis
SLC27A5	-4.0321158490000002	1.04E-7	LIHC	Glycolysis
SLC39A5	-3.8995862319999999	2.9634000000000003E-4	LIHC	Glycolysis
SLC13A5	-3.8217181920000001	7.3092199999999995E-4	LIHC	Glycolysis
SLC6A1	-3.5304095329999998	4.9799999999999998E-6	LIHC	Glycolysis
SLC22A1	-3.4432071720000001	1.0390178E-2	LIHC	Glycolysis
SLC17A2	-3.3710725099999999	2.6730730000000002E-3	LIHC	Glycolysis
SLC17A4	-2.9877885540000002	4.3500199999999998E-4	LIHC	Glycolysis
SLC51A	-2.8577729679999999	4.433658E-3	LIHC	Glycolysis
SLC47A1	-2.8573878920000002	7.3499999999999998E-5	LIHC	Glycolysis
SLC22A25	-2.7918053490000001	8.1286329999999997E-3	LIHC	Glycolysis
SLC6A12	-2.5719401770000001	1.3151210999999999E-2	LIHC	Glycolysis
SLC16A11	-2.567167634	1.9334599000000001E-2	LIHC	Glycolysis
SLC15A1	-2.551909067	4.5695281999999997E-2	LIHC	Glycolysis
SLC30A10	-2.453236296	4.6229929999999997E-3	LIHC	Glycolysis
SLC7A9	-2.3598885159999998	7.2770999999999999E-3	LIHC	Glycolysis
SLC17A1	-2.313772331	4.207996E-2	LIHC	Glycolysis
SLC46A1	-1.740614431	2.6467729999999998E-3	LIHC	Glycolysis
SLC2A4RG	-1.6459881709999999	1.834664E-3	LIHC	Glycolysis
SLC25A10	-1.5985485859999999	2.9528186000000001E-2	LIHC	Glycolysis
SLC25A12	1.779916743	4.4167786000000001E-2	LIHC	Glycolysis
SLC9A1	1.801040363	2.3990399999999999E-3	LIHC	Glycolysis
SLC35E4	1.8398942069999999	9.4795139999999996E-3	LIHC	Glycolysis
SLC44A3-AS1	1.843666161	3.2527385999999998E-2	LIHC	Glycolysis
SLC4A7	1.8596308539999999	1.9896079999999999E-3	LIHC	Glycolysis

SLC9A9	2.027530257	7.9768760000000008E-3	LIHC	Glycolysis
SLC16A6	2.0552706779999999	1.4292005999999999E-2	LIHC	Glycolysis
SLC7A7	2.3580328650000002	1.6158200000000001E-4	LIHC	Glycolysis
SLC8A1	2.396510041	6.1600000000000007E-5	LIHC	Glycolysis
SLC22A15	2.3966289810000001	4.8213058000000003E-2	LIHC	Glycolysis
SLC7A8	2.4004100689999999	1.2683799999999999E-3	LIHC	Glycolysis
SLC11A1	2.4458698270000001	5.0852500000000001E-4	LIHC	Glycolysis
SLC1A5	2.5077273510000002	5.1270500000000002E-4	LIHC	Glycolysis
SLC4A11	2.7751012099999999	1.800837E-3	LIHC	Glycolysis
SLC7A11	2.8659955849999998	9.1380179999999995E-3	LIHC	Glycolysis
SLC38A5	2.8758176010000001	2.0588799999999999E-4	LIHC	Glycolysis
SLC7A1	2.90230202	7.6141900000000005E-4	LIHC	Glycolysis
SLC25A24	2.9170925900000002	2.62E-5	LIHC	Glycolysis
SLC2A3	3.0288614300000001	2.7300000000000002E-7	LIHC	Glycolysis
SLC35F2	3.0695066139999998	2.9899999999999998E-5	LIHC	Glycolysis
SLC2A5	3.25797296	1.1515218000000001E-2	LIHC	Glycolysis
SLC38A1	3.282436653	2.1299999999999999E-5	LIHC	Glycolysis
SLC6A8	3.6562567920000002	7.2799999999999995E-7	LIHC	Glycolysis
SLC4A3	3.6690209540000001	4.9017199999999998E-4	LIHC	Glycolysis
SLCO4A1	3.7152284990000002	4.9799999999999998E-5	LIHC	Glycolysis
SLC16A3	3.71574859	5.2999999999999998E-11	LIHC	Glycolysis
SLC2A1	3.8390998920000001	4.2999999999999996E-9	LIHC	Glycolysis
SLC6A6	4.1701629069999999	2.8699999999999999E-8	LIHC	Glycolysis
SLC34A2	5.5970570439999996	8.6362199999999998E-4	LIHC	Glycolysis
SLC5A2	-2.5103655919999999	9.7600000000000001E-5	LUAD	Glycolysis
SLC5A9	-2.2647514439999998	8.7995049999999991E-3	LUAD	Glycolysis
SLC26A5	-2.0524057529999999	3.2521609999999999E-2	LUAD	Glycolysis
SLC25A27	-1.9032948460000001	9.4628209999999997E-3	LUAD	Glycolysis
SLC2A5	2.1715957850000001	2.5886120000000001E-3	LUAD	Glycolysis

SLC6A8	2.2011643950000002	2.3446E-4	LUAD	Glycolysis
SLC2A3	2.3451838669999998	6.19E-6	LUAD	Glycolysis
SLC16A1	2.7707391029999999	1.2699999999999999E-6	LUAD	Glycolysis
SLCO4A1	2.9482832019999998	7.3200000000000002E-6	LUAD	Glycolysis
SLC16A3	2.9973438510000001	3.0799999999999998E-16	LUAD	Glycolysis
SLC2A1	4.0959020119999998	1.09E-31	LUAD	Glycolysis
SLC16A3	2.1282484099999999	1.9300000000000002E-5	LUSC	Glycolysis
SLC6A8	2.3398784099999999	1.1507730000000001E-2	LUSC	Glycolysis
SLC2A1	2.4894867399999998	3.1953E-4	LUSC	Glycolysis
SLC20A1	2.140918128	3.7507914000000003E-2	PAAD	Glycolysis
SLC22A18	2.3393987009999999	3.6480951999999997E-2	PAAD	Glycolysis
SLC22A18AS	2.3945499080000001	4.2983502E-2	PAAD	Glycolysis
SLC7A11	2.7451568150000001	4.1720766999999999E-2	PAAD	Glycolysis
SLCO4A1	3.1276339320000002	6.9513350000000003E-3	PAAD	Glycolysis
SLC16A3	3.4253156520000001	7.00558E-4	PAAD	Glycolysis
SLC2A1	4.2790108719999997	7.8299999999999996E-9	PAAD	Glycolysis
SLC25A27	-1.3834838	1.6088210000000001E-3	PRAD	Glycolysis
SLC39A5	-1.293927982	2.725309E-3	PRAD	Glycolysis
SLC29A1	1.029383666	8.2575200000000008E-3	PRAD	Glycolysis
SLC25A25	1.066682353	1.7447326999999999E-2	PRAD	Glycolysis
SLC37A2	1.1046613059999999	4.9445784E-2	PRAD	Glycolysis
SLC6A6	1.1988420500000001	7.0192839999999998E-3	PRAD	Glycolysis
SLC7A5	1.2252057949999999	2.377922E-2	PRAD	Glycolysis
SLC6A20	1.3966229370000001	4.0662210999999997E-2	PRAD	Glycolysis
SLC2A3	1.43994358	1.022443E-2	PRAD	Glycolysis
SLC18A2	1.592595293	2.5542727000000001E-2	PRAD	Glycolysis
SLC10A6	1.6230116459999999	3.741879E-3	PRAD	Glycolysis
SLC25A27	-2.7268373399999999	1.3699999999999999E-5	SKCM	Glycolysis
SLC15A2	-2.3872844569999998	2.8726422000000001E-2	SKCM	Glycolysis

SLC35E4	1.759200382	2.6049177999999999E-2	SKCM	Glycolysis
SLC16A13	1.958329521	1.4820165E-2	SKCM	Glycolysis
SLC22A18AS	2.2650523410000001	3.3409845000000001E-2	SKCM	Glycolysis
SLC1A4	2.4091893209999999	3.633776E-3	SKCM	Glycolysis
SLC27A3	2.506609734	1.2854389000000001E-2	SKCM	Glycolysis
SLC2A6	2.66971048	1.1336300000000001E-4	SKCM	Glycolysis
SLC11A1	2.7630801279999999	1.31E-5	SKCM	Glycolysis
SLC6A12	2.7740746399999998	8.0831299999999996E-4	SKCM	Glycolysis
SLC2A1	2.932869905	1.07E-16	SKCM	Glycolysis
SLC16A6	3.1799493139999999	3.6178531E-2	SKCM	Glycolysis
SLC2A3	3.5721462939999999	5.8500000000000001E-17	SKCM	Glycolysis
SLC16A3	4.0305572310000004	5.8500000000000001E-17	SKCM	Glycolysis

Table A.1: Differentially expressed SLC transporters in Acidosis - A full list of hits across the 3 analysis streams. Cut offs: $\log_2$(Fold change) ≥ 1, adjusted P value $\leq$ 0.05. CA - Carbonic anhydrases

Appendix B

Differentially expressed SLC transporters in hypoxia

gene_name	log2FC	adj.P.Val	cancer	Analysis
SLC25A24P1	-2.639402332	1.5568323E-2	BRCA	Hypoxia
SLC12A4	1.266071857	1.0918535E-2	BRCA	Hypoxia
SLC43A3	1.415958126	1.2009614E-2	BRCA	Hypoxia
SLC16A3	1.5001980150000001	2.2080605E-2	BRCA	Hypoxia
SLC1A3	1.506627988	9.0298960000000008E-3	BRCA	Hypoxia
SLC16A1	1.576692781	1.6114186999999999E-2	BRCA	Hypoxia
SLC1A7	1.6090919560000001	3.7962831000000002E-2	BRCA	Hypoxia
SLC16A7	1.6364629020000001	3.9491120000000003E-3	BRCA	Hypoxia
SLC38A4	1.7537232380000001	3.9610490999999998E-2	BRCA	Hypoxia
SLC24A2	1.846793551	3.4391788999999999E-2	BRCA	Hypoxia
SLC16A10	1.8716234839999999	4.4029900000000001E-4	BRCA	Hypoxia
SLC2A5	2.0285681370000002	8.3999999999999992E-6	BRCA	Hypoxia
SLC66A1L	2.0866646310000001	2.4620099999999998E-4	BRCA	Hypoxia
SLCO4A1	2.1281172879999999	1.28348E-4	BRCA	Hypoxia
SLC2A3	2.2644347680000001	2.5399999999999999E-16	BRCA	Hypoxia
SLC6A17	2.3432104909999998	9.8499999999999995E-5	BRCA	Hypoxia
SLC38A5	2.3557369119999998	1.7700000000000001E-9	BRCA	Hypoxia

SLC28A3	2.4205324090000002	4.1894499999999999E-4	BRCA	Hypoxia
SLC5A1	2.5052279820000001	2.6387939999999999E-3	BRCA	Hypoxia
SLC22A3	2.5778916999999999	1.99E-8	BRCA	Hypoxia
SLC2A12	2.7777413850000001	1.0500000000000001E-9	BRCA	Hypoxia
SLC6A14	3.6608311919999998	3.6399999999999999E-6	BRCA	Hypoxia
SLC34A2	3.945416018	1.8300000000000001E-6	BRCA	Hypoxia
SLC22A11	-2.7586329040000002	1.723848E-2	COAD	Hypoxia
SLC25A27	-2.0509178239999999	1.0188020000000001E-3	COAD	Hypoxia
SLC2A6	1.746443991	1.6317786000000001E-2	COAD	Hypoxia
SLC31A2	1.7560368289999999	2.8572239999999998E-3	COAD	Hypoxia
SLC24A3	1.8418877570000001	2.93718E-2	COAD	Hypoxia
SLC2A3	1.8843656259999999	1.6020733999999998E-2	COAD	Hypoxia
SLC22A17	1.8914756260000001	5.7908539999999998E-3	COAD	Hypoxia
SLC11A1	1.9825018190000001	6.1325620000000003E-3	COAD	Hypoxia
SLC37A2	2.0006242599999999	1.0655136000000001E-2	COAD	Hypoxia
SLC15A3	2.0055649550000001	8.92E-5	COAD	Hypoxia
SLC4A11	2.012613993	4.7795362000000001E-2	COAD	Hypoxia
SLC2A5	2.0222240189999998	4.083611E-3	COAD	Hypoxia
SLC16A3	2.0315309130000001	8.9318899999999996E-4	COAD	Hypoxia
SLC16A2	2.1231777350000001	7.7029799999999999E-4	COAD	Hypoxia
SLC6A8	2.1543653059999999	5.975078E-3	COAD	Hypoxia
SLC4A4	2.7908156210000001	5.0831909999999999E-3	COAD	Hypoxia
SLC6A14	2.8589803140000001	2.8238640999999998E-2	COAD	Hypoxia
SLC6A11	5.6535889199999998	4.6313295999999997E-2	ESCA	Hypoxia
SLC25A48	-3.0630289290000001	3.1633544999999999E-2	GBM	Hypoxia
SLC2A1	1.9490105360000001	5.8301710000000003E-3	GBM	Hypoxia
SLC39A8	1.9997730419999999	1.0241399999999999E-2	GBM	Hypoxia
SLC49A3	2.0468610699999998	2.0762321E-2	GBM	Hypoxia
SLC22A18	2.11706796	1.7753741E-2	GBM	Hypoxia

SLCO4A1	2.1367178889999998	3.3414894000000001E-2	GBM	Hypoxia
SLC2A5	2.4385690000000002	1.1210619E-2	GBM	Hypoxia
SLC39A14	2.5663520879999999	3.9600000000000002E-6	GBM	Hypoxia
SLC6A6	2.9743659400000002	1.6652600000000001E-4	GBM	Hypoxia
SLC11A1	3.0114802599999999	9.963350000000001E-4	GBM	Hypoxia
SLC10A6	3.0212466170000001	2.1891649999999999E-3	GBM	Hypoxia
SLC16A10	3.202091647	1.5742830000000001E-3	GBM	Hypoxia
SLC2A3	3.3789566990000002	8.9700000000000003E-8	GBM	Hypoxia
SLC16A3	3.486832508	1.6999999999999999E-7	GBM	Hypoxia
SLC1A6	-3.3679922759999998	4.2799999999999997E-6	LGG	Hypoxia
SLC17A8	-3.33096484	7.0479199999999998E-4	LGG	Hypoxia
SLC17A6	-2.5621461870000002	1.7826732000000001E-2	LGG	Hypoxia
SLC8A2	-2.415684224	9.8911000000000008E-4	LGG	Hypoxia
SLC25A21-AS1	-2.1096268949999999	1.8454669999999999E-3	LGG	Hypoxia
SLC7A14	-2.0236604699999998	2.8994954E-2	LGG	Hypoxia
SLCO5A1	-1.939833685	1.542419E-3	LGG	Hypoxia
SLC1A1	-1.8664278379999999	7.9691199999999999E-4	LGG	Hypoxia
SLC26A10	-1.848540581	1.862743E-3	LGG	Hypoxia
SLC8A3	-1.8221976390000001	1.1721209999999999E-2	LGG	Hypoxia
SLC25A21	-1.7599810469999999	4.1509915000000001E-2	LGG	Hypoxia
SLC25A27	-1.7191898539999999	3.4100000000000002E-5	LGG	Hypoxia
SLC9A3-AS1	-1.5887239200000001	2.2898720000000001E-3	LGG	Hypoxia
SLC66A3	1.483024042	3.7024470000000002E-3	LGG	Hypoxia
SLC49A3	1.5170263639999999	9.5105799999999994E-3	LGG	Hypoxia
SLC12A7	1.639517544	4.2402960000000002E-3	LGG	Hypoxia
SLC2A3	1.6866444789999999	3.970739E-3	LGG	Hypoxia
SLC8B1	1.715039711	2.0000000000000002E-5	LGG	Hypoxia

SLC2A12	1.775010253	4.1514509999999996E-3	LGG	Hypoxia
SLC25A43	1.775194597	4.8853568999999999E-2	LGG	Hypoxia
SLC25A45	1.787176745	1.1534850000000001E-3	LGG	Hypoxia
SLC16A5	1.846349223	5.5500000000000001E-5	LGG	Hypoxia
SLC37A2	1.882660126	7.1929299999999997E-4	LGG	Hypoxia
SLC35G2	1.9071147610000001	1.1351519999999999E-3	LGG	Hypoxia
SLC15A3	1.9342573190000001	4.1199999999999999E-5	LGG	Hypoxia
SLC16A4	1.941234082	3.4222499999999998E-4	LGG	Hypoxia
SLC9A7P1	1.978245816	4.5376879999999998E-3	LGG	Hypoxia
SLC17A9	2.13213315	2.5400000000000002E-7	LGG	Hypoxia
SLC2A9	2.1463247609999998	4.9700000000000002E-8	LGG	Hypoxia
SLC43A3	2.1554934609999998	3.29E-5	LGG	Hypoxia
SLC7A7	2.2187826839999998	2.2700000000000001E-8	LGG	Hypoxia
SLC25A24	2.4000854519999999	4.8799999999999997E-10	LGG	Hypoxia
SLC1A5	2.504338138	6.0299999999999999E-10	LGG	Hypoxia
SLC2A5	2.5523388420000002	2.5600000000000002E-7	LGG	Hypoxia
SLC44A3	2.573484922	3.7599999999999999E-8	LGG	Hypoxia
SLC16A3	2.727668274	1.52E-11	LGG	Hypoxia
SLC2A10	2.8439492830000002	5.1499999999999998E-8	LGG	Hypoxia
SLC44A3-AS1	2.985853058	9.1700000000000004E-9	LGG	Hypoxia
SLC47A2	3.204279235	1.77E-5	LGG	Hypoxia
SLC11A1	3.7790094110000001	1.07E-14	LGG	Hypoxia
SLC39A5	-3.072513453	1.0317457E-2	LIHC	Hypoxia
SLC66A3	1.6382206850000001	3.4286944999999999E-2	LIHC	Hypoxia
SLC4A7	2.031087554	1.6714099999999999E-4	LIHC	Hypoxia
SLC8A1	2.0974098830000001	1.45228E-3	LIHC	Hypoxia
SLC25A24	2.670534516	3.9634000000000002E-4	LIHC	Hypoxia
SLC2A3	2.7680729839999998	9.7100000000000002E-6	LIHC	Hypoxia

SLC4A4	2.9648631600000002	4.6539870000000001E-3	LIHC	Hypoxia
SLC6A6	3.1686210899999998	3.8399999999999998E-5	LIHC	Hypoxia
SLC24A3	3.1781796029999998	2.24014E-4	LIHC	Hypoxia
SLC1A1	3.8196190099999998	1.630685E-3	LIHC	Hypoxia
SLC26A5	-2.3616633220000001	2.4464400000000002E-4	LUAD	Hypoxia
SLC25A27	-2.3016047319999999	5.0000000000000002E-5	LUAD	Hypoxia
SLC4A5	-1.7638646499999999	1.9425595E-2	LUAD	Hypoxia
SLC15A3	1.533362348	5.0001087E-2	LUAD	Hypoxia
SLC10A3	1.581190874	4.2548145000000002E-2	LUAD	Hypoxia
SLC35E4	1.58170495	3.7365394000000003E-2	LUAD	Hypoxia
SLC7A7	1.6143905549999999	4.3292089999999997E-3	LUAD	Hypoxia
SLC16A2	1.6614488759999999	2.4628644000000002E-2	LUAD	Hypoxia
SLC31A2	1.6989327400000001	1.2694570000000001E-3	LUAD	Hypoxia
SLC45A1	1.9181656140000001	6.2035470000000002E-3	LUAD	Hypoxia
SLC16A1	2.0569847609999998	4.7593289999999996E-3	LUAD	Hypoxia
SLC6A8	2.1289629200000002	1.8937000000000001E-4	LUAD	Hypoxia
SLCO4A1-AS1	2.2916147599999999	4.4286923999999998E-2	LUAD	Hypoxia
SLC2A5	2.4284262490000001	1.0000000000000001E-5	LUAD	Hypoxia
SLC2A3	2.529587195	2.37E-8	LUAD	Hypoxia
SLCO4A1	2.8867138680000002	2.7300000000000001E-6	LUAD	Hypoxia
SLC16A3	3.0122688210000002	7.3799999999999992E-15	LUAD	Hypoxia
SLC2A1	3.373575808	3.2300000000000002E-12	LUAD	Hypoxia
SLC25A25-AS1	-2.0383091310000001	4.1212900000000001E-4	LUSC	Hypoxia
SLC16A3	1.534292641	4.8814791000000003E-2	LUSC	Hypoxia
SLC39A8	1.756348974	8.4171799999999998E-3	LUSC	Hypoxia
SLC2A1	1.9887451169999999	2.1164529999999999E-3	LUSC	Hypoxia
SLC1A3	2.0244932640000002	3.5054460000000002E-3	LUSC	Hypoxia

SLC2A3	2.238316492	2.2419200000000001E-4	LUSC	Hypoxia
SLC22A3	2.2798578300000001	2.7951554E-2	LUSC	Hypoxia
SLC24A3	2.3680416310000001	2.55367E-4	LUSC	Hypoxia
SLC38A5	2.4130314959999999	3.1691110000000001E-3	LUSC	Hypoxia
SLC34A2	2.741900072	3.8391451E-2	LUSC	Hypoxia
SLC10A6	2.7480112349999999	2.9081340000000002E-3	LUSC	Hypoxia
SLC20A1	2.4138603829999998	2.7405260000000001E-3	PAAD	Hypoxia
SLC11A1	2.56522849	9.4122779999999996E-3	PAAD	Hypoxia
SLC37A2	2.8691708029999998	6.0289899999999997E-3	PAAD	Hypoxia
SLC16A3	3.1281912740000002	3.9198130000000003E-3	PAAD	Hypoxia
SLC2A1	3.331981275	1.714438E-3	PAAD	Hypoxia
SLC2A3	3.4388692839999999	1.2500000000000001E-5	PAAD	Hypoxia
SLC45A2	-2.3777226169999999	2.1816954E-2	PRAD	Hypoxia
SLC23A3	-1.602653391	4.6544217999999998E-2	PRAD	Hypoxia
SLC43A3	1.418860051	4.377649E-3	PRAD	Hypoxia
SLCO2A1	1.471654649	9.926809E-3	PRAD	Hypoxia
SLC40A1	1.591793944	3.7649010000000002E-3	PRAD	Hypoxia
SLC9A7P1	1.6834217389999999	1.437192E-2	PRAD	Hypoxia
SLC7A5	1.6936254230000001	2.3260212999999998E-2	PRAD	Hypoxia
SLC12A4	1.7196431219999999	4.7899999999999999E-8	PRAD	Hypoxia
SLC2A9	1.739754639	1.01826E-4	PRAD	Hypoxia
SLC1A7	1.762972145	4.0595149999999997E-3	PRAD	Hypoxia
SLC46A3	1.768995783	8.4499999999999994E-5	PRAD	Hypoxia
SLC38A5	1.7784402070000001	4.3145599999999998E-4	PRAD	Hypoxia
SLC10A6	1.8009151510000001	6.1095339999999998E-3	PRAD	Hypoxia
SLC16A4	1.8044445579999999	3.1600000000000002E-5	PRAD	Hypoxia
SLC52A1	1.932157492	1.0996268999999999E-2	PRAD	Hypoxia
SLC35F4	1.981126376	8.6823399999999995E-4	PRAD	Hypoxia
SLC5A1	2.0120517659999999	1.9951627999999999E-2	PRAD	Hypoxia

SLC7A3	2.0848919509999999	1.8807648E-2	PRAD	Hypoxia
SLC16A2	2.0929975970000001	7.1699999999999998E-9	PRAD	Hypoxia
SLCO3A1	2.147715378	2.64E-9	PRAD	Hypoxia
SLC47A1	2.2173210509999999	7.0999999999999998E-7	PRAD	Hypoxia
SLC51B	2.2538023269999998	1.72E-6	PRAD	Hypoxia
SLC26A9	2.2714406220000001	3.6852880000000001E-3	PRAD	Hypoxia
SLC19A3	2.2916733269999998	2.08252E-4	PRAD	Hypoxia
SLC38A3	2.3639373479999999	2.4000000000000001E-5	PRAD	Hypoxia
SLC24A3	2.4022241219999998	4.7099999999999998E-8	PRAD	Hypoxia
SLC2A3	2.4045708970000002	7.2600000000000002E-9	PRAD	Hypoxia
SLC22A3	2.4299755479999998	2.646888E-3	PRAD	Hypoxia
SLC15A1	2.5450643839999998	7.4802699999999996E-4	PRAD	Hypoxia
SLC39A2	2.5540656259999999	5.0010059999999997E-3	PRAD	Hypoxia
SLC16A7	2.5846663639999998	7.79E-10	PRAD	Hypoxia
SLC16A5	2.6408640929999998	5.7100000000000002E-8	PRAD	Hypoxia
SLC2A4	2.687271859	9.05E-9	PRAD	Hypoxia
SLC6A14	2.7719887600000002	4.66482E-4	PRAD	Hypoxia
SLC8A1	2.7992031590000002	6.6E-10	PRAD	Hypoxia
SLC27A6	2.9665691170000001	1.29E-5	PRAD	Hypoxia
SLC18A2	2.9739423999999999	2.9200000000000002E-7	PRAD	Hypoxia
SLC2A5	3.090992655	3.0600000000000001E-7	PRAD	Hypoxia
SLC14A1	3.281270197	7.9700000000000006E-8	PRAD	Hypoxia
SLC34A2	3.448801038	1.66291E-4	PRAD	Hypoxia
SLC7A4	4.0775418190000003	6.7000000000000004E-7	PRAD	Hypoxia
SLC5A8	4.5390395760000004	8.5500000000000005E-10	PRAD	Hypoxia
SLC9A9	2.296047518	4.6656464000000002E-2	READ	Hypoxia
SLC24A3	2.3741999690000002	3.7099791E-2	READ	Hypoxia
SLC2A3	2.7573632539999999	8.9096309999999995E-3	READ	Hypoxia
SLC25A27	-2.5457554930000001	5.0538600000000003E-4	SKCM	Hypoxia

SLC2A1	1.7811571500000001	2.4337749999999998E-2	SKCM	Hypoxia
SLC43A2	1.8127789809999999	4.1208720000000003E-3	SKCM	Hypoxia
SLC31A2	1.940188274	5.8910359999999997E-3	SKCM	Hypoxia
SLC20A1	2.0050884089999998	5.8910359999999997E-3	SKCM	Hypoxia
SLC22A4	2.008874804	3.7761560000000001E-3	SKCM	Hypoxia
SLC45A1	2.0591265129999998	3.0941711E-2	SKCM	Hypoxia
SLC35G2	2.0772129910000001	3.5774711000000001E-2	SKCM	Hypoxia
SLCO2B1	2.1231407029999998	4.1151651999999997E-2	SKCM	Hypoxia
SLC12A8	2.1276996100000001	1.1844439999999999E-2	SKCM	Hypoxia
SLC2A5	2.3303895030000001	4.204719E-3	SKCM	Hypoxia
SLC2A3	2.440159945	1.8247900000000001E-4	SKCM	Hypoxia
SLC11A1	2.5235202189999999	2.4988499999999998E-4	SKCM	Hypoxia
SLC22A3	2.5660884469999998	3.2310966000000003E-2	SKCM	Hypoxia
SLC24A3	2.5908116329999999	3.7572356000000001E-2	SKCM	Hypoxia
SLC16A3	2.7101484280000001	1.0697899999999999E-4	SKCM	Hypoxia
SLC9A7	2.7773547129999998	6.3686700000000005E-4	SKCM	Hypoxia

Table B.1: Differentially expressed SLC transporters in Hypoxia - A full list of hits in the hypoxia stream. Cut offs: $\log_2$(Fold change) ≥ 1, adjusted P value ≤ 0.05